From Lewis Superacidic Aluminum Pentafluoroorthotellurates to Perfluorinated Tritylium and Fluoronium Ions

Inaugural-Dissertation
to obtain the academic degree
Doctor rerum naturalium (Dr. rer. nat.)

submitted to the Department of Biology, Pharmacy, Chemistry
of Freie Universität Berlin

by

Kurt F. Hoffmann

2022

The work for this dissertation was done in the group of Prof. Dr. Sebastian Hasenstab-Riedel from January 2018 until October 2022 at the Institute of Chemistry and Biochemistry at Freie Universität Berlin.

I declare that this dissertation is my own work except where stated contrary. This dissertation has not been submitted to obtain any other degree.

Kurt F. Hoffmann

Date of Disputation: 16.12.2022

First referee: Prof. Dr. Sebastian Hasenstab-Riedel

Second referee: Prof. Dr. Thomas Braun

Acknowledgements

At first, I want to thank Prof. Dr. Sebastian Hasenstab-Riedel for giving me the opportunity to undertake my doctoral thesis in his group and for being an engaged, supportive supervisor, who always had an open ear for discussions and suggestions.
I want to thank Prof. Dr. Thomas Braun for acting as second referee for this thesis and for his supervision and input during our cooperation in the CRC 1349. Additionally, I am grateful to the other members of the disputation committee for their time.
I would like to thank Dr. habil. Helmut Beckers, Dr. Simon Steinhauer, Dr. Anja Wiesner and Dr. Julia Bader for their very helpful scientific discussions and advice during the course of my studies, their help with measurements and their careful correction of my manuscripts.
Furthermore, I want to thank all collaboration partners with whom I was working together during my doctoral studies: Minh Bui, Dr. Mike Ahrens and Prof. Dr. Thomas Braun, Cody Ross Pitts, Muhammad Kazim, Prof. Thomas Lectka, Susanne Rupf and Dr. Moritz Malischewski.
I want to thank the students Abdulrahman Radwan, Hannes Aberhan, David Battke and Ariane Wieseke who worked under my supervision during their internships and bachelor thesis.
A big thanks goes to all current and former members of the AG Riedel for their helpfulness and the good working atmosphere they created. Especially, I would like to express my gratitude to the teflate sub-group including the teflate running club. It was a pleasure having you all around at numerous lunch and coffee breaks, BBQ sessions and other AK events. A special thanks goes to Patrick Pröhm for being the greatest lab-mate during my time as doctoral student. I want to thank you for the many insightful discussions we had, be it on chemistry or the life beyond, and for being a good friend. I hope we'll stick to this also in the future!
Also, I want to express my gratitude towards Dr. Carsten Müller and Marie Nickel for their excellent coordination within the CRC 1349 and their valuable advice in all bureaucratic matters. Furthermore, I am grateful for the opportunities this CRC gave me in form of manifold scientific talks and conference visits as well as financial support.
I want to express my thanks to all working groups in the inorganic chemistry department, the technical staff, the secretaries, the lab-shop people, the glass-blowers, the employees at the HPC center at ZEDAT and the workshop crew for ensuing a smoother and less troubled life as a doctoral student.
I thank Dr. Anja Wiesner, Dr. Alberto Pérez-Bitrián and Dr. Patrick Pröhm for carefully proof-reading my thesis and their valuable advice in this matter.
Finally, I would like to thank my family, my friends and my beloved partner! I want to thank you for the endless support and encouragement you gave me during this time and words can't express how happy I am to share my life with you.

Abstract

The properties and reactivity of Lewis superacidic aluminum pentafluoroorthotellurates are investigated. An improved synthesis for the dimeric $[Al(OTeF_5)_3]_2$ was developed, yielding a pure product with an enhanced thermal stability. Different solvent adducts were synthesized, resulting in monomeric complexes of the Lewis acid with up to three solvent molecules attached. The complexes of $Al(OTeF_5)_3$ with toluene, fluorobenzene and sulfuryl chloride fluoride remained Lewis superacidic, as quantum-chemical calculations confirmed. Additionally, the high Lewis acidity of $[Al(OTeF_5)_3]_2$ and its solvent adducts were further verified by experimental methods.

Two different routes for the synthesis of the perfluorinated trityl cation $[C(C_6F_5)_3]^+$ were established. One utilizes the Lewis superacid $[Al(OTeF_5)_3(OSOClF)_2]$, the other the corresponding Brønsted superacid $[H–C_6H_4F_2][Al(OTeF_5)_4]$. A crystallographic characterization of this cation in conjunction with the weakly coordinating anion $[Al(OTeF_5)_4]^-$ was achieved for the first time. These routes finally give access to the perfluortrityl cation in SO_2ClF and organic solvents such as *ortho*-difluorobenzene. This improved handling enabled insights into the reactivity of this cation as hydride abstractor and oxidation reagent, which was proven by experimental and theoretical methods.

Organic divalent fluoronium ions were only investigated by spectroscopic studies, while a characterization in the solid state so far did not yield success. In this thesis, the synthesis and crystallographic analysis of a symmetrical $[C–F–C]^+$ fluoronium ion is reported. The vibrational spectrum of the fluoronium salt is discussed and the nature of the bonding situation in this type of cations are quantum-chemically studied and compared with heavier halonium homologues.

Besides the isolation and characterization of elusive cations with strong Lewis acids, the synthesis of a novel solid Lewis superacid is reported. Hereby, the reaction of a mixture of $AlCl_3$ and$[Al(OTeF_5)_3]_2$ with CCl_3F leads to an anion-doped aluminum chlorofluoride $AlCl_{0.1}F_{2.8}(OTeF_5)_{0.1}$. This material was studied by PDF analysis, EXAFS and MAS NMR spectroscopy, confirming an intact $OTeF_5$ group. A reaction with CD_3CN and subsequent IR spectroscopy revealed the Lewis superacidic nature of the material. Lastly, the catalytic activity of the material in dehydrofluorination reactions was tested.

Kurzzusammenfassung

Die Eigenschaften und die Reaktivität von Lewis-supersauren Aluminiumpentafluoroorthotelluraten wurden untersucht. Es wurde eine verbesserte Synthese für dimeres $[Al(OTeF_5)_3]_2$ entwickelt, die ein reineres Produkt mit erhöhter thermischer Stabilität ergibt. Es wurden verschiedene Lösungsmitteladdukte synthetisiert, wobei monomere Komplexe der Lewis-Säure mit bis zu drei gebundenen Lösungsmittelmolekülen erhalten wurden. Die Komplexe von $Al(OTeF_5)_3$ mit Toluol, Fluorbenzol und Sulfurylchloridfluorid gelten immernoch als Lewis-Supersäuren, was durch quantenchemische Berechnungen bestätigt wurde. Darüber hinaus wurde die hohe Lewis-Azidität von $[Al(OTeF_5)_3]_2$ und seinen Lösungsmitteladdukten durch experimentelle Methoden weiter verifiziert.

Es wurden zwei unterschiedliche Routen zur Synthese des perfluorierten Tritylkations $[C(C_6F_5)_3]^+$ entwickelt. Die erste Route nutzt die Lewis-Supersäure $[Al(OTeF_5)_3(OSOClF)_2]$, während die zweite Route die korrespondierende Brønsted Supersäure $[H–C_6H_4F_2][Al(OTeF_5)_4]$ verwendet. Das schwach koordinierende Anion $[Al(OTeF_5)_4]^-$ ermöglichte die kristallographische Charakterisierung dieses Kations mittels Einkristall-Röntgenstrukturanalyse. Die vorgestellten Synthesrouten führen so erstmalig zur Handhabung des Perfluortrityl-Kations in SO_2ClF und organischen Lösungsmitteln wie *ortho*-Difluorbenzol. Dies erlaubte Einblicke in die Reaktivität dieses Kations als Hydridabstraktor und Oxidationsreagenz, was mit experimentellen und theoretischen Methoden nachgewiesen wurde.

Organische, divalente Fluoroniumionen wurden bisher nur durch spektroskopische Studien untersucht, während eine Charakterisierung im festen Zustand bisher nicht möglich war. In dieser Arbeit wird über die Synthese und kristallographische Analyse eines symmetrischen $[C–F–C]^+$ Fluoroniumions berichtet. Darüber hinaus wird das Schwingungsspektrum des Fluoroniumsalzes diskutiert und die Bindungssituation in dieser Art von Kation quantenchemisch untersucht und mit schwereren Halonium-Homologen verglichen.

Neben der Isolierung und Charakterisierung von schwer-fassbaren Kationen mit starken Lewis-Säuren wird über die Synthese einer neuartigen festen Lewis-Supersäure berichtet. Dabei führt die Reaktion einer Mischung aus $AlCl_3$ und $[Al(OTeF_5)_3]_2$ mit CCl_3F zu einem anionen-dotierten Aluminiumchlorfluorid $AlCl_{0.1}F_{2.8}(OTeF_5)_{0.1}$. Dieses Material wurde mittels PDF-Analyse, EXAFS- und MAS-NMR-Spektroskopie untersucht, wodurch die Intakthaltung der $OTeF_5$ Gruppe bestätigt werden konnte. Eine Reaktion mit CD_3CN und anschließende Untersuchung mittels IR-Spektroskopie zeigten die Lewis-supersauren Eigenschaften des Materials. Schließlich wurde die katalytische Aktivität des Materials in Dehydrofluorierungsreaktionen getestet.

List of Abbreviations

ACF aluminum chlorofluoride

BP86 Becke-Perdew 1986

Cp cyclopentadienyl, $-(C_5H_5)$

DFT density-functional theory

Eq equation

Et ethyl, $-(CH_2CH_3)$

et al. et alii/aliae, and others

EXAFS extended X-ray absorption fine structure

Fc ferrocene, $[Fe(C_5H_5)_2]$

FIA fluoride ion affinity

FLP frustrated Lewis pair

GEI global electrophilicity index

HDF hydrodefluorination

HIA hydride ion affinity

hs high surface

i-Pr *iso*-propyl, $-(CH(CH_3)_2)$

IR infrared

LA Lewis acid

LB Lewis base

LSA Lewis superacid

LUMO lowest unoccupied molecular orbital

MAS magic-angle spinning

Me methyl, $-(CH_3)$

Mes mesityl, $-(C_6H_2 2,4,5-(CH_3))$

NMR nuclear magnetic resonance

o-DFB *ortho*-difluorobenzene

o-tol *ortho*-tolyl, $-(2\text{–}(CH_3)C_6H_5)$

OTf triflate, $-(OSO_2CF_3)$

PDF pair distribution function

Ph phenyl, $-(C_6H_5)$

PhF fluorobenzene

SC-XRD single-crystal X-ray diffraction

t-Bu *tert*-butyl, $-(C(CH_3)_3)$

THF tetrahydrofurane

TPD temperature-programmed desorption

UV-vis ultraviolet-visible

WCA weakly coordinating anion

Contents

1. Introduction **1**

1.1. Acid-Base Concepts . . . 1

1.1.1. Scaling of Acidity . . . 1

1.2. Pentafluoroorthotellurates . . . 4

1.3. Lewis Superacids . . . 5

1.3.1. Neutral Lewis Superacids . . . 5

1.3.2. Cationic Lewis Superacids . . . 10

1.3.3. Solid Lewis Superacids . . . 12

1.4. Applications of Lewis Superacids . . . 12

1.4.1. Catalysis . . . 12

1.4.2. Reactive Cation Synthesis . . . 14

1.4.3. Frustrated Lewis Pairs . . . 15

1.5. Brønsted Superacids . . . 17

1.6. Weakly Coordinating Anions . . . 18

2. Objectives **23**

3. Publications **25**

3.1. Insights on the Lewis Superacid $Al(OTeF_5)_3$: Solvent Adducts, Characterization and Properties 25

3.2. The Tris(pentafluorophenyl)methylium Cation: Isolation and Reactivity . . . 41

3.3. Structural proof of a $[C–F–C]^+$ fluoronium cation . . . 49

3.4. An Amorphous Teflate Doped Aluminium Chlorofluoride: A Solid Lewis Superacid for the Dehydrofluorination of Fluoroalkanes . . . 57

4. Conclusion and Outlook **63**

4.1. Conclusion . . . 63

4.2. Outlook . . . 66

5. References **69**

6. List of Publications **81**

A. Supporting Information of Publications **83**

A.1. Insights on the Lewis Superacid $Al(OTeF_5)_3$: Solvent Adducts, Characterization and Properties 83

A.2. The Tris(pentafluorophenyl)methylium Cation: Isolation and Reactivity . . . 109

A.3. Structural proof of a $[C–F–C]^+$ fluoronium cation . . . 136

A.4. An Amorphous Teflate Doped Aluminium Chlorofluoride: A Solid Lewis Superacid for the Dehydrofluorination of Fluoroalkanes . . . 153

1. Introduction

1.1. Acid-Base Concepts

A great fundamental of chemistry is the understanding of acid-base concepts. The first explanation of this chemical phenomenon was given by Arrhenius, who investigated the ionic dissociation of different acids in water.[1] He came to the conclusion that acids yield hydrogen ions, H^+, upon dissociation, while bases yield hydroxide ions, OH^-. This concept was further refined by Lowry and Brønsted independently, which added more generality to it, leading to the well-known definition for Brønsted acids and bases: *Acids are proton donators (HA) and bases are proton acceptors (B).*[2,3] This interaction of an acid and a base is depicted in equation 1. An acid-base pair that only differs by one proton is referred to as conjugate. The proton transfer can occur in both directions and is dependent on the relative acidity of HA compared to its conjugate acid HB^+. Note that in the condensed phase, B can also be a solvent molecule and the acid can also ionize while the protons are coordinated by one or more solvent molecules. Furthermore, in the case of autoprotolysis another acid molecule can act as the base B.

$$HA + B \rightleftharpoons A^- + HB^+ \tag{1}$$

The unifying species of both, the Arrhenius and the Brønsted-Lowry concepts, is the proton H^+. Due to its empty *1s* orbital, the proton is not subject to electronic repulsion and its high electron affinity and polarizing effect renders it extremely reactive. Therefore, in the condensed phase it is always found bound to other molecules. In 1938, G. N. Lewis generalized this concept and defined: *Acids are electron-pair acceptors and bases are electron-pair donors.*[4] According to this definition, H^+ is a Lewis acid/electron-pair acceptor. This concept follows that a reaction between a Lewis acid LA and a Lewis base LB results in the formation of an adduct as shown in equation 2.

$$LA + :LB \rightleftharpoons LA{-}LB \tag{2}$$

A third concept which is more focused on solid oxides and fluxes thereof was introduced by Lux and Flood. They investigated the behavior of molten oxides and claimed an acid as "oxide ion acceptor" and the corresponding base as "oxide ion donor".[5,6] While this concept seems to have a limited field of applicability, it is foremost important for industrial processes such as the production of glass or metallurgy.[7]

1.1.1. Scaling of Acidity

The ideal parameter to gauge the acidity of a Brønsted acid in a certain medium is the proton activity. For the most common medium H_2O, a convenient measure for the Brønsted acidity is the pH scale, which was firstly introduced by Sørensen.[8] It is defined as negative decadic logarithm of the proton activity in water (cf. Eq. 3) and it is accurate in dilute acidic solutions in which the acid is completely dissociated.

$$\mathrm{pH} = -\log\left(a_{\mathrm{H}^+}\right) \tag{3}$$

For concentrated aqueous solutions, which have undisscociated acid molecules, or non-aqueous systems a different approach is needed. In 1932, Hammett and Deyrup introduced a new scale, which is based on the protonation of a weakly basic indicator B with a known dissociation constant $\mathrm{p}K_{\mathrm{HB}^+}$ (see equation 4).[9] The degree of protonation can then be measured with experimental methods such as UV-vis, IR or NMR spectroscopy or electrochemical techniques.[10]

$$H_0 = \mathrm{p}K_{\mathrm{HB}^+} - \log\left(\frac{[\mathrm{HB}^+]}{\mathrm{B}}\right) \tag{4}$$

Since the Hammett acidity scale is only applicable to liquid media, for gaseous or solid Brønsted acids different methods are needed. A convenient procedure to estimate the strength of solid Brønsted acids was developed by Fărcaşiu and Ghenciu. They utilize the protonation of mesityl oxide and its thereby induced chemical shift difference of the C_α and C_β atoms (see Figure 1). A strong acid shifts the equilibrium to the right-hand site of the equation due to the increased degree of protonation, which consequently leads to an increased chemical shift difference. This difference $\Delta\delta(^{13}\mathrm{C})$ can be measured by ^{13}C NMR spectroscopy.[11]

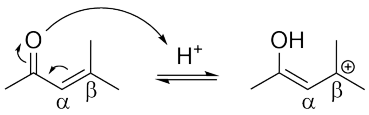

Figure 1. Protonation of mesityl oxide.

Finally, more recent approaches use quantum-chemical calculations to avoid the solvent-dependence and obtain a unified view on Brønsted acidity. In this method, the ideal proton gas is used as reference point, enabling the calculation of a solvent-independent absolute pH value for an acid in question.[12,13]

While the aforementioned methods can be used to quantitatively scale the Brønsted acidity of certain compounds, establishing a corresponding unified scale for the determination of the strength of Lewis acids is not as straightforward. The reason for this is the missing common denominator for Lewis acid-base interactions, as it is the case for the proton transfer in Brønsted acid-base interactions. In fact, the acidity of different Lewis acids may differ drastically depending on the choice of the Lewis base. An important qualitative theory was developed by Pearson, which judged the donor-acceptor interactions of different Lewis acids and bases depending on their hardness or softness.[14] Hereby, hard acids are described as small, unpolarizable, electropositive acceptor atoms while hard bases are unpolarizable electronegative donor atoms. The opposite holds true for soft acids and bases. Pearson's principle now states that hard acids preferably interact with hard bases, forming mostly electrostatic bonds, while soft acids rather bind to soft bases through more covalent interactions. Drago and Wayland attempted to formulate this concept by introducing electrostatic E and covalent C parameters for acids and bases, which can be used to predict the binding enthalpy of an acid-base pair.[15] Nevertheless, these qualitative concepts also have their limitations, e.g. when it comes to rationalizing ambident reactivities in organic reactions.[16]

For the quantitative estimation of Lewis acidity a large variety of methods have been reported in literature, both experimental and theoretical. In the following section, the most established examples will be introduced. Early works by Bartlett *et al.* suggested the fluoride ion affinity (FIA) for the assessment of Lewis acidity.[17] In this concept the binding of a Lewis acid to a fluoride ion is considered and the negative

reaction enthalpy of Lewis acid-base complexation is defined as the fluoride ion affinity (cf. Eq. 5). Hereby, the FIA should correlate with the strength of a certain Lewis acid. The fluoride ion was chosen due to its high basicity, small size and capability to form acid-base complexes with a broad variety of Lewis acids. Experimentally, the measure of the reaction enthalpy was realized by lattice energy calculations or ion cyclotron resonance experiments.[18,19]

$$\mathrm{LA\,(g) + F^-\,(g) \xrightarrow{FIA\,=\,-\Delta H} [LA{-}F]^-\,(g)} \tag{5}$$

Since these FIA values showed large discrepancies depending on the used method and also require an extensive experimental setup, a quantum-chemical approach was introduced by Christe and co-workers.[20,21] Because the calculation of a "naked" fluoride atom F^- on lower levels of theory is problematic, an isodesmic reaction with COF_2 is considered. These isodesmic reactions allow reliable calculations of reaction enthalpies on DFT level even for large Lewis acids (Eq. 6). In order to obtain the correct FIA value, the calculated reaction enthalpy has to be corrected by the experimental FIA value for COF_2, which acts as so-called anchor point (Eq. 7).

$$\mathrm{LA\,(g) + [COF_3]^-\,(g) \xrightarrow{DFT\,calculation} [LA{-}F]^-\,(g) + COF_2} \tag{6}$$

$$\mathrm{[COF_3]^-\,(g) \xrightleftharpoons{experimental} COF_2 + F^-\,(g)} \tag{7}$$

A different established reference system for these isodesmic reactions is based on trimethylsilylfluoride Me_3SiF.[22] In this case, the anchor point energy was not obtained experimentally, but calculated on a high level of theory.

Following the principle of Pearson, fluoride ions are one of the hardest Lewis bases and the highest FIA values are therefore achieved with hard Lewis acids. In order to also describe softer Lewis acids appropriately, a similar affinity scale was introduced, which is based on a hydride ion as Lewis base, known as hydride ion affinity.[23,24] Other ion affinity scales which are used frequently are the chloride and methide ion affinity scales, in which Me_3SiCl and Me_4Si are used respectively as anchor points.[22] Furthermore, it is important to distinguish between cationic and neutral Lewis acids. Since routine quantum-chemical calculations assume reactions in the gas-phase, the FIA values for cationic molecules are highly exaggerated because of the absence of any solvation enthalpies. This overestimation can be partially addressed through solvent-models for the FIA calculations.[25,26] A different experimental method utilizes acetonitrile as a Lewis base and probe in vibrational spectroscopy. Hereby, a blue shift of the C≡N stretching mode is observed upon the formation of an acetonitrile-Lewis acid complex, when compared to neat acetonitrile.[27] The magnitude of the blue-shift should correlate to the Lewis acidity. A pitfall is the Fermi resonance, appearing in the similar wavenumber region as the C≡N stretching mode, which requires the use of deuterated acetonitrile in order to circumvent this misinterpretation.[28]

Gutmann and Beckett proposed the usage of NMR spectroscopy to determine the Lewis acidity. In their method, the complexes of a Lewis acid and triethylphopshine oxide Et_3PO are investigated. Such complexes exhibit a change in the chemical shift of the bound Et_3PO in the ^{31}P NMR spectrum when compared to free Et_3PO.[29,30] This chemical shift difference is then used to correlate the acidity of the parent Lewis acid. An alternative method was developed by Childs and co-workers, who used *trans*-crotonaldehyde as a Lewis base and the induced shift of the H3 proton upon binding for Lewis acidity measurements.[31]

Nevertheless, both methods can result in misleading trends, since steric effects, intramolecular stabilization of the Lewis acid, multiple bonded donor molecules and general electronegativity and polarizabilty of the Lewis acid heavily influence the obtained values. Therefore, it is recommended to consider only similar types of Lewis acids for a meaningful comparison.[32]

A conceptually different approach on scaling Lewis acidity is the global electrophilicity index (GEI). The concept itself is already known since 1999 for estimating the ability of a molecule to take up electrons,[33] but it was in 2018 when Stephan and co-workers introduced the GEI as a metric for Lewis acidity.[34] An advantage of this method is the fast applicability and the independence of any Lewis base as reference. Nevertheless, effects directly arising from the interaction between acid and base such as deformation energy or repulsion are systematically neglected.

Conclusively, every technique has its advantages and drawbacks, making it necessary to use different methods for estimating the Lewis acidity of a certain compound. As recently reported, three different aspects of Lewis acidity can be distinguished, namely global, effective and intrinsic Lewis acidity.[35] Hereby, global Lewis acidity can be described as the thermodynamic tendency of a Lewis acid to form Lewis acid-base complexes, which follows closely the definition by IUPAC.[36] Associated physical values are the reaction enthalpy ΔH and Gibbs energy ΔG and the most frequently used scale for it is the previously described FIA. The effective Lewis acidity covers induced changes in physicochemical properties of Lewis bases which interact with the Lewis acid in question. These acid properties are best investigated with methods like Gutmann-Beckett or IR spectroscopy on acetonitrile adducts. Finally, intrinsic Lewis acidity describes the acidity of the free, uncoordinated Lewis acids without the use of any reference base, as exemplary desribed for the GEI method.

1.2. Pentafluoroorthotellurates

The pentafluoroorthotellurate group $[OTeF_5]^-$, also abbreviated as *teflate*, is the conjugate base of the pentafluoroorthotelluric acid $HOTeF_5$. Its octahedral coordination at the Te center with five fluoride ligands results in a characteristic AB_4 spin system, which is easily detectable by NMR spectroscopy. Additionally, vibrational spectra of pentafluoroorthotellurates show unique bands.[37] The pentafluoroorthotelluric acid $HOTeF_5$ was firstly discovered by Engelbrecht and Sladky by the reaction of $BaTeO_4$ and HSO_3F in 1964.[38] At room temperature this compound is a volatile, glass-like solid and contact with water leads to its decomposition into telluric acid $Te(OH)_6$ and HF. Later, a more convenient route to obtain $HOTeF_5$ was developed by reacting $Te(OH)_6$ and HSO_3F.[39] Besides the acid $HOTeF_5$, typical reactants to introduce the pentafluoroorthotellurate ligand into main group and transition metal compounds are $B(OTeF_5)_3$, $AgOTeF_5$ and $Xe(OTeF_5)_2$.[37] In Equations 8, 9, 10 and 11 some exemplary teflate transfer reactions are shown.[38,40–42] While in the case of $B(OTeF_5)_3$ and $AgOTeF_5$ the reactions can be described as metathesis reactions with the formation of BF_3 and AgF as driving force, reactions with $Xe(OTeF_5)_2$ are based on an oxidative addition. Lesser used but still effective transfer reagents are $ClOTeF_5$ and $Me_3SiOTeF_5$.[43,44]

$$HOTeF_5 + KCl \longrightarrow KOTeF_5 + HCl \tag{8}$$

$$B(OTeF_5)_3 + SbF_3 \longrightarrow Sb(OTeF_5)_3 + BF_3 \tag{9}$$

$$4\,AgOTeF_5 + SiCl_4 \longrightarrow Si(OTeF_5)_4 + 4\,AgCl \tag{10}$$

$$Xe(OTeF_5)_2 + I(OTeF_5)_3 \longrightarrow I(OTeF_5)_5 + Xe \tag{11}$$

The teflate group possesses strong electron-withdrawing properties which are comparable to that of fluorine. These properties have been investigated by different methods such as comparison of the chemical shift differences of the compounds Me–X and Et–X (X = F, Cl, Br, I, $OTeF_5$) in ^1H NMR spectra and the preference of equatorial $OTeF_5$ substitution on square-pyramidal $IF_x(OTeF_5)_{5-x}$ (x = 1, 2, 3, 4).[42,45,46] Additionally, Mössbauer, ^{125}Te and ^{129}Xe NMR spectroscopy on different analogue teflate and fluoride complexes were carried out for this purpose.[47] The electron-withdrawing properties of $OTeF_5$ are reflected by its reactivity, such as the successful stabilization and isolation of compounds in high oxidation states, e.g. $Te(OTeF_5)_6$ and $Xe(OTeF_5)_6$, which were formerly only known with fluoride ligands.[48–50] A striking difference between the teflate and the fluoride ligand is their size. The higher sterical demand of $OTeF_5$ leads to a reduced tendency to act as bridging ligand and can prevent oligomerization as shown in the case of $Au(OTeF_5)_3$. The gold-based pentafluoroorthotellurate dimerizes in the solid state, whereas AuF_3 results in a polymeric structure.[51,52] The negative charge of the teflate group is distributed over the whole periphery of the ligand, leading to low intermolecular interactions. Therefore, neutral pentafluoroorthotellurate compounds such as $Ti(OTeF_5)_4$ and $U(OTeF_5)_6$ possess a low vapor pressure and are sublimable at moderate temperatures despite their size and high molecular weight.[53,54] Combined with its high oxidation stability, these properties renders the $OTeF_5$ group ideal for weakly coordinating anions. Furtheremore, the assumed lack of π-backbonding in $OTeF_5$ complexes results in an increased Lewis acidity of pentafluoroorthotellurate complexes when compared to its fluoride analogues. Both, weakly coordinating anions and Lewis acids based on pentafluoroorthotellurates will be discussed in the following sections.

1.3. Lewis Superacids

Historically, different claims about the threshold for Lewis superacidity have been made, e.g. Olah's suggestion to define Lewis acids that are stronger than the frequently used Friedel-Crafts catalyst $AlCl_3$ as Lewis superacids (LSA).[55] Nevertheless, these suggestions tend to be arbitrary, since the acidity is always dependent on the used Lewis base. The contemporary accepted definition was given by Krossing and is: *Molecular Lewis acids, which are stronger than monomeric SbF_5 in the gas-phase are Lewis superacids.*[56] As mentioned in the previous section, a convenient tool to quantitatively measure the strength for gas-phase Lewis acids is the fluoride ion affinity. In Figure 2 an overview of FIA values calculated on different levels of theory for a broad range of different Lewis superacids is given. When it comes to designing a new Lewis superacid, certain requirements should be considered: Besides the choice of the central atom, the most efficient way to reach high acidities includes the introduction of electron-withdrawing ligands. Furthermore, it is important to prevent an oligomerization of the acid by using bulky ligands. A classical example for decreased acidity due to oligomerization are aluminum trihalides such as $AlCl_3$ and $AlBr_3$.[57] Another determining factor is the reorganization energy of a Lewis acid upon Lewis base binding, which can heavily influence its effective acidity.[58] In the following, different classes of Lewis superacids will be presented, which adapt these aforementioned design principles.

1.3.1. Neutral Lewis Superacids

The most commonly used, convenient strong Lewis acid is SbF_5. Under ambient conditions, this compound is a highly viscous, corrosive, moisture-sensitive liquid composed of fluoride-bridged, polymeric molecules.

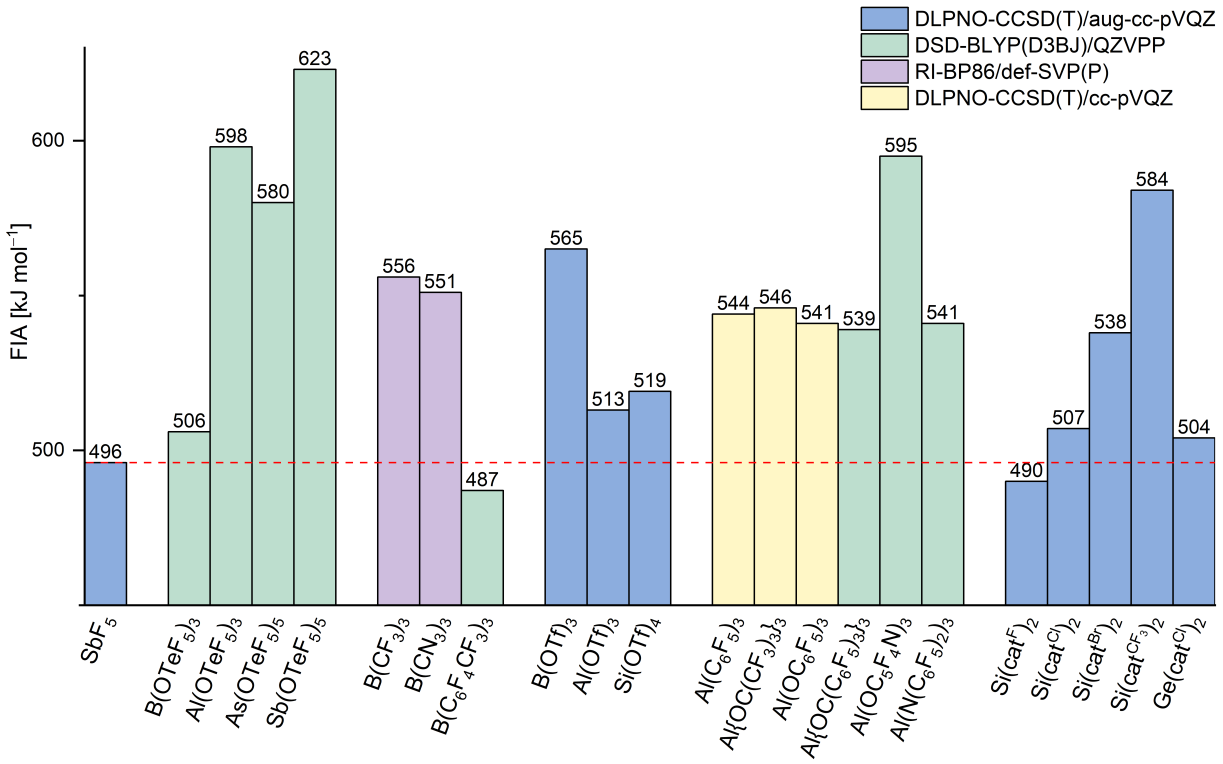

Figure 2. Fluoride ion affinities of neutral Lewis superacids (Tf = $[SO_2CF_3]^-$, cat^X = $[o\text{-}C_6X_4O_2]^{2-}$ with X = F, Cl, Br, CF_3).[22,59]

Solid SbF_5 was reported to possess a tetrameric structure.[60] It has found widespread application as fluoride abstractor in the synthesis of highly reactive cations and was one of the key chemicals for the development of carbocation chemistry (see also section 1.4.2). A limitation is its high oxidation potential, which can lead to unwanted side reactions. A theoretical work revealed the increased Lewis acidity of $[SbF_5]_n$ oligomers (n = 2, 3, 4) and therefore concentrated solutions of SbF_5 can be considered as Lewis superacids.[61]

Boron trihalides BX_3 (X = F, Cl, Br) are quintessential Lewis acids and are used as textbook models for explaining Lewis acidity.[62] They are not considered as Lewis superacids as they do not surpass the acidty of SbF_5, as shown by the lower FIA values of BF_3 (346 kJ mol^{-1}), BCl_3 (404 kJ mol^{-1}) and BBr_3 (428 kJ mol^{-1}) compared to SbF_5 (496 kJ mol^{-1}).[59] Nevertheless, there are ways to enhance the acidity of three-coordinate boron acids, mainly by substituting the halide ligands with more electronegative or sterically demanding groups. For example, $B(CF_3)_3$, possesses a FIA of 556 kJ mol^{-1} as determined by quantum-chemical calculations.[59] While the uncoordinated $B(CF_3)_3$ still remains elusive due to the thermodynamically favored α-fluoride elimination, several adduct-stabilized compounds have been obtained.[63] These include stable nitrile complexes as well as reactive carbonyl adducts.[64,65] Interestingly, the carbonyl compound is formed by solvolysis of a single CF_3 ligand of $K[B(CF_3)_4]$ in concentrated H_2SO_4. The closely related carbonyl adducts of $B(C_2F_5)_3$ and $B(C_3F_7)_3$ were also reported in the literature but showed a similar instability.[66] More stable derivatives are accessible by using fluorinated aryl substituents. While the most famous representative $B(C_6F_5)_3$ does not display superacidic behavior in terms of fluoride ion affinity (448 kJ mol^{-1}), its high hydride ion affinity makes it a widely used soft Lewis acid. This

chemically stable compound is synthesized in large quantities by reacting boron trihalides with $Li(C_6F_5)$ or analogue Grignard reagents[67] and finds widespread application as co-catalyst for polymerization reactions, classical organic Lewis acid catalysis and as component of frustrated Lewis pairs.[68–72] By *para*-fluoride substitution with CF_3 groups, the even stronger derivative tris(*p*-perfluorotolyl)borane $B(p\text{-}(CF_3)C_6F_4)_3$ is accessible and its reported catalytic reactivities further supports its high acidity.[73]

A different electron-withdrawing ligand is the trifluoromethanesulfonate $[OSO_2CF_3]^-$ group, abbreviated as *triflate* OTf, which gave access to the Lewis superacids $B(OTf)_3$, $Al(OTf)_3$ and $Si(OTf)_4$ (see Figure 3 and Figure 5). The boron derivate $B(OTf)_3$ was reported in 1977 and synthesized by treating BCl_3 with $HOSO_2CF_3$.[74] The compound is a monomeric species, which is volatile and stable up to 100 °C. It is easily soluble in weakly coordinating solvents such as CH_2Cl_2.[75] Furthermore, it was successfully applied as catalyst for Friedel-Crafts reactions,[76] in the preparation of $XeOTf_2$[77] and in the synthesis of the supersilylating reagent $Me_3SiB(OTf)_4$.[78] In contrast, the higher isostructural homologue $Al(OTf)_3$ oligomerizes, its reactivity being thereby reduced.[76] Nevertheless, it was successfully used as co-catalyst in organic reactions, e.g. etherifications,[79,80] the synthesis of dimethoxymethane[81] and aminolysis of epoxides.[82] Recently, the multigram synthesis of the Lewis superacid $Si(OTf)_4$ starting from SiI_4 and equimolar amounts of AgOTf was reported.[83] It was shown that $Si(OTf)_4$ reacts with soft Lewis bases such as isocyanides, thioethers and carbonyls forming adduct-complexes, while reactions with CPh_3Cl lead to C–Cl cleavage and subsequent chloride/triflate exchange.

Even stronger Lewis acids are accessible by introduction of the pentafluoroorthotellurate $[OTeF_5]^-$ group, also abbreviated as *teflate*. This class of ligand is known for its strong electron-withdrawing properties, which are comparable to those of fluorine, but being sterically more demanding as described in Section 1.2. Several Lewis acids based on teflates have been already reported, such as $B(OTeF_5)_3$, $As(OTeF_5)_5$ and more recently $Al(OTeF_5)_3$, which possess exceptionally high FIA values (see Figure 2). In fact, the compound $Sb(OTeF_5)_5$ is assumed to be one of the strongest possible neutral Lewis acids, yet its synthetic preparation as pristine species or solvent adduct remains a challenge.[40,84] Similar to the triflate analogue, $B(OTeF_5)_3$ is a monomeric, sublimable compound and is prepared by reacting BCl_3 with teflic acid.[41] So far, it was mainly used as a teflate-transfer reagent, which led to the isolation of $As(OTeF_5)_5$,[40] $Sb(OTeF_5)_3$[40] and $Xe(OTeF_5)_n$ (n = 4,6).[50,85] Different synthetic approaches for the synthesis of the five-fold coordinated $As(OTeF_5)_5$ are reported in literature and it is expected to show a remarkable acidity.[40,59,86] Interestingly, only one report shows the usage of $As(OTeF_5)_5$ as a reactant for the synthesis of the arsenium cations $AsCl_3^+$ and $AsBr_3^+$.[87] More recently, the preparation of the aluminum analogue $[Al(OTeF_5)_3]_2$ based on the reaction of $AlEt_3$ and $HOTeF_5$ in *n*-pentane was reported. A vibrational spectroscopy analysis indicated the dimerization of this compound in the solid state and revealed a high Lewis acidity proven by the strong blue-shift of the C≡N stretching mode of its acetonitrile adduct.[88]

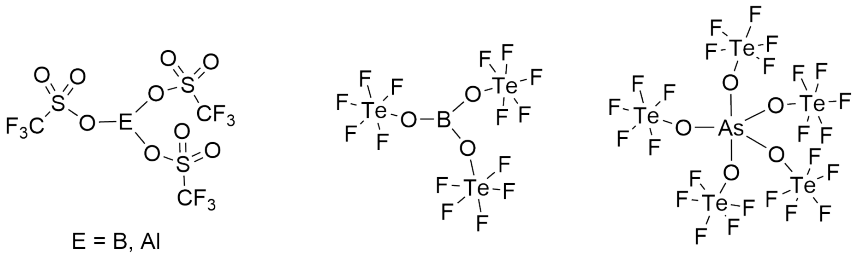

Figure 3. Lewis structures of $E(OSO_2CF_3)_3$ (E = B, Al), $B(OTeF_5)_3$ and $As(OTeF_5)_5$.[40,41,74,76]

A fruitful approach in the design of new Lewis superacids is the combination of an aluminum center with perfluorinated aryl, alkoxy and aryloxy ligands, leading to a variety of new compounds (see Figure 4). Compared to boron, aluminum is a more electropositive element and the lower reorganization energy of aluminum Lewis acids often results in better acceptor properties.[58] Consequently, the compound $Al(C_6F_5)_3$ shows a drastically increased Lewis acidity (FIA = 544 kJ mol^{-1}) when compared to the boron derivative $B(C_6F_5)_3$ (FIA = 448 kJ mol^{-1}).[59] The compound $Al(C_6F_5)_3$ is able to form adduct complexes with very weak basic donors, such as toluene or benzene,[89] is prone to hydrolysis[90] and reacts with chlorine-containing solvents such as CH_2Cl_2.[91] Attempts to obtain a solvent-free form of the acid revealed its shock- and temperature-sensitive nature, which eventually can lead to explosions.[92] The first preparation was achieved as the THF adduct by reacting $AlClMe_2$ and C_6F_5Li in THF.[93] Later, with the ligand exchange reaction of $AlMe_3$ with $B(C_6F_5)_3$ in arene solvents a more convenient route was reported.[89] In 2016, the first crystallographic characterization of the solvent-free compound was published, revealing the intermolecular stabilization of the Lewis acidic Al center via *ortho*-F bridging.[94] Furthermore, this compound found application in frustrated Lewis-pair chemistry and as catalyst for alkene polymerization, cross-couplings, hydrosilylation and hydrodefluorination.[95–99] Recently, partially fluorinated triaryl alanes with Lewis superacidic behavior have been reported and effectively applied in catalytic hydroboration reactions.[100]

The substitution of phenyl groups with perfluorphenolato ligands also leads to superacidic Lewis acids.[59] The compound $Al(OC_6F_5)_3$ exists as dimeric structure in the solid state, as proven by single-crystal X-ray diffraction, and was used as catalyst for polymerization reactions.[101] An influential investigation on aluminum-based Lewis acids has been done by the group of Krossing with their reports on perfluoroalkoxy derivatives, such as $Al\{OC(CF_3)_3\}_3$. This compound was first obtained as solvent-stabilized fluorobenzene adduct $[Al\{OC(CF_3)_3\}_3(PhF)]$.[56] Later, different solvent-stabilized adducts with SO_2 and *o*-DFB were obtained.[102] The solvent-free substance was also reported, but is unstable at room temperature due to an intramolecular fluoride abstraction leading to fluoride-bridged dimers and trimers under epoxide elimination.[102] A fluoride-bridged adduct with Me_3SiF was prepared, which either reacts as fluoride abstractor with hard Lewis bases or as silylating reagent with softer bases.[103] Additionally, this silyl fluoride adduct gives synthetic access to the fluoride-bridged weakly coordinating anion $[\{(CF_3)_3CO\}_3Al–F–Al\{OC(CF_3)_3\}_3]^-$.[104] The analogue chloride-bridged adduct $Me_3Si–Cl–Al\{OC(CF_3)_3\}_3$ is only stable at temperatures below 0 °C.[105] Other applications of $Al\{OC(CF_3)_3\}_3$ include its usage as component in a binary Brønsted superacid[106,107] and its role as reactant for the preparation of phosphino-phosphonium cations.[108]

Recently, two new aluminum Lewis acids were introduced, namely $Al\{OC(C_6F_5)_3\}_3$ and $Al\{N(C_6F_5)_2\}_3$.[109,110] Both Al centers are sterically well-shielded by the bulky tritylalcoholate and amide ligands, which allows the isolation of the solvent-free, room temperature stable acids as monomers. Both acids show similar FIA values ($Al\{OC(C_6F_5)_3\}_3$: 539 kJ mol^{-1}; $Al\{N(C_6F_5)_2\}_3$: 541 kJ mol^{-1}) and their acidity was further gauged by the Gutmann-Beckett method and a competitive fluoride abstraction from anionic $[SbF_6]^-$. Furthermore, for both aluminum acids several neutral solvent adducts and anionic halide complexes were reported.[110,111] An exceptionally high fluoride ion affinity was calculated for an aluminum Lewis acid based on perfluoropyridinoxy ligands $Al(OC_5F_4N)_3$ (FIA = 595 kJ mol^{-1}). Attempts to prepare its neat form by reacting $AlEt_3$ and 3.1 equivalents of HOC_5F_4N resulted in the formation of an insoluble oligomerization product. Nevertheless, addition of strongly donating solvents like acetonitrile and diethyl ether lead to soluble dimeric adducts.[112]

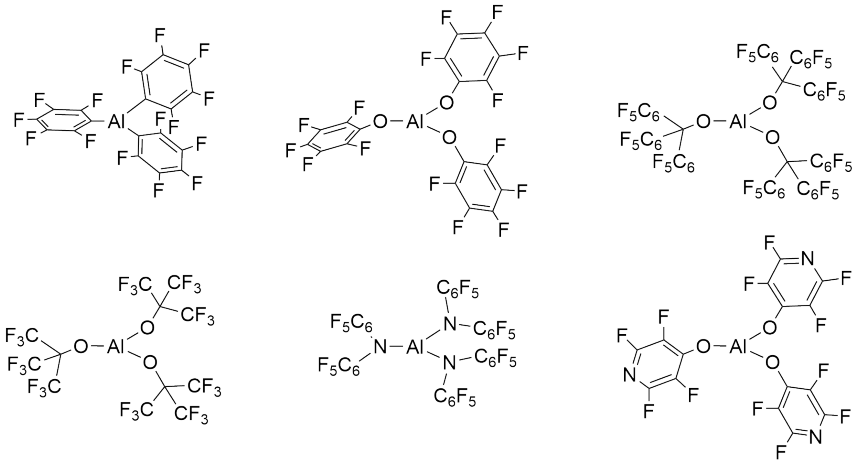

Figure 4. Lewis structures of $Al(C_6F_5)_3$, $Al(OC_6F_5)_3$, $Al\{OC(C_6F_5)_3\}_3$, $Al\{OC(CF_3)_3\}_3$, $Al\{N(C_6F_5)_2\}_3$ and $Al(OC_5F_4N)_3$.[94,101,102,109,110,112]

A recently emerging class of Lewis superacids is based on perhalogenated catecholato ligands $[o\text{-}C_6X_4O_2]^{2-}$ (X = F, Cl, Br, CF_3), also abbreviated as $[cat^X]^{2-}$ (see Figure 5). The neutral bis(perhalocatecholato)silanes $Si(cat^X)_2$ (X = F, Cl, Br) have been prepared by the reaction of the corresponding tetrahalocatechol and $HSiCl_3$ in MeCN and yielded the acetonitrile adducts of these Lewis acids.[113–115] These adducts are available on a multi-gram scale and were structurally characterized. While the bis(perfluorocatecholato)silane $Si(cat^F)_2$ only displays a mild Lewis acidty, the perchloro and perbromo derivatives can be classified as Lewis superacids. The increase in Lewis acidity going from $Si(cat^F)_2$ to $Si(cat^{Br})_2$ can be rationalized by the decrease of π back-donation from the halogen lone pairs to the phenyl rings, resulting in a more effective electron-withdrawal by the chloride and bromide substituents. The compounds $Si(cat^X)_2$ (X=F, Cl, Br) successfully catalysed the hydrodefluorination of 1-fluoroadamantane.[115] Nevertheless, their applicability is limited due to the low solubility and thereby reduced catalytic activity.[114] Attempts to obtain the solvent-free form indicated the oligomerization of these bis(perhalocatecholato)silanes and led in the case of $Si(cat^F)_2$ to the formation of macrocycles.[116] The reactivity of these oligomerized silanes is still not completely quenched. For example, polymeric $[Si(cat^{Cl})_2]_n$ was used for the formation of hypercoordinated silicates by reaction with Lewis bases such as halides, acetates and triflates.[117] By introducing a pertrifluoromethylated derivative $Si(cat^{CF_3})_2$, a more soluble compound became accessible.[118] Additionally, it possesses a very high fluoride ion affinity (584 kJ mol^{-1}) and is used for various deoxygenation and carbonyl-olefin methathesis reactions. So far, the solvent-free $Si(cat^{CF_3})_2$ is not available due to adduct complex formation even with weak bases such as disiloxanes. Combining catecholato ligands with germanium as metal center gives access to the water-tolerant Lewis superacid $Ge(cat^{Cl})_2$.[119] Its facile preparation by treatment of germanium oxide GeO_2 with tetrachlorocatechol in water allows a broad applicability. The species was characterized as water and acetonitrile adducts. In aprotic donor solvents $Ge(cat^{Cl})_2$ displays a reactivity as Lewis acid catalyst, but in protic solvents $Ge(cat^{Cl})_2$ gives access to a strong Brønsted acid reactivity.

In 2022, Inoue and co-workers reported the preparation of a perfluorinated bispinacolato silane $Si(pin^F)_2$ (see Figure 5).[120] In contrast to the bis(catecholato)silanes, the perfluoropinacol ligand increases the solubility of the resulting Lewis acid. The compound was characterized as acetonitrile adduct by vibrational and NMR spectrosopy, as well as by single-crystal X-ray diffraction. The FIA value of $Si(pin^F)_2$ does not

surpass the FIA of SbF_5, still the experimental fluoride abstraction from $AgSbF_6$ is observed. Besides its catalytic activity in hydrodefluorinaton reactions, $Si(pin^F)_2$ also successfully abstracts a fluoride from Et_3SiF.

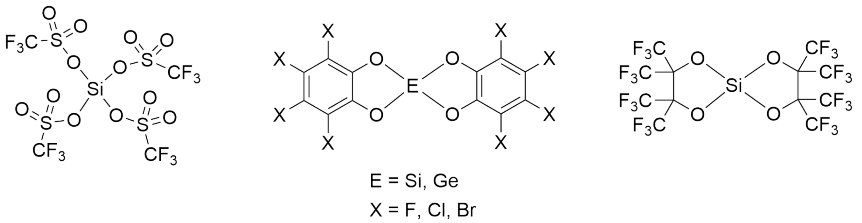

Figure 5. Lewis structures of $Si(OSO_2CF_3)_4$, $E(cat^X)_2$ (E = Si, Ge; X = F, Cl, Br) and $Si(pin^F)_2$.[83,114,115,118–120]

Besides the presented main-group Lewis acids, there are also several transition-metal Lewis acids known.[121,122] Lewis superacidic candidates are mainly metal pentafluorides of the type MF_5 (M = Ru, Rh, Os, Ir, Pt, Au) as quantum-chemical calculations have shown.[123,124] Nevertheless, besides they reactivity as Lewis acids, these transition-metal complexes often possess an even stronger reactivity as oxidizers. Therefore, their synthetic use as Lewis acids has been limited so far.

1.3.2. Cationic Lewis Superacids

Cationic Lewis superacids (see Figure 6) can be classified as a distinct branch in the field of Lewis acid chemistry. As already mentioned, a direct comparison with neutral Lewis acids based on theoretical methods such as FIA or GEI might be misleading, because electrostatic attraction and charge neutralization may result in extremely high values and consequently overestimate the Lewis acidity. The usage of a solvent-model can counteract these effects and lead to an appropriate dampening of the ion affinities of cationic LSAs. Usually, a highly reactive cation needs to be stabilized by a robust counterion. So called weakly coordinating anions are generally good candidates and will be addressed in a later chapter (see Section 1.6). In the current section, the most important representatives of cationic Lewis superacids and their properties are discussed.

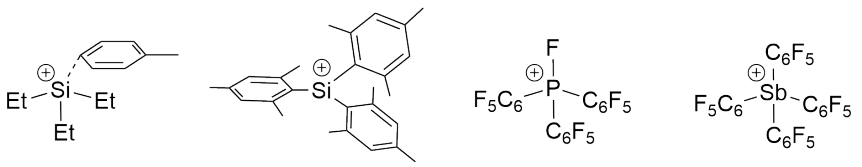

Figure 6. Lewis structures of $[Et_3Si(\eta^1\text{-}C_7H_8)]^+$, $[Mes_3Si]^+$, $[(C_6F_5)_3PF]^+$ and $[(C_6F_5)_4Sb]^+$.[125–128]

A highly important class of cationic Lewis superacids are trivalent silylium ions $[SiR_3]^+$ (R = alkyl, aryl). Compared to their carbon congeners, trivalent silylium derivatives show a higher electrophilicity. In fact, strong interaction of $[SiR_3]^+$ with weak donor solvents and counterions are common. This even led to a debate, if such cations can exist in a "free", non-coordinated form in the condensed phase.[129] Finally, the crystallographic characterization of non-coordinated $[Mes_3Si][HCB_{11}Me_5Br_6]$ in the solid state was reported in 2002.[126] Hereby, a combination of an appropriate weakly coordinating anion, non-nucleophilic solvent and sterically demanding substituents at the Si center were the key to success. Aside this fringe

case of a truly free silylium cation, a range of different Lewis acid-base adducts were already known. After the pioneering work by Corey, who introduced a synthetic access to silylium cations by treatment of silanes with the hydride acceptor $[CPh_3]^+$,[130] the isolation of arene-coordinated $[Et_3Si(toluene)][B(C_6F_5)_4]$ and the contact ion pair $[i\text{-}Pr_3Si][HCB_{11}H_5Br_6]$ were reported.[125,131] Besides the stabilization of these cations by solvent molecules and counterions, a viable approach is the intramolecular stabilization. Remarkable examples are ferrocene-stabilized silylium ions,[132] hydrogen-bridged bis(silyl)cations[133] and π arene-stabilized silylium cations.[134,135] A comprehensive review covering the rich chemistry of silylium ions was recently published.[136] While ^{29}Si NMR spectroscopy is a useful tool to determine the silylium ion character and gives spectroscopic insights into possible coordination phenomena, it does not necessarily correlate with the Lewis acidity of these cations. A more promising approach is the aforementioned Gutmann-Beckett method. In Figure 7, a ranking based on the $\Delta\delta^{31}P$ shift difference of different silylium cations together with other Lewis acids is depicted.[25] This trend is also correlating with the calculated FIA values for the differently substituted sililyium cations. Following up on the understanding of their isolation, silylium cations were successfully applied in Lewis acid catalysis, e.g. for bond-activation chemistry and rearrangement reactions.[137] A special attention should be paid to their capability for C–F bond activation, which allowed hydrodefluorination reactions on unreactive perfluoroalkyl groups, which will be discussed in section 1.4.[138]

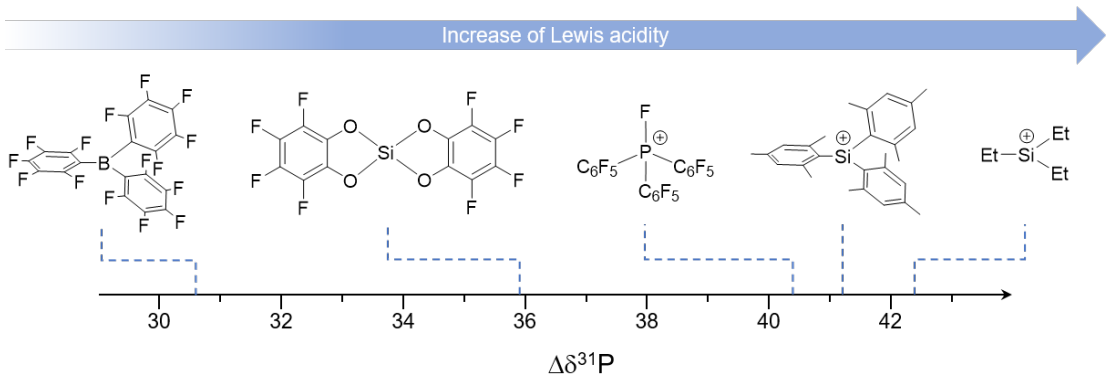

Figure 7. Gutmann-Beckett chemical shift differences of different Lewis acid with Et_3PO.[25]

Neutral phosphorus(V) Lewis acids such as PF_5 and Wittig reagents are well-described in literature, but their acidity does not allow a classification as Lewis superacids (e.g. FIA (PF_5) = 384 kJ mol^{-1}).[59] In 2013, the cationic phosphonium cation $[(C_6F_5)_3PF]^+$ was reported, showing a remarkable reactivity as catalyst for hydrodefluorination reactions, which is usually only achieved by strong Lewis acids.[127] Interestingly, the Lewis acidity stems from the energetically low-lying σ^* orbital of the P–F bond. A limitation is their incompatibility with water. A workaround was found by substituting the F atom attached to the phosphonium center with a CF_3 group. Nevertheless, the air and water stability of the $[(C_6F_5)_3PCF_3]^+$comes with the expense of a decreased Lewis acidity.[139] Recently, an air-stable derivative of the higher homologue antimony(V) was reported, namely the $[Sb(C_6F_5)_4]^+$ ion (see Figure 6).[128] This cation was able to abstract a fluoride from $[SbF_6]^-$ and could be further used for hydrodefluorination reactions.

1.3.3. Solid Lewis Superacids

Besides the molecular Lewis superacids, also solid materials with superacidic behavior are known. The reactivity of such solid materials can be classified in Lewis and Brønsted acidic behavior and is determined by the chemical composition and the surface structure of these materials. Since such reactive sites on the solid surface can vary and usually are heterogeneous, quantum-chemical methods for scaling the Lewis acidity of these surfaces is complicated. Therefore, most experimental methods utilize adsorption reactions of probe molecules, which then can be further analyzed. A typical example is the aforementioned method based on aceonitrile adsorption followed by analysis of the C≡N stretching mode. The obtained shift-difference can be compared to molecular Lewis acids to obtain a meaningful correlation. Similarly, solid Lewis superacids can then be classified as solid acids which induce a higher blue-shift of the C≡N stretching mode compared to SbF_5.[140] A different commonly used method is the adsorption and temperature-programmed desorption (TPD) of volatile bases such as NH_3 and pyridine, which gives insights in the type and strength of the acidic surface sites. Also, solid-state NMR spectroscopy is a useful tool for estimating the acidity of solid materials. While metal oxides are thoroughly investigated, they tend to be mostly Brønsted acidic in nature and possess Lewis acidic character only as side reactivity. But highly Lewis acidic solid materials are accessible, e.g. based on aluminum halides. While AlF_3 in its most-stable crystalline phase α-AlF_3 does not show any significant Lewis acidity, the surface structure can be altered to obtain highly acidic phases.[140] Most prominent examples are aluminum chlorofluoride (ACF, $AlCl_xF_{3-x}(x = 0.3–0.05)$) and *high surface*-$AlF_3$ (*hs*-AlF_3), which both exhibit a Lewis acidity comparable to SbF_5 and can be considered as solid Lewis superacids. Aluminum chlorofluoride is obtained by treating $AlCl_3$ suspended in CCl_4 with the fluorinating reagent CCl_3F, which leads to an amorphous powder.[141] *Hs*-AlF_3 is synthesized by a sol-gel process, starting from $Al(O\textit{i}\text{-}Pr)_3$ and HF, followed by a fluorination with CF_2Cl_2 or $CHClF_2$.[142] The high Lewis acidity of these kind of materials stems from the distortion of the bulk structure either by chloride or isopropoxide ligands. In 2022, a new type of solid Lewis superacid was reported, based on the reaction of the fluorobenzene adduct $[(PhF)Al(OC(CF_3)_3)_3)]$ with partially dehydroxylated silica (Aerosil $SiO_{2–700}$).[143] The well-defined material of the type $[\equiv SiOAl\{OC(CF_3\}_3)_2(O(Si\equiv)_2)]$ possesses a higher FIA than the molecular Lewis acid $[(PhF)Al\{OC(CF_3)_3\}_3)]$ and was used in the methide abstraction of $Cp_2Zr(CH_3)_2$. Solid Lewis superacids are especially promising for large scale processes, since they can be applied in heterogeneous catalysis.

1.4. Applications of Lewis Superacids

1.4.1. Catalysis

A steadily growing field of application for Lewis superacids is their use in catalysis. This is especially true for silylium cations. Their importance is broadly covered by recent reviews and here only the most groundbreaking results will be briefly discussed.[136,137,144] As described in the previous chapter, the isolation of a "free" trivalent silylium cation was a challenge, but after its accomplishment the high affinity for nucleophiles of these cations could be further utilized. An important contribution in this field was given by Ozerov *et al.*, who used silylium cations for the activation of C–F bonds by performing a hydrodefluorination reaction (see Figure 8).[145] This is remarkable, since the C–F bond is rather strong and their selective activation and transformation under mild conditions is an active field of research.[146]

For the initial step a silylium ion must be generated. For this procedure most commonly the tritylium

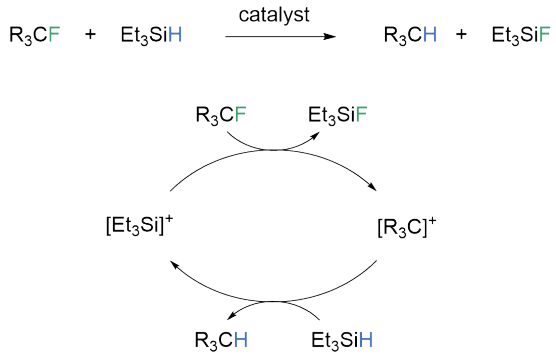

Figure 8. Reaction equation of the silylium-catalyzed hydrodefluorination and its established mechanism.

cation $[C(C_6H_5)_3]^+$ in combination with a suitable WCA, e.g. $[B(C_6F_5)_4]^-$, is used as hydride abstraction reagent on a hydrosilane such as Et_3SiH. The so-formed silylium cation cleaves the C–F bond of the substrate, forming a carbocation and the silyl fluoride Et_3SiF. In the last step, the carbocation reacts with another equivalent of hydrosilane, thereby regenerating the silylium species and forming the C–H bond. The counterion plays a crucial role, because the efficiency of the catalytic reaction is dependent on the stability of the counterion towards highly reactive silylium ions.[145,147] Using this reaction route in conjunction with the very robust carborane anion $[HCB_{11}H_5Cl_6]^-$ the hydrodefluorination of highly fluorinated alkyl compounds such as *n*-$C_4F_9C_2H_5$ with high turnover numbers was possible.[138]

Hydrodefluorination reactions have also been achieved with mixtures of Lewis superacids and hydrosilanes instead of preforming a silylium cation with tritylium cations. Chen and co-workers reported the efficient hydrodefluorination of CPh_3F with $Et_3Si–H–Al(C_6F_5)_3$ and stochiometric amounts of hydrosilane.[95] In their proposed mechanism, the hydride-bridged adduct acts as precatalyst, forming the fluoride-bridged $Et_3Si–F–Al(C_6F_5)_3$ after the first C–F cleavage, which then acts as active catalyst. In a similar fashion, perhalogenated biscatecholato and bispinacolato silanes can promote the hydrodefluorination of 1-fluoroadamantane in the presence of hydrosilanes.[115,120] Furthermore, $Al(C_6F_5)_3$ was used for the alkynyldefluorination of aliphatic C–F bonds, by adding the Lewis acid to a mixture of a C–F bond containing substrate and trimethylsilyl acetylides.[96]

Lewis superacids have been successfully employed in polymerization reactions. The adduct $Me_3Si–F–Al\{OC(CF_3)_3\}_3$ is an efficient initiator for isobutene polymerization. Similarly, $Al(C_6F_5)_3$ acts as coinitiator in the cationic polymerization of isobutylene in aqueous media.[148] Along with $Al(OC_6F_5)_3$, these acids can also be used for ring-opening polymerizations.[91] Besides the previous discussed C–F activation and polymerization reactions, molecular Lewis superacids can also be used for classical Lewis-acid catalysis such as Friedel-Crafts-type reactions,[76,149,150] hydrosilylation of olefins,[95] Diels-Alder reactions,[151,152] aldol condensations[151,153] or deoxyfluorination reactions.[118,154]

For heterogeneous catalysis, the solid Lewis superacid ACF (see subsection 1.3.3) can be utilized together with hydrosilanes to achieve hydrodefluorination reactions of fluorinated methanes and fluoroolefins such as the refrigerants 2,3,3,3-tetrafluoropropene and 1,3,3,3-tetrafluoropropene.[155,156] Hereby, upon loading of ACF with trimethylsilane, a silylium-like species is formed on the Lewis acid surface, that is then promoting the hydrodefluorination.[155] These silylium-like species were analyzed via solid-state MAS NMR spectroscopy. When germanes instead of silanes are employed, a hydrogermylation of the fluoroolefins is observed.[156] In 2022, also the chlorodefluorination of fluoromethane and fluoroolefins with trimethylsilyl

chloride in the presence of ACF was reported.[157] Another prominent example for Lewis superacid-based heterogenous catalysis is *hs*-AlF_3, which acts as catalyst for selective dehydrofluorination reactions. This was shown with 3-chloro-1,1,1,3-tetrafluorobutane, in which the usage of *hs*-AlF_3 as catalyst yielded >99 % conversion with a selectivity towards dehydrofluorination of 100 %.[158] In 2019, an analogue reactivity was also shown for ACF.[159] In order to form dehydrochlorination products, the presence of a silane is again necessary.[160] Furthermore, ACF can be employed as heterogeneous catalyst for the hydroarylation of olefins under very mild reaction conditions. This even holds true for highly fluorinated arenes such as 1,3,5-triflurobenzene and pentafluorobenzene.[161]

1.4.2. Reactive Cation Synthesis

A fundamental field of research is the generation of highly reactive or unstable molecules, which have remained elusive for a long time and can act as model compounds to further broaden the understanding of relevant concepts in chemistry. In the current section, some remarkable examples synthesized by the use of LSAs are presented. Please note that silylium cations are omitted since they are already discussed in depth in a previous section.

One of the biggest milestones in this regard has been the area of carbocation chemistry.[162] The first stable carbocation was the tritylium ion $[C(C_6H_5)_3]^+$, which was obtained by dissolution of the chloride $C(C_6H_5)_3Cl$ in concentrated sulfuric acid.[163] Nowadays, the tritylium ion is mainly applied in synthetic chemistry as hydride abstraction reagent.[136,164] With the goal in mind to obtain long-lived alkylium ions, Olah *et al.* understood the crucial role of Brønsted and Lewis superacids in order to synthesize such cations. In the 70's and 80's, he reported an enormous number of carbocationic compounds and was honored with a Nobel Prize in 1994.[165] A remarkable breakthrough was the discussion about the existence about "non-classical" carbocations, i.e. cationic carbon centers, which have five or more bonding partners (carbonium ions) in contrast to the "classical" trivalent carbenium ions. An illustrative example of a "non-classical" carbocation is the norbornyl cation. It was accessible by the reaction of a halide norbornyl precursor with SbF_5, but only analyzed by NMR spectroscopy (see Figure 9).[166–168] Still, the nature of the norbornyl cation was long under discussion, since it could have been also described as a pair of rapidly equilibrating "classical" carbocations.[169,170] In 2013, the unambiguous proof of its "non-classical" character was given in form of a crystal structure at 40 K, which was obtained by the reaction of norbornyl bromide with aluminum bromide in CH_2Br_2.[171]

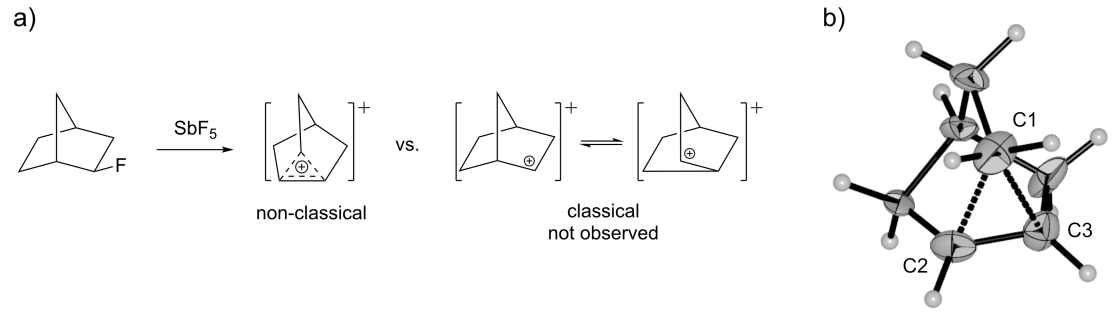

Figure 9. a) First synthesis of the non-classical norbornyl carbonium ion. b) Molecular structure in the solid state of the norbornyl cation. The counterion has been omitted for clarity.[172]

A different class of elusive cations are halonium ions. These type of compounds are defined as ions of the form $[R_2X]^+$, where X can be any halogen.[36] The isolation of these types of cations marked an important step towards the understanding of Friedel-Crafts-type reaction mechanisms. Halonium ions can further be divided into organic (adjacent atoms R are carbon atoms) and inorganic representatives (adjacent atoms R are non-carbon atoms). A large variety of inorganic halonium ions is accessible by the reaction with strong Lewis acids such as SbF_5. Prominent examples are interhalonium ions of the type $[XF_n]^+$ (X = Cl, Br, I; n = 2, 4, 6).[173–178] Organic halonium ions on the other hand can be synthesized by reacting RX (R = alkyl, X = Cl, Br, I) with SbF_5 in low-nucleophilic solvents such as SO_2 or SO_2ClF to obtain $[R_2X][SbF_5X]$ via halogen abstraction by the Lewis acid.[179,180] These organic derivatives can be further used as strong alkylation reagents.[179] Organic fluoronium ions were so far only detected by spectroscopic methods (see Figure 10). These include a three-membered cyclic fluoronium ion as well as a F-protonated fluorobenzene, while Gabbaï and co-workers reported a rapidly equilibrating fluoronium ion which they observed via NMR spectroscopy.[181–183] Lectka *et al.* succeeded in detecting a symmetrical C–F–C fluoronium ion in solution by NMR spectroscopy, which was controversially discussed in literature.[184–187]

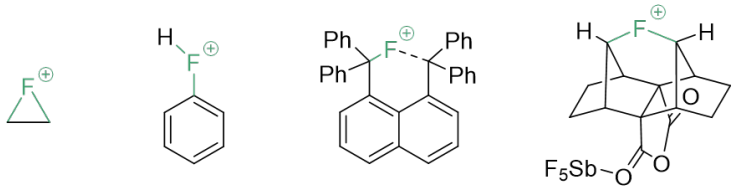

Figure 10. Lewis structures of spectroscopically characterized C–F–C fluoronium ions.[181–183,186]

Finally, in the field of noble-gas chemistry, cations containing such elements have been mainly generated with the help of Lewis superacids. The first synthesis of a noble gas cation was carried out by Bartlett in 1966 with the reaction of xenon gas, fluorine and the strong Lewis acid PtF_5, which resulted in the isolation of crystalline $[XeF_5][PtF_6]$.[188,189] The lower oxdiation state analogues $[XeF]^+$[190,191] and $[Xe_2F_3]^+$[190,192] are accessible by reaction of the corresponding neutral xenon fluoride with SbF_5. Following a similar route, the first krypton cations $[KrF]^+$ and $[Kr_2F_3]^+$ have been isolated.[193] Furthermore, by using AuF_5 on XeF_6, a fluoride-bridged xenononium cation $[Xe_2F_{11}]^+$ was obtained.[194] Despite the fluorine-based cationic xenon and krypton species, no heavier halogen could be implemented in such compounds. Only in the case of Xe(II) the pentafluoroorthotellurate analogue $[Xe(OTeF_5)][Sb(OTeF_5)_6]$ has been reported.[195]

1.4.3. Frustrated Lewis Pairs

In the thriving field of frustrated Lewis pair (FLP) chemistry, Lewis superacids have already found use.[72] In general, the concept of frustrated Lewis pairs is based on acid-base combinations, which thermodynamically favor an adduct formation but are sterically prevented from doing so. This results in "frustration" of the Lewis pair (see Figure 11). This "frustration" can be used for the controlled activation and heterolysis of small molecules, such as H_2, CO_2, SO_2, olefins or alkynes.[196–200]

The reactivity derives from an unquenched acidity and basicity of the FLP that allows it to cooperatively act as an electron donor and acceptor.[201] Some exemplary reactions are shown in Figure 12 below. A well-known example for such an acid-base pair are the compounds $B(C_6F_5)_3$ and $P(t\text{-}Bu)_3$, which have been used for dihydrogen splitting.[202]

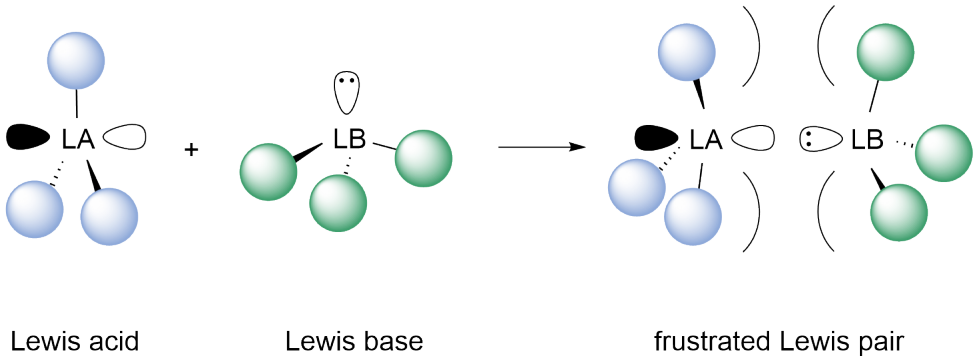

Figure 11. Model of a frustrated Lewis pair. The green and blue spheres represent sterically demanding substituents.

This chemistry is not limited to intermolecular FLPs, since there are also intramolecular representatives known, such as the aryl-bridged $(C_6H_2Me_3)P(C_6F_4)B(C_6F_5)_2$ (cf. Figure 12) or ethylene-linked $(Mes_2P)C_2H_4(B(C_6F_5)_2)$.[203,204]

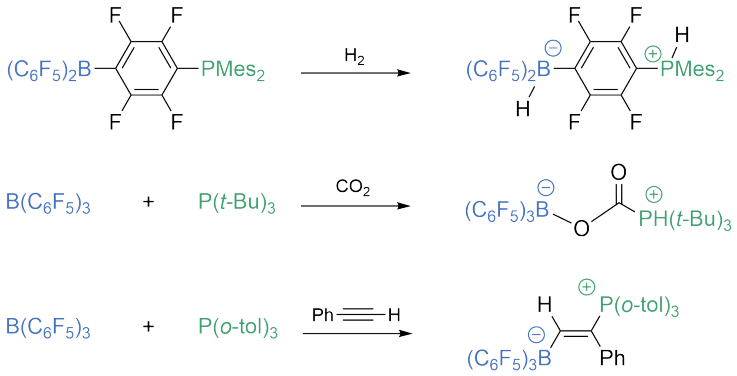

Figure 12. Exemplary reactions with frustrated Lewis pairs.

The in FLPs typically used $B(C_6F_5)_3$ can also be exchanged with the more acidic analogue $Al(C_6F_5)_3$. A recent theoretical study discusses the influence of these two Lewis acids on C–F bond activation of three different fluorobutanes. The aluminum-based FLP is thermodynamically more favored and shows a lower free energy barrier in all cases.[205] Also experimental applications of $Al(C_6F_5)_3$ as acid in an FLP were reported. In combination with phosphines PR_3 (R=*t*-Bu and Mes) they have been used for the activation of H_2 and subsequent hydride transfer to olefins as well as the C–H activation of isobutylene.[97,98] Furthermore, these FLPs form frustrated radical pairs $[R_3P\cdot][\cdot O(Al(C_6F_5)_3)_2]$ when reacted with N_2O.[99]

The activation of CO_2 with different FLPs consisting of phosphine bases and aluminum-based acids has been intensively studied. The system $PMes_3/AlX_3$ (X = Cl, Br, I) forms the complex $Mes_3PC(OAlX_3)_2$.[206] If an excess of CO_2 is used, the dissociation of the AlX_3 moiety is observed, yielding a mixture of $Mes_3PC(OAlX_2)_2OAlX_3$, $[Mes_3PX][AlX_4]$ and the elimination of CO. The sterical more demanding $Al(C_6F_5)_3$ in conjunction with P(*o*-tol)$_3$ forms the related complex (*o*-tol)$_3$PC(OAl$(C_6F_5)_3)_2$. The latter complex does not show any elimination of CO, instead it can be thermally transformed to the complex (*o*-tol)$_3$PC(O)OAl$(C_6F_5)_3$. A structural proof of this insertion product was shown with the closely related species (*o*-tol)$_3$PC(O)OAl$\{OC(CF_3)_3\}_3$.

Chen and co-workers studied a scope of different Lewis acid and base combinations for the Lewis pair polymerization of conjugated polar alkenes.[207] Herein, FLPs based on the Lewis acid $Al(C_6F_5)_3$ and sterically demanding phosphines or N-heterocyclic carbenes turned out to be most active and efficient. Furthermore, they isolated and structurally characterized phosphonium and imidazolium enolaluminate zwitterions and identified them as active species in the polymerization process supporting a bimolecular, activated-monomer propagation mechanism.[208]

An example for a silylium cation acting as a constituent of an FLP was reported by Müller and coworkers, who could show the capture of CO_2 by combining $P(t\text{-}Bu)_3$ and $[Si(C_6Me_5)_3][B(C_6F_5)_4]$.[209]

1.5. Brønsted Superacids

A well-accepted definition for Brønsted superacids was given by Gillespie, who stated that superacids are acidic media which exceed the acidity of 100 % sulfuric acid.[210,211] This definition was recently refined by Krossing and Leito, who distinguished between medium and molecular superacidity.[13,212] Medium superacidity is analogue to Gillespie's definition, but is further specified using a unified acidity scale.[12] Herein, a superacidic medium is one which has a greater absolute chemical potential of a proton in a given solvent S $\mu_{abs}(H^+, S)$ than a proton in 100 % H_2SO_4 with $\mu_{abs}(H^+, H_2SO_4(l))$.[213] Molecular superacidity, on the other hand, refers to neutral or ionic molecular acid, which is a stronger acid than H_2SO_4. This can either be determined by $pK_{a,S}$ values in a given medium in the condensed phase or via gas-phase acidities in the gas phase.[214,215] As mentioned above, there are several techniques for determining the acidity of Brønsted acids, while for highly acidic and non-aqueous media, the Hammett-acidity scale H_0 is the most common measure.[211,216] Classical examples for primary Brønsted superacids are triflic acid HSO_3CF_3, fluorosulfonic acid HSO_3F and anhydrous hydrogen fluoride *a*HF. Note, that in the case of *a*HF already traces of water can lead to a drastically diminished acidity.[217] In Figure 13, these acids are shown along their corresponding H_0 values of the Hammett-acidity function.[10] When these acids are coupled with strong Lewis acids, an extreme increase of the Brønsted acidity can be achieved. Such systems are known as binary or conjugate Brønsted superacids and the most prominent examples are "magic acid", a mixture of HSO_3F and SbF_5, or mixtures of HF and SbF_5.[10] These compounds paved the way for the field of carbocation chemistry, since the "stable-ion conditions" of such superacidic media allowed the observation of carbocations in solution.[165,218,219] In these binary acids, the Lewis acid forms a complex with the conjugate base of the Brønsted acid, forming a larger counterion and resulting in a higher ionization and thus a higher acidity of the Brønsted acid.[220] A drawback of these binary superacids are their strongly oxidizing nature or an unintended coordination of the employed Lewis acid as a competitive reaction besides the protonation.

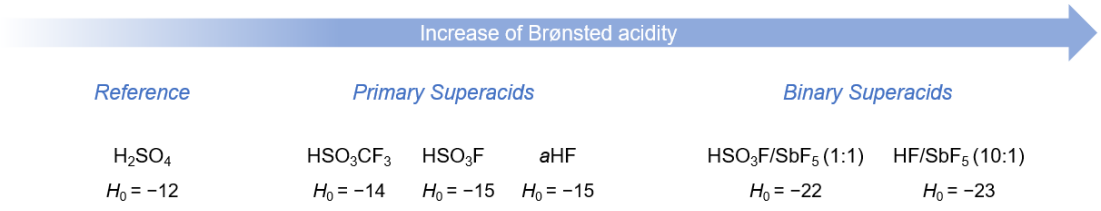

Figure 13. Overview of different Brønsted superacids.[10]

Modern Brønsted superacids often consist of a salt with an associated H^+ or protonated solvent molecule as cation and a weakly coordinating counterion. A widely used example is Brookhart's acid, which is comprised of protonated diethylether $[H(OEt_2)_2]^+$ and a WCA such as $[B(C_6F_5)_4]^-$, $[B(C_6H_3\text{–}3,5\text{–}(CF_3)_2)_4]^-$ or $[Al\{OC(CF_3\}_3)_4]^-$.[221–224] These acids can also be isolated as solids but are not as acidic as the binary Brønsted superacids HSO_3F/SbF_5 and HF/SbF_5. To increase the Brønsted acidity, either less basic solvents or solvent-free conditions are desired. In the case of the anion $[Al\{O(CF_3)_3\}_4]^-$, the "free" acid was reported and used to protonate mesitylene.[106] Brønsted acids based on the weakly coordinating carborane anions possess the general formula $H[HCB_{11}Y_5X_6]$ (Y = H, X; X = F, Cl, Br, I) and count towards the strongest accessible Brønsted superacids.[225] These compounds are capable to protonate extreme weak bases such as benzene, fullerene C_{60}, alkanes or CO_2.[226–230] Their chemical robustness and low nucleophilicity allows these transformation without unwanted side reactions or coordination of the anion. In the case of $H[HCB_{11}Cl_{11}]$, a molecular structure in the solid state was obtained, which revealed a polymeric, proton-bridged structure of this Brønsted acid.[231] In 2017, the synthesis of a Brønsted superacid based on aluminum pentafluoroorthotellurates was reported.[88] These acids are directly formed in solution by reacting $HOTeF_5$ with $AlEt_3$ in aromatic solvents such as benzene or *o*-DFB. Thereby, the weakly coordinating anion $[Al(OTeF_5)_4]^-$ alongside the protonated aryl is formed and can be directly used for further protonation reaction. For example, this Brønsted acidic system has been used for the protonation and characterization of white phosporus P_4 or the synthesis of the strong methylating reagent $[Me_2Cl][Al(OTeF_5)_4]$.[232,233] In Table 1, a strength ranking of different Brønsted superacids based on the protonation of mesityl oxide is given.

Table 1. Brønsted acidity ranking according to the protonation of mesityl oxide (see Figure 1).

Brønsted acid	$\Delta\delta$ (^{13}C) [ppm]
$H[Al(OTeF_5)_4]$	87.9[a]
$H[CHB_{11}Cl_{11}]$	84.0[b]
$H[CHB_{11}H_5Cl_6]$	83.8[b]
$H[CHB_{11}H_5Br_6]$	83.8[b]
$H[CHB_{11}H_5I_6]$	83.3[b]
HSO_3F	73.8[b]
HSO_3CF_3	72.9[b] (70.3[a])
$HN(SO_2CF_3)_2$	72.0[b]
H_2SO_4	64.3[b]
$HOTeF_5$	46.6[a]

[a]in *o*-DFB.[88] [b]in liquid SO_2.[226]

1.6. Weakly Coordinating Anions

Strongly interwoven with the research of Lewis and Brønsted superacids is the field of weakly coordinating anions (WCAs). These are typically univalent anions, whose charge is ideally delocalized over a large molecule. All nucleophilic and basic sites of the molecule should be sterically shielded in order to prevent interaction with electrophilic cations. Furthermore, the anion should possess a low polarizability and a high chemical robustness.[234] These properties make "pseudo-gas-phase conditions"[235] in solution approachable and renders this class of anions well suited for a range of applications in modern chemistry. Most prominently, WCAs are used for the stabilization, isolation and characterization of extremely reactive or labile cations. These range from highly oxidative cations such as XeF^+ to strong electrophiles like silylium cations (see Section 1.4.2), as well as weakly bound coordination complexes such as $[Ag(Cl_2)]^+$.[236]

Furthermore, WCAs are employed as important components for catalysis, room temperature ionic liquids and electrolytes.[237–241] The different classes of modern WCAs (cf. Figure 14) and their advantages and limitations will be briefly discussed in this section.

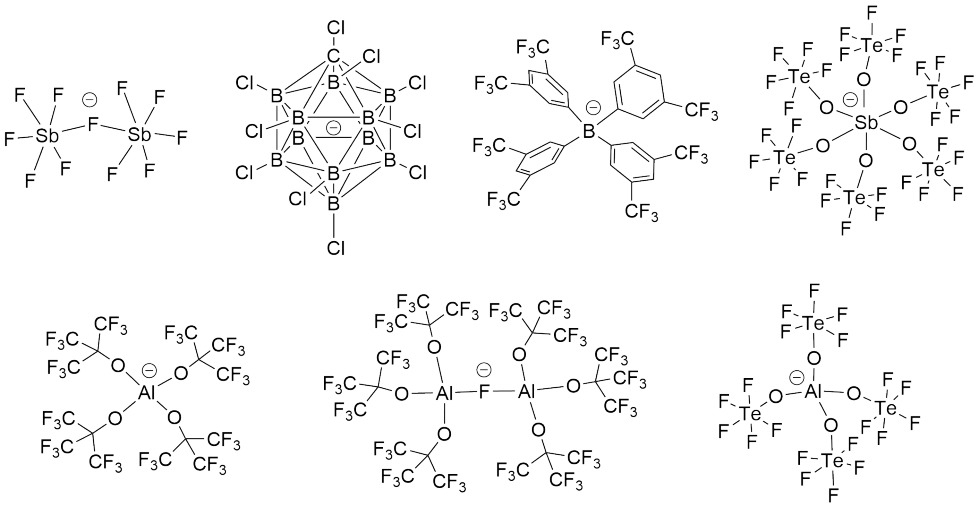

Figure 14. Lewis structures of different weakly coordinating anions: $[Sb_2F_{11}]^-$, $[CHB_{11}Cl_{11}]^-$ $[B(C_6H_3\text{–}3,5\text{–}(CF_3)_2)_4]^-$, $[Sb(OTeF_5)_6]^-$, $[Al\{OC(CF_3)_3\}_4]^-$, $[\{(CF_3)_3CO\}_3Al\text{–}F\text{–}Al\{OC(CF_3)_3\}_3]^-$, $[Al(OTeF_5)_4]^-$.

While the "classic" WCA $[SbF_6]^-$[242,243] was proven by single-crystal X-ray diffraction to display strong interactions with cations, its coordinating ability can be decreased by replacement with di-, tri or tetranuclear derivatives of the form $[Sb_nF_{5n+1}]^-$ (n = 2, 3, 4).[244–246] These anions can be handled in weakly basic solvents such as HF, SO_2ClF or SO_2 and are accessible directly from its Lewis acid SbF_5. They show a remarkable resistance against oxidation, as shown by the successful isolation of strong oxidizers such as $[XeF_5]^+$[247] or $[KrF]^+$,[193] polyhalonium ions $[Br_2]^+$[248] or $[Br_5]^+$[249] and the first gold-xenon complex $[Au(Xe)_4]^{2+}$.[250]

The class of fluorinated alkyl- and arylborate anions is based on the replacement of fluoride ligands in the anion $[BF_4]^-$ by partially fluorinated or perfluorinated alkyl or aryl substituents. Noteworthy and already well-investigated examples are the anions $[B(C_6F_5)_4]^-$[67] and $[B(C_6H_3\text{–}3,5\text{–}(CF_3)_2)_4]^-$,[251,252] also known as $BArF_{20}$ or $BArF_{24}$, which are both commercially available. These type of anions are useful for the stabilization of strong electrophiles and nowadays they are used as standard anions in the field of silylium ion catalysis.[144] Furthermore, these borate anions find application in olefin polymerization catalysis.[237,253] A drawback of this compound class is its instability towards strongly oxidizing compounds and its tendency for coordination via the phenyl rings, forming π-arene complexes with the metal cations.[254] This tendency can be diminished by the usage of perfluorinated aryl rings or alkyl-based ligands. The only homoleptical representative $[B(CF_3)_4]^-$ is accessible in good yields by the reaction of salts of the type $M[B(CN)_4]^-$ with ClF_3 in anhydrous HF.[255] More recently, a route utilizing $[NEt_3Me][ClF_4]$ and BF_3 to convert $[B(CN)_4]^-$ into a mixture of $[B(CF_3)_x(CN)_{4-x}]^-$ (x = 0, 1, 2, 3, 4) was reported.[256] These anions exhibits a high (electro)chemical robustness and promising properties in conducting salts for lithium ion batteries or as component in ionic liquids.[257] In 2013, a dendronized derivative of the borate anion was reported, which even reached nanometer-sized particles.[258] For the heavier homologue gallium, the synthesis of the weakly coordinating anion $[Ga(C_2F_5)_4]^-$ was reported in 2019 and more recently used as component

in ionic liquids.[259,260] Interestingly, salts of the analogue aluminum-based anion $[Al(C_2F_5)_4]^-$ are also accessible, but show a reduced stability when compared to the gallium derivatives.[261,262] Furthermore, larger fluoride-bridged anions of the type $F_m[M(C_6F_5)_3]_n^{m-}$ (M = Al, Ga; m = 1, 2; n = 1, 2, 3) were reported, which showed a remarkable activity when used as co-catalyst for olefin polymerization.[263,264]

A related class of WCAs are fluorinated alkoxy- or aryloxy aluminates. Besides numerous reported examples such as $[Al(OC_6F_5)_4]^-$[265] or $[Al\{OC(Ph)_2(CF_3)\}_4]^-$,[266] the most prominent representative is $[Al\{OC(CF_3)_3\}_4]^-$. This compound is easily accessible in a multi-gram scale by treatment of $LiAlH_4$ with the corresponding alcohol and a variety of useful precursors are available.[267] This anion possesses only a very low coordinative ability and allowed the isolation of weakly bound complexes such as $[Ag(P_4)_2]^+$,[268,269] $[Ag(X_2)]^+$ (X = Cl, Br, I)[236] or $[M(CO)_7]^+$ (M = Nb, Ta).[270] Furthermore, it is robust against highly electrophilic cations such as $[CI_3]^+$[271] and $[Si(C_6Me_5)_3]^+$.[272] Additionally, its performance as co-catalyst in polymerization or hydrogenation reactions is often superior than the aforementioned borate anions or traditionally used aluminoxanes.[273–275] The promising role of perfluoroalkoxy aluminates as components in ionic liquids was discussed in a review.[239] It is also possible to form the fluoride-bridged complex ion $[\{(CF_3)_3CO\}_3Al–F–Al\{OC(CF_3)_3\}_3]^-$ starting from the previously mentioned Lewis acid-base adduct $Me_3Si–F–Al\{OC(CF_3)_3\}_3$. This very bulky anion shows an even more decreased coordinative strength and an improved stability against electrophiles and was previously only known as a decomposition product of $[Al\{OC(CF_3)_3\}_4]^-$.[103,104,276] This fluoride-bridged anion allowed the isolation of a handful of fragile carbonyl transition metal complexes such as $[Cr(CO)_6]^+$,[277] $[Ni(CO)_4]^+$[278] or $[(Mes)Nb(CO)_4]^+$.[279]

Conceptually different is the class of polyhedral carborane anions. The archetypical anion $[HCB_{11}H_{11}]^-$ was first reported in 1986, already claimed as least coordinating anion,[280] while still being susceptible towards electrophilic substitution.[225] By replacing hydrogen atoms with methyl and halogen substituents, their properties in terms of stability, solubility and coordinative strength can be tuned, leading to a large variety of this compound class.[281–283] A drawback of carborane anions is that they can only be synthesized in milligram-scale batches during an expensive and time-consuming multi-step procedure.[284,285] Nevertheless, efforts were reported which aim to overcome this problem.[286] Carborane anions show remarkable properties in terms of chemical robustness towards strong electrophiles. With the anion $[HCB_{11}Me_5Br_6]^-$, the first isolation of a "free" silylium cation $[Si(Mes)_3]^+$ succeeded.[126] Furthermore, extremely strong solid-phase Brønsted acids such as $H[CHB_{11}F_{11}]$ or $H[CHB_{11}H_5Cl_6]$ are accessible (cf. Table 1). Closely related to this type of polyhedral anions are dodecarboranes $[B_{12}H_{12}]^{2-}$ and their halogenated derivatives.[287,288] These compounds are accessible in gram-scale quantities and despite them being two-fold negatively charged, dodecaboranes show similar properties then the carborane analogues.[289] For example, Brønsted superacids $H_2[B_{12}X_{12}]$ (X = Cl, Br) have been reported, which are able to protonate benzene.[290] Also, contact ion pairs of silylium cations such as $[Et_3Si]_2[B_{12}Cl_{12}]$ have been synthesized and applied to hydrodefluorination reactions.[291,292] To improve the solubility and reduce the coordinative strength, a substituent can be replaced by an ammonium group, resulting in single-charged derivatives of the type $[Me_3N–B_{12}X_{11}]^-$ (X=F, Cl).[293,294]

Another class of weakly coordinating anions is based on the pentafluoroorthotellurate group $[OTeF_5]^-$. As mentioned above, this ligand is known for its strong electron-withdrawing properties and in combination with its steric bulk and chemical robustness gives rise to this type of anions such as $[B(OTeF_5)_4]^-$ or $[Sb(OTeF_5)_6]^-$.[37,45,295] While the boron derivative was used for the first isolation of $[Tl]^+$ and silver-carbonyl complexes $[Ag(CO)_n]^+$ (n = 1, 2),[296,297] they are still prone to ligand abstraction by sufficient small electrophiles such as $[SiPh_3]^+$ or non-coordinated $[Ag]^+$.[298–300] Hexacoordinated anions such as

$[As(OTeF_5)_6]^-$ or $[Sb(OTeF_5)_6)]^-$ are less prone to such decomposition pathways, as their basic sites are sterically more shielded.[295] The oxidation resistance of pentafluoroorthotellurate anions allowed the isolation of the xenonium compound $[Xe(OTeF_5)][Sb(OTeF_5)_6]$.[195,301] The latter has been further used for the synthesis of highly reactive carbocations $[CX_3]^+$ (X = Cl, Br, $OTeF_5$).[302] More recently, the aluminum- and gallium-based pentafluoroorthotellurate anions $[Al(OTeF_5)_4]^-$ and $[Ga(OTeF_5)_4]^-$ were reported.[88,303] These anions play a crucial role in the synthesis and stabilization of protonated white phosphorus or the dimethylchloronium salt $[Me_2Cl][Al(OTeF_5)_4]$ as mentioned in the previous chapter.[232,233,304]

Further noteworthy mentions are trifluormethanesulfonamides $[N(SO_2R^F)_2]^-$ and triflides $[C(SO_2R^F)_3]^-$ ($R^F = F, C_2F_5, C_4F_9$).[305] The former is used as WCA in catalytic reactions, ionic liquids and electrolytes in lithium-ion batteries, while the latter has been applied in Friedel-Crafts and Diels-Alder reactions.[240,306–309]

In Figure 15 the structures and their electrostatic potentials for an exemplary overview of WCAs is shown. Hereby, the "classical" WCAs $[SbF_6]^-$ and $[Sb_2F_{11}]^-$ display a rather high negative potential at the surrounding fluoride atoms, while the larger, modern WCAs disperse the negative charge over a large number of atoms. Note that nucleophilic sites such as the oxygen atoms in $[Al\{OC(CF_3)_3\}_4]^-$ are shielded, e.g. by bulky perfluoro-*tert*-butyl groups.

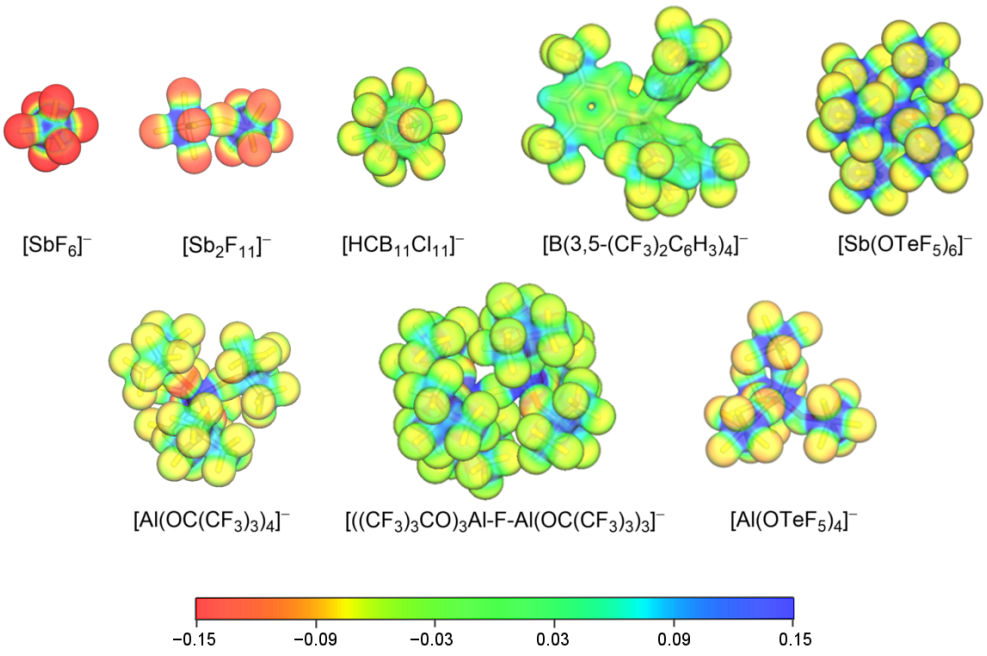

Figure 15. Calculated electrostatic potentials mapped onto isodensity surfaces (isovalue: 0.025 e^-Bohr^{-3}) for a set of different weakly coordinating anions. Calculations were performed on BP86/def-SV(P) level of theory.

2. Objectives

The pentafluoroorthotellurate group is known for its strong electron-withdrawing properties and, in conjunction with its sterical demand, enables the synthesis of very strong Lewis acids such as $B(OTeF_5)_3$ and $As(OTeF_5)_5$. However, their implementation in synthetic chemistry is rather confined.

Based on quantum-chemical calculations, the Lewis acidic aluminum pentafluoroorthotellurate $Al(OTeF_5)_3$ shows a high fluoride ion affinity, surpassing most of the synthetically accessible Lewis superacids (cf. Figure 2).[59] In previous studies the synthesis of $Al(OTeF_5)_3$ is only briefly mentioned and its full potential still has to be examined in depth.[88]

The first objective of this thesis is the development of an improved synthesis and a thorough investigation of the Lewis superacid $Al(OTeF_5)_3$. Besides a structural characterization in the solid state, also the reactivity in solution and towards weak bases is of interest.

The second objective is the utilization of Lewis superacids for the synthesis of elusive and reactive cations. Hereby, the high Lewis acidity in combination with the formation of robust weakly coordinating anions should be a key principle for the successful isolation and characterization of the cations. As Lewis acids the aforementioned $Al(OTeF_5)_3$ and the well-studied SbF_5 should be used. One interesting synthetic target is the perfluorinated tritylium cation $[C(C_6F_5)_3]^+$. So far, this species was only observed by NMR and UV-vis spectroscopy and could only be formed in superacidic media.[310,311] Theoretical investigations revealed its promising potential as strong hydride abstraction reagent.[26] For this purpose, a synthetic access in organic solvents along with a more detailed characterization is crucial. Another viable candidate is an organic fluoronium species with a formally positive charged fluorine atom symmetrically bound to two organic residues. To date, only spectroscopic evidence of one organic fluoronium cation was reported, but the existence of such compounds has been object to debate.[186,187] A structural proof accompanied with theoretical and spectroscopic analysis to further elucidate this bonding phenomenon are therefore of high interest.

As seen above, solid-state Lewis acids like ACF are already successfully employed in C–F activation reactions. A promising approach to enhance the reactivity of such materials might be achieved by doping with sterically demanding and electron-withdrawing groups. The last objective aims to introduce the pentafluoroorthotellurate moiety as dopant into the structure of the solid Lewis acid aluminum chlorofluoride. A reproducible synthesis route for a multi-gram scale should be developed.

3. Publications

3.1. Insights on the Lewis Superacid $Al(OTeF_5)_3$: Solvent Adducts, Characterization and Properties

Kurt F. Hoffmann, Anja Wiesner, Simon Steinhauer and Sebastian Riedel*
Chem. Eur. J. **2022**, e202201958

DOI: 10.1002/chem.202201958

©The Authors. Chemistry - A European Journal published by Wiley-VCH GmbH.

Author Contribution:
Kurt F. Hoffmann performed experiments and calculations, analyzed data and wrote the manuscript. Anja Wiesner and Kurt F. Hoffmann acquired and refined the SC-XRD data. Simon Steinhauer and Sebastian Riedel supervised the project, provided scientific guidelines and suggestions and revised the manuscript.

Chemistry–A European Journal
Research Article
doi.org/10.1002/chem.202201958
Chemistry Europe
European Chemical Societies Publishing
www.chemeurj.org

Insights on the Lewis Superacid $Al(OTeF_5)_3$: Solvent Adducts, Characterization and Properties**

Kurt F. Hoffmann,[a] Anja Wiesner,[a] Simon Steinhauer,[a] and Sebastian Riedel*[a]

Abstract: Preparation and characterization of the dimeric Lewis superacid $[Al(OTeF_5)_3]_2$ and various solvent adducts is presented. The latter range from thermally stable adducts to highly reactive, weakly bound species. DFT calculations on the ligand affinity of these Lewis acids were performed in order to rank their remaining Lewis acidity. An experimental proof of the Lewis acidity is provided by the reaction of solvent-adducts of $Al(OTeF_5)_3$ with $[PPh_4][SbF_6]$ and $OPEt_3$, respectively. Furthermore, their reactivity towards chloride and pentafluoroorthotellurate salts as well as $(CH_3)_3SiCl$ and $(CH_3)_3SiF$ is shown. This includes the formation of the dianion $[Al(OTeF_5)_5]^{2-}$.

Introduction

For a long time antimony pentafluoride was considered the strongest Lewis acid in the condensed phase.[1] In the last two decades, a new class of Lewis superacids emerged, which are defined as Lewis acids with a higher fluoride ion affinity (FIA) than molecular SbF_5 in the gas-phase (calc. FIA:[2] 493 kJ mol^{-1} on BP86/def-SV(P); exptl. FIA:[3] 506 ± 63 kJ mol^{-1}) and thereby surpass the latter in terms of acidity and manageability (cf. Figure 1).[4,5] More recent examples of group 13 Lewis superacids are $B(C_6F_4CF_3)_3$,[6] $Al(C_6F_5)_3$[7] (including partially fluorinated derivatives[8]), $Al[OC(CF_3)_3]_3$,[9] $Al[N(C_6F_5)_2]_3$,[10] $Al(OC_5F_4N)_3$,[11] $Al[OC(C_6F_5)_3]_3$[12] and a comprehensive review was recently published.[13] However, one of the drawbacks of such compounds is their strong interaction with solvent molecules or their own ligand system, resulting in a drastically lowered Lewis acidity. Regarding the manageability, important properties of Lewis superacids are the isolability as a neat substance as well as the thermal stability.

In 2017 we reported first attempts of the synthesis of the Lewis acid $Al(OTeF_5)_3$.[14] With a FIA of 591 kJ mol^{-1} for its molecular unit it can be counted as one of the strongest known isolable Lewis acids. The compound was analyzed by IR and Raman spectroscopy, revealing the dimeric form $[Al(OTeF_5)_3]_2$ in the solid state. Still, its temperature sensitivity made the handling of the compound tedious as it rapidly decomposed at temperatures above 0 C, which might be accounted to impurities (see below).

Herein we report on an improved synthesis of $[Al(OTeF_5)_3]_2$, which can be prepared on a multigram scale. The Lewis superacid is room-temperature stable for several hours and isolable as an adduct-free, amorphous powder. With this neat Lewis acid in hand, we investigated its complexation with a broad range of different solvents, ranging from thermally stable, strongly bound adducts to weakly bound, reactive species. We then further elaborate on the reactivity of these so formed solvent-adducts.

Results and Discussion

In our previous study we firstly reported on the formation of the Lewis acid $[Al(OTeF_5)_3]_2$ by the reaction of triethylaluminium, $AlEt_3$, with teflic acid, $HOTeF_5$, in *n*-pentane in a stoichiometric ratio of 1 : 3.[14] This reaction yields a colorless powder which is unstable at room temperature. Analyzing a solution of this product in SO_2ClF by low-temperature NMR spectroscopy revealed the presence of residual alkyl moieties that presumably led to a decreased thermal stability (decomposition above 0 C) of this compound. Therefore, an improved synthesis of the dimeric $[Al(OTeF_5)_3]_2$ by employing different reactants and conditions was needed.

In our new approach $AlMe_3$ was used as a starting material (cf. Scheme 1). Analogue to the reported synthesis with $AlEt_3$, treatment in *n*-pentane with 3 equivalents of $HOTeF_5$ and warming of the mixture from −196 C to −40 C results in the formation of a colorless precipitate. After removing the solvent, a yet again temperature-sensitive powder remains. Low-temperature NMR measurements in SO_2ClF show the presence of a methyl group at −0.01 ppm in the ^{1}H NMR spectrum, indicating an incomplete substitution of the methyl groups by $-OTeF_5$ (teflate) groups at the aluminum center. In the ^{19}F NMR spectrum, two sets of signals for magnetically inequivalent $-OTeF_5$ groups are observed, while the ^{27}Al NMR shows a broad signal at 48 ppm, typical for a tetrahedrally coordinated Al

[a] K. F. Hoffmann, Dr. A. Wiesner, Dr. S. Steinhauer, Prof. Dr. S. Riedel
Fachbereich für Biologie, Chemie, Pharmazie
Institut für Chemie und Biochemie – Anorganische Chemie
Fabeckstraße 34/36, 14195 Berlin (Germany)
E-mail: s.riedel@fu-berlin.de

[**] A previous version of this manuscript has been deposited on a preprint server (https://doi.org/10.26434/chemrxiv-2022-9z6j7).

Supporting information for this article is available on the WWW under https://doi.org/10.1002/chem.202201958

© 2022 The Authors. Chemistry - A European Journal published by Wiley-VCH GmbH. This is an open access article under the terms of the Creative Commons Attribution License, which permits use, distribution and reproduction in any medium, provided the original work is properly cited.

© 2022 The Authors. Chemistry - A European Journal published by Wiley-VCH GmbH

Chemistry–A European Journal
Research Article
doi.org/10.1002/chem.202201958
Chemistry Europe
European Chemical Societies Publishing

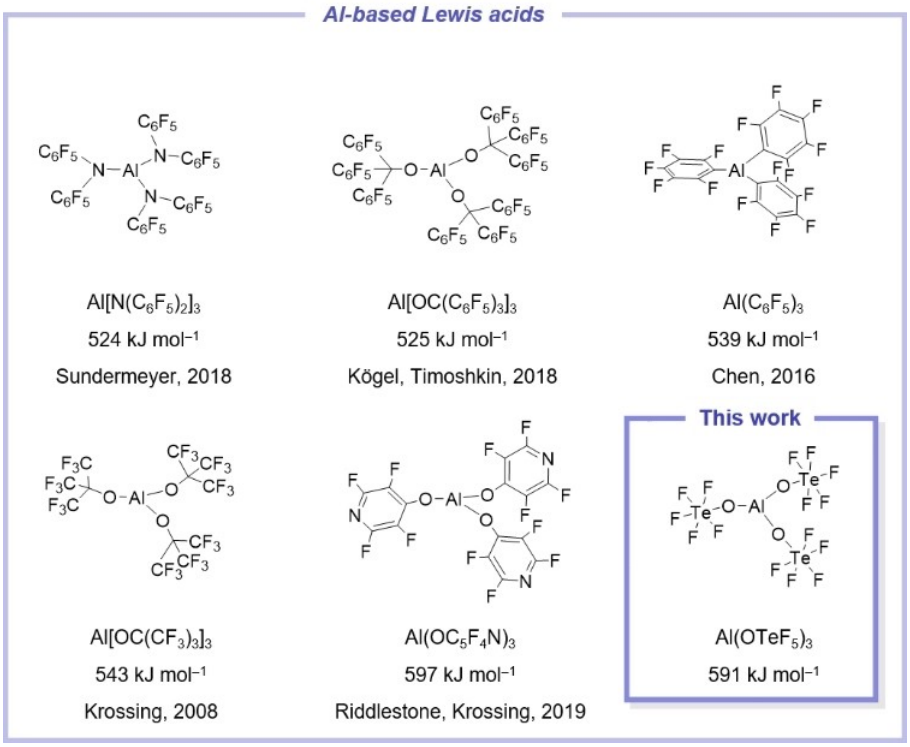

Figure 1. Modern aluminum-based Lewis superacids and their corresponding fluoride ion affinity. FIA values were calculated on the BP86/def-SV(P) level of theory. Me_3SiF was used as anchor point.[2]

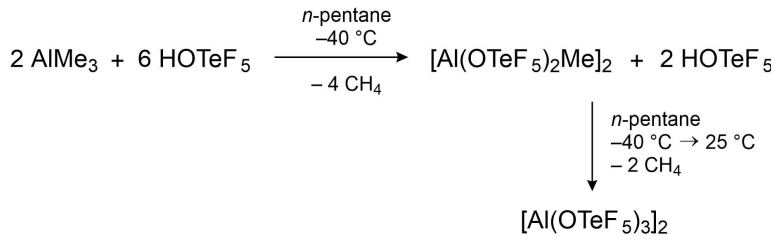

Scheme 1. Improved synthesis of the Lewis acid $[Al(OTeF_5)_3]_2$.

center. Single crystals suitable for low-temperature single crystal X-ray diffraction grew in a cooled *ortho*-difluorobenzene (*o*-DFB) solution and the molecular structure of the neutral dimer $[Al(OTeF_5)_2Me]_2$ was obtained (cf. Figure 2). The dimer bridged by two $-OTeF_5$ groups crystallizes in the monoclinic space group $P2_1/n$.

Each of the aluminum centers is coordinated by a methyl group, a terminal teflate group and two bridging teflate moieties, leading to a heavily distorted tetrahedral coordination sphere with bond angles between 79.2(2) and 118.5(3) . The bridging Al–O bond distances are elongated (d(Al1-O1) = 188.2(5), d(Al1-O1′) = 189.0(6) pm) compared to the terminal Al–O bond distance (d(Al1-O2) = 172.3(6) pm). The latter are comparable to Al–O bond distances in salts of the anion $[Al(OTeF_5)_4]^-$ (e.g., d(Al–O) in $[PPh_4][Al(OTeF_5)_4]$ = 173.4(2) pm).[14] This difference in bond distances is analogue to the difference in bond distances of bridging and terminal perfluoroalcoholates in the compound $Et_2Al(\mu\text{-}OR_f)_2Al(Et)(OR_f)$ with $OR_f = OC(CF_3)_3$) reported by Krossing et al.[15] The Al–C bond distances (d(Al1-C1) = 192.3(8) pm) are shortened when compared to the molecular structure of dimeric $[AlMe_3]_2$, underlining the increased Lewis acidity of the Al centers in $[Al(OTeF_5)_2Me]_2$.[16] Recently, we reported on a comparable molecular structure of the higher homologue gallium $Et_2Ga(\mu$-

© 2022 The Authors. Chemistry - A European Journal published by Wiley-VCH GmbH

Chemistry–A European Journal | Research Article
doi.org/10.1002/chem.202201958
Chemistry Europe
European Chemical Societies Publishing

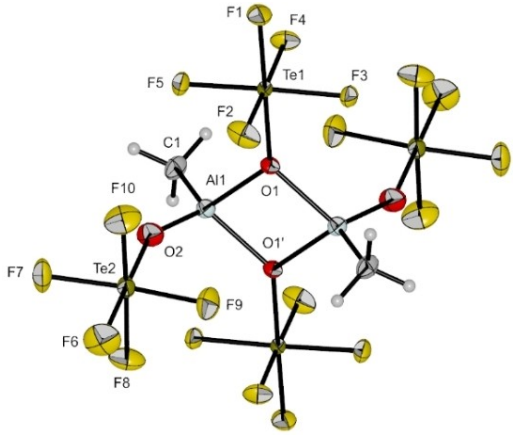

Figure 2. Molecular structure of $[Al(OTeF_5)_2Me]_2$ in the solid state. Thermal ellipsoids set up to 50% probability. Selected bond lengths [pm] and angles [ ]: Al1-O1 188.2(5), Al1-O2 172.3(6), Al1-O1′ 189.0(6), Al1-C1 192.3(8), O1-Al1-C1 117.1(3), O1-Al1-O2 107.1(3), O1-Al1-O1′ 79.2(2), C1-Al1-O2 118.3(4), C1-Al1-O1′ 118.5(3), O2-Al1-O1′ 110.1(3).

$OTeF_5)_2Ga(Et)(OTeF_5)$.[17] Further investigations by IR and Raman vibrational spectroscopy confirm the presence of the dimeric $[Al(OTeF_5)_2Me]_2$. More details can be found in the Supporting Information.

To obtain the fully teflate-substituted Lewis acid $[Al(OTeF_5)_3]_2$, either starting from $AlMe_3$ and $HOTeF_5$ or $[Al(OTeF_5)_2Me]_2$, a slight excess of teflic acid and further heating to room-temperature is needed. Removing the solvent at reduced pressure again leads to the isolation of a colorless powder. The comparison of recorded IR and Raman spectra of $[Al(OTeF_5)_3]_2$ to $[Al(OTeF_5)_2Me]_2$ shows the absence of residual methyl groups (cf. spectra in Supporting Information). Furthermore, this product is stable for several hours at room temperature and can be stored at −20 C under an argon atmosphere for months without any decomposition.

Solvent adducts

The reactivity and acidity of the Lewis acid $[Al(OTeF_5)_3]_2$ in further reactions is clearly dependent on the solvent that is used. In the following section the interaction of the dimer $[Al(OTeF_5)_3]_2$ with different solvents is described. While either no solubility at low temperatures or decomposition was observed with non-polar solvents such as alkanes and methylene chloride, a number of different solvent adducts are obtained with stronger donors (cf. Figure 3).

In our previous work, we briefly discussed the synthesis of the solvent-adduct $[Al(OTeF_5)_3(MeCN)]$ by the reaction of $HOTeF_5$ with $AlEt_3$ in n-pentane and the subsequent addition of equimolar amounts of MeCN.[14] For this work we extended the range of nitriles and used acetonitrile as well as benzonitrile (PhCN) as solvent (cf. Scheme 2) and further analyzed the formed compounds by NMR and, in the case of the benzonitrile adduct, also by SC-XRD. In both cases the removal of all volatiles yields a room-temperature stable colorless powder in almost quantitative yields, which can be stored under an argon-atmosphere at room temperature for several months without any sign of decomposition.

NMR-spectroscopic investigation of the nitrile adducts reveal an octahedral coordination sphere at the Al center in solution, by showing very broad signals in the typical range of octahedrally coordinated aluminum centers between −10 and −25 ppm.[18] This indicates the formation of $[Al(OTeF_5)_3(MeCN)_3]$

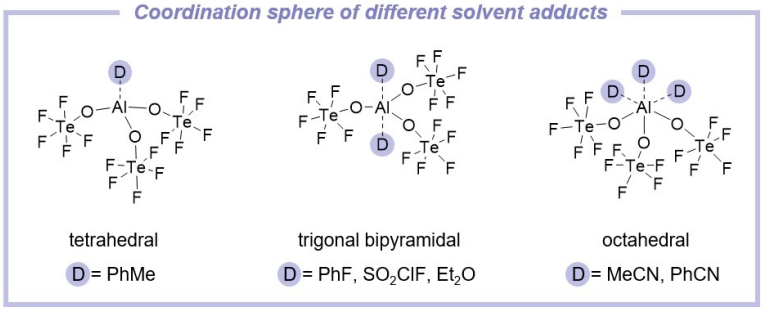

Figure 3. Summary of structurally characterized solvent adducts of the Lewis acid $Al(OTeF_5)_3$.

$$AlEt_3 + 3\,HOTeF_5 \xrightarrow[-3\,C_2H_6]{RCN,\ -40\,^{\circ}C \rightarrow 25\,^{\circ}C} [Al(OTeF_5)_3(RCN)_3] \qquad R = Me, Ph$$

Scheme 2. Synthesis of nitrile solvent-adducts $[Al(OTeF_5)_3(RCN)_3]$.

© 2022 The Authors. Chemistry - A European Journal published by Wiley-VCH GmbH

Chemistry–A European Journal | Research Article
doi.org/10.1002/chem.202201958
Chemistry Europe
European Chemical Societies Publishing

$$2\ [Al(OTeF_5)_3(RCN)_3] \rightleftharpoons [Al(OTeF_5)_2(RCN)_4]^+ + [Al(OTeF_5)_4(RCN)_2]^-$$

Scheme 3. Equilibrium between the neutral nitrile adduct of $Al(OTeF_5)_3$ and its autoionized ion-pair. (R = Me, Ph).

and $[Al(OTeF_5)_3(PhCN)_3]$, which is further supported by crystallographic evidence in the case of PhCN (see below). The ^{19}F NMR spectra intriguingly show three sets of AB_4 spin systems, indicating three magnetically inequivalent $-OTeF_5$ groups. This is explained by an equilibrium of the neutral solvent adduct $[Al(OTeF_5)_3(RCN)_3]$ (R = MeCN or PhCN) and an autoionized ion-pair of the type $[Al(OTeF_5)_2(RCN)_4][Al(OTeF_5)_4(RCN)_2]$ (cf. Scheme 3). Analogous autoionization products are known for other aluminum halides, such as $AlBr_3$ and $AlCl_3$, in tetrahydrofurane.[19]

Dissolution of $[Al(OTeF_5)_3(RCN)_3]$ in less nucleophilic solvents like CH_2Cl_2 or *o*-DFB leads to a complete autoionization and the formation of $[Al(OTeF_5)_4]^-$ next to $[Al(OTeF_5)_2(RCN)_4]^+$ and $[Al(OTeF_5)_4(RCN)_2]^-$. In addition, the exchange of all $-OTeF_5$ groups is observed in the corresponding ^{19}F,^{19}F EXSY NMR measurement (see Supporting Information for more details).

In the case of the benzonitrile adduct colorless single crystals suitable for SC-XRD could be obtained. The compound $[Al(OTeF_5)_3(PhCN)_3]$ crystallizes in the monoclinic space group $P2_1/c$ with three molecules per asymmetric unit (cf. Figure 4). The octahedral complex possesses a facial coordination sphere. The Al–O bond lengths lie between 181.4(3) and 183.4(3) pm and are shorter than the Al–O bond distances of the two other known six-fold coordinated aluminum pentafluoro-orthotellurates $[Li(thf)_4][Al(OTeF_5)_4(thf)_2]$ and $[Ag(thf)_6][Al(OTeF_5)_4(thf)_2]$.[20]

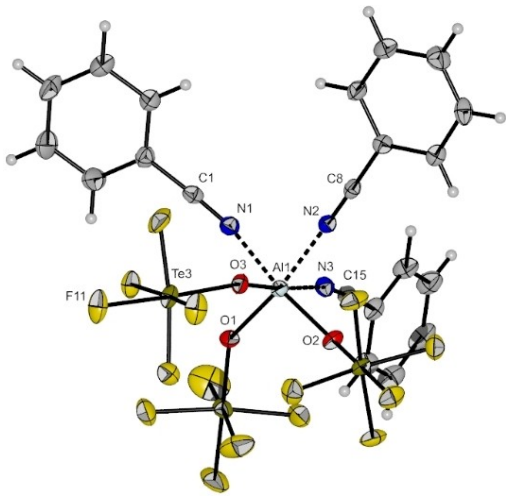

Figure 4. Molecular structure of $[Al(OTeF_5)_3(PhCN)_3]$ in the solid state. Thermal ellipsoids set up to 50% probability. Selected bond lengths [pm] and angles [ ]: Al1-O1 182.5(3), Al1-O2 183.4(3), Al1-O3 183.2(3), Al1-N1 203.7(3), Al1-N2 200.3(3), Al1-N3 203.6(3), O1-Al1-O2 98.34(13), O1-Al1-O3 93.94(13), O2-Al1-O3 96.04(12), N1-Al1-N2 84.62(13), N1-Al1-N3 87.38(13), N2-Al1-N3 88.95(13).

The Al–N bond distances range from 200.3(3) to 203.7(3) pm. All of the O–Al–O bond angles are with an average of 95.8 larger than the N–Al–N bond angles with an average of 86.7 , leading to a slight distortion of the coordination sphere.

To enable a structural characterization of the autoionized species, bipyridine (bipy) is added to a solution of $[Al(OTeF_5)_3(PhCN)_3]$ in CH_2Cl_2. A similar approach was recently reported by Gerken et al. for the autoionization of SbF_5.[21] The anticipated salt $[Al(OTeF_5)_2(bipy)_2][Al(OTeF_5)_4(bipy)]$ crystallizes in the triclinic space group $P\bar{1}$ (cf. Figure 5). The molecular structure shows two octahedrally coordinated aluminum complexes. The anionic fragment shows Al–O bond distances between 183.9(2) and 188.0(2) pm which are comparable to the reported Al–O bond distances in $[Al(OTeF_5)_4(thf)_2]^-$.[20] The Al–O bond distances of the cation are in a similar range and not shortened as one might expect. The same holds true for the Al–N bond distances in anion and cation.

Compared to the neat Lewis acid $[Al(OTeF_5)_3]_2$, the nitrile adducts form room-temperature stable compounds and can be easily handled. The main drawback is the quenched Lewis acidity due to the coordination of the nitrile molecules. In order to preserve a high reactivity of the underlying Lewis acid we aimed to prepare adducts with weaker donor solvents. Therefore, the solid dimer $[Al(OTeF_5)_3]_2$ was dissolved in fluorobenzene and SO_2ClF, respectively (cf. Scheme 4).

Dissolution of $[Al(OTeF_5)_3]_2$ in fluorobenzene at 0 C results in a light green, clear solution. Warming the mixture to room-temperature leads to visible decomposition of the compound. Low-temperature NMR spectroscopic measurements revealed the presence of a single aluminum species in the ^{27}Al NMR spectrum. The broad signal at −46.1 ppm is in the typical range for tetrahedrally coordinated Al centers and in agreement with the chemical shift of the literature-known $[Al\{OC(CF_3)_3\}_3(PhF)]$, thus pointing to the formation of $[Al(OTeF_5)_3(PhF)]$.[5] The ^{19}F NMR spectrum shows signals corresponding to one AB_4 spin system with F_a at −40.7 ppm and F_b at −46.1 ppm with a coupling constant of $^2J_{FF} = 191$ Hz. A signal for the coordinated PhF could not be observed in the ^{19}F NMR spectrum since the spectra were recorded in fluorobenzene. Therefore, an exchange of the solvent molecules bound to the Al center can be expected. Attempts to isolate the compound as a neat substance did not yield in any success.

$$0.5\ [Al(OTeF_5)_3]_2 \xrightarrow[\text{or}\ SO_2ClF]{C_6H_5F} [Al(OTeF_5)_3D_2]$$

D = C_6H_5F or SO_2ClF

Scheme 4. Neutral adduct formation with weakly donating solvents.

© 2022 The Authors. Chemistry - A European Journal published by Wiley-VCH GmbH

Chemistry–A European Journal | Research Article
doi.org/10.1002/chem.202201958
Chemistry Europe
European Chemical Societies Publishing

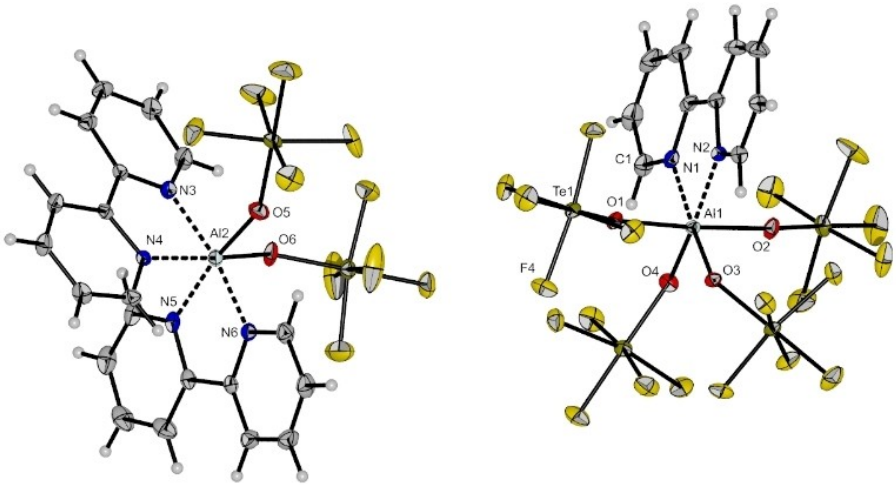

Figure 5. Molecular structure of $[Al(OTeF_5)_2(bipy)_2][Al(OTeF_5)_4(bipy)]$ in the solid state. Thermal ellipsoids set up to 50% probability. Al1-O1 188.0(2), Al1-O2 187.6(3), Al1-O3 183.9(2), Al1-O4 184.9(2), Al1-N1 204.6(3), Al1-N2 205.7(3), Al2-O5 183.1(3), Al2-O6 183.6(3), Al2-N3 200.8(3), Al2-N4 204.2(3), Al2-N5 203.5(3), Al2-N6 200.7(3), O1-Al1-O2 176.22(12), N1-Al1-O3 171.29(12), N2-Al1-O4 168.58(12), N3-Al2-N6 170.09(13), N4-Al2-O6 169.85(12), N5-Al2-O5 170.22(13).

Concentration of a solution of $[Al(OTeF_5)_3]_2$ in PhF and further cooling to −40 C resulted in yellow-green single crystals which were examined by single crystal X-ray diffraction. Instead of a tetrahedral aluminum complex, the five-fold coordinated complex $[Al(OTeF_5)_3(PhF)_2]$ was found (cf. Figure 6). The compound crystallizes in the monoclinic space group $P2_1/n$. In this structure the aluminum center has a trigonal-bipyramidal coordination sphere with three –$OTeF_5$ groups in the equatorial plane and two fluorobenzene molecules in the axial positions. The Al–O bond lengths range from 172.7(2) to 173.1(2) pm and the bond angles between the Al–O bonds lie between 115.04(11) and 123.41(11) . The fluorobenzene molecules coordinate the aluminum center via their fluorine atom. With bond lengths of d(Al1-F17) = 197.9(2) pm and d(Al1-F18) = 197.4(2) pm, the Al–F bonds are elongated compared to the ones reported for the tetrahedral Lewis superacid adduct $[Al\{OC(CF_3)_3\}_3(PhF)]$ (d(Al–F) = 186.4(2) pm).[5] Analogous to the findings of Krossing et al.,[5] the C–F bond lengths of the bound fluorobenzene molecules are elongated by about 7 pm compared to neat fluorobenzene.[22]

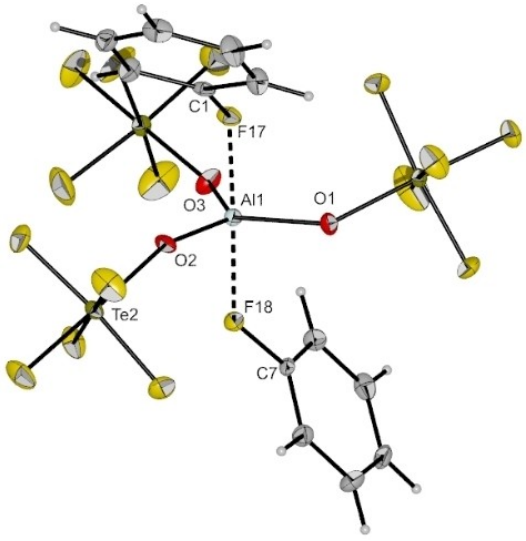

Figure 6. Molecular structure of $[Al(OTeF_5)_3(PhF)_2]$ in the solid state. Thermal ellipsoids set up to 50% probability. Selected bond lengths [pm] and angles [ ]: Al1-O1 172.7(2), Al1-O2 172.4(2), Al1-O3 173.1(2), Al1-F17 197.9(2), Al1-F18 197.4(2), C1-F17 142.4(3), C7-F18 142.4(3), O1-Al1-O2 123.41(11), O1-Al1-O3 115.04(11), O2-Al1-O3 121.56(11), C7-F18-Al1 135.03(16), C1-F17-Al1 134.03(16).

Changing the solvent and treating solid $[Al(OTeF_5)_3]_2$ with an excess of SO_2ClF results in a clear colorless solution. In contrast to the experiments with fluorobenzene, this mixture is sufficiently stable at room temperature. Interestingly, the adduct formation with SO_2ClF yields the trigonal-bipyramidal complex $[Al(OTeF_5)_3(SO_2ClF)_2]$ in solution and in the solid state. The ^{27}Al NMR spectrum shows a very broad signal at 34.0 ppm (FWHM = 2200 Hz), which lies between the typical regions of four-fold and six-fold coordinated Al centers. Similar to the experiments with PhF, the ^{19}F NMR spectrum shows only one AB_4 spin system belonging to the three magnetically equivalent –$OTeF_5$ groups.

A colorless powder is isolated by removing all volatiles at reduced pressure. This powder is stable for several hours at room temperature and was analyzed by IR and Raman spectroscopy. Besides the typical bands of $Al(OTeF_5)_3$ in the IR spectrum, additional bands at 1436 (Raman: 1428) and 1188 (Raman: 1182) cm^{-1} for the SO_2 stretching vibrations of the

© 2022 The Authors. Chemistry - A European Journal published by Wiley-VCH GmbH

Chemistry–A European Journal | Research Article
doi.org/10.1002/chem.202201958
Chemistry Europe
European Chemical Societies Publishing

coordinated SO_2ClF molecules are observed. Compared to free SO_2ClF ($\nu_{as}(SO_2) = 1455\ cm^{-1}$, $\nu_s(SO_2) = 1224\ cm^{-1}$) these bands are slightly red-shifted, which indicates a coordination of the SO_2ClF molecules via the oxygen atom.[23]

After concentrating the solution of $[Al(OTeF_5)_3(SO_2ClF)_2]$ and slowly cooling it to −80 C single crystals suitable for single crystal X-ray diffraction were obtained. The compound $[Al(OTeF_5)_3(SO_2ClF)_2]$ crystallizes in the triclinic space group $P\bar{1}$ (cf. Figure 7). Analogous to the molecular structure of $[Al(OTeF_5)_3(PhF)_2]$, the $-OTeF_5$ groups build the equatorial plane and the SO_2ClF molecules are bound in axial position to the central aluminum atom, resulting in a trigonal bipyramidal coordination sphere. For the Al–O bonds between aluminum and the teflate groups an average bond distance of 174.3 pm with average bond angles of 119.9 is found, which is comparable to the distances and angles in $[Al(OTeF_5)_3(PhF)_2]$. As already discovered by vibrational spectroscopy, the SO_2ClF molecules are bound by their oxygen atoms with Al–O bond lengths of 210.4(6) and 198.9(6) pm. To the best of our knowledge, only one other example of a molecular structure with an oxygen-bound SO_2ClF molecule has been reported so far, which is $[Xe(OTeF_5)(SO_2ClF)][Sb(OTeF_5)_6]$. Here, the SO_2ClF molecule is coordinated to the $[Xe(OTeF_5)]^+$ cation.[24]

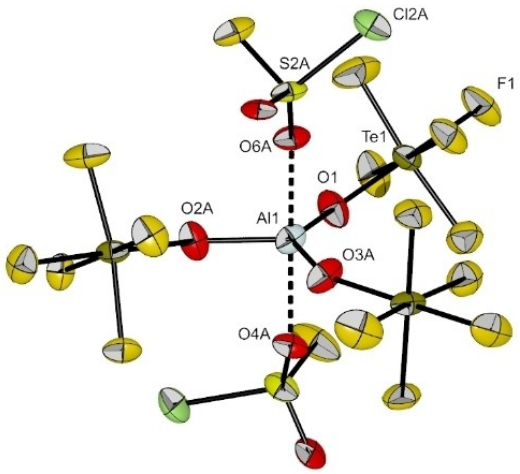

Figure 7. Molecular structure of $[Al(OTeF_5)_3(SO_2ClF)_2]$ in the solid state. Thermal ellipsoids set up to 50% probability. Selected bond lengths [pm] and angles [ ]: Al1-O1 172.0(3), Al1-O2 A 177.9(6), Al1-O3 A 173.4(4), Al1-O4 A 210.4(6), Al1-O6 A 198.9(6), O1-Al1-O2 A 114.76(19), O1-Al1-O3 A 131.9(2), O2 A-Al1-O3 A 113.02(6).

A remarkable example for a weakly coordinated aluminum complex was shown by Cowley, Jones, and coworkers, when they first synthesized the arene complexes $[Al(C_6F_5)_3(\eta^1\text{-}C_6H_6)]$ and $[Al(C_6F_5)_3(\eta^1\text{-}C_7H_8)]$ starting from $AlMe_3$ and $B(C_6F_5)_3$ in benzene or toluene.[25] Own attempts to form an arene adduct in an analoguous route with $B(OTeF_5)_3$ as $-OTeF_5$ group transfer reagent were unsuccessful. Also dissolving the solid $[Al(OTeF_5)_3]_2$ in toluene led to the decomposition of the Lewis acid. The failed reaction can be explained by the low binding energy of a toluene complex compared to the dimeric species and will be discussed in a later section.

Nevertheless, it was possible to obtain an arene adduct by a detour (cf. Scheme 5). In the first step, a solution of $AlEt_3$ in toluene is treated with 4 equivalents of $HOTeF_5$, which leads to the protonation of toluene, thereby forming the strong Brønsted acid $[H\text{-}C_7H_8][Al(OTeF_5)_4]$. Similar procedures are already described in the literature.[14,26] In the next step, a slight excess of triethylsilane, Et_3SiH, is added to the mixture, followed by a gas formation accompanied by the decolorization of the bright orange solution. Upon addition of Et_3SiH, presumably the cationic silylium species $[SiEt_3]^+$ is formed alongside the evolution of gaseous H_2, which is a sufficiently strong electrophile to abstract an $-OTeF_5$ group from the anion $[Al(OTeF_5)_4]^-$. Thereby, $Et_3SiOTeF_5$ and the Lewis acid $Al(OTeF_5)_3$ are formed, the latter of which is stabilized by the present toluene. Warming the reaction mixture above −40 C results in the visible decomposition of the sample. Therefore, the reaction solution was analyzed by low-temperature NMR spectroscopy. The ^{19}F NMR spectrum reveals two magnetically inequivalent $-OTeF_5$ groups, assigned to the formed $Et_3SiOTeF_5$ and the solvent-adduct $[Al(OTeF_5)_3(\eta^1\text{-}C_7H_8)]$. In the ^{27}Al NMR spectrum a broad signal at 48 ppm for $[Al(OTeF_5)_3(\eta^1\text{-}C_7H_8)]$ is observed. The ^1H and ^{29}Si NMR spectra confirm the presence of $Et_3SiOTeF_5$ and residual Et_3SiH.

Further cooling of the reaction mixture to −80 C led to colorless crystals suitable for single crystal X-ray diffraction. The compound $[Al(OTeF_5)_3(\eta^1\text{-}C_7H_8)]\cdot C_7H_8$ crystallizes in the monoclinic space group $P2_1/c$ (cf. Figure 8). The aluminum center is distorted tetrahedrally coordinated by three $-OTeF_5$ ligands and a toluene molecule via its *para*-carbon atom. The Al–O bond lengths are in the same range as the aforementioned solvent

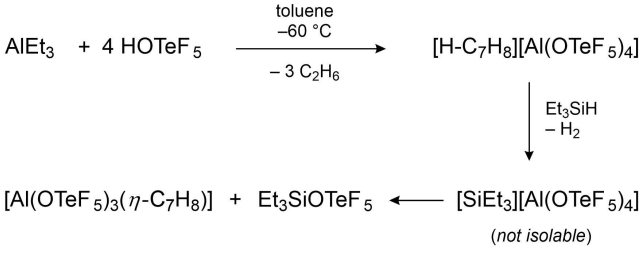

Scheme 5. Proposed mechanism for the formation of the toluene adduct $[Al(OTeF_5)_3(\eta^1\text{-}C_7H_8)]$.

© 2022 The Authors. Chemistry - A European Journal published by Wiley-VCH GmbH

Chemistry–A European Journal | Research Article
doi.org/10.1002/chem.202201958
Chemistry Europe
European Chemical Societies Publishing

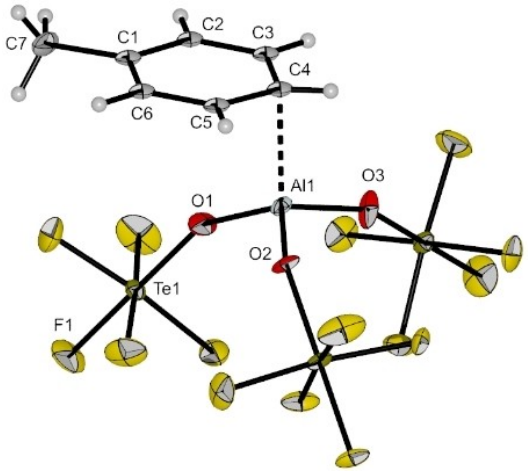

Figure 8. Molecular structure of $[Al(OTeF_5)_3(\eta^1\text{-}C_7H_8)]$ in the solid state. Thermal ellipsoids set up to 50% probability. Selected bond lengths [pm] and angles [ ]: Al1-O1 171.3(7), Al1-O2 173.4(7), Al1-O3 172.6(8), Al1-C4 214.3(10), O1-Al1-O2 114.2(4), O1-Al1-O3 112.9(4), O1-Al1-C4 111.1(4), O2-Al1-O3 110.4(4), O2-Al1-C4 105.1(4), O3-Al1-C4 102.3(4), Al1-C4-C5 91.7(6), Al1-C4-C3 95.8(6).

adducts $[Al(OTeF_5)_3(SO_2ClF)_2]$ and $[Al(OTeF_5)_3(PhF)_2]$. The average Al–O bond angle of 112.5 is close to the ideal tetrahedral angle. The Al1-C4 bond distance of 214.3(10) pm is significantly shorter than in the complexes $[Al(C_6F_5)_3(\eta^1\text{-}C_6H_6)]$ and $[Al(C_6F_5)_3(\eta^1\text{-}C_7H_8)]$ (d(Al-$C_{toluene}$) = 236.6(2) pm and d(Al-$C_{benzene}$) = 234.2(6) pm).[25] An analoguous coordination motif was reported by Lambert et al. in the molecular structure of $[Et_3Si(\eta^1\text{-}C_7H_8)][B(C_6F_5)_4]$, whereby the highly Lewis acidic silylium ion is η^1-coordinated by toluene (d(Si-$C_{toluene}$) = 218 pm).[27] The geometry at the C4 atom indicates a sp^2 hybridization (∠(C3-C4-C5) = 119.4(10)) and the donor-acceptor bond between Al and C is therefore best described as a π-arene complex (∠(Al1-C4-C3) = 95.8(6) and ∠(Al1-C4-C5) = 91.7(6)). This is further supported by the maintained planarity of the toluene molecule (largest torsion angle: 3.9) and similar aromatic C–C bond lengths (ranging between 137.6(14) and 141.2(14) pm). The contrary case of a Wheland-type σ-complex would require a sp^3 hybridized carbon atom C4 with bond angles close to 109 , alternating C–C bond lengths and a loss of planarity of the aromatic ring.

In order to estimate the ligand affinity of the Lewis acid $Al(OTeF_5)_3$ towards the different solvents and judge the remaining Lewis acidity of the solvent adducts, the fluoride ion affinities and the complexation energies of the adducts have been calculated on the BP86/def-SV(P) and B3LYP/def2-TZVPP level of theory. The results are summarized in Table 1. For the discussion of the calculated FIA values, the BP86/def-SV(P) level of theory and the isodesmic reactions with trimethylsilane as anchor are used to allow a comparison with a previously reported FIA calculation.[2,28]

In general, by expanding the ligand coordination sphere of the aluminum center starting from a tetrahedral over a trigonal bipyramidal to an octahedral coordination, a decrease of the Lewis acidity is observed. For the tetrahedrally coordinated complexes, the Lewis acidity of the Al center decreases in the order toluene > SO_2ClF > PhF > MeCN > PhCN > Et_2O. This is also reflected in the experiment, whereby the complex stability increases in the same order. This trend is also in agreement with experimental donor numbers of the respective solvents.[29] The calculated FIA values of the experimentally observed complexes $[Al(OTeF_5)_3(PhF)_2]$, $[Al(OTeF_5)_3(SO_2ClF)_2]$ and $[Al(OTeF_5)_3(\eta^1\text{-}C_7H_8)]$ still surpass the fluoride ion affinity of

Table 1. Calculated fluoride ion affinities (FIA) and complexation energies of various solvent adducts of $Al(OTeF_5)_3$.

compound	FIA [kJ mol^{-1}] BP86/def-SV(P)	B3LYP/def2-TZVPP	reaction			$\Delta_R H$ [kJ mol^{-1}] BP86/def-SV(P)	B3LYP/def2-TZVPP
$Al(OTeF_5)_3$	591	637		–		–	–
$[Al(OTeF_5)_3]_2$	569	584	2 $Al(OTeF_5)_3$	→	$[Al(OTeF_5)_3]_2$	−21.9	−53.6
tetrahedral coordination							
$[Al(OTeF_5)_3(\eta^1\text{-}C_7H_8)]$	566	590	$Al(OTeF_5)_3 + C_7H_9$	→	$[Al(OTeF_5)_3(\eta^1\text{-}C_7H_8)]$	−25.1	−47.1
$[Al(OTeF_5)_3(SO_2ClF)]$	584	580	$Al(OTeF_5)_3 + SO_2ClF$	→	$[Al(OTeF_5)_3(SO_2ClF)]$	−7.7[a]	−57.0
$[Al(OTeF_5)_3(PhF)]$	581	581	$Al(OTeF_5)_3 + PhF$	→	$[Al(OTeF_5)_3(PhF)]$	−9.3[a]	−56.0
$[Al(OTeF_5)_3(MeCN)]$	493	499	$Al(OTeF_5)_3 + MeCN$	→	$[Al(OTeF_5)_3(MeCN)]$	−97.9	−138.3
$[Al(OTeF_5)_3(PhCN)]$	481	489	$Al(OTeF_5)_3 + PhCN$	→	$[Al(OTeF_5)_3(PhCN)]$	−110.1	−148.7
$[Al(OTeF_5)_3(Et_2O)]$	477	493	$Al(OTeF_5)_3 + Et_2O$	→	$[Al(OTeF_5)_3(Et_2O)]$	−114.6	−144.7
trigonal bipyramidal coordination							
$[Al(OTeF_5)_3(SO_2ClF)_2]$	555	571	$Al(OTeF_5)_3 + 2\ SO_2ClF$	→	$[Al(OTeF_5)_3(SO_2ClF)_2]$	−35.9	−66.6
$[Al(OTeF_5)_3(PhF)_2]$	540	564	$Al(OTeF_5)_3 + 2\ PhF$	→	$[Al(OTeF_5)_3(PhF)_2]$	−50.9	−73.2
$[Al(OTeF_5)_3(OEt_2)_2]$	408	474	$Al(OTeF_5)_3 + 2\ Et_2O$	→	$[Al(OTeF_5)_3(Et_2O)_2]$	−183.0	−163.4
octahedral coordination							
$[Al(OTeF_5)_3(MeCN)_3]$	368	441	$Al(OTeF_5)_3 + 3\ MeCN$	→	$[Al(OTeF_5)_3(MeCN)_3]$	−223.0	−196.5
$[Al(OTeF_5)_3(PhCN)_3]$	348	435	$Al(OTeF_5)_3 + 3\ PhCN$	→	$[Al(OTeF_5)_3(PhCN)_3]$	−243.1	−202.6

[a] Those values seem unreliable due to basis set limitation. The calculations were repeated with a larger basis set (BP86/def-TZVP) and are found to give a more consistent value: $\Delta_R H$ ($Al(OTeF_5)_3 + SO_2ClF \rightarrow [Al(OTeF_5)_3(SO_2ClF)]$) = −21.3 kJ mol^{-1}; $\Delta_R H$ ($Al(OTeF_5)_3 + PhF \rightarrow [Al(OTeF_5)_3(PhF)]$) = −26.7 kJ mol^{-1}.

© 2022 The Authors. Chemistry - A European Journal published by Wiley-VCH GmbH

Chemistry–A European Journal | Research Article
doi.org/10.1002/chem.202201958
Chemistry Europe
European Chemical Societies Publishing

molecular SbF_5 (FIA: 493 kJ mol^{-1}) and therefore a high reactivity can be expected. The calculations also reveal significantly lower fluoride ion affinities of the nitrile adducts $[Al(OTeF_5)_3(MeCN)_3]$ and $[Al(OTeF_5)_3(PhCN)_3]$ than SbF_5. Regarding the calculated complexation enthalpies $\Delta_R H$, the results based on the calculations with B3LYP/def2-TZVPP level of theory are discussed and the following trend is observed: If the FIA value of a Lewis acid-solvent adduct is low, the corresponding complexation reaction is highly exothermic. The $\Delta_R H$ values also allow to estimate whether a complexation of $[Al(OTeF_5)_3]_2$ with a solvent is possible. Only in the case of $[Al(OTeF_5)_3(\eta^1\text{-}C_7H_8)]$ the dimerization is thermodynamically favored compared to the toluene-adduct formation ($\Delta_R H$ ($[Al(OTeF_5)_3]_2$) = −53.6 kJ mol^{-1}, $\Delta_R H$ ([$Al(OTeF_5)_3(\eta^1\text{-}C_7H_8)$]) = −47.1 kJ mol^{-1}). This explains why the toluene adduct is not accessible directly by dissolving dimeric $[Al(OTeF_5)_3]_2$ in toluene.

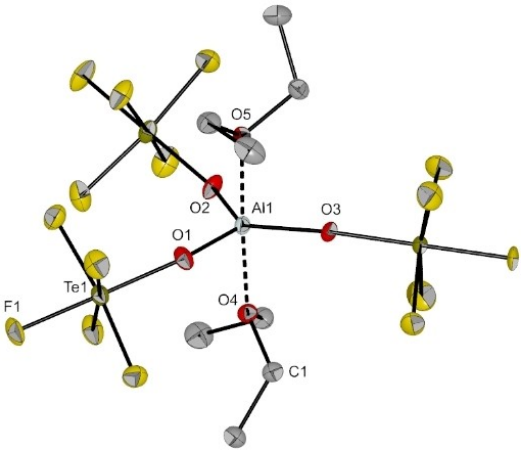

Figure 9. Molecular structure of $[Al(OTeF_5)_3(Et_2O)_2]$ in the solid state. Thermal ellipsoids set up to 50% probability. Selected bond lengths [pm] and angles [ ]: Al1-O1 176.0(2), Al1-O2 176.4(2), Al1-O3 174.8(2), Al1-O4 195.7(2), Al1-O5 197.1(3), O1-Al1-O2 119.82(12), O1-Al1-O3 116.90(13), O2-Al1-O3 123.27(13).

Reactivity of solvent adducts

From the computational study we know that the adducts $[Al(OTeF_5)_3(SO_2ClF)_2]$ and $[Al(OTeF_5)_3(PhF)_2]$ still remain very strong Lewis acids. Therefore, they were treated with different reactants, including stronger Lewis bases such as the phosphine oxide $OPEt_3$ and diethyl ether. Additionally, reactions with chloride sources were conducted, including the salt $[PPh_4]Cl$ and trityl chloride, CPh_3Cl (cf. Scheme 6).

In some cases, it was not possible to successfully form a solvent-adduct by just adding an excess of solvent to the neat Lewis acid $[Al(OTeF_5)_3]_2$. This problem could be circumvented by starting from weakly bound adducts. As an example, we added a small excess of diethyl ether to $[Al(OTeF_5)_3(SO_2ClF)_2]$ in SO_2ClF, resulting in the formation of the diethyl ether adduct. By slowly cooling the reaction mixture to −80 C it was possible to obtain colorless crystals of the product. The compound $[Al(OTeF_5)_3(Et_2O)_2]$ crystallizes in the triclinic space group $P\bar{1}$ (cf. Figure 9). Similar to the adducts with PhF and SO_2ClF, the complex possesses a trigonal bipyramidal coordination sphere at the Al center. The bond distances between the aluminum and the oxygen atom of Et_2O (d(Al1-O4) = 195.7(2) and d(Al1-O5) = 197.1(3) pm) are comparable to the analogue bond lengths in literature-known $[Al(OC_5F_4N)_3(Et_2O)_2]$.[11] This reflects well on the similar Lewis acidity of the two compounds.

An established method for experimentally gauging the acidity of a Lewis acid is the Gutmann-Beckett method, in which the ^{31}P NMR chemical shift of triethylphosphine oxide, $OPEt_3$, in a Lewis acid complex is analyzed in respect to free $OPEt_3$.[30] By reacting an equimolar amount of $OPEt_3$ with $[Al(OTeF_5)_3]_2$ in SO_2ClF it was possible to obtain the tetrahedral complex $[Al(OTeF_5)_3OPEt_3]$. Note that any excess of the phosphine will lead to multiple coordination to the Al center and therefore result in ambiguous signals in the corresponding NMR spectra. The ^{31}P NMR of this compound gave a signal at 83.9 ppm. Compared to free $OPEt_3$ (δ in CD_2Cl_2: 50 ppm) this resonance is shifted by 33.9 ppm and clearly surpasses other aluminum based Lewis superacids such as $Al(C_6F_5)_3$ ($\Delta\delta$: 26.0 ppm)[31] and $Al[OC(C_6F_5)_3]_3$ ($\Delta\delta$: 23.9 ppm).[12] This high value is also in line with the calculated FIA of $Al(OTeF_5)_3$. Therefore, this compound combines both, a high global (according to FIA) and effective (according to GB method) Lewis acidity.[32]

By cooling a concentrated solution of $[Al(OTeF_5)_3OPEt_3]$ in SO_2ClF colorless crystals were obtained. The compound $[Al(OTeF_5)_3OPEt_3]$ crystallizes in the orthorhombic space group

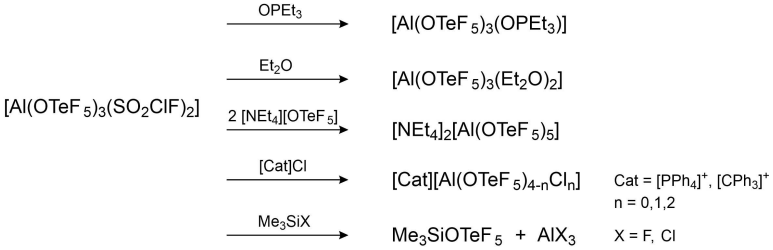

Scheme 6. Reactions of solvent adducts of $Al(OTeF_5)_3$ with different substrates.

© 2022 The Authors. Chemistry - A European Journal published by Wiley-VCH GmbH

Chemistry–A European Journal
Research Article
doi.org/10.1002/chem.202201958
Chemistry Europe
European Chemical Societies Publishing

Pbca (cf. Figure 10). The complex has a distorted tetrahedral coordination sphere and the Al–O bond lengths of the pentafluoroorthotellurate groups range between 173.3(3) and 174.1(3) pm and are comparable to the Al–O bonds in the tetrahedral complex $[Al(OTeF_5)_3(\eta^1\text{-}C_7H_8)]$. Interestingly, the Al–O bond length of the $OPEt_3$ moiety is the shortest with 171.3(3) pm, which indicates a strong interaction of the Lewis basic $OPEt_3$ with the Al center.

To further validate the high fluoride ion affinity of these solvent adducts, $[Al(OTeF_5)_3(SO_2ClF)_2]$ was reacted with the salt $[PPh_4][SbF_6]$ in SO_2ClF aiming to abstract one fluoride atom of the anion $[SbF_6]^-$. Upon addition of the phosphonium salt, the precipitation of a brown solid was observed. Analysis by NMR spectroscopy reveals the formation of the salt $[PPh_4][Al(OTeF_5)_4]$ and small amounts of $HOTeF_5$. This outcome can be rationalized by the successful initial abstraction of a fluoride from $[SbF_6]^-$, followed by ligand scrambling which leads to the formation of the anion $[Al(OTeF_5)_4]^-$ and precipitation of presumably insoluble AlF_3. Additionally, side reactions of SbF_5 with the cation led to the formation of HF which then further reacts with $[Al(OTeF_5)_4]^-$ to $HOTeF_5$. This explains why no signals of SbF_5 could be detected in the ^{19}F NMR spectrum.

By adding equimolar amounts of $[NEt_4]OTeF_5$ to a solution of $[Al(OTeF_5)_3(SO_2ClF)_2]$ in SO_2ClF it is possible to form the already known anion $[Al(OTeF_5)_4]^-$. Interestingly, increasing the amount of $[NEt_4][OTeF_5]$ leads to a further coordination of $OTeF_5$ groups to the central Al atom. Therefore, by adding a two-fold excess of the ammonium salt gave the di-anion $[Al(OTeF_5)_5]^{2-}$, which could be analyzed by NMR and vibrational spectroscopy. The solubility of this compound is very limited. Furthermore, we succeeded in the crystallization of $[NEt_4]_2[Al(OTeF_5)_5]$ by forming this species on an alternative route (see Supporting Information).

The compound $[NEt_4]_2[Al(OTeF_5)_5]$ crystallizes in the monoclinic spacegroup $P2_1/c$ (cf. Figure 11). The anion possesses a distorted trigonal bipyramidal coordination sphere at the Al center. The average Al–O bond distances of the axial teflate ligands are with 185.7 ppm slightly elongated when compared to the equatorial Al–O distances (average *d*(Al–O): 179.6 pm).

Addition of the phosphonium salt $[PPh_4]Cl$ to a solution of $[Al(OTeF_5)_3(PhF)_2]$ in fluorobenzene led to the formation of the mixed aluminate salts $[Al(OTeF_5)_{4-n}Cl_n]^-$ ($n=0,1,2,3$). The ^{27}Al NMR spectrum of this reaction shows three sharp signals at 80.5, 65.1, and 47.6 ppm, corresponding to the $[Al(OTeF_5)_2Cl_2]^-$, $[Al(OTeF_5)_3Cl]^-$, and $[Al(OTeF_5)_4]^-$ ions.[14] These resonances are flanked by ^{125}Te satellites of the corresponding isotopologues. In the ^{19}F NMR spectrum three AB_4 patterns are observed, which are assigned to the chloroaluminates by their integral ratio.

Treating the adduct $[Al(OTeF_5)_3(SO_2ClF)_2]$ with trityl chloride CPh_3Cl in SO_2ClF immediately yields an intense yellow solution, already indicating the formation of the carbocation $[CPh_3]^+$. Analysis by NMR spectroscopy shows beside the formation of the desired cation again a mixture of anions $[Al(OTeF_5)_{4-n}Cl_n]^-$ ($n=0,1,2,3$) as mentioned above (more details in Supporting Information). A similar ligand scrambling of the anion was reported by Riddlestone et al. when they treated the Lewis acid $Al(OC_5F_4N)_3$ with trityl chloride.[11]

In an attempt to obtain halogen-bridged adducts of the form $[Al(OTeF_5)_3(Me_3SiF)]$ and $[Al(OTeF_5)_3(Me_3SiCl)]$[33] in analogy to the literature-known $[Al\{OC(CF_3)_3\}_3(Me_3SiF)]$ and $[Al\{OC(CF_3)_3\}_3(Me_3SiCl)]$,[15] we treated $[Al(OTeF_5)_3(SO_2ClF)_2]$ with the respective trimethylsilyl halides. Instead of the desired reaction,

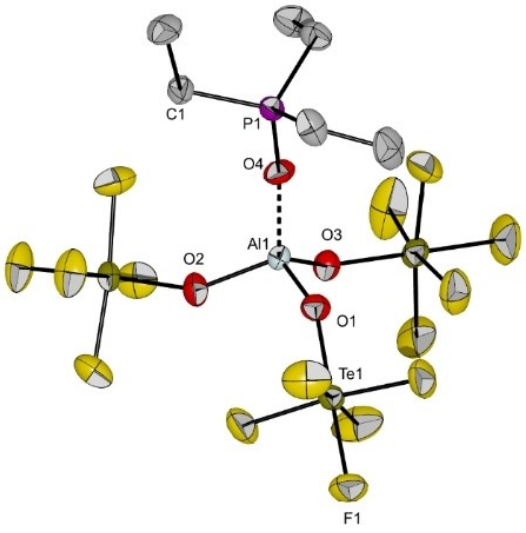

Figure 10. Molecular structure of $[Al(OTeF_5)_3(OPEt_3)]$ in the solid state. Thermal ellipsoids set up to 50% probability. Selected bond length [pm] and angles [ ]: Al1-O1 174.1(3), Al1-O2 173.3(3), Al1-O3 173.6(3), Al1-O4 171.3(3), P1-O4 153.2(3), O1-Al1-O2 108.16(14), O1-Al1-O3 111.56(13), O1-Al1-O4 106.78(14), O2-Al1-O3 106.97(15), O2-Al1-O4 113.13(15), O3-Al1-O4 110.28(14), Al1-O4-P1 159.9(2).

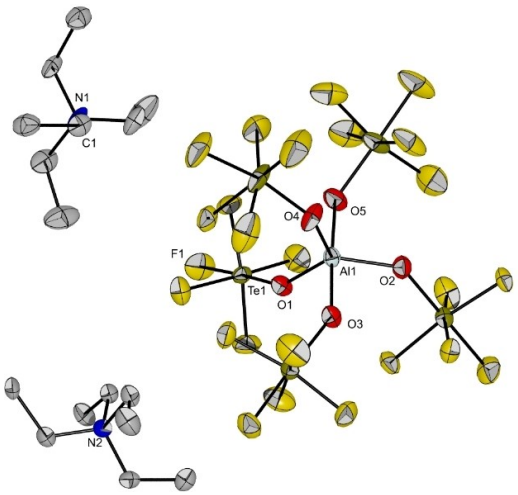

Figure 11. Molecular structure of $[NEt_4]_2[Al(OTeF_5)_5]$ in the solid state. Thermal ellipsoids set up to 50% probability. Selected bond length [pm] and angles [ ]: Al1-O1 178.6(4), Al1-O2 180.4(4), Al1-O3 186.7(4), Al1-O4 179.7(4), Al1-O5 184.6(4), O1-Al1-O2 125.3(2), O1-Al1-O4 118.6(2), O2-Al1-O4 115.9(2), O3-Al1-O5 176.7(2).

© 2022 The Authors. Chemistry - A European Journal published by Wiley-VCH GmbH

Chemistry–A European Journal | Research Article
doi.org/10.1002/chem.202201958
Chemistry Europe
European Chemical Societies Publishing

the formation of the species $Me_3SiOTeF_5$ is observed in both cases by NMR spectroscopy.[34] Moreover, in the reaction of $[Al(OTeF_5)_3(SO_2ClF)_2]$ with Me_3SiCl the formation of $AlCl_3$ is observed in the ^{27}Al NMR spectrum, while in the case of Me_3SiF a colorless, insoluble solid precipitates, which is likely insoluble AlF_3. Subsequently, a substitution of the $-OTeF_5$ groups by the halogen atom of the trimethylsilyl halides takes place. This is due to two reasons: The high Lewis acidity and the steric accessibility of the Al atom in $[Al(OTeF_5)_3(SO_2ClF)_2]$ allow a dynamic ligand exchange. Further, the formation of $Me_3SiOTeF_5$ and AlF_3 are thermodynamically favored and therefore drive the reaction.

Conclusion

In this work we report the improved synthesis of the Lewis superacid $Al(OTeF_5)_3$ in its neat dimeric form in gram-scale, as well as the synthesis and characterization of a variety of solvent adducts. These range from octahedral complexes with strong donor molecules to extremely weakly bound tetrahedral complexes. Theoretical calculations on the complexation energies and fluoride ion affinities of these adducts show that, depending on the solvent, the reactivity of the Lewis acid can be controlled, while a very high acidity is retained. Experimental validation of its Lewis acidity by the Gutmann Beckett method and fluoride abstraction from a hexafluoroantimonate salt confirm the Lewis superacidity of $Al(OTeF_5)_3$. As expected, fluoride and chloride abstractions can be easily realized with this species, but the accessibility of the aluminum center can also lead to ligand scrambling. This allows $Al(OTeF_5)_3$ and its solvent-adducts to be used in the future whenever an extreme high fluoride ion affinity is needed, a recent example being the successful synthesis of the perfluorinated trityl cation.[35]

Experimental Section

All preparative work was carried out using standard Schlenk techniques. Glassware was greased with Triboflon III. The pentafluoroorthotelluric acid $HOTeF_5$ was prepared as described elsewhere.[36] All solid materials were handled inside a glove box with an atmosphere of dry argon ($O2 < 0.5$ ppm, $H2O < 0.5$ ppm). All solvents were freshly dried with CaH_2 before use and stored on molecular sieve. $HSiEt_3$, $FSiMe_3$ and $ClSiMe_3$ were degassed prior to use and CPh_3Cl was dried in dynamic vacuum overnight and stored in a dry argon box. Raman spectra were recorded on a Bruker MultiRAM II equipped with a low-temperature Ge detector (1064 nm, 50–100 mW, resolution 4 cm^{-1}). IR spectra were measured on a Bruker ALPHA FTIR spectrometer equipped with a diamond ATR attachment in a glove box filled with argon (resolution 4 cm^{-1}). NMR spectra were recorded on a JEOL 400 MHz ECS or ECZ spectrometer. All reported chemical shifts were referenced to the Ξ values given in IUPAC recommendations of 2008 using the ^2H signal of the deuterated solvent as internal reference.[37] Chemical shifts and coupling constants of ^{19}F NMR spectra are given as simulated by *gNMR*.[38] Crystal data were collected with MoK_α radiation on a Bruker D8 Venture diffractometer with a CMOS area detector. Single crystals were picked at −40 C under nitrogen atmosphere and mounted on a 0.15 mm Micromount using perfluoroether oil. The structures were solved with the *ShelXT*[39] structure solution program using intrinsic phasing and refined with the *ShelXL*[40] refinement package using least squares on weighted F2 values for all reflections using OLEX2.[41] Deposition Number(s) 2165632 (for $[Al(OTeF_5)_2Me]_2$), 2165805 (for $[Al(OTeF_5)_3(PhCN)_3]$), 2165786 (for $[Al(OTeF_5)_2(bipy)_2]$/$[Al(OTeF_5)_4(bipy)]$), 2161784 (for $[Al(OTeF_5)_3(PhF)_2]$), 2161790 (for $[Al(OTeF_5)_3(SO_2ClF)_2]$), 2165797 (for $[Al(OTeF_5)_3(\eta^1\text{-}C_7H_8)]$), 2165785 (for $[Al(OTeF_5)_3(OEt_2)_2]$), 2167629 (for $[NEt_4]_2[Al(OTeF_5)_5]$), 2170700 (for $[Al(OTeF_5)_3(OPEt_3)]$) contain(s) the supplementary crystallographic data for this paper. These data are provided free of charge by the joint Cambridge Crystallographic Data Centre and Fachinformationszentrum Karlsruhe Access Structures service. The *Turbomole* program[42] was used to perform calculations at the unrestricted Kohn-Sham DFT level, using the BP86 or B3LYP hybrid functional[43] (with RI[44]) in conjunction with basis sets def-SV(P) and def2-TZVPP.[45] Minima on potential energy surfaces were characterized by normal mode analysis. Thermochemical data is provided without counterpoise correction but including zero-point energy correction as obtained from harmonic vibrational frequencies.

$[AlMe(OTeF_5)_2]_2$: Pentafluoroorthotelluric acid, $HOTeF_5$, (726 mg, 3.00 mmol) was condensed onto a frozen solution of $AlMe_3$ (72 mg, 1.00 mmol) in *n*-pentane at −196 C. After connection of a bubbler, the mixture was slowly warmed to −30 C resulting in the formation of a colorless precipitate under gas evolution. Evaporation of all volatiles led to the isolation of a colorless powder (503 mg, 96%). The solid compound can be stored at −30 C without visible decomposition. Crystals suitable for SC-XRD were grown by slowly cooling a concentrated solution in *ortho*-difluorobenzene to −40 C. ^1H NMR (400 MHz, SO_2ClF, ext. [D6]acetone, −40 C): $\delta = -0.01$ (s, Al-CH_3) ppm. ^{19}F NMR (377 MHz, SO_2ClF, ext. [D6]acetone, −40 C): $\delta = -39.3$ (m, 1F, F_a $^2J_{FF} = 187$ Hz, bridging $-OTeF_5$), −40.5 (m, 1F, F_a, $^2J_{FF} = 185$ Hz, terminal $-OTeF_5$), −45.3 (m, 4F, F_b, terminal $-OTeF_5$), −45.9 (m, 4F, F_b, bridging $-OTeF_5$) ppm. ^{27}Al NMR (104 MHz, SO_2ClF, ext. [D6]acetone, −40 C): $\delta = 48.2$ (br, s, FWHM = 520 Hz). IR (ATR, 25 C): $\tilde{\nu} = 1452$ (vw), 1220 (w), 977 (m), 868 (w), 736 (s), 709 (vs), 692 (vs), 593 (m) cm^{-1}. FT-Raman (25 C): $\tilde{\nu} = 2977$ (w), 2920 (s), 1220 (m), 986 (w), 850 (w), 723 (vs), 689 (m), 675 (s), 664 (m), 649 (m), 357 (m), 330 (m), 309 (m), 275 (m), 229 (w), 215 (w), 134 (s) cm^{-1}.

Improved synthesis of $[Al(OTeF_5)_3]_2$: An excess of $HOTeF_5$ (1234 mg, 5.10 mmol) was condensed onto a frozen solution of $AlMe_3$ (105 mg, 1.46 mmol) in n-pentane at −196 C. The mixture was warmed to −30 C and vigorously stirred until the gas evolution ceased. A colorless solid precipitated. Afterwards, the solution was further heated to room temperature and stirred for an additional 20 minutes, which gave rise to a continued formation of gas. Subsequently, all volatiles were pumped off leading to the isolation of a colorless powder (1063 mg, 98%). IR (ATR, 25 C): $\tilde{\nu} =$ 1009 (m), 976 (m), 860 (vw), 746 (m), 704 (vs), 670 (s), 656 (s), 571 (w) cm^{-1}. FT-Raman (25 C): $\tilde{\nu} = 1023$ (vw), 731 (m), 706 (s), 688 (vs), 664 (s), 613 (w), 379 (w), 327 (m), 311 (m), 136 (m) cm^{-1}.

$[Al(OTeF_5)_3(MeCN)_3]$: $AlEt_3$ (148 mg, 1.3 mmol) was dissolved in 10 mL of MeCN. Three equivalents $HOTeF_5$ (944 mg, 3.9 mmol) were condensed onto the frozen solution at −196 C. Warming up the mixture to room temperature under constant stirring led to a gas evolution. After 30 minutes, all volatiles were removed under reduced pressure until a colorless powder was obtained (1.12 g, 99%). ^1H NMR (400 MHz, CD_3CN, 22 C): $\delta = 2.0$ (s, MeCN) ppm. ^{19}F NMR (377 MHz, CD_3CN, 22 C): $\delta = -31.7$ (m, 1F, F_a, $^2J_{FF} = 185$ Hz, $[Al(OTeF_5)_4(MeCN)_2]^-$, 20%), −32.7 (m, 1F, F_a, $^2J_{FF} = 185$ Hz, $[Al(OTeF_5)_2(MeCN)_4]^+$, 10%), −33.1 (m, 1F, F_a, $^2J_{FF} = 185$ Hz, $[Al(OTeF_5)_3(MeCN)_3]$), 100%), −45.5 (m, 4F, F_b, $[Al(OTeF_5)_4(MeCN)_2]^-$), −45.75 (m, 4F, F_b, $[Al(OTeF_5)_2(MeCN)_4]^+$), −45.8 (m, 4F, F_b, $[Al(OTeF_5)_3(MeCN)_3]$) ppm. ^{27}Al NMR (104 MHz, CD_3CN, 22 C): $\delta =$

© 2022 The Authors. Chemistry - A European Journal published by Wiley-VCH GmbH

Chemistry–A European Journal | Research Article doi.org/10.1002/chem.202201958 | Chemistry Europe European Chemical Societies Publishing

−11.7 (br, $[Al(OTeF_5)_4(MeCN)_2]^-$), −16.4 (br, $[Al(OTeF_5)_3(MeCN)_3]$), −21.6 (br, $[Al(OTeF_5)_2(MeCN)_4]^+$) ppm. IR (ATR, 25 C): $\tilde{\nu}$ = 3019 (vw), 2950 (vw), 2339 (w), 2312 (w), 1418 (vw), 1371 (vw), 1035 (vw), 950 (m), 904 (m), 678 (vs), 626 (w), 553 (w), 467 (s), 448 (s) cm^{-1}. FT-Raman (25 C): $\tilde{\nu}$ = 3019 (vw), 2951 (vs), 2342 (s), 2314 (m), 1422 (vw), 1374 (w), 962 (w), 684 (s), 628 (m), 433 (m), 340 (w), 299 (w) cm^{-1}.

$[Al(OTeF_5)_3(PhCN)_3]$: $AlEt_3$ (200 mg, 1.75 mmol) was dissolved in 10 mL of PhCN. Three equivalents $HOTeF_5$ (1270 mg, 5.3 mmol) were condensed onto the frozen solution at −196 C. Warming up the mixture to room temperature under constant stirring led to a gas evolution. The obtained colorless solution was concentrated under reduced pressure until a colorless powder was obtained (1.78 g, 95%). In PhCN: ^1H NMR (400 MHz, PhCN, ext. [D6]acetone, 22 C): δ = 7.38 (m, PhCN) ppm. ^{19}F NMR (377 MHz, PhCN, ext. [D6]acetone, 22 C): δ = −29.4 (m, 1F, F_a, $^2J_{FF}$ = 188 Hz, $[Al(OTeF_5)_3(PhCN)_3]$, 50%), −30.2 (m, 1F, F_a, $^2J_{FF}$ = 188 Hz, $[Al(OTeF_5)_4(PhCN)_2]^-$, 100%), −30.6 (m, 1F, F_a, $^2J_{FF}$ = 188 Hz, $[Al(OTeF_5)_2(PhCN)_4]^+$), 50%), −43.4 (m, 4F, F_b, $[Al(OTeF_5)_3(PhCN)_3]$), −43.5 (m, 4F, F_b, $[Al(OTeF_5)_4(PhCN)_2]^-$), −43.6 (m, 4F, F_b, $[Al(OTeF_5)_2(PhCN)_4]^+$) ppm. ^{27}Al NMR (104 MHz, PhCN, ext. [D6]acetone, 22 C): δ = −13.0 (br, FWHM = 1720 Hz) ppm. In CD_2Cl_2: ^1H NMR (400 MHz, CD_2Cl_2, 22 C): δ = 7.69 (br, m, PhCN) ppm. ^{19}F NMR (377 MHz, CD_2Cl_2, 22 C): δ = −33.6 (m, 1F, F_a, $^2J_{FF}$ = 189 Hz, $[Al(OTeF_5)_2(PhCN)_4]^+$, 34%), −38.7 (m, 1F, F_a, $^2J_{FF}$ = 188 Hz, $[Al(OTeF_5)_4]^-$, 68%), −38.8 (m, 1F, F_a, $^2J_{FF}$ = 188 Hz, $[Al(OTeF_5)_3(PhCN)_3]$), 100%), −44.3 (m, 4F, F_b, $[Al(OTeF_5)_2(PhCN)_4]^+$), −45.0 (m, 4F, F_b, $[Al(OTeF_5)_4]^-$), −46.0 (m, 4F, F_b, $[Al(OTeF_5)_3(PhCN)_3]$) ppm. ^{27}Al NMR (104 MHz, CD_2Cl_2, 22 C): δ = 46.8 (s, $[Al(OTeF_5)_4]^-$), −9.3 (br, s, $[Al(OTeF_5)_3(PhCN)_3]$), −17 (br, s, $[Al(OTeF_5)_2(PhCN)_4]^+$) ppm. IR (ATR, 25 C): $\tilde{\nu}$ = 3069 (vw), 3039 (vw), 2284 (m), 1597 (w), 1489 (w), 1450 (w), 942 (m), 902 (m), 756 (m), 676 (vs), 626 (m), 560 (m), 516 (m), 455 (s) cm^{-1}. FT-Raman (25 C): $\tilde{\nu}$ = 3078 (m), 2293 (vs), 2231 (m), 1598 (s), 1206 (w), 1183 (w), 988 (s), 774 (vw), 685 (m), 627 (m), 603 (w), 464 (m) cm^{-1}. Crystals suitable for SC-XRD were grown by cooling a concentrated solution in PhCN slowly to −40 C.

$[Al(OTeF_5)_3(SO_2ClF)_2]$: In a Schlenktube with a greaseless Teflon valve, an excess of SO_2ClF (~2 mL) was condensed onto solid $[Al(OTeF_5)_3]_2$ (104 mg, 0.07 mmol). By subsequent warming of this mixture to −30 C a colorless, clear solution was obtained. Removal of all volatiles at 0 C led to the isolation of a colorless powder (124 mg, 91%). NMR samples were prepared by directly dissolving $[Al(OTeF_5)_3]_2$ in SO_2ClF in a J. Young NMR tube. ^{19}F NMR (377 MHz, SO_2ClF, ext. [D6]acetone, 22 C): δ = −41.5 (m, 1F, F_a, $^2J_{FF}$ = 187 Hz), −45.9 (m, 4F, F_b) ppm. ^{27}Al NMR (104 MHz, SO_2ClF, ext. [D6]acetone, 22 C): δ = 34 (br, s, FWHM = 2200 Hz) ppm. IR (ATR, 25 C): $\tilde{\nu}$ = 1436 (w), 1188 (w), 969 (m), 890 (w), 853 (w), 745 (m), 701 (vs), 663 (s), 572 (m), 476 (w), 447 (w) cm^{-1}. FT-Raman (25 C): $\tilde{\nu}$ = 1428 (vw), 1182 (vw), 703 (vs), 658 (s), 446 (s), 329 (s), 307 (s), 243 (m), 136 (m) cm^{-1}. Crystals suitable for SC-XRD were grown by cooling a concentrated solution in SO_2ClF slowly to −80 C.

$[Al(OTeF_5)_3(PhF)_2]$: Treatment of solid $[Al(OTeF_5)_3]_2$ (50 mg, 0.03 mmol) at −30 C with 1 mL of PhF and subsequently stirring the mixture led to the slow dissolution of the solid material and formation of a green solution. Warming the solution to 0 C facilitates the solution process. Evaporation of the solvents led to a greenish powder, which decomposes at room temperature to a dark, oily substance. NMR samples were prepared by directly dissolving $[Al(OTeF_5)_3]_2$ in PhF in a J. Young NMR tube. ^1H NMR (400 MHz, C_6H_5F, ext. [D6]acetone, −40 C): δ = 6.7 (m, 5 H, C_6H_5F) ppm. ^{19}F NMR (377 MHz, C_6H_5F, ext. [D6]acetone, −40 C): δ = −40.7 (m, 1F, F_a, $^2J_{FF}$ = 191 Hz), −46.1 (m, 4F, F_b) ppm. ^{27}Al NMR (104 MHz, C_6H_5F, ext. [D6]acetone, −40 C): δ = 46.1 (br, s) ppm. Crystals suitable for SC-XRD were grown by cooling a concentrated solution in PhF slowly to −40 C.

$[Al(OTeF_5)_3(OPEt_3)]$: To a cooled solution of $[Al(OTeF_5)_3]_2$ (104 mg, 0.13 mmol) in SO_2ClF at −30 C solid $OPEt_3$ (17 mg, 0.84 mmol) was added under an argon stream. Stirring of the mixture led to a slightly yellow solution and crystals were grown by concentrating the mixture and subsequently cooling to −80 C. Removing all volatiles under reduced pressure gave a colorless powder, which was washed with *n*-pentane and dried again (109 mg, 89%). ^1H NMR (400 MHz, CD_2Cl, 22 C): δ = 2.13 (m, 6H, $-OPEt_3$), 1.31 (m, 9H, $-OPEt_3$) ppm. ^{19}F NMR (377 MHz, CD_2Cl, 22 C): δ = −38.7 (m, 1F, F_a, $^2J_{FF}$ = 188.2 Hz), −45.3 (m, 4F, F_b) ppm. ^{27}Al NMR (104 MHz, CD_2Cl, 22 C): δ = 46.3 (s, $[Al(OTeF_5)_3(OPEt_3)]$) ppm. $^{31}P\{^1H\}$ NMR (162 MHz, CD_2Cl, 22 C): δ = 83.9 (s, $-OPEt_3$) ppm. IR (ATR, 25 C): $\tilde{\nu}$ = 2994 (vw), 2956 (vw), 2922 (vw), 2894 (vw), 1460 (w), 1409 (w), 1277 (w), 1139 (m), 1048 (w), 928 (s), 793 (m), 783 (m), 691 (vs), 651 (s), 442 (m) cm^{-1}. FT-Raman (25 C): $\tilde{\nu}$ = 2997 (m), 2957 (s), 2925 (s), 2895 (m), 2765 (vw), 1470 (w), 1410 (w), 1235 (vw), 1043 (w), 985 (w), 794 (vw), 696 (vs), 648 (vs), 551 (w), 433 (m), 332 (s), 302 (m), 235 (m), 140 (m) cm^{-1}.

$[Al(OTeF_5)_3(Et_2O)_2]$: To a cooled solution of $[Al(OTeF_5)_3]_2$ (120 mg, 0.08 mmol) in SO_2ClF at −30 C a slight excess of Et_2O (0.02 mL, 0.20 mmol) was added under an argon stream. Stirring of the mixture led to a dark colored solution. Concentrating the mixture under reduced pressure and subsequent cooling to −80 C yielded the formation of colorless crystals suitable for SC-XRD measurement. Attempts to isolate the crystals by removing all volatiles led to decomposition of the sample.

$[Al(OTeF_5)_3(\eta^1\text{-}C_7H_8)]$: $AlEt_3$ (93 mg, 0.82 mmol) was dissolved in 2 mL of toluene, the solution was frozen at −196 C and $HOTeF_5$ (593 mg, 2.45 mmol) was condensed on top. Warming the mixture to −30 C under stirring gave a yellow/orange colored, biphasic solution. After stirring for 10 minutes the mixture was cooled to −50 C and a slight excess of $HSiEt_3$ (0.15 mL, 1.00 mmol) was added via a syringe. A gas evolution and the decolorization of the solution was observed. Warming the solution above −40 C led to decomposition. ^1H NMR (400 MHz, C_7H_8, ext. [D6]acetone, −60 C): δ = 0.63 (t, 9H, $^2J_{HH}$ = 8 Hz, $-CH_3$, $Et_3SiOTeF_5$), 0.28 (quart, 6H, $-CH_2-$, $Et_3SiOTeF_5$) ppm. ^{19}F NMR (377 MHz, C_7H_8, ext. [D6]acetone, −60 C): δ = −37.5 (m, 1F, F_a, $^2J_{FF}$ = 191 Hz, $Et_3SiOTeF_5$, 33%), −38.6 (m, 1F, F_a, $^2J_{FF}$ = 191 Hz, $[Al(OTeF_5)_3(tol)]$, 100%), −42.9 (m, 4F, F_b, $Et_3SiOTeF_5$), −44.1 (m, 4F, F_b, $[Al(OTeF_5)_3(tol)]$) ppm. ^{27}Al NMR (104 MHz, C_7H_8, ext. [D6]acetone, −60 C): δ = 48.4 (br, FWHM = 237 Hz) ppm. Crystals suitable for SC-XRD were grown within 2 days by cooling a concentrated solution slowly to −80 C.

Formation of $[C(C_6H_5)_3][Al(OTeF_5)_{4-n}Cl_n]$ (n = 0,1,2,3): To a cooled solution of $[Al(OTeF_5)_3]_2$ (66 mg, 0.045 mmol) in SO_2ClF at −30 C a stoichiometric amount of $C(C_6H_5)_3Cl$ (24 mg, 0.09 mmol) was added under an argon stream, which resulted in the formation of a clear, bright yellow solution. The mixture was brought to room temperature and stirred for 15 minutes. Subsequently, all volatiles were removed under reduced pressure. The remaining yellow solid was washed with *n*-pentane and dried again, resulting in a yellow powder (88.3 mg, 96%). ^1H NMR (400 MHz, CD_2Cl_2, 22 C): δ = 8.30 (br, 3H, *para*-H), 7.92 (br, 6H, *meta*-H), 7.70 (br, 6H, *ortho*-H) ppm. ^{19}F NMR (377 MHz, CD_2Cl_2, 22 C): δ = −36.8 (m, 1F, F_a, $^2J_{FF}$ = 189 Hz, $[AlCl_2(OTeF_5)_2]^-$, 11%), −37.7 (m, 1F, F_a, $^2J_{FF}$ = 190 Hz, $[AlCl(OTeF_5)_3]^-$, 84%), −38.0 (m, 1F, F_a, $^2J_{FF}$ = 189 Hz, $[AlCl_3(OTeF_5)]^-$, 1%), −38.6 (m, 1F, F_a, $^2J_{FF}$ = 191 Hz, $[Al(OTeF_5)_4]^-$, 100%), −44.7 (m, 4F, F_b, $[AlCl_2(OTeF_5)_2]^-$), −45.4 (m, 4F, F_b, $[AlCl(OTeF_5)_3]^-$), −45.6 (m, 4F, F_b, $[AlCl_3(OTeF_5)]^-$), −45.9 (m, 4F, F_b, $[Al(OTeF_5)_4]^-$) ppm. ^{27}Al NMR (104 MHz, CD_2Cl_2, 22 C): δ = 92.8 (s, $[Al(OTeF_5)Cl_3]^-$), 79.5 (s, $[Al(OTeF_5)_2Cl_2]^-$; d, $[Al(OTeF_5)(O^{125}TeF_5)Cl_2]^-$, $^2J(^{27}Al,^{125}Te)$ = 20 Hz), 64.1 (s, $[Al(OTeF_5)_3Cl]^-$; d, $[Al(OTeF_5)_2(O^{125}TeF_5)Cl]^-$, $^2J(^{27}Al,^{125}Te)$ = 43 Hz), 47.0 (s, $[Al(OTeF_5)_4]^-$; d, $[Al(OTeF_5)_3(O^{125}TeF_5)]^-$, $^2J(^{27}Al,^{125}Te)$ = 72 Hz) ppm. IR (ATR, 25 C): $\tilde{\nu}$ = 1621 (vw), 1579 (s), 1483 (m), 1450 (m), 1355 (s), 1295 (m), 1187 (m), 1171 (w), 995 (m), 980 (m), 926 (s),

© 2022 The Authors. Chemistry - A European Journal published by Wiley-VCH GmbH

Chemistry–A European Journal | Research Article doi.org/10.1002/chem.202201958 | Chemistry Europe European Chemical Societies Publishing

843 (w), 809 (w), 770 (w), 686 (vs), 622 (s), 607 (s), 536 (s), 467 (m), 425 (w), 403 (m) cm^{-1}. FT-Raman (25 C): $\tilde{\nu}$ = 3071 (w), 1597 (s), 1583 (vs), 1485 (m), 1357 (s), 1298 (w), 1186 (m), 1174 (w), 1027 (w), 998 (m), 916 (w), 697 (w), 623 (w), 468 (w), 405 (m), 287 (s), 143 (m) cm^{-1}.

Formation of $[PPh_4][Al(OTeF_5)_{4-n}Cl_n]$ (n = 0,1,2,3): In a J. Young NMR tube, a cooled solution of $[Al(OTeF_5)_3]_2$ (100 mg, 0.07 mmol, 0.5 equiv.) in PhF at 0 C was treated with a stoichiometric amount of $[PPh_4]Cl$ (50 mg, 0.14 mmol, 1 equiv.). A colorless, clear solution formed, which was analyzed by NMR spectroscopy. Signals of the cation in the ^{1}H NMR spectrum are partly overlaid by solvent signals. ^{1}H NMR (400 MHz, C_6H_5F, ext. [D6]acetone, 22 C): δ = 7.42 (m, 4H, *para*-H, $[PPh_4]^+$) 7.26 (m, 8H, *meta*-H, $[PPh_4]^+$), 7.1–6.7 (PhF) ppm. ^{19}F NMR (377 MHz, C_6H_5F, ext. [D6]acetone, 22 C): δ = −36.1 (m, 1F, F_a, $^2J_{FF}$ = 189 Hz, $[AlCl_2(OTeF_5)_2]^-$, 5 %), −37.2 (m, 1F, F_a, $^2J_{FF}$ = 190 Hz, $[AlCl(OTeF_5)_3]^-$, 44 %), −38.2 (m, 1F, F_a, $^2J_{FF}$ = 191 Hz, $[Al(OTeF_5)_4]^-$, 100 %), −44.0 (m, 4F, F_b, $[AlCl_2(OTeF_5)_2]^-$), −44.7 (m, 4F, F_b, $[AlCl(OTeF_5)_3]^-$), −45.3 (m, 4F, F_b, $[Al(OTeF_5)_4]^-$) ppm. ^{27}Al NMR (104 MHz, C_6H_5F, ext. [D6]acetone, 22 C): δ = 80.5 (s, $[Al(OTeF_5)_2Cl_2]^-$), 65.1 (s, $[Al(OTeF_5)_3Cl]^-$), 47.6 (s, $[Al(OTeF_5)_4]^-$) ppm. ^{31}P NMR (162 MHz, C_6H_5F, ext. [D6]acetone, 22 C): δ = 23.0 (m, $[PPh_4]^+$) ppm.

$[NEt_4][OTeF_5]$: $[NEt_4]Cl$ (445 mg, 2.69 mmol, 1 equiv.) was dissolved in *o*-DFB (20 mL). The solution was cooled with liquid nitrogen and degassed. $HOTeF_5$ (659 mg, 2.75 mmol, 1 equiv.) was condensed onto the solution. A bubbler was connected to the flask and the reaction mixture was stirred at room temperature until gas formation was no longer observed. After removal of the solvent in vacuo a yellow solid was obtained (952 mg, 96 % yield). ^{1}H NMR (401 MHz, *o*-DFB, ext. [D6]acetone, 22 C): δ = 3.21 (quart, 8H, $^3J_{HH}$ = 7.3 Hz, $[N(CH_2CH_3)_4]^+$), 1.32 (tt, 12H, $^3J_{HH}$ = 7.3 Hz, J_{HN} = 1.9 Hz, $[N(CH_2CH_3)_4]^+$) ppm. ^{19}F NMR (377 MHz, *o*-DFB, ext. [D6]acetone, 22 C): δ = −28.96 (m, $1F_a$), −42.97 (m, $4F_b$) ppm. IR (ATR, 25 C): $\tilde{\nu}$ = 3000 (w), 1478 (m), 1458 (m), 1397 (m), 1183 (m), 1031 (w), 1002 (m), 864 (m), 762 (m), 674 (s), 632 (vs), 577 (s), 465z (w) cm^{-1}. This compound was already reported in literature.[46]

Formation of $[NEt_4]_2[Al(OTeF_5)_5]$: A cooled solution of $[Al(OTeF_5)_3]_2$ (100 mg, 0.07 mmol, 0.5 equiv.) in SO_2ClF at 0 C was treated with two equivalents of $[NEt_4][OTeF_5]$ (97 mg, 0.26 mmol, 2 equiv.). The mixture was stirred for 12 h which resulted in a colorless suspension formed. All volatiles were removed under reduced pressure, which gave a colorless powder (180 mg, 94 %). For crystallization, a solution of $[NEt_4][Al(OTeF_5)_4]$ in *o*-DFB was treated with equimolar amounts of $[NEt_4][OTeF_5]$ and then slowly cooled down to −40 C which resulted in the growth of colorless crystals suitable for SC-XRD. ^{1}H NMR (400 MHz, $C_6H_4F_2$, ext. [D6]acetone, 22 C): δ = 3.02 (quart., 8H, $^3J_{HH}$ = 7.3 Hz, $[N(CH_2CH_3)_4]^+$), 1.14 (m, 12H, $[N(CH_2CH_3)_4]^+$) ppm. ^{19}F NMR (377 MHz CD_2Cl_2, 22 C): δ = −45.4 (br, m, 4F, F_b, FWHM = 340 Hz), ppm. ^{27}Al NMR (104 MHz, $C_6H_4F_2$, ext. [D6]acetone, 22 C): δ = 48.7 (br, FWHM = 550 Hz) ppm. IR (ATR, 25 C): $\tilde{\nu}$ = 3003 (w), 1486 (m), 1457 (w), 1443 (w), 1396 (m), 1368 (w), 1305 (w), 1238 (w), 1173 (m), 1068 (w), 1052 (w), 999 (m), 898 (s), 783 (m), 678 (vs), 620 (m), 535 (m), 511 (m), 486 (m) cm^{-1}.

Reaction of $[Al(OTeF_5)_3(SO_2ClF)_2]$ with $[PPh_4][SbF_6]$: In a J. Young NMR tube, a cooled solution of $[Al(OTeF_5)_3]_2$ (40 mg, 0.025 mmol, 0.5 equiv.) in SO_2ClF at −30 C was treated with a stoichiometric amount of $[PPh_4][SbF_6]$ (30 mg, 0.05 mmol, 1 equiv.). The mixture was brought to room temperature and a yellowish solution together with a brown precipitate formed. The sample was analyzed by NMR spectroscopy. ^{1}H MR (400 MHz, SO_2ClF, ext. [D6]acetone, 22 C): δ = 8.34 (m, 4H, *para*-H, $[PPh_4]^+$), 8.18 (m, 8H, *meta*-H, $[PPh_4]^+$), 8.07 (m, 8H, *ortho*-H, $[PPh_4]^+$), 6.87 ($HOTeF_5$) ppm. ^{19}F NMR (377 MHz, SO_2ClF, ext. [D6]acetone, 22 C): δ = −39.5 (m, 1F, F_a, $^2J_{FF}$ = 191 Hz, $[Al(OTeF_5)_4]^-$, 100 %), −44.0 (m, 1F, F_a, $^2J_{FF}$ = 191 Hz, $HOTeF_5$, 10 %), −46.4 (m, 4F, F_b, $[Al(OTeF_5)_4]^-$), −47.8 (m, 4F, F_b, $HOTeF_5$) ppm. ^{27}Al NMR (104 MHz, SO_2ClF, ext. [D6]acetone, 22 C): δ = 47.4 (s, $[Al(OTeF_5)_4]^-$) ppm. ^{31}P NMR (162 MHz, SO_2ClF ext. [D6]acetone, 22 C): δ = 23.9 (m, $[PPh_4]^+$) ppm.

Reaction of $[Al(OTeF_5)_3(SO_2ClF)_2]$ with Me_3SiCl: In a J. Young NMR tube, a cooled solution of $[Al(OTeF_5)_3]_2$ (63 mg, 0.04 mmol) in SO_2ClF at −30 C was treated with a slight excess of trimethylsilyl chloride (13 mg, 0.12 mmol) by condensing it onto the solution. Shaking the mixture resulted in a clear, slightly yellow solution. The mixture was brought to room temperature and analyzed by NMR spectroscopy. ^{1}H NMR (400 MHz, SO_2ClF, ext. [D6]acetone, 22 C): δ = 0.88 (s, 9H, $-CH_3$, Me_3SiCl), 0.86 (m, 9H, $-CH_3$, $Me_3SiOTeF_5$) ^{19}F NMR (377 MHz, SO_2ClF, ext. [D6]acetone, 22 C): δ = −40.5 (m, 1F, F_a, $^2J_{FF}$ = 185 Hz, $Me_3SiOTeF_5$), −44.3 (m, 4F, F_b, $Me_3SiOTeF_5$) ppm. ^{29}Si NMR (80 MHz, SO_2ClF, ext. [D6]acetone, 22 C): δ = 39.1 ($Me_3SiOTeF_5$), 31.0 (s, Me_3SiCl) ppm. ^{27}Al NMR (104 MHz, SO_2ClF, ext. [D6]acetone, 22 C): δ = 91.7 (br, s, $AlCl_3$, FWHM = 910 Hz) ppm.

Reaction of $[Al(OTeF_5)_3(SO_2ClF)_2]$ with Me_3SiF: In a J. Young NMR tube, a cooled solution of $[Al(OTeF_5)_3]_2$ (50 mg, 0.03 mmol) in SO_2ClF at −30 C was treated with an excess of trimethylsilyl fluoride (11 mg, 0.12 mmol) by condensing it onto the solution. Shaking the mixture resulted in a clear colorless solution. After the mixture was brought to room temperature a colorless precipitate formed. The solution was analyzed by NMR spectroscopy. ^{1}H NMR (400 MHz, SO_2ClF, ext. [D6]acetone, 22 C): δ = 0.88 (m, 9H, $-CH_3$, $Me_3SiOTeF_5$), 0.71 (br, m, 9H, $-CH_3$, Me_3SiF) ppm. ^{19}F NMR (377 MHz, SO_2ClF, ext. [D6]acetone, 22 C): δ = −40.5 (m, 1F, F_a, $^2J_{FF}$ = 185 Hz, $Me_3SiOTeF_5$), −44.3 (m, 4F, F_b, $Me_3SiOTeF_5$), −158.0 (br, m, 1F, Me_3SiF) ppm. ^{29}Si NMR (80 MHz, SO_2ClF, ext. [D6]acetone, 22 C): δ = 39.4 (m, $Me_3SiOTeF_5$), 32.6 (br, Me_3SiF) ppm.

Acknowledgements

Funded by the Deutsche Forschungsgemeinschaft (DFG, German Research Foundation) – Project-ID 387284271 – SFB 1349. Computing time was made available by the High-Performance Computing Center at the ZEDAT, Freie Universität Berlin. Also, we would like to acknowledge the assistance of the Core Facility BioSupraMol supported by the DFG. Open Access funding enabled and organized by Projekt DEAL.

Conflict of Interest

The authors declare no conflict of interest.

Data Availability Statement

The data that support the findings of this study are available from the corresponding author upon reasonable request.

Keywords: aluminum · coordination chemistry · fluorine chemistry · Lewis superacids · pentafluoroorthotellurate

[1] G. A. Olah, G. K. Surya Prakash, R. Molnr, J. Sommer, *Superacid Chemistry*, John Wiley & Sons, Inc, Hoboken, NJ, USA, **2009**.
[2] H. Böhrer, N. Trapp, D. Himmel, M. Schleep, I. Krossing, *Dalton Trans.* **2015**, *44*, 7489.

© 2022 The Authors. Chemistry - A European Journal published by Wiley-VCH GmbH

Chemistry–A European Journal | Research Article doi.org/10.1002/chem.202201958 | Chemistry Europe European Chemical Societies Publishing

[3] H. D. B. Jenkins, H. K. Roobottom, J. Passmore, *Inorg. Chem.* **2003**, *42*, 2886.
[4] K. O. Christe, D. A. Dixon, D. McLemore, W. W. Wilson, J. A. Sheehy, J. A. Boatz, *J. Fluorine Chem.* **2000**, *101*, 151.
[5] L. O. Müller, D. Himmel, J. Stauffer, G. Steinfeld, J. Slattery, G. Santiso-Quiñones, V. Brecht, I. Krossing, *Angew. Chem. Int. Ed. Engl.* **2008**, *47*, 7659; *Angew. Chem.* **2008**, *120*, 7772.
[6] L. A. Körte, J. Schwabedissen, M. Soffner, S. Blomeyer, C. G. Reuter, Y. V. Vishnevskiy, B. Neumann, H.-G. Stammler, N. W. Mitzel, *Angew. Chem. Int. Ed. Engl.* **2017**, *56*, 8578; *Angew. Chem.* **2017**, *129*, 8701.
[7] a) J. Chen, E. Y.-X. Chen, *Dalton Trans.* **2016**, *45*, 6105; b) T. Belgardt, J. Storre, H. W. Roesky, M. Noltemeyer, H.-G. Schmidt, *Inorg. Chem.* **1995**, *34*, 3821.
[8] D. M. C. Ould, J. L. Carden, R. Page, R. L. Melen, *Inorg. Chem.* **2020**, *59*, 14891.
[9] A. Kraft, N. Trapp, D. Himmel, H. Böhrer, P. Schlüter, H. Scherer, I. Krossing, *Chem. Eur. J.* **2012**, *18*, 9371.
[10] J. F. Kögel, D. A. Sorokin, A. Khvorost, M. Scott, K. Harms, D. Himmel, I. Krossing, J. Sundermeyer, *Chem. Sci.* **2018**, *9*, 245.
[11] I. M. Riddlestone, S. Keller, F. Kirschenmann, M. Schorpp, I. Krossing, *Eur. J. Inorg. Chem.* **2019**, *2019*, 59.
[12] J. F. Kögel, A. Y. Timoshkin, A. Schröder, E. Lork, J. Beckmann, *Chem. Sci.* **2018**, *9*, 8178.
[13] L. Greb, *Chem. Eur. J.* **2018**, *24*, 17881.
[14] A. Wiesner, T. W. Gries, S. Steinhauer, H. Beckers, S. Riedel, *Angew. Chem. Int. Ed. Engl.* **2017**, *56*, 8263; *Angew. Chem.* **2017**, *129*, 8375.
[15] A. Martens, O. Petersen, H. Scherer, I. Riddlestone, I. Krossing, *Organometallics* **2018**, *37*, 706.
[16] R. G. Vranka, E. L. Amma, *J. Am. Chem. Soc.* **1967**, *89*, 3121.
[17] A. Wiesner, L. Fischer, S. Steinhauer, H. Beckers, S. Riedel, *Chem. Eur. J.* **2019**, *25*, 10441.
[18] J. Mason, *Multinuclear NMR*, Springer US, Boston, MA, **1987**.
[19] a) K. Knabel, H. Nöth, *Z. Naturforsch. B* **2005**, *60*, 1027; b) N. C. Means, C. M. Means, S. G. Bott, J. L. Atwood, *Inorg. Chem.* **1987**, *26*, 1466.
[20] K. F. Hoffmann, A. Wiesner, N. Subat, S. Steinhauer, S. Riedel, *Z. Anorg. Allg. Chem.* **2018**, *644*, 1344.
[21] F. O'Donnell, D. Turnbull, S. D. Wetmore, M. Gerken, *Chem. Eur. J.* **2021**, *27*, 16334.
[22] G. Portalone, G. Schultz, A. Domenicano, I. Hargittai, *J. Mol. Struct.* **1984**, *118*, 53.
[23] a) T. Birchall, R. J. Gillespie, *Spectrochim. Acta* **1966**, *22*, 681; b) R. J. Gillespie, E. A. Robinson, *Spectrochim. Acta* **1962**, *18*, 1473.
[24] a) P. Ulferts, K. Seppelt, *Z. Anorg. Allg. Chem.* **2004**, *630*, 1589; b) H. P. A. Mercier, M. D. Moran, J. C. P. Sanders, G. J. Schrobilgen, R. J. Suontamo, *Inorg. Chem.* **2005**, *44*, 49.
[25] G. S. Hair, A. H. Cowley, R. A. Jones, B. G. McBurnett, A. Voigt, *J. Am. Chem. Soc.* **1999**, *121*, 4922.
[26] A. Wiesner, S. Steinhauer, H. Beckers, C. Müller, S. Riedel, *Chem. Sci.* **2018**, *9*, 7169.
[27] J. B. Lambert, S. Zhang, C. L. Stern, J. C. Huffman, *Science* **1993**, *260*, 1917.
[28] P. Erdmann, J. Leitner, J. Schwarz, L. Greb, *ChemPhysChem* **2020**, *21*, 987.
[29] a) V. Gutmann, *Electrochim. Acta* **1976**, *21*, 661; b) Y. Marcus, *J. Solution Chem.* **1984**, *13*, 599.
[30] a) U. Mayer, V. Gutmann, W. Gerger, *Monatsh. Chem.* **1975**, *106*, 1235; b) M. A. Beckett, G. C. Strickland, J. R. Holland, K. Sukumar Varma, *Polymer* **1996**, *37*, 4629.
[31] S. Mummadi, D. Kenefake, R. Diaz, D. K. Unruh, C. Krempner, *Inorg. Chem.* **2017**, *56*, 10748.
[32] P. Erdmann, L. Greb, *Angew. Chem. Int. Ed. Engl.* **2022**, *61*, e202114550; *Angew. Chem.* **2022**, *134*, 508.
[33] a) M. Rohde, L. O. Müller, D. Himmel, H. Scherer, I. Krossing, *Chem. Eur. J.* **2014**, *20*, 1218; b) A. Martens, P. Weis, M. C. Krummer, M. Kreuzer, A. Meierhöfer, S. C. Meier, J. Bohnenberger, H. Scherer, I. Riddlestone, I. Krossing, *Chem. Sci.* **2018**, *9*, 7058.
[34] M. A. Ellwanger, C. von Randow, S. Steinhauer, Y. Zhou, A. Wiesner, H. Beckers, T. Braun, S. Riedel, *Chem. Commun.* **2018**, *54*, 9301.
[35] K. F. Hoffmann, D. Battke, P. Golz, S. M. Rupf, M. Malischewski, S. Hasenstab-Riedel, *Angew. Chem. Int. Ed. Engl.* **2022**, e202203777; *Angew. Chem.* **2022**.
[36] K. Seppelt, D. Nothe, *Inorg. Chem.* **1973**, *12*, 2727.
[37] R. K. Harris, E. D. Becker, S. M. Cabral de Menezes, P. Granger, R. E. Hoffman, K. W. Zilm, *Pure Appl. Chem.* **2008**, *80*, 59.
[38] *gNMR V 5.0*, Adept Scientific, **2005**.
[39] G. M. Sheldrick, *Acta Crystallogr. Sect. A* **2008**, *64*, 112.
[40] G. M. Sheldrick, *Acta Crystallogr. Sect. C* **2015**, *71*, 3.
[41] O. V. Dolomanov, L. J. Bourhis, R. J. Gildea, J. A. K. Howard, H. Puschmann, *J. Appl. Crystallogr.* **2009**, *42*, 339.
[42] TURBOMOLE GmbH, *TURBOMOLE V7.3. a development of University of Karlsruhe and Forschungszentrum Karlsruhe GmbH*, **2018**.
[43] a) A. D. Becke, *Phys. Rev. A* **1988**, *38*, 3098; b) C. Lee, W. Yang, R. G. Parr, *Phys. Rev. B* **1988**, *37*, 785; c) S. H. Vosko, L. Wilk, M. Nusair, *Can. J. Phys.* **1980**, *58*, 1200.
[44] M. Sierka, A. Hogekamp, R. Ahlrichs, *J. Chem. Phys.* **2003**, *118*, 9136.
[45] F. Weigend, R. Ahlrichs, *Phys. Chem. Chem. Phys.* **2005**, *7*, 3297.
[46] K. Moock, K. Seppelt, *Z. Anorg. Allg. Chem.* **1988**, *561*, 132.

Manuscript received: June 27, 2022
Accepted manuscript online: July 28, 2022
Version of record online: ■■, ■■■

© 2022 The Authors. Chemistry - A European Journal published by Wiley-VCH GmbH

RESEARCH ARTICLE

The dimeric Lewis superacid [$Al(OTeF_5)_3]_2$ and its solvent adducts are ready to test their strength in terms of fluoride ion affinity. While some of them are still highly reactive, others had too much coordinating solvent and remain stable but comparably unreactive. In here, their preparation, characterization and reactivity are reported in detail.

*K. F. Hoffmann, Dr. A. Wiesner, Dr. S. Steinhauer, Prof. Dr. S. Riedel**

1 – 14

Insights on the Lewis Superacid $Al(OTeF_5)_3$: Solvent Adducts, Characterization and Properties

3.2. The Tris(pentafluorophenyl)methylium Cation: Isolation and Reactivity

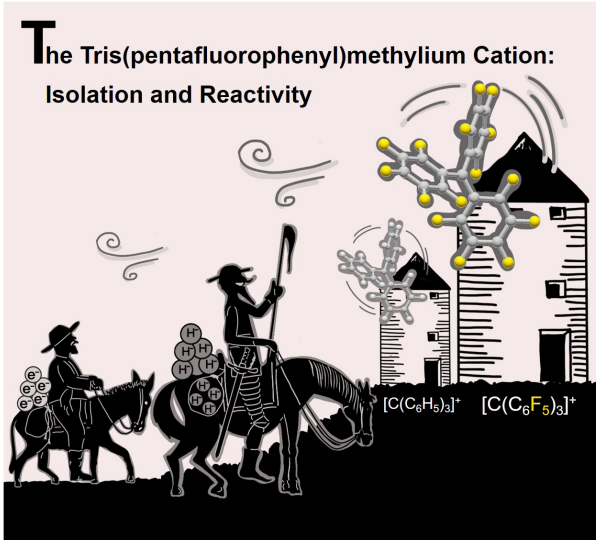

Kurt F. Hoffmann, David Battke, Paul Golz, Susanne M. Rupf, Moritz Malischewski and Sebastian Riedel*
Angew. Chem. Int. Ed. **2022**, *61*, e202203777
Angew. Chem. **2022**, *134*, e202203777
DOI: 10.1002/anie.202203777
DOI: 10.1002/ange.202203777
©The Authors. Published by Wiley-VCH GmbH

Author Contribution:
Kurt F. Hoffmann designed the project, performed experiments, analyzed data and wrote the manuscript. David Battke performed experiments during his Bachelor thesis under supervision of Kurt F. Hoffmann. Paul Golz optimized the synthesis of starting materials. Susanne M. Rupf performed the CV measurements. Moritz Malischweski revised the manuscript. Sebastian Riedel supervised the project and revised the manuscript.

GDCh Communications Angewandte International Edition Chemie www.angewandte.org

Check for updates

VIP Fluorine Very Important Paper

How to cite:
International Edition: doi.org/10.1002/anie.202203777
German Edition: doi.org/10.1002/ange.202203777

The Tris(pentafluorophenyl)methylium Cation: Isolation and Reactivity

*Kurt F. Hoffmann, David Battke, Paul Golz, Susanne M. Rupf, Moritz Malischewski, and Sebastian Riedel**

Abstract: Herein, we present two different routes for the synthesis of the perfluorinated trityl cation, which allowed the handling of the free, uncoordinated species in organic solvents for the first time. The usage of the weakly coordinating anion $[Al(OTeF_5)_4]^-$ and its derivatives allows the characterization of this species by NMR spectroscopy and most importantly by single-crystal X-ray diffraction. The high hydride ion affinity of the cation is shown by hydrogen abstraction from isobutane. Furthermore, cyclic voltammetry reveals its oxidative potential which is supported by the reaction with tris(4-bromophenyl)amine, giving rise to the formation of the ammoniumyl radical cation, also known as "magic blue".

The trityl cation $[C(C_6H_5)_3]^+$ is known as a versatile compound for hydride and methide abstraction reactions and in combination with weakly coordinating anions it finds widespread application in modern chemistry, e.g. as co-catalyst in olefin polymerization[1] or as key reagent in the generation of silylium cations.[2] More recently, the application of tritylium cations as components in frustrated radical pairs was reported.[3] Still, they are viable reagents for hydride abstraction and recently enabled the isolation of a phosphorus dication.[4] Its reactivity can be even further enhanced by replacing the H atoms of the phenyl groups by F atoms.

A theoretical study by Dutton et al.[5] on the Lewis acidity of the perfluorinated trityl cation in terms of calculated ion affinities towards small Lewis bases showed a strong increase of the Lewis acidity compared to its non-fluorinated analogue and even surpassed the isoelectronic tris(pentafluorophenyl) borane $B(C_6F_5)_3$. This becomes evident when comparing the calculated gas-phase fluoride ion affinity (FIA) and hydride ion affinity (HIA) of the perfluorinated trityl cation (FIA: 697 kJ mol^{-1}; HIA: 955 kJ mol^{-1}) with its non-fluorinated analogue (FIA: 599 kJ mol^{-1}; HIA: 801 kJ mol^{-1}) and $B(C_6F_5)_3$ (FIA: 403 kJ mol^{-1}; HIA: 455 kJ mol^{-1}). The effect of fluorination of the phenyl groups was further studied by Stephan et al. as well as Mayr and Horn. They reported on an increase of the global electrophilicity index[6] and the rate of hydride transfer reactions,[7] respectively.

The first formation and NMR spectroscopic investigations of the perfluorinated trityl cation were reported independently by the groups of Filler and Olah in the 1960s.[8,9] Their synthesis was based on the reaction of the alcohol $C(C_6F_5)_3OH$ with neat oleum or "magic acid" (HSO_3F/SbF_5). Nevertheless, it was not possible to isolate a salt of this compound.

Dutton et al. recently followed up on this approach using triflic acid.[10] While they observed the successful formation of the perfluorinated trityl cation $[C(C_6F_5)_3]^+$ in neat triflic acid, only the contact ion pair $C(C_6F_5)_3OTf$ is formed in organic solvents such as *ortho*-dichlorobenzene. Still, this compound possessed a certain reactivity as a hydride acceptor which they proved by the reaction of $C(C_6F_5)_3OTf$ with triethylsilane resulting in the partial formation of tris(pentafluorophenyl)methane $HC(C_6F_5)_3$.

In contrast to the previous described routes for the synthesis of the perfluorinated trityl cation, our approach starts from tris(pentafluorophenyl)methyl chloride **1** and the Brønsted superacid $[H\text{-}C_6F_2H_4][Al(OTeF_5)_4]$ (cf. Figure 1). This Brønsted superacid is formed by reacting $AlEt_3$ and $HOTeF_5$ in *ortho*-difluorobenzene (*o*-DFB) and is generally used to generate cations in two ways; via the protonation of weak bases and via the elimination of gaseous HCl out of chloride sources.[11–13] Taking advantage of this reactivity, we

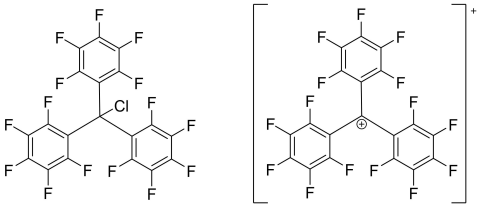

1 **2**

Figure 1. Lewis structures of the precursor tris(pentafluorophenyl)methyl chloride **1** and the product tris(pentafluorophenyl)methylium **2.**

[*] K. F. Hoffmann, D. Battke, P. Golz, S. M. Rupf, M. Malischewski, Prof. Dr. S. Riedel
Fachbereich für Biologie, Chemie, Pharmazie, Institut für Chemie und Biochemie—Anorganische Chemie
Fabeckstraße 34/36, 14195 Berlin (Germany)
E-mail: s.riedel@fu-berlin.de

© 2022 The Authors. Angewandte Chemie International Edition published by Wiley-VCH GmbH. This is an open access article under the terms of the Creative Commons Attribution License, which permits use, distribution and reproduction in any medium, provided the original work is properly cited.

© 2022 The Authors. Angewandte Chemie International Edition published by Wiley-VCH GmbH

GDCh Communications Angewandte International Edition Chemie

added chloride **1** to a solution of $[H\text{-}C_6F_2H_4][Al(OTeF_5)_4]$ followed by an immediate color change from yellow to an intense purple as well as the evolution of HCl gas (cf. Scheme 1). At the same time, the weakly coordinating properties of the anion $[Al(OTeF_5)_4]^-$ stabilizes the perfluorinated trityl cation.

Analysis of the solution by low-temperature NMR spectroscopy confirmed the successful formation of the desired species. In the ^{19}F NMR spectrum the signals observed at a chemical shift of −112.6, −127.7 and −154.3 ppm with relative integrals of 3:6:6 correspond to the *para*-, *ortho*- and *meta*-fluorine atoms of the perfluorinated trityl cation **2** and are in agreement with already reported spectra of the cation in "magic acid" and neat triflic acid.[9,10] Furthermore, a signal set corresponding to an AB_4 pattern appears at chemical shifts of −40.1 and −47.2 ppm with a $^2J_{FF}$ coupling constant of 186 Hz belonging to the pentafluoro-orthotellurate groups of the anion $[Al(OTeF_5)_4]^-$.[11,12] In the ^{27}Al NMR spectrum the signal of the anion is found at 47 ppm.[11,12] Repeating the NMR experiments at room temperature leads to the following changes: In the ^{19}F NMR spectrum the signals of cation **2** are broadened and a new set of signals at −142.9, −154.3 and −162.7 ppm appear. This is assigned to the already reported decomposition product $HCPh^F{}_3$.[10] Its formation probably occurs via hydrogen abstraction of the cation from the solvent *o*-DFB. After 24 hours, the signals of the cation are not observable anymore. Also, this decomposition reaction slowly proceeds at −40 C, since needle-shaped single crystals of $HCPh^F{}_3$ grew in a concentrated solution of $[C(C_6F_5)_3][Al(OTeF_5)_4]$ in *o*-DFB (cf. Figure 2).[14] Attempts to prepare the cation by reacting perfluorotrityl chloride **1** and pentafluoro-orthotelluric acid did not show any reaction. This underlines that a rather strong Brønsted superacid is required to achieve the HCl elimination in this reaction.

Nevertheless, by layering a solution of $[C(C_6F_5)_3][Al(OTeF_5)_4]$ in a mixture of *o*-DFB and dichloromethane with *n*-pentane at −80 C it was possible to obtain dark purple, plate-shaped single crystals suitable for x-ray diffraction. The compound crystallizes in the monoclinic space group *C*2/*c* (cf. Figure 3).[14] Similar to the non-fluorinated trityl cation, the phenyl rings are arranged in a propeller-like manner. The sum of angles around the central carbon atom (C1) is 359.9(9) , which is in line with free trityl cations.[15] The closest cation-anion contact lies between a *para*-fluorine atom of a phenyl ring and a fluorine atom of a pentafluoro-orthotellurate group (d(F3–F15) = 268.7(10) pm) and is slightly shorter than the sum of the van-der-Waals radii ($d(F–F)_{vdW}$ = 294 pm). The distance between C1 to the closest anionic fluorine atom (F10) is 289.7(3) pm. This distance is slightly decreased compared to the non-fluorinated trityl analogue $[C(C_6H_5)_3][Al(OTeF_5)_4]$ (closest d-(C···F): 303.3(3) pm) and is probably caused by the enhanced electrophilicity of cation **2**.[11] The average dihedral angles of the phenyl rings in cation **2** are with 36.78 slightly larger compared to the non-fluorinated analogue with an average dihedral angle of 31.14 .

In a second approach the Lewis superacid $Al(OTeF_5)_3$ was used as starting material instead of the Brønsted superacid $[H\text{-}C_6F_2H_4][Al(OTeF_5)_4]$. By dissolving solid $[Al(OTeF_5)_3]_2$ in an excess of SO_2ClF a clear solution is formed. Upon addition of solid perfluorotrityl chloride **1**, an immediate change of color to intense purple is observed (cf. Scheme 2).

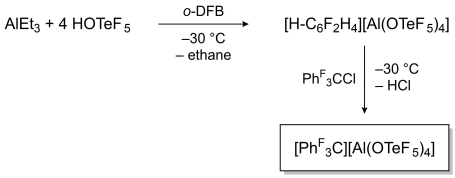

Scheme 1. Synthesis of the perfluorinated trityl cation via a Brønsted acidic route.

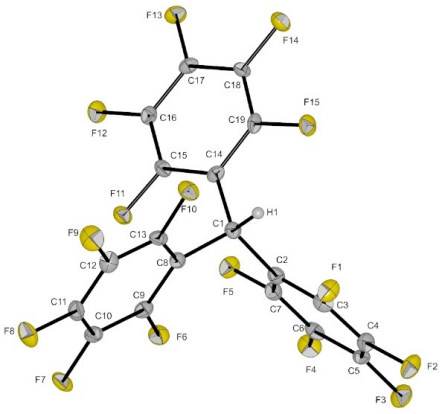

Figure 2. Molecular structure of $HC(C_6F_5)_3$ in the solid state. Thermal ellipsoids set at 50% probability. Selected bond lengths [pm] and angles [ ]: C1–C2 153.5(4), C1–C8 152.7(4), C1–C14 153.6(4); C2-C1-C14 113.5(2), C8-C1-C2 114.6(2), C8-C1-C14 113.4(2).

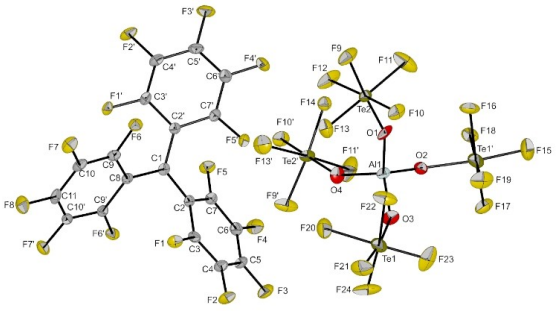

Figure 3. Molecular structure of $[C(C_6F_5)_3][Al(OTeF_5)_4]$ in the solid state. Thermal ellipsoids set at 50% probability. Selected bond lengths [pm] and angles [ ]: C1–C2 143.2(6), C1–C8 144.9(10); C2-C1-C8 119.8(3), C2-C1-C2′ 120.5(6), C2′-C1-C8 119.8(3).

© 2022 The Authors. Angewandte Chemie International Edition published by Wiley-VCH GmbH

GDCh Communications Angewandte International Edition Chemie

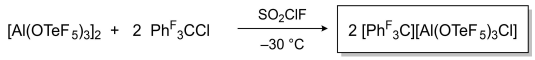

Scheme 2. Synthesis of the perfluorinated trityl cation via a Lewis acidic route.

An analysis of the reaction mixture by low-temperature NMR spectroscopy showed the successful formation of the perfluorinated trityl cation. The formed anion $[Al(OTeF_5)_3Cl]^-$ is presumably in an equilibrium between the fully pentafluoro-orthotellurate-substituted anion $[Al(OTeF_5)_4]^-$ and an anion with two chlorido and two pentafluoro-orthotellurate ligands $[Al(OTeF_5)_2Cl_2]^-$. The ^{19}F NMR spectrum shows again the signals of the cation **2** at −109.6, −125.5 and −152.3 ppm. Additionally, three different AB_4 signal sets are observed between −35 and −50 ppm. They correspond to the equilibrating anions $[Al(OTeF_5)_{4-x}Cl_x]^-$ ($x=0,1,2$). The ^{27}Al NMR also shows three different signals, assigned to $[Al(OTeF_5)_4]^-$ at 48 ppm, $[Al(OTeF_5)_3Cl]^-$ at 65 ppm and $[Al(OTeF_5)_2Cl_2]^-$ at 80 ppm.[11] The ^{13}C NMR spectrum shows the signals of cation **2**. Surprisingly, the signal of the central carbon atom at 175 ppm is 36 ppm upfield-shifted compared to the non-fluorinated trityl cation.[11] This phenomenon may occur due to π donation of the adjacent fluorine atoms to the central carbon atom and are in agreement with findings of Dutton et al.[10] Warming the reaction mixture to room-temperature did not lead to a decolorization. Still, the corresponding NMR spectra at room temperature indicate decomposition of the compound within 15 minutes. The successful formation of the cation via a Lewis acidic reaction pathway is in contrast to previous experimental findings, in which only an reaction at the *para*-fluorine atom instead of an attack at the chloride bound to the central carbon atom was observed when halide abstraction reagents were used.[10] Attempts to isolate the compound by evaporation of all volatiles led to a viscous, dark purple oil, which could not be further characterized so far.

Quantum-chemical calculations were performed to understand the electronic properties of the perfluorinated trityl cation. In the top part of Figure 4, the plotted electrostatic potential of the perfluorinated and non-fluorinated trityl cation is shown. In the case of the $[C(C_6H_5)_3]^+$ ion the positive electrostatic potential is located at the central carbon atom as well as on the peripheral hydrogen atoms, while the negative potential is located near the aromatic ring. In the case of the $[C(C_6F_5)_3]^+$ ion the distribution of the electrostatic potential is changed: All carbon atoms possess a rather positive electrostatic potential. Due to the strong electron-withdrawing properties of the fluorine substituents, the peripheral F atoms accumulate a more negative electrostatic potential. A closer look on the fluorine substituents reveals the lowest electrostatic potential at the *meta*-fluorine atoms compared to the *para*- and *ortho*-fluorine atoms. The bottom part of Figure 4 depicts the lowest unoccupied molecular orbitals (LUMO) of $[C(C_6H_5)_3]^+$ and $[C(C_6F_5)_3]^+$, mainly centered on the unoccupied p-orbital of the central carbon atom. The LUMO

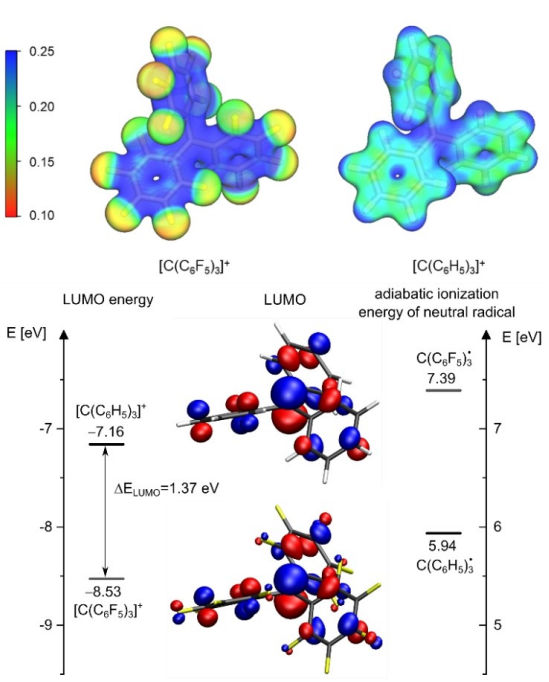

Figure 4. Top: Plotted electrostatic potential of perfluorinated and non-fluorinated trityl cations (in E_H, isovalue: 0.025). Bottom: Plotted Lowest Unoccupied Molecular Orbitals of $[C(C_6F_5)_3]^+$ and $[C(C_6H_5)_3]^+$ along with the calculated difference of LUMO energy and the adiabatic ionization energy. Calculations were performed at RI-B3LYP/def2-TZVPP level of theory.

energy of $[C(C_6F_5)_3]^+$ is lowered by 1.37 eV compared to $[C(C_6H_5)_3]^+$, which reflects the increased electrophilicity. Furthermore, the adiabatic ionization energy of the neutral radical species $C(C_6F_5)_3^\bullet$ and $C(C_6H_5)_3^\bullet$ show a difference of 1.45 eV. Consequently, this should lead to an increased oxidation potential of the fluorinated trityl cation compared to the non-fluorinated analogue.

As quantum-chemical calculations of Couchman et al. already indicated, a high hydride ion affinity is expected for the perfluorinated trityl cation (calculated gas-phase hydride affinities: $[C(C_6F_5)_3]^+ = 955\ kJ\,mol^{-1}$ vs. $[C(C_6H_5)_3]^+ = 801\ kJ\,mol^{-1}$).[5] This is experimentally supported by the observed formation of the side-product tris(pentafluorophenyl)methane in the crystallization attempts of compound $[C(C_6F_5)_3][Al(OTeF_5)_4]$. In order to elaborate on the experimental hydride affinity of cation **2**, the generation of the *tert*-butyl cation by means of a hydrogen abstraction on isobutane was undertaken. A similar reaction was shown by Reed and co-workers, who prepared a *tert*-butyl cation by treating the very strong methylation reagent $Me(CHB_{11}Me_5Br_6)$ with isobutane and thereby formed methane and the *tert*-butyl cation.[16] Therefore, a solution of $[C(C_6F_5)_3][Al(OTeF_5)_3Cl]$ in SO_2ClF was prepared by the prior described reaction (cf. Scheme 2) and

© 2022 The Authors. Angewandte Chemie International Edition published by Wiley-VCH GmbH

treated with an excess of isobutane. The reaction was then monitored by low-temperature NMR spectroscopy (cf. Scheme 3). The recorded spectra can be found in the Supporting Information.

While at −60 C no reaction occurred, warming the reaction mixture to 0 C gave insight into the reaction progress. In the ^{19}F NMR spectrum the decrease of the signals corresponding to cation **2** is observed while a new set of signals at −142.9, −154.9 and −163.0 ppm emerges, which belongs to the formation of $HCPh^F_3$. The singlet of $HCPh^F_3$ in the ^{1}H NMR spectrum appears at 6.8 ppm. In the ^{27}Al NMR spectrum the signals of the mixed anions $[Al(OTeF_5)_3Cl]^-$ and $[Al(OTeF_5)_2Cl_2]^-$ vanished, while the homoleptic anion $[Al(OTeF_5)_4]^-$ remains stable. The signals of the isobutane at 2.2 and 1.5 ppm in the ^{1}H NMR spectrum as well as at 24.3 and 23.6 ppm in the ^{13}C NMR spectrum are severely broadened, indicating a dynamic process. These observations confirm a successful hydride abstraction by the $[C(C_6F_5)_3]^+$ ion while the formed *tert*-butyl cation might undergo a dynamic exchange with the remaining isobutane or even the present chloride anions of the mixed anion species. Such processes already have been described in literature.[17] Nevertheless, these experiments clearly underline the high hydride ion affinity of cation **2** by cleanly converting the cation to the perfluorinated trityl methane. For further details see Supporting Information.

The influence of the fluorine substitution pattern of the phenyl rings in trityl cations on its electrophilicity and stability has been already discussed in literature.[18] However, there are no reports on the change of its oxidative potential by introduction of more electron-withdrawing substituents. The tris(pentafluorophenyl)-methyl radical has already been mentioned in a previous publication and was synthesized by the reduction of the $[C(C_6F_5)_3]^+$ cation with $TiCl_3$.[19] Therefore, it should be feasible to analyze a solution of $[C(C_6F_5)_3][Al(OTeF_5)_4]$ in *o*-DFB by cyclic voltammetry. The experiment gave an irreversible oxidation wave at E_{pa} = 1.11 V against Fc/Fc^+ (cf. Figure 5), which surpasses the formal oxidative potential of its non-fluorinated analogue by a remarkable 1.22 V (cf. Table 1). This strong increase of the oxidative potential can be explained by the increase of the ionization energy, induced by the fluorine substitution (see above). A similar effect on the oxidation potential was observed when the group of Krossing et al. investigated fluorine-substituted dihydrophenanzine derivatives.[20]

In order to show the oxidative potential of the cation **2** experimentally, it was reacted with ferrocene and tris(4-bromophenyl)amine, respectively. In the case of ferrocene addition, an immediate color change to green is observed, due to the formation of the ferrocenium cation $[FeCp_2]^+$. The addition of tris(4-bromophenyl)amine to a solution of $[C(C_6F_5)_3][Al(OTeF_5)_4]$ in *o*-DFB lead to a deep-blue colored reaction mixture, indicating the successful formation of the ammoniumyl radical cation (cf. Scheme 4), also known as "magic blue". Subsequently the tris(pentafluorophenyl)methyl radical $Ph^F_3C^\bullet$ must have been formed. For further characterization, both reaction mixtures were analyzed by EPR spectroscopy. The EPR spectrum of the reaction of ferrocene with $[C(C_6F_5)_3][Al(OTeF_5)_4]$ gave one broadened signal with a *g* value of 2.0031, which corresponds to the $Ph^F_3C^\bullet$ radical and is in line

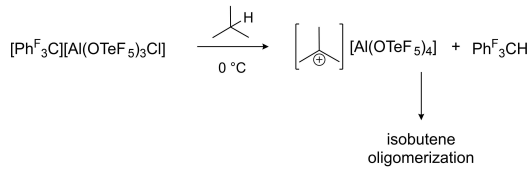

Scheme 3. Reaction of the perfluorinated trityl cation with isobutane performed in SO_2ClF.

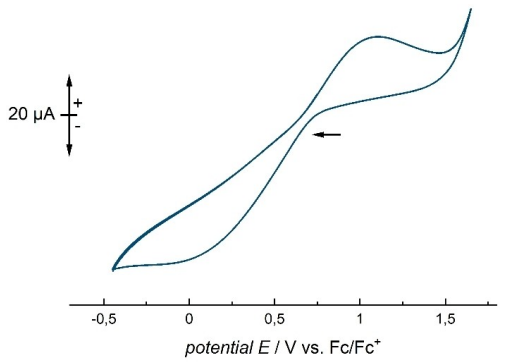

Figure 5. Cyclic voltammogram of a 0.078 M solution of $[C(C_6F_5)_3][Al(OTeF_5)_4]$ in *ortho*-difluorobenzene at −35 C. Scan rate: 100 mV s^{-1}. Irreversible oxidation wave at 1.11 V.

Table 1: Formal redox potentials (V vs. Fc/Fc^+) of selected compounds.

Oxidant	Solvent	E [a]
$[N(C_6H_4Br\text{-}2,4,6)_3]^+$	MeCN	1.40[21]
$[N(C_6H_4Br\text{-}2,4)_3]^+$	MeCN	1.18[21]
$[CPh_3^F]^+$	*o*-DFB	1.11
$[NO]^+$	CH_2Cl_2	1.00[22]
$[N(C_6H_4Br\text{-}4)_3]^+$	CH_2Cl_2	0.74[21]
$[FeCp_2]^+$		0.00
$[CPh_3]^+$	MeCN	−0.11[23]

[a] Values have been corrected accordingly: Fc/Fc^+ $E_{1/2}$ = 0.31 V vs. SCE (0.56 V vs. NHE).

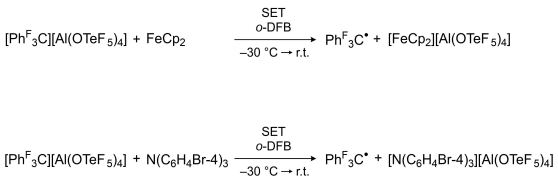

Scheme 4. Reaction of the perfluorinated trityl cation with ferrocene (top) and tris(4-bromophenyl)amine (bottom).

© 2022 The Authors. Angewandte Chemie International Edition published by Wiley-VCH GmbH

with the literature reported *g* value for this species.[19] The signal of the $[FeCp_2]^+$ cation is not expected, since the measurement was performed at room temperature and it is known that this species can only be observed at temperatures below 78 K.[24] The EPR spectrum of the reaction between $[C(C_6F_5)_3][Al(OTeF_5)_4]$ and the tris(4-bromophenyl)amine shows two overlapping broad signals, which correspond to the ammoniumyl radical cation and the perfluorinated trityl radical (see Figures S16). This is in agreement with literature, where a severely broadened signal for the tris(4-bromophenyl)ammoniumyl radical cation was reported.[25]

In conclusion, we report on two novel synthesis routes for the preparation of the perfluorinated trityl cation $[C(C_6F_5)_3]^+$. By using the weakly coordinating anion $[Al(OTeF_5)_4]^-$ it was now possible to structurally characterize this interesting species. In conjunction with theoretical and experimental methods like EPR, NMR and CV the cation $[C(C_6F_5)_3]^+$ is further investigated. These new synthetic routes allow it to handle this delicate species in its free form in organic solvents such as *o*-DFB. Moreover, we have experimentally shown its remarkable hydride ion affinity and its high oxidation potential.

Note Added in Proof

Since the publication of this work as an Accepted Article, an article by Ozerov et al. has been published, which reports on the synthesis and reactivity of partially fluorinated trityl cation salts.[25]

Acknowledgements

Funded by the Deutsche Forschungsgemeinschaft (DFG, German Research Foundation)—Project-ID 387284271—SFB 1349 and the ERC Project HighPotOx. Computing time was made available by the High-Performance Computing Center at the ZEDAT, Freie Universität Berlin. Also, we would like to acknowledge the assistance of the Core Facility BioSupraMol supported by the DFG. Open Access funding enabled and organized by Projekt DEAL.

Conflict of Interest

The authors declare no conflict of interest.

Data Availability Statement

The data that support the findings of this study are available from the corresponding author upon reasonable request.

Keywords: High Hydride Affinity · Perfluorinated Trityl Cation · Strong Oxidizer · Superacids · Weakly Coordinating Anions

[1] a) E. Y. Chen, T. J. Marks, *Chem. Rev.* **2000**, *100*, 1391; b) D. S. McGuinness, A. J. Rucklidge, R. P. Tooze, A. M. Z. Slawin, *Organometallics* **2007**, *26*, 2561; c) J. Bah, J. Franzén, *Chem. Eur. J.* **2014**, *20*, 1066.
[2] H. F. T. Klare, L. Albers, L. Süsse, S. Keess, T. Müller, M. Oestreich, *Chem. Rev.* **2021**, *121*, 5889.
[3] a) Z. Dong, C. Pezzato, A. Sienkiewicz, R. Scopelliti, F. Fadaei-Tirani, K. Severin, *Chem. Sci.* **2020**, *11*, 7615; b) A. Dasgupta, E. Richards, R. L. Melen, *Angew. Chem. Int. Ed.* **2021**, *60*, 53; *Angew. Chem.* **2021**, *133*, 53.
[4] P. Mehlmann, T. Witteler, L. F. B. Wilm, F. Dielmann, *Nat. Chem.* **2019**, *11*, 1139.
[5] S. A. Couchman, D. J. D. Wilson, J. L. Dutton, *Eur. J. Org. Chem.* **2014**, 3902.
[6] A. R. Jupp, T. C. Johnstone, D. W. Stephan, *Dalton Trans.* **2018**, *47*, 7029.
[7] M. Horn, H. Mayr, *Eur. J. Org. Chem.* **2011**, 6470.
[8] R. Filler, C.-S. Wang, M. A. McKinney, F. N. Miller, *J. Am. Chem. Soc.* **1967**, *89*, 1026.
[9] G. A. Olah, M. B. Comisarow, *J. Am. Chem. Soc.* **1967**, *89*, 1027.
[10] E. G. Delany, S. Kaur, S. Cummings, K. Basse, D. J. D. Wilson, J. L. Dutton, *Chem. Eur. J.* **2019**, *25*, 5298.
[11] A. Wiesner, T. W. Gries, S. Steinhauer, H. Beckers, S. Riedel, *Angew. Chem. Int. Ed.* **2017**, *56*, 8263; *Angew. Chem.* **2017**, *129*, 8375.
[12] K. F. Hoffmann, A. Wiesner, N. Subat, S. Steinhauer, S. Riedel, *Z. Anorg. Allg. Chem.* **2018**, *644*, 1344.
[13] A. Wiesner, S. Steinhauer, H. Beckers, C. Müller, S. Riedel, *Chem. Sci.* **2018**, *9*, 7169.
[14] Deposition Numbers 2154970 (for $C(C_6F_5)_3H$) and 2153771 (for $[C(C_6F_5)_3][Al(OTeF_5)_4]$) contain the supplementary crystallographic data for this paper. These data are provided free of charge by the joint Cambridge Crystallographic Data Centre and Fachinformationszentrum Karlsruhe Access Structures service.
[15] C. Bolli, J. Derendorf, C. Jenne, H. Scherer, C. P. Sindlinger, B. Wegener, *Chem. Eur. J.* **2014**, *20*, 13783.
[16] T. Kato, C. A. Reed, *Angew. Chem. Int. Ed.* **2004**, *43*, 2908; *Angew. Chem.* **2004**, *116*, 2968.
[17] a) D. Mirda, D. Rapp, G. M. Kramer, *J. Org. Chem.* **1979**, *44*, 2619; b) F. Kalchsclimid, E. Mayer, *Z. Naturforsch. B* **1979**, *34*, 548.
[18] M. Horn, H. Mayr, *J. Phys. Org. Chem.* **2012**, *25*, 979.
[19] C. Trapp, C.-S. Wang, R. Filler, *J. Chem. Phys.* **1966**, *45*, 3472.
[20] M. Schorpp, T. Heizmann, M. Schmucker, S. Rein, S. Weber, I. Krossing, *Angew. Chem. Int. Ed.* **2020**, *59*, 9453; *Angew. Chem.* **2020**, *132*, 9540.
[21] W. Schmidt, E. Steckhan, *Chem. Ber.* **1980**, *113*, 577.
[22] J. K. Kochi, *Acc. Chem. Res.* **1992**, *25*, 39.
[23] H. Volz, W. Lotsch, *Tetrahedron Lett.* **1969**, *10*, 2275.
[24] R. Prins, F. J. Reinders, *J. Am. Chem. Soc.* **1969**, *91*, 4929.
[25] F. A. Bell, A. Ledwith, D. C. Sherrington, *J. Chem. Soc. C* **1969**, 2719.[26] S. O. Gunther, C.-I. Lee, E. Song, N. Bhuvanesh, O. V. Ozerov, *Chem. Sci.* **2022**, *13*, 4972.

Manuscript received: March 14, 2022
Accepted manuscript online: April 13, 2022
Version of record online: ■■, ■■

© 2022 The Authors. Angewandte Chemie International Edition published by Wiley-VCH GmbH

GDCh Communications Angewandte International Edition Chemie

Communications

Fluorine

K. F. Hoffmann, D. Battke, P. Golz,
S. M. Rupf, M. Malischewski,
S. Riedel* _____ **e202203777**

The Tris(pentafluorophenyl)methylium Cation: Isolation and Reactivity

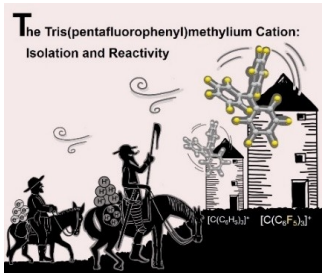

Two brave knights worrying for their hydrides and electrons are caught in the storm of a small tritylium and a giant perfluorotritylium windmill. Herein, the structural proof of the perfluorinated trityl cation and its remarkable hydride ion affinity and oxidation potential compared to its non-fluorinated analogue are reported.

© 2022 The Authors. Angewandte Chemie International Edition published by Wiley-VCH GmbH

3.3. Structural proof of a [C–F–C]$^+$ fluoronium cation

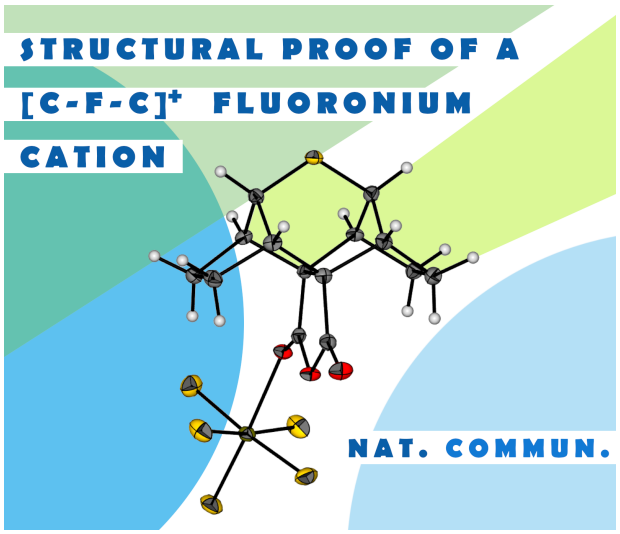

Kurt F. Hoffmann, Anja Wiesner, Carsten Müller, Simon Steinhauer, Helmut Beckers, Muhammad Kazim, Cody Ross Pitts, Thomas Lectka* and Sebastian Riedel*
Nat. Commun. **2021**, *12*, 5275.

DOI: 10.1038/s41467-021-25592-6

©The Authors. Published by Springer Nature.

Author Contribution:
Kurt F. Hoffmann carried out the synthetic work and analytical characterization. Anja Wiesner performed preliminary experiments on the system. Carsten Müller and Kurt F. Hoffmann performed DFT calculations. Carsten Müller performed the bonding analysis. Simon Steinhauer acquired the SC-XRD data. Helmut Beckers assisted with vibrational data analysis. Muhammad Kazim and Cody Ross Pitts synthesized the precursor. Kurt F. Hoffmann wrote the paper, all authors discussed and commented on the manuscript. Thomas Lectka and Sebastian Riedel directed and coordinated the research.

nature COMMUNICATIONS

ARTICLE

https://doi.org/10.1038/s41467-021-25592-6 OPEN

Structural proof of a $[C–F–C]^+$ fluoronium cation

Kurt F. Hoffmann[1], Anja Wiesner[1], Carsten Müller[1], Simon Steinhauer[1], Helmut Beckers[1], Muhammad Kazim[2], Cody Ross Pitts[2,3], Thomas Lectka[2]✉ & Sebastian Riedel[1]✉

Organic fluoronium ions can be described as positively charged molecules in which the most electronegative and least polarizable element fluorine engages in two partially covalent bonding interactions to two carbon centers. While recent solvolysis experiments and NMR spectroscopic studies on a metastable $[C–F–C]^+$ fluoronium ion strongly support the divalent fluoronium structure over the alternative rapidly equilibrating classical carbocation, the model system has, to date, eluded crystallographic analysis to confirm this phenomenon in the solid state. Herein, we report the single crystal structure of a symmetrical $[C–F–C]^+$ fluoronium cation. Besides its synthesis and crystallographic characterization as the $[Sb_2F_{11}]^-$ salt, vibrational spectra are discussed and a detailed analysis concerning the nature of the bonding situation in this fluoronium ion and its heavier halonium homologues is performed, which provides detailed insights on this molecular structure.

[1] Fachbereich Biologie, Chemie, Pharmazie, Institut für Chemie und Biochemie – Anorganische Chemie, Freie Universität Berlin, Berlin, Germany. [2] Department of Chemistry, Johns Hopkins University, Baltimore, MD, USA. [3] Present address: Department of Chemistry, University of California, Davis, Davis, CA, USA. ✉email: lectka@jhu.edu; s.riedel@fu-berlin.de

According to IUPAC, halonium ions are defined as ions of the form $[R_2X]^+$, where X may be any halogen[1]. In the case of organic halonium ions, R is defined as a cyclic or open-chained hydrocarbon backbone. Since they were first discussed as reactive intermediates in organic halogenation reactions in 1937[2], a large variety of stable and structurally characterizable iodo-[3,4], bromo-[5,6], and chloronium[7–9] salts of the type $[C–X–C]^+$ have been synthesized[10,11]. On the other hand, fluoronium cations, in which a divalent fluorine atom (as depicted in a simplifying Lewis dot structure) is symmetrically bound to two carbon atoms, have only been reported thus far in spectroscopic investigations. For instance, Morton et al. first detected a three-membered cyclic fluoriranium ion as an intermediate in mass-spectrometry experiments[12], while Gabbaï and coworkers obtained the structure of a diphenylnaphthylmethylium cation that shows an intramolecular bonding interaction to an adjacent fluorine substituent, allowing a description as an unsymmetrically bridged fluoronium cation (Fig. 1a)[13].

In 2013, Lectka et al. presented the transient generation of a symmetrically bridged fluoronium cation in solution starting from a rigid double-norbornyl type precursor. Its formation as a fleeting reactive intermediate was indicated through isotopic labeling experiments[14,15]. Finally, in 2018 they supported the formation of the aforementioned fluoronium ion by NMR spectroscopy[16,17]; yet, the structural proof of this organic fluoronium ion in the solid state remained a lofty goal. In addition to these few spectroscopic examples of carbon-based fluoronium cations, some inorganic fluoronium cations have been investigated in the past. Motz and Bartmann published in 1988 a crystal structure of the simplest fluoronium ion $[H_2F]^+$ [18]. A crystal structure of a cyclic disilylfluoronium salt was reported by Müller and coworkers in 2006, followed by the structure of an open-chained bissilylated fluoronium cation by Schulz in 2009[19–21]. More recently in 2018, Kraus presented examples of a fluorine atom coordinated by two BrF_2 units (Fig. 1a)[22,23].

In this work, we present a modified synthesis and structural investigation of the carbon-based double-norbornyl type fluoronium ion **1** (Fig. 1) as the $[Sb_2F_{11}]^-$ salt by single-crystal X-ray diffraction. Furthermore, the bonding schemes of $[C–X–C]^+$ (X = F, Cl, Br, I) are discussed and compared through detailed AIM analyses, and the properties of **1** are further analyzed by vibrational spectroscopy.

Results

Synthesis and characterization. Our approach is, in principle, based on utilizing the strong Lewis acid SbF_5 as a fluoride ion abstractor[16,17]. Herein, neat SbF_5 was substituted by the crystalline solvent-adduct $SbF_5·SO_2$ due to its slightly weakened acidic character and more convenient handling (Fig. 1b). By adding precursor **2** to a cooled mixture of $SbF_5·SO_2$ in SO_2ClF, a yellow solution is formed. Partial evaporation of the SO_2ClF and consecutive slow cooling of the reaction mixture afforded single crystals suitable for X-ray diffraction.

The compound $[\mathbf{1}][Sb_2F_{11}]·(SO_2ClF)_3$ (Fig. 2, more detailed structure in Supplementary Fig. 1 including a comprehensive list of crystal data in Supplementary Tables 1–3) crystallizes in the centrosymmetric monoclinic space group $P2_1/c$ along with three solvent molecules per asymmetric unit. A nearly symmetrical C–F–C bonding array is observed. The bridging fluorine atom F1 and its adjacent carbon atoms feature bond lengths of 156.6(3) and 158.5(3) pm with an overall C1–F1–C2 bond angle of 115.78(15)°. This is consistent with the data of the computed quantum-chemical structure of cation **1** with C–F bond distances of 157.4 and 160.1 pm and a C–F–C angle of 115.32° (B3LYP/cc-pVTZ). Compared to the unsymmetrical bridging fluorine atom in Gabbaï's bis-naphthalene complex with C–F distances of 142.4 and 244.4 pm, the distances in cation **1** are in between[13]. No interaction between anion and cation can be observed, although as predicted in previous publications, a single SbF_5 coordinates to the anhydride function of the cation. The coordinating SbF_5 is slightly bent out of the anhydride plane with a dihedral angle < (O2–C14–O1–Sb1) = 19.0(4)°, resulting in a C_1 symmetry of the cation. Lectka et al. previously assumed C_s symmetry from their NMR analysis of this compound[16,17].

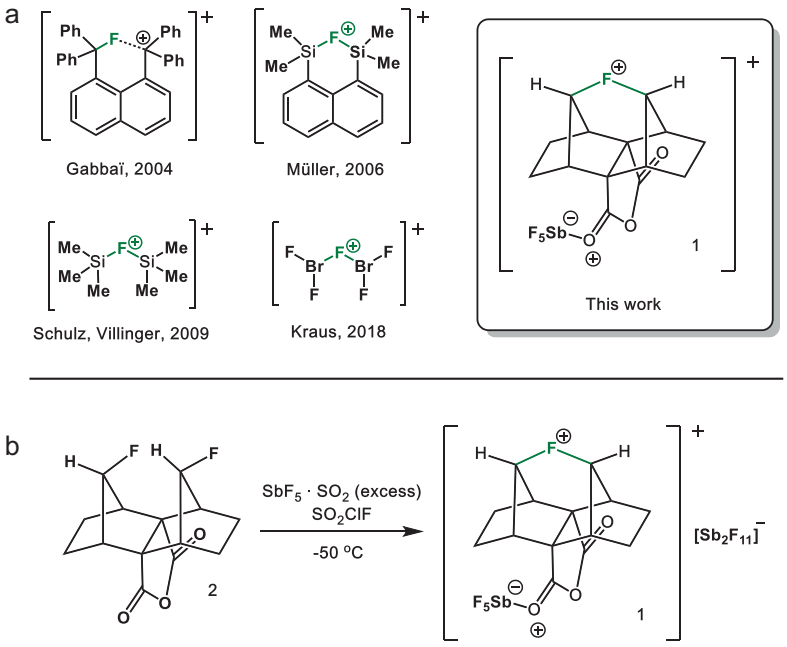

Fig. 1 Overview of fluoronium ions in the condensed phase. a Crystallographically characterized fluoronium ions[16,17,19–23]. Note that the formal charges shown inside a circle do not represent the actual charge of the corresponding atoms. **b** Synthesis of the fluoronium salt $[\mathbf{1}][Sb_2F_{11}]$.

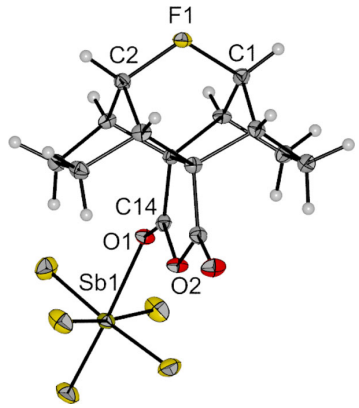

Fig. 2 Molecular structure of the fluoronium ion 1 as its $[Sb_2F_{11}]\cdot(SO_2ClF)_3$ salt in the solid state. Anion and solvent molecules are not depicted. Thermal ellipsoids set to 50% probability. Selected bond lengths [pm] and angles [°]: F1–C1 156.6(3), F1–C2 158.7(3), C1–F1–C2 115.64(17), O2–C14–O1–Sb1 19.0(4).

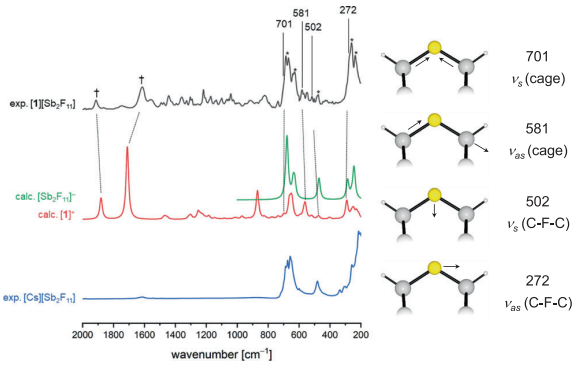

Fig. 3 Vibrational analysis of fluoronium 1. Left: Experimental infrared spectra of [**1**][Sb_2F_{11}] (black) and [Cs][Sb_2F_{11}] (blue) at −40 °C, as well as calculated spectra of cation **1** (red) and anion $[Sb_2F_{11}]^-$ (green) at B3LYP/def2-TZVPP level of theory. Bands of the anion are denoted with an asterisk in the experimental spectrum and bands associated with the carbonyl group are denoted with a dagger. Right: Approximate representation and assignment of selected C–F–C normal modes of **1** (see text, only displacements involving the C–F–C unit are shown).

The vacuum-dried crystalline material was investigated by IR spectroscopy at −40 °C. The experimental spectrum of [**1**][Sb_2F_{11}] (see Fig. 3, black trace) was assigned guided by calculated vibrational spectra of cation **1** and anion $[Sb_2F_{11}]^-$ and by comparison with the spectrum of precursor **2** (Supplementary Fig. 3 and Supplementary Table 5), and an experimental spectrum of [Cs][Sb_2F_{11}]. This allows the assignment of characteristic vibrational modes at 581 cm^{-1} (calc. 560 cm^{-1}) and 502 cm^{-1} (calc. 471 cm^{-1}) carrying significant in-plane C–F–C stretching character. Although the region around 690 cm^{-1} and 260 cm^{-1} are dominated by strong Sb_2F_{11} vibrations two additionally fluorine-involved modes are tentatively assigned to shoulders at 272 cm^{-1} (calc. 291 cm^{-1}) and 701 cm^{-1} (calc. 699 cm^{-1}). In addition, the coordination of SbF_5 to one of the carbonyl groups of **1** leads to a splitting of the C=O bands at 1913 (ν(C=O)) and 1614 (ν(C=O···SbF_5)) cm^{-1} (marked by a dagger symbol in Fig. 3). For a complete list of recorded IR vibrations and their assignment see also the methods section.

In Table 1 we present a comparison of the C–F–C stretching modes for the acyclic dimethyl halonium ions $[Me_2X]^+$ (X = F, Cl, Br and I) with those of the C_{2v} symmetric double-norbornyl halonium ions $[DNTX]^+$ (without coordination of an additional SbF_5 group). Generally, such a comparison is hampered by the more complex and rigid cage shape of the $[DNTX]^+$ derivatives, since the division of such cage vibrations into certain stretching and ring deformations is more arbitrary and the vibrational coupling between different cage vibrations is more serious than for the simple dimethyl analogs. In Fig. 3 and Table 1 we present a tentative assignment of characteristic vibrations of **1** and the symmetric $[DNTX]^+$ ions, respectively. A closer look reveals that the C–X–C stretching coordinates of the $[DNTX]^+$ ions contribute to several normal modes such as an in-phase and an out-of-phase cage vibration, denoted as ν_s(cage) and ν_{as}(cage) in Table 1 and Fig. 3, respectively, in which mainly the two carbon atoms vibrate along the C–X coordinates, as well as to two lower-lying modes which carry dominant halogen atom displacements, and which are thus denoted as ν_s(C–X–C) and ν_{as}(C–X–C) stretching vibrations (for more details see Supplementary Movie 1). As a consequence, the ν_s(cage) frequencies change only slightly from $\nu_s = 724\ cm^{-1}$ ($[DNTF]^+$) to $709\ cm^{-1}$ ($[DNTI]^+$), while the ν_s(C–X–C) stretching frequencies in the $[DNTX]^+$ ions are strongly reduced from $\nu_s = 488\ cm^{-1}$ for X = F down to $365\ cm^{-1}$ for X = I (Table 1).

The C–F–C stretching vibrations of **1** and the symmetric $[DNTF]^+$ cation are strongly red-shifted compared to conventional monovalent C–F vibrations (usually observed between 1300 and 900 cm^{-1})[24], indicating the weakened C–F bonds in these fluoronium derivatives. This is in line with similar findings of Dopfer et al. and their calculations on phenylfluoronium $[F\text{–}C_6H_6F]^+$[25]. Also, the significantly higher frequency of the symmetric compared to the antisymmetric C–F–C stretching modes for the $[DNTX]^+$ cations is remarkable and in striking contrast to spectroscopic investigations of acyclic dialkyl halonium salts[26,27].

In addition, the comparison of the frequencies of the cyclic $[DNTX]^+$ ions with those of the $[Me_2X]^+$ derivatives reveals further interesting features: while the ν_{as}(C–X–C) vibrations of the $[DNTX]^+$ ions generally occur at lower frequencies than those of the $[Me_2X]^+$ analogs, the two antisymmetric vibrations of $[DNTF]^+$ are even lower in frequency than those of $[DNTCl]^+$ (Table 1). We tentatively attribute these characteristic spectroscopic properties to different bonding properties of the C–X–C bonds in $[DNTF]^+$ and $[Me_2F]^+$ on the one hand and the $[DNTCl]^+$ cation on the other. A distortion along the antisymmetric stretching coordinate is expected to change the overall wave-function by increasing the relative weight of a carbo-cationic resonance structure with unequal C–F–C bond distances, and, consequently, the stabilization of this carbo-cationic resonance structure by suitable carbon substituents in a fluoronium equilibrium structure should result in a lower antisymmetric stretching frequency. This assumption was previously supported by an almost linear decrease in ν_{as}(C–Cl–C) on the number of methyl groups n in the acyclic chloronium cations $[(H_3C)_n(H_{3-n}C)_2Cl]^+$ ($n = 0$–3)[27]. Thus, lower ν_{as}(C–X–C) frequencies are to be expected for the $[DNTX]^+$ cations with secondary carbon substituents compared to the $[Me_2X]^+$ series. Also, entropic effects likely contribute to the stabilization of the cyclic $[DNTX]^+$ cations. In addition, we have carried out a vibrational analysis of $[DNTX]^+$ cations, with X = F and Cl, in which the hydrogen atoms of the H–C groups next to X are substituted by R = F, CH_3, and CF_3 (denoted as $[R_2DNTX]^+$ in Supplementary Table 4). With the exception of the fluorinated derivative $[F_2DNTF]^+$ (R = F) all other computed derivatives form stable symmetric halonium cations and for $[F_2DNTF]^+$, we have

Table 1 Comparison of selected computed vibrational frequencies and C-X-C bond angles of dimethyl halonium ions $[Me_2X]^+$ (X = F, Cl, Br, I) and double-norbornyl type halonium ions $[DNTX]^+$ (C_{2v} symmetry) at def2-TZVPP/B3LYP level of theory.

		ν_s (cage)	ν_s (C-X-C)	ν_{as} (cage)	ν_{as} (C-X-C)	<(C-X-C)
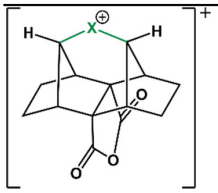	$[DNTF]^+$	724 (6)	488 (6)	588 (29)	304 (34)	115°
	$[DNTCl]^+$	711 (11)	386 (4)	657 (22)	313 (3)	98°
	$[DNTBr]^+$	710 (15)	368 (4)	651 (19)	253 (2)	92°
	$[DNTI]^+$	709 (18)	365 (3)	649 (14)	234 (1)	86°

		ν_s (C-X-C)	δ (C-X-C)	ν_{as} (C-X-C)	<(C-X-C)
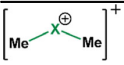	$[Me_2F]^+$	659 (12)	264 (1)	677 (100)	121°
	$[Me_2Cl]^+$	561 (41)	228 (1)	604 (100)	105°
	$[Me_2Br]^+$	500 (55)	187 (4)	517 (100)	101°
	$[Me_2I]^+$	470 (41)	160 (3)	484 (52)	98°

Frequencies are given in cm^{-1}. Relative intensities are given in brackets.

analyzed the C_{2v} symmetric fluoronium transition state, connecting two equivalent carbo-cationic minimum structures (Supplementary Fig. 2). For R = CH_3 and F, which both support an asymmetric carbo-cationic structure the fluoronium ions (X = F) show lower ν_{as}(C–X–C) frequencies than the chloronium analogs (X = Cl), which is in line with the above assumption. In contrast, the trifluoromethylated derivatives (R = CF_3), which disfavors an ionic structure, show similar ν_{as}(C–X–C) frequencies for X = F and Cl (Supplementary Table 4).

Bonding analysis. Previous quantum-chemical studies focused on the atomic or partial charge of the fluorine atom in order to contest its classification as a fluoronium ion[28]. Atomic charges, however, strongly depend on the computational level and are not uniquely defined[29]. In the present case, a non-exhaustive selection of population analyses yields atomic charges for the bridging fluorine atom of −0.260 (NBO; all charges are given in atomic units), −0.136 (Mulliken), −0.132 (CHELPG), −0.521 (AIM), −0.094 (Merz–Kollmann), +0.058 (Voronoi) (for more details see Supplementary Table 6). For all methods, the neighboring carbon atoms yield a positive partial charge.

Perhaps a more relevant aspect is how the fluorine atom is bound to its two neighboring sp^3-carbon atoms. As pointed out elsewhere, an AIM analysis shows two bond critical points (BCPs), indicating a chemical bond[16,17]. Judging from the different properties at these BCPs ($\rho_{BCP} = 0.95$ Å^{-3}; $\nabla^2\rho_{BCP} = -6.43$ Å^{-5}; $ELF_{BCP} = 0.43$; $|V|/G = 2.05$) the bonds are barely covalent due to the strong fluorine-specific repulsion between lone pairs of the fluorine atom and the C–F σ-bonds and are best described as charge shift bonds[30,31]. This bond character differs significantly from the one in $[H–F–H]^+$ ($\rho_{BCP} = 2.03$ Å^{-3}; $\nabla^2\rho_{BCP} = -68.44$ Å^{-5}; $ELF_{BCP} = 0.98$; $|V|/G = 16.44$), which is genuinely covalent[32].

To compare cation **1** to its heavier analogs, the fluorine atom was replaced by other halogens. The positions of the halogen atoms, the two neighboring carbon atoms, and the two nearest hydrogen atoms were re-optimized, while all other atoms were kept fixed. Table 2 lists the most important properties of the BCPs in these four systems and in $[H–F–H]^+$.

As the X–C bond distance increases the X–C bond becomes less polarized and the BCP approaches the mid-point of the X–C bond path. With increasing bond length, the electron density and its curvature at the BCP decreases, although the number of electrons associated with this bond increases, which can be seen from raising ELF (electron localization function) values and delocalization indices DLI_{X-C}. The covalent character in the chlorine analog is slightly larger than in the fluoronium cation and decreases again for the bromonium and iodonium cation. Nevertheless, it never reaches values typical for genuine covalent bonds as in $[H–F–H]^+$. In Fig. 4, ELF maps for the fluoronium and chloronium cations are shown for the C–X–C plane (X = F, Cl; left) and the one perpendicular to that containing the halogen lone pairs (right; bromonium and iodonium ELF maps in Supplementary Fig. 4). All four systems clearly indicate covalent interactions between carbon and the halogen atom, with the fluoronium cation resembling the least genuine covalent interaction and the chloronium cation the most. In the former, the valence electrons of the fluorine atom seem the least polarized, resembling almost the ELF map of an ion. This might be reinforced by the adjacent hydrogen atoms that draw electron density from the lone pair region in the C–F–C plane, which can be considered as a fluorine-specific interaction. For the other halonium cations, the valence shell is clearly separated into a maximum along the C–X bond path and two distinguished lone pairs.

In all, our results—loosely analogous to the reported norbornyl cation crystal structure in 2013[33]—definitively verify the nearly symmetrical structure of a controversial and often regarded as "impossible" species.

Methods

General considerations. All preparative work was carried out using standard Schlenk techniques. Glassware was greased with Triboflon III. All solid materials were handled inside a glove box with an atmosphere of dry argon ($O_2 < 0.5$ ppm, $H_2O < 0.5$ ppm). SO_2ClF was stored over CaH_2 before use. Precursor **2**, $SbF_5{\cdot}SO_2$ and $CsSb_2F_{11}$ were made as reported[16,17,34,35].

IR. Low-temperature IR spectra were recorded on a Nicolet iS50 with a diamond ATR attachment and a home-build contraption which was cooled by a stream of liquid nitrogen to −40 °C.

X-ray crystallography. All data were recorded on a Bruker D8 Venture diffractometer with a CMOS area detector using a Mo*K*α radiation source. In a nitrogen atmosphere suitable single crystals were coated and picked in perfluoroether oil at −80 °C and subsequently mounted on a 0.15 mm Micromount. The structure solution and refinement were performed in OLEX2[36] utilizing the ShelXT[37] structure solution program with intrinsic phasing and the ShelXL[38] refinement package using least-squares on weighted F2 values for all reflections.

Table 2 Computed properties of the bonds to the halogen atom in different double-norbornyl type halonium ions: bond length (r_{X-C}); deviation of the BCP from the mid-point of the bond ($r_{BCP-X} - ½r_{X-C}$; for negative values, the BCP is closer to the halogen atom, for positive values, vice versa); electron density at the BCP (ρ_{BCP}); Laplacian at the BCP ($\nabla^2\rho_{BCP}$); ELF at the BCP (ELF_{BCP}); value of the ELF maximum along the bond path (ELF_{max}); ratio of the absolute potential and the kinetic energy density at the BCP ($|V|/G$); localization index of the valence electrons at the halogen atom ($^{val}LI_X$); delocalization index of the bonds with the halogen atom (DLI_{X-C}); localization index of the valence electrons at the carbon or hydrogen atom bound to the halogen atom ($^{val}LI_{C/H}$).

System	r_{X-C} [Å]	$r_{BCP-X} - 1/2r_{X-C}$ [Å]	ρ_{BCP} [Å^{-3}]	$\nabla^2\rho_{BCP}$ [Å^{-5}]	ELF_{BCP}	ELF_{max}	$\|V\|/G$	$^{val}LI_X$	DLI_{X-C}	$^{val}LI_{C/H}$
Fluoronium	1.5871	0.20	0.946	−6.432	0.43	-	2.05	6.72	0.58	1.84
Chloronium	1.8852	0.17	0.964	−2.614	0.80	0.87	2.49	5.82	0.85	1.91
Bromonium	2.0236	0.16	0.849	−1.616	0.82	0.83	2.40	4.73	0.89	1.95
Iodonium	2.2006	0.14	0.729	−1.099	0.80	0.82	2.33	5.32	0.94	2.03
$[H-F-H]^+$	0.9679	0.35	2.027	−68.62	0.98	-	16.5	7.42	0.27	0.01

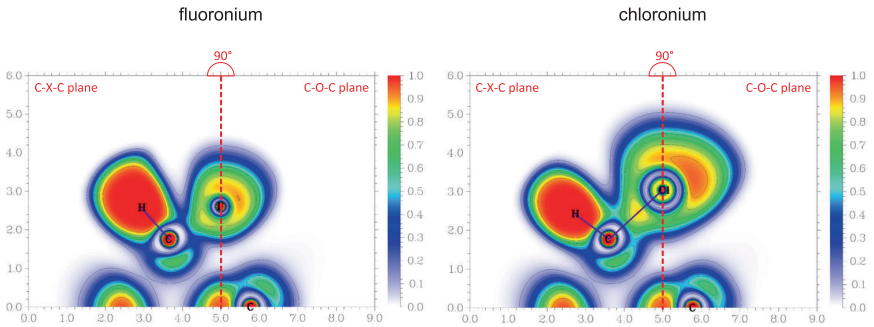

Fig. 4 Electron localization in Fluoro- and Chloronium. Electron localization function in the C–X–C plane (X = F, Cl) of 1 (left) and its chloronium analog (right) and in their C–O–C planes containing the halogen's lone pairs, perpendicular to the former one. Both planes are merged at the molecule's O–X axis (dashed red line). ELF is defined from 0.0 (white) to 1.0 (red); contours are drawn in intervals of 0.1.

Computational details. Calculations were performed with the Gaussian[39] program, using the B3LYP DFT functional applying Dunnings cc-pVTZ basis set[40–42] for all atoms except iodine for which a fully relativistic pseudopotential replacing 28 core electrons and the corresponding triple-ζ basis set[43,44] was used. All population analyses, AIM analysis, as well as the calculation and visualization of ELF plots, were performed with the Multiwfn program[45]. In addition, the Turbomole program[46] was used to perform calculations at the unrestricted Kohn–Sham DFT level, using the B3LYP hybrid functional[47–49] in conjunction with the valence triple-ζ basis set with two sets of polarization functions (def2-TZVPP)[50].

Crystallization of fluoronium salt [1][Sb_2F_{11}]. After $SbF_5{\cdot}SO_2$ (26 mg, 0.093 mmol) was filled into a Schlenk tube, SO_2ClF was condensed into the vessel forming a clear solution at −50 °C. Precursor **2** (20 mg, 0.075 mmol) was added via a funnel to the reaction vessel and the mixture was shaken until a homogenous yellow solution was formed. After the partial evacuation of the solvent, the mixture was slowly cooled to −80 °C. Over the course of two weeks, yellow crystals started to grow which could be analyzed via X-ray diffraction.

Pumping off all volatiles from the crystalline material under reduced pressure produced an orange powder, of which a sample for low-temperature IR measurements was prepared.

IR (ATR, −40 °C): $\tilde{\nu}$ = 2990 (w, ν (C–H)), 2914 (w, ν (C–H)), 1913 (m, ν (C=O)), 1746 (w), 1614 (s, ν_{as}(C=O···Sb)), 1562 (m), 1492 (w), 1475 (w), 1443 (m), 1394 (w), 1359 (m), 1327 (w), 1304 (m), 1292 (w), 1275 (w), 1258 (w), 1218 (m), 1172 (m), 1136 (w), 1100 (m), 1068 (w), 1056 (w), 1042 (w), 1025 (w), 988 (w), 918 (w), 870 (w), 822 (m, ν_{as}(C–O–C)), 793 (w), 736 (w), 701 (sh, ν_s(C–F–C)), 685 (vs, ν(Sb–F)), 669 (vs, ν(Sb–F)), 640 (s, ν(Sb–F)), 629 (s, ν(Sb–F)), 581(s, ν_{as}(C–F–C)), 551 (m), 516 (m, δ(C–F–C)), 502 (m), 476 (m, ν (Sb–F–Sb)), 430 (w), 417 (w), 408 (w), 384 (w), 364 (w), 272 (sh, ρ (C–F–C)), 237 (vs, δ(Sb–F–Sb)), 181 (w), 172 (w) cm^{-1}. (vs = very strong, s = strong, m = medium, w = weak, sh = shoulder).

Data availability

Crystallographic data (excluding structure factors) for structures reported in this study have been deposited at the Cambridge Crystallographic Data Centre (CCDC) and can be obtained free of charge via www.ccdc.cam.ac.uk/data_request/cif on quoting the depository number CCDC-2049161. All other data generated or analyzed during this study are provided in this Article and the Supplementary Information.

Received: 29 March 2021; Accepted: 11 August 2021;
Published online: 06 September 2021

References

1. McNaught, A. D. & Wilkinson, A. *IUPAC. Compendium of Chemical Terminology (the "Gold Book)* 2nd edn (Blackwell Scientific Publications, Oxford, 1997).
2. Roberts, I. & Kimball, G. E. The halogenation of ethylenes. *J. Am. Chem. Soc.* **59**, 947–948 (1937).
3. Grushin, V. V. Cyclic diaryliodonium ions: old mysteries solved and new applications envisaged. *Chem. Soc. Rev.* **29**, 315–324 (2000).
4. Bailly, F., Barthen, P., Frohn, H.-J. & Köckerling, M. Aryl(pentafluorophenyl) iodonium tetrafluoroborate: Allgemeine Synthesesmethode, typische Eigenschaften und strukturelle Gemeinsamkeiten. *Z. Anorg. Allg. Chem.* **626**, 2419–2427 (2000).
5. Brown, R. S. et al. Stable bromonium and iodonium ions of the hindered olefins adamantylideneadamantane and bicyclo[3.3.1]nonylidenebicyclo[3.3.1] nonane. X-ray structure, transfer of positive halogens to acceptor olefins, and ab initio studies. *J. Am. Chem. Soc.* **116**, 2448–2456 (1994).
6. Frohn, H.-J., Giesen, M., Welting, D. & Bardin, V. V. Bis(perfluoroorganyl) bromonium salts [(RF)2Br]Y (RF=aryl, alkenyl, and alkynyl). *J. Fluor. Chem.* **131**, 922–932 (2010).
7. Stoyanov, E. S., Stoyanova, I. V., Tham, F. S. & Reed, C. A. Dialkyl chloronium ions. *J. Am. Chem. Soc.* **132**, 4062–4063 (2010).
8. Hämmerling, S. et al. A very strong methylation agent: $[Me_2Cl][Al(OTeF_5)_4]$. *Angew. Chem. Int. Ed.* **58**, 9807–9810 (2019).
9. Hämmerling, S. et al. Ein sehr starkes Methylierungsmittel: $[Me_2Cl][Al(OTeF_5)_4]$. *Angew. Chem.* **131**, 9912–9915 (2019).

10. Olah, G. A., Laali, K. K., Wang, Q. & Prakash, G. K. S. *Onium Ions* (Wiley, New York, NY, 1998).
11. Olah, G. A. *Halonium Ions* (Wiley, New York, NY, 1975).
12. Viet, N., Cheng, X. & Morton, T. H. Three-membered cyclic fluoronium ions in gaseous ion-neutral complexes. *J. Am. Chem. Soc.* **114**, 7127–7132 (1992).
13. Wang, H., Webster, C. E., Pérez, L. M., Hall, M. B. & Gabbaï, F. P. Reaction of the 1,8-bis(diphenylmethylium)naphthalenediyl dication with fluoride: formation of a cation containing a C-F→C bridge. *J. Am. Chem. Soc.* **126**, 8189–8196 (2004).
14. Struble, M. D., Scerba, M. T., Siegler, M. & Lectka, T. Evidence for a symmetrical fluoronium ion in solution. *Science* **340**, 57–60 (2013).
15. Struble, M. D., Holl, M. G., Scerba, M. T., Siegler, M. A. & Lectka, T. Search for a symmetrical C-F-C fluoronium ion in solution: kinetic isotope effects, synthetic labeling, and computational, solvent, and rate studies. *J. Am. Chem. Soc.* **137**, 11476–11490 (2015).
16. Pitts, C. R., Holl, M. G. & Lectka, T. Spectroscopic characterization of a $[C–F–C]^+$ fluoronium ion in solution. *Angew. Chem. Int. Ed.* **57**, 1924–1927 (2018).
17. Pitts, C. R., Holl, M. G. & Lectka, T. Spectroscopic characterization of a $[C–F–C]^+$ fluoronium ion in solution. *Angew. Chem.* **130**, 1942–1945 (2018).
18. Mootz, D. & Bartmann, K. The fluoronium ions H_2F^+ and $H_3F_2^+$: characterization by crystal structure analysis. *Angew. Chem. Int. Ed. Engl.* **27**, 391–392 (1988).
19. Panisch, R., Bolte, M. & Müller, T. Hydrogen- and fluorine-bridged disilyl cations and their use in catalytic C-F activation. *J. Am. Chem. Soc.* **128**, 9676–9682 (2006).
20. Lehmann, M., Schulz, A. & Villinger, A. Bisilylated halonium ions: $[Me_3Si–X–SiMe_3][B(C_6F_5)_4]$ (X=F, Cl, Br, I). *Angew. Chem. Int. Ed.* **48**, 7444–7447 (2009).
21. Lehmann, M., Schulz, A. & Villinger, A. Bisilylated halonium ions: $[Me_3Si–X–SiMe_3][B(C_6F_5)_4]$ (X=F, Cl, Br, I). *Angew. Chem.* **121**, 7580 (2009).
22. Ivlev, S. I., Karttunen, A. J., Buchner, M. R., Conrad, M. & Kraus, F. The interhalogen cations $[Br_2F_5]^+$ and $[Br_3F_8]^+$. *Angew. Chem. Int. Ed.* **57**, 14640–14644 (2018).
23. Ivlev, S. I., Karttunen, A. J., Buchner, M. R., Conrad, M. & Kraus, F. Die Interhalogenkationen $[Br_2F_5]^+$ und $[Br_3F_8]^+$. *Angew. Chem.* **130**, 14850–14855 (2018).
24. Nakamoto, K. *Infrared and Raman Spectra of Inorganic and Coordination Compounds A: Theory and Applications in Inorganic Chemistry* (John Wiley & Sons Inc, Hoboken, N.J., 2009).
25. Solcà, N. & Dopfer, O. Protonation of gas-phase aromatic molecules: IR spectrum of the fluoronium isomer of protonated fluorobenzene. *J. Am. Chem. Soc.* **125**, 1421–1430 (2003).
26. Minkwitz, R. & Gerhard, V. On dimethylhalonium salts – $CH_3ClCH_3^+MF_6^-$, $CH_3BrCH_3^+MF_6^-$, $CH_3ICH_3^+MF_6^-$– and dimethylmethylendiiodonium salts $(CH_3ICH_2ICH_3)_2^+(MF_6^-)_2$ (M = As, Sb). *Z. Naturforsch. B Chem. Sci.* **46**, 561–565 (1991).
27. Stoyanov, E. S. Chemical properties of dialkyl halonium ions (R_2Hal^+) and their neutral analogues, methyl carboranes, CH_3-($CHB_{11}Hal_{11}$), where Hal = F, Cl. *J. Phys. Chem. A* **121**, 2918–2923 (2017).
28. Christe, K. O., Haiges, R., Rahm, M., Dixon, D. A. & Vasiliu, M. Misconceptions on fluoronium ions and hypervalent fluorine cations. *J. Fluor. Chem.* **204**, 6–10 (2017).
29. Mao, J. X. Atomic charges in molecules: a classical concept in modern computational chemistry. *PDJ* **2**, 15–18 (2014).
30. Shaik, S. et al. Charge-shift bonding: a new and unique form of bonding. *Angew. Chem. Int. Ed.* **59**, 984–1001 (2020). *Angew. Chem.* **132**, 996–1013 (2020).
31. Shaik, S. et al. Charge-shift bonding: a new and unique form of bonding. *Angew. Chem.* **132**, 996–1013 (2020).
32. Espinosa, E., Alkorta, I., Elguero, J. & Molins, E. From weak to strong interactions: a comprehensive analysis of the topological and energetic properties of the electron density distribution involving X-H···F-Y systems. *J. Chem. Phys.* **117**, 5529–5542 (2002).
33. Scholz, F. et al. Crystal structure determination of the nonclassical 2-norbornyl cation. *Science* **341**, 62–64 (2013).
34. Aynsley, E. E., Peacock, R. D. & Robinson, P. L. New inorganic compounds involving antimony pentafluoride. *Chem. Ind.* 1117 (1951).
35. Benkič, P., Brooke Jenkins, H. D., Ponikvar, M. & Mazej, Z. Synthesis and characterisation of alkali metal and thallium polyfluoroantimonates, ASb_nF_{5n+1} (n = 2, 3). *Eur. J. Inorg. Chem.* **2006**, 1084–1092 (2006).
36. Dolomanov, O. V., Bourhis, L. J., Gildea, R. J., Howard, J. A. K. & Puschmann, H. OLEX 2: a complete structure solution, refinement and analysis program. *J. Appl. Cryst.* **42**, 339–341 (2009).
37. Sheldrick, G. M. A short history of SHELX. *Acta Crystallogr. A* **64**, 112–122 (2008).
38. Sheldrick, G. M. Crystal structure refinement with SHELXL. *Acta Cryst. C* **71**, 3–8 (2015).
39. Frisch, M. J. et al. *Gaussian 16* (Gaussian, Inc., Wallingford CT, 2016).
40. Dunning, T. H. Gaussian basis sets for use in correlated molecular calculations. I. The atoms boron through neon and hydrogen. *J. Chem. Phys.* **90**, 1007–1023 (1989).
41. Woon, D. E. & Dunning, T. H. Gaussian basis sets for use in correlated molecular calculations. III. The atoms aluminum through argon. *J. Chem. Phys.* **98**, 1358–1371 (1993).
42. Wilson, A. K., Woon, D. E., Peterson, K. A. & Dunning, T. H. Gaussian basis sets for use in correlated molecular calculations. IX. The atoms gallium through krypton. *J. Chem. Phys.* **110**, 7667–7676 (1999).
43. Peterson, K. A., Figgen, D., Goll, E., Stoll, H. & Dolg, M. Systematically convergent basis sets with relativistic pseudopotentials. II. Small-core pseudopotentials and correlation consistent basis sets for the post-*d* group 16-18 elements. *J. Chem. Phys.* **119**, 11113–11123 (2003).
44. Peterson, K. A., Shepler, B. C., Figgen, D. & Stoll, H. On the spectroscopic and thermochemical properties of ClO, BrO, IO, and their anions. *J. Phys. Chem. A* **110**, 13877–13883 (2006).
45. Lu, T. & Chen, F. Multiwfn: a multifunctional wavefunction analyzer. *J. Comput. Chem.* **33**, 580–592 (2012).
46. TURBOMOLE GmbH. *TURBOMOLE V7.3* (a development of University of Karlsruhe and Forschungszentrum Karlsruhe GmbH, 1989–2018).
47. Becke, A. D. Density-functional exchange-energy approximation with correct asymptotic behavior. *Phys. Rev. A.* **38**, 3098–3100 (1988).
48. Lee, C., Yang, W. & Parr, R. G. Development of the Colle-Salvetti correlation-energy formula into a functional of the electron density. *Phys. Rev. B.* **37**, 785–789 (1988).
49. Vosko, S. H., Wilk, L. & Nusair, M. Accurate spin-dependent electron liquid correlation energies for local spin density calculations: a critical analysis. *Can. J. Phys.* **58**, 1200–1211 (1980).
50. Weigend, F. & Ahlrichs, R. Balanced basis sets of split valence, triple zeta valence and quadruple zeta valence quality for H to Rn: design and assessment of accuracy. *Phys. Chem. Chem. Phys.* **7**, 3297–3305 (2005).

Acknowledgements

We thank J. Heberle and D. Ehrenberg for scientific discussions. We gratefully acknowledge the Zentraleinrichtung für Datenverarbeitung (ZEDAT) of the Freie Universität Berlin for the allocation of computer time. Funded by the Deutsche Forschungsgemeinschaft (DFG, German Research Foundation)—Project-ID 387284271—SFB 1349. M.K. thanks JHU for a William Hooper Grafflin Fellowship (M.K.) and the National Science Foundation (NSF) (Grant CHE 1800510) (T.L.) for financial assistance.

Author contributions

K.F.H. carried out the synthetic work and analytical characterization. A.W. performed preliminary experiments on the system. C.M. and K.F.H. performed DFT calculations. C.M. performed the bonding analysis. S.S. acquired the XRD data. H.B. assisted with vibrational data analysis. M.K. and C.R.P. synthesized precursor 2. K.F.H. wrote the paper, all authors discussed and commented on the manuscript. T.L. and S.R. directed and coordinated the research.

Funding

Open Access funding enabled and organized by Projekt DEAL.

Competing interests

The authors declare no competing interests.

Additional information

Supplementary information The online version contains supplementary material available at https://doi.org/10.1038/s41467-021-25592-6.

Correspondence and requests for materials should be addressed to T.L. or S.R.

Peer review information *Nature Communications* thanks Karl Christe and the anonymous reviewer(s) for their contribution to the peer review of this work.

Reprints and permission information is available at http://www.nature.com/reprints

Publisher's note Springer Nature remains neutral with regard to jurisdictional claims in published maps and institutional affiliations.

Open Access This article is licensed under a Creative Commons Attribution 4.0 International License, which permits use, sharing, adaptation, distribution and reproduction in any medium or format, as long as you give appropriate credit to the original author(s) and the source, provide a link to the Creative Commons license, and indicate if changes were made. The images or other third party material in this article are included in the article's Creative Commons license, unless indicated otherwise in a credit line to the material. If material is not included in the article's Creative Commons license and your intended use is not permitted by statutory regulation or exceeds the permitted use, you will need to obtain permission directly from the copyright holder. To view a copy of this license, visit http://creativecommons.org/licenses/by/4.0/.

© The Author(s) 2021

3.4. An Amorphous Teflate Doped Aluminium Chlorofluoride: A Solid Lewis Superacid for the Dehydrofluorination of Fluoroalkanes

Minh Bui, Kurt F. Hoffmann, Thomas Braun*, Sebastian Riedel*, Christian Heinekamp, Kerstin Scheurell, Gudrun Scholz, Tomasz M. Stawski, Franziska Emmerling

DOI: 10.26434/chemrxiv-2022-vr6fm

©The Authors.

Author Contribution:
Kurt F. Hoffmann designed and performed the synthesis of ACF-teflate and conducted preliminary tests on its catalytic activity with the isomerization of 1,2-dibromohexafluoropropane. Minh Bui performed the reaction studies and analytical characterization. Franziska Emmerling and Tomasz Stawski wrote the proposals for the measurements on the synchrotrons BESSY II and Diamond Light Source. Christian Heinekamp and Tomasz Stawski evaluated the data from the synchrotrons. Kerstin Scheurell and Gudrun Scholz performed the solid-state NMR spectroscopic experiments. Minh Bui wrote the paper with support from Thomas Braun, all authors discussed the results and contributed to the manuscript. Thomas Braun and Sebastian Riedel supervised the project.

An Amorphous Teflate Doped Aluminium Chlorofluoride: A Solid Lewis Superacid for the Dehydrofluorination of Fluoroalkanes

Minh Bui,[a] Kurt Hoffmann,[b] Thomas Braun,*[a] Sebastian Riedel,*[b] Christian Heinekamp,[a],[c] Kerstin Scheurell,[a] Gudrun Scholz,[a] Tomasz M. Stawski,[c] Franziska Emmerling[a],[c]

Abstract: An anion doped aluminium chlorofluoride $AlCl_{0.1}F_{2.8}(OTeF_5)_{0.1}$ (ACF-teflate) was synthesized. The material contains pentafluoroorthotellurate (teflate) groups, which mimic fluoride ions electronically, but are sterically more demanding. They are embedded into the amorphous structure. The latter was studied by PDF analysis, EXAFS data and MAS NMR spectroscopy. The mesoporous powder is a Lewis superacid, and ATR-IR spectra of adsorbed CD_3CN reveal a blue-shift of the adsorption band by 73 cm^{-1}, which is larger than the shift for SbF_5. Remarkably, ACF-teflate catalyzes dehydrofluorination reactions of monofluoroalkanes to yield olefins in C_6D_6. In these cases, no Friedel-Crafts products were formed.

Amorphous aluminium fluoride-based catalysts can be considered as very strong Lewis-acids.[1] Nanoscopic aluminium chlorofluoride (ACF, $AlCl_xF_{3-x}$, with x = 0.3-0.05) exhibits a Lewis-acidity comparable to SbF_5.[1c,2] It has been synthesized by fluorination of $AlCl_3$ with CCl_3F and applied in a variety of conversions such as C-H activation, fluorination, defluorination or Friedel-Crafts type conversions.[3] Especially hydrodefluorination type reactions can be promoted by the presence of silanes and silylium-type surface species might play a crucial role to induce the C–F bond cleavage reactions.[3c,4] A variety of other Lewis-acidic amorphous aluminium fluoride type catalyst were developed such as the mesoscopic *high-surface*-AlF_3.[5] Fluorination of γ-Al_2O_3-700 with $CHClF_2$ also gives a highly Lewis-acidic mesoporous catalyst.[6] In the presence of Et_3SiH dehydrofluorination of fluoropentane was found, albeit with very low selectivity. A Nb doped Al hydroxide fluoride was obtained by reaction of Al isopropoxide with aqueous HF, and post-fluorination of the produced xerogel with $CHClF_2$ at higher temperatures. It is also mesoscopic, but shows Lewis-acidic and Brønsted acidic properties.[7] In all of these materials Lewis-acidity and amorphicity are mainly due to the distortion of the bulk structure by chloride or isopropoxide groups.

The pentafluoroorthotellurate group ([$^-$OTeF$_5$], teflate group) is an interesting substitute for fluoride, because the teflate group mirrors its electron withdrawing properties, but is considerably bulkier.[8] It can be considered as chemical inert towards electrophiles. The monomeric aluminium teflate $Al(OTeF_5)_3$ exhibits a much higher Lewis acidity compared to the one of SbF_5. However, a dimeric structure $[Al(OTeF_5)_3]_2$ in the solid state has been suggested, which lowers the Lewis acidity.[9] Nevertheless, it can be considered as a soluble molecular counterpart of AlF_3 phases.[10]

Herein, we report on an unprecedented strategy to design properties of an aluminium fluoride. Controlled anion doping with teflate groups by using $[Al(OTeF_5)_3]_2$ yielded an amorphous aluminium chlorofluoride (ACF-teflate). The sterically demanding [$^-$OTeF$_5$] moieties preset a pronounced distortion of the bulk material, which induces the Lewis superacidity. As a result, ACF-teflate is an active catalyst for the dehydrofluorination of fluoroalkanes at room temperature to yield olefins.

Fluorination of a mixture of $AlCl_3$ and 5 mol% $Al(OTeF_5)_3$ by treatment with $CFCl_3$ at low temperature was achieved to obtain a pale yellow powder after removal of the generated CCl_4 (Equation 1). The surface properties of ACF-teflate were assessed by gas N_2 adsorption experiments and BET analysis. The adsorption isotherm for ACF-teflate features at low pressure a type II like shape. A type H4 hysteresis indicates slit-like pores on the surface (see SI).[11] ACF-teflate is mesoporous and BJH analysis reveals a larger pore size (31 Å) than in ACF (12 Å), but a smaller surface area (220 m^2g^{-1} vs 330 m^2g^{-1} for ACF).[12]

$$AlCl_3 + 0.05\ Al(OTeF_5)_3 \xrightarrow[\text{2h, -30°C}\ -\ CCl_4]{\text{excess of } CCl_3F} \underset{\text{ACF-teflate}}{AlCl_{0.1}F_{2.8}(OTeF_5)_{0.1}} \quad (1)$$

Powder XRD studies revealed an amorphous nature for ACF-teflate. In the DSC profile an exothermic event was observed at approximately 450 °C, which indicates a crystallization process (see SI). TGA shows a mass loss in a range from 100 until 300 °C, whereas at 180 °C sublimation of $AlCl_3$ sets in. After heating up to 600 °C a mass loss of nearly 16 % was detected. Powder XRD data that were measured after heating, were assigned to β-AlF_3, as it was also found for ACF.[13]

STEM measurements at ACF-teflate reveal agglomerates consisting of spherical particles. The sizes of the agglomerates are in a range of 1-2 µm, whereas the single particles have a diameter of approximately 50 nm. Energy dispersive X-ray (EDX) analysis and elemental mappings (Figure 1) disclose that Al, Cl, F, O and Te are distributed homogenously over the entire agglomerate. This confirms the implementation of tellurium containing entities into the ACF structure. The EDX analysis suggests a chemical formula for the ACF-teflate of $AlCl_{0.1}F_{2.8}(OTeF_5)_{0.1}$.

[a] M. Bui, Prof. Dr. T. Braun, C. Heinekamp, Dr. K. Scheurell, Dr. G. Scholz, Priv.-Doz. Dr. F. Emmerling
Department of Chemistry, Humboldt-Universität zu Berlin
Brook-Taylor-Straße 2, D-12489 Berlin, Germany
E-mail: thomas.braun@chemie.hu-berlin.de
[b] K. Hoffmann, Prof. Dr. S. Riedel
Institut für Chemie und Biochemie, Freie Universität Berlin
Fabeckstraße 34/36, D-14195 Berlin, Germany
E-Mail: s.riedel@fu-berlin.de
[c] C. Heinekamp, Dr. Tomasz M. Stawski, Priv.-Doz. Dr. F. Emmerling
BAM Federal Institute for Materials Research and Testing
Richard-Willstätter-Straße 11, D-12489 Berlin, Germany

Supporting information for this article is given via a link at the end of the document.

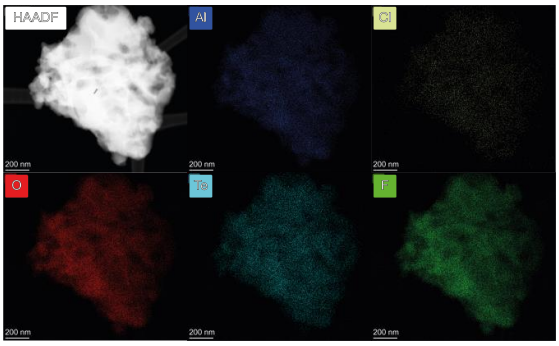

Figure 1. Elemental Mapping of ACF-teflate by STEM and EDX analysis.

MAS NMR data for ACF-teflate were measured and compared with those of ACF and $[Al(OTeF_5)_3]_2$. The latter were not reported before. The ^{27}Al MAS NMR spectrum for ACF-teflate shows a broad signal at –16 ppm, which is typical for strongly distorted $[AlF_6]$ moieties.[14] This signal has an increased line width by 150 Hz than the signal for ACF, suggesting a higher disorder and amorphicity.[15] A minor signal at 44 ppm was observed at a characteristic shift for $[AlX_4]$ entities, where X are either oxygen or fluorine atoms.[16] In the ^{27}Al MAS NMR spectrum of $[Al(OTeF_5)_3]_2$ a signal in the range between 34 and –18 ppm was observed, with a shape, typically associated with a second order quadrupolar coupling (see SI). DMFIT was used to determine an isotropic chemical shift ($\delta_{iso}(^{27}Al)$) of about 59 ppm, which is a characteristic value for fourfold coordinated aluminium species. This also confirms the dimeric structure $[Al(OTeF_5)_3]_2$ in the solid state. A second distinct signal at 13 ppm was detected that develops during the measurement. It can be associated to a sixfold coordinated aluminium entity $[AlF_xO_{6-x}]$ (x = 0-1) [14c,16b],and arises presumably from decomposition of $[Al(OTeF_5)_3]_2$ above room temperature. A ^{19}F MAS NMR spectrum of ACF-teflate shows three signals at –164, –47 and –42 ppm (Figure 2). The very broad signal at –164 ppm can be assigned to distorted $[AlF_6]$ octahedra. The signal is slightly shifted downfield when compared to the one for ACF (–167 ppm).[2b,14a] The resonance shows an increase of the line width by approximately 700 Hz when compared to the signal for ACF indicating a higher degree of disorder for ACF-teflate. The fairly sharp signal at –47 ppm with a shoulder at –42 ppm suggests the presence of two types of distinct teflate groups that remained their identity to a large part. $[Al(OTeF_5)_3]_2$ also shows two distinct signals in the ^{19}F NMR spectrum at –34 and –46 ppm with an intensity ratio of nearly 1:2, presumably for bridging and terminal teflate groups (Figure 3). Accordingly, the ^{19}F MAS NMR spectrum of $[Ph_4P][Al(OTeF_4)]$[9] exhibits only one signal at –44 ppm for all fluorine atoms bound at the teflate groups (see SI). Finally, spin-echo ^{19}F MAS NMR experiments of ACF-teflate were done to investigate the chemical environment of the teflate groups in the bulk. By increasing the dipolar evolution time, the signals for the teflate groups remain sharp, which suggests a lower dipolar interaction with their environment. The spin-echo experiments did also reveal a small signal at –195 ppm, which is indicative for the presence of surface bound terminal fluorides (see SI).[2b,14a]

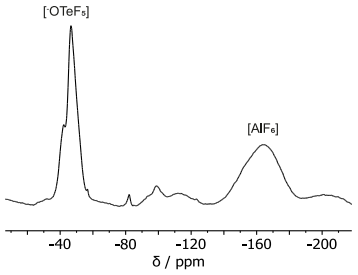

Figure 2. ^{19}F MAS NMR spectrum ($\tilde{\nu}_{rot}$: 20 kHz) of ACF-teflate.

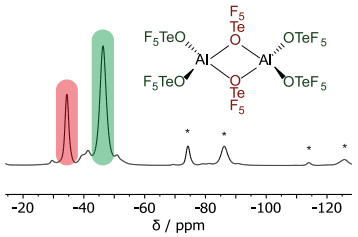

Figure 3. ^{19}F MAS NMR spectrum ($\tilde{\nu}_{rot}$: 15 kHz) for $[Al(OTeF_5)_3]_2$. Asterisks (*) represent spinning sidebands; Lewis structure of $[Al(OTeF_5)_3]_2$ with bridging (red) and terminal (green) $[OTeF_5]$ groups.

The amorphous nature of ACF-teflate and, for comparison, also ACF were then further investigated by synchrotron-based total scattering measurements at a wavelength of 0.161669 Å (76.7 keV). The pair distribution functions (PDF) displayed in Figure 4 confirm the amorphous and highly-disordered nature of both materials, since any structural coherence is below r = 4 Å. This is in contrast to crystalline $AlCl_3$ and AlF_3 samples, for which the coherence extends far beyond 4 Å (Figure 4, black lines). In addition, no distinct Al–Cl bond separations can be estimated from the PDF for ACF and ACF-teflate.

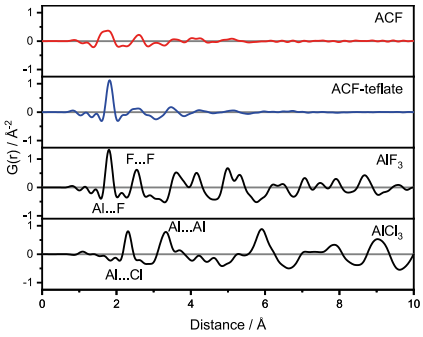

Figure 4. Pair Distribution Functions (PDF) of ACF, ACF-teflate, commercial AlF_3 and $AlCl_3$ from High-Energy X-ray Diffraction (HEXD, wavelength 0.161669 Å) data obtained at I15-1 Diamond Light Source.

ACF-teflate reveals a peak for Al···F separations at octahedral coordinated Al centers at approximately 1.82 Å. The peak can also partially be contributed by the Te···F bonds of the teflate groups, for which distances are reported between 1.82 – 1.84 Å.[9] In contrast ACF displays a broader feature, which seems to be due to two overlapping atomic distances at 1.6 and 1.8 Å. No shoulder can be detected for the peak shape at 1.82 Å for ACF-

teflate. This indicates that the reported coordination distances in [$^-$OTeF$_5$] groups are still intact.
EXAFS data at the Te K-edge at 31831.7 eV investigating the teflate coordination sphere are consistent with the observation from the pdf. The magnitude plot of χ in real space depicts a shift of 0.08 Å for ACF-teflate compared to the Te(OH)$_6$ reference sample (Figure 5). The bond separation for ACF-teflate was calculated to be 1.82 Å, which is in accordance with the reported Te···F distances in crystal structures of [$^-$OTeF$_5$] containing compounds.[9] The distance Te···O in Te(OH)$_6$ was determined to be 1.92 Å, which fits well with the literature value of 1.91 Å.[17] One cannot differentiate between Te···O and Te···F distances, due to the comparable electron densities of oxygen and fluorine atoms.

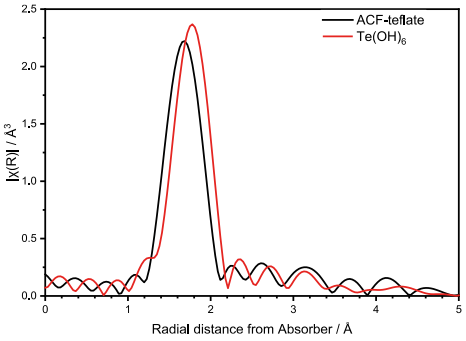

Figure 5. Magnitude of χ in real space from normalized Te K-edge data at 31831.7 eV of ACF-teflate and Te(OH)$_6$.

To confirm the presence of teflate-like groups ATR-IR spectra were measured (Figure 6). A very broad band at 608 cm^{-1} can be assigned to Al–F entities, as it was also found for ACF. Another vibrational band of lower intensity for aluminium fluoride entities was observed at 863 cm^{-1}. Additionally, a band for Te–F moiety was found at 705 cm^{-1} as well as Al–O vibrational bands at 986 and 1040 cm^{-1}.

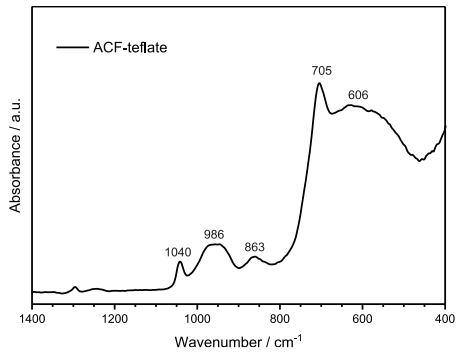

Figure 6. ATR-IR spectrum ACF-teflate.

Infrared spectroscopic data of adsorbed deuterated acetonitrile can be used to assess Lewis-acidic sites at the surfaces. For comparison ATR-IR spectra of molecular CD_3CN and [Al(OTeF$_5$)$_3$(CD_3CN)] as well as CD_3CN loaded ACF, and ACF-teflate are depicted in Figure 7. The C≡N vibrational band of CD_3CN was observed at 2258 cm^{-1} and serves as reference point for the materials. The band of ACF-teflate loaded with CD_3CN appears at 2331 cm^{-1}, which corresponds to a blue-shift of 73 cm^{-1}. Thus ACF-teflate can be classified as Lewis superacid, as it possesses a higher Lewis acidity than molecular SbF_5, whose corresponding CD_3CN adduct shows a blue shift of 56 cm^{-1}.[18] For comparison, [Al(OTeF$_5$)$_3$(CD_3CN)] and the adduct of ACF with CD_3CN show a blue-shift of the CN stretching mode to higher frequencies by 70 and 69 cm^{-1}, respectively.[9,12]
NH_3-TPD experiments were used to derive information on the nature of acidic surface sites. The TPD profile of ACF-teflate shows a peak between 180 and 220 °C with its maximum at 208 °C, which can be attributed to weak acidic sites. A larger peak which appears in the range between 330 and 380 °C, reaching its maximum at 349 °C, corresponds to medium/strong acids sites (see SI). The peak intensity ratio is 3:1, indicating a predominately presence of medium/strong acidic sites on the surface. The peak above 500 °C is probably due to the decomposition of the material.

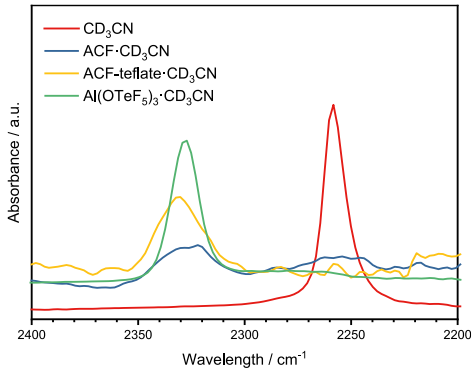

Figure 7. ATR-IR spectra for CD_3CN as well as CD_3CN loaded ACF, ACF-teflate and [Al(OTeF$_5$)$_3$(CD_3CN)].

To evaluate the catalytic activity of highly Lewis-acidic ACF-teflate, the isomerization of 1,2-dibromohexafluoropropane into 2,2-dibromohexafluoropropane was tested. The reaction is only catalyzed by strongly Lewis acidic centers,[5,19] and for ACF-teflate a conversion of 70 % at room temperature within 2 h was obtained. ACF-teflate was then used as catalyst for C–F bond activation reactions. Remarkably, in the presence of Et_3SiH and fluoropentane or fluoroheptane dehydrofluorination was observed to yield H_2 as well as 2-*E*/*Z*-pentene and the *E*/*Z* isomers of 2-and 3-heptane. (Scheme 1). No Friedel-Crafts reactions were found, although the reactions were run in C_6D_6 and it can be assumed that carbenium-like species might play a role as intermediates.[3a-c] They can be generated initially or by reaction with silylium-type ions. [3b,3c] The latter are formed after an interaction of silanes at the ACF-teflate surface. Mechanistically, a reaction with fluoroalkanes would then result in C–F bond cleavage to give the fluorosilane and carbenium-type ions. Subsequently, in the presence of silane dihydrogen and the olefinic products are formed. Though, with difluoromethane and 1,1-difluoroethane, the Friedel-Crafts products were observed (Scheme 1), which supports the assumption for the presence of intermediate carbenium-like species. Note also that treatment of fluoropentane with silane at ACF yielded Friedel-Crafts products.[3b] Thus, the properties of the system ACF-teflate/Et_3SiH are distinct. However, in a broader sense it resembles observations, which have been reported with ACF/Et_3GeH, but for the latter dehydrofluorination

steps were only observed at higher temperature.[3b] Note that molecular Al(I) complexes can undergo an oxidative addition of fluoroalkenes to form organoaluminium fluorides.[20] Ichikawa and co-workers reported on a cyclisation of 1-fluoronaphthalenes *via* aromatic C–F bond activation induced by Al(III) reagents.[21]

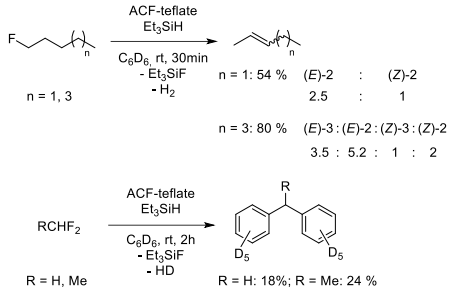

Scheme 1: Catalytic reactions at ACF-teflate

When ACF-teflate samples were loaded with Et_3SiH or fluoropentane a mass gain of 8% or 3 %, respectively, was determined after removal of excess silane under vacuum. This indicates a preference for silane binding over fluoroalkane immobilization. In order to estimate the interaction of silane with ACF-teflate, the latter was treated with silane and the properties of the resulting silane-loaded material was studied spectroscopically. In the ^{27}Al MAS NMR spectrum a signal at –16 ppm was observed that shows an increased line width by 150 Hz when compared to the signal for ACF-teflate, which indicates a slightly less ordered aluminium fluoride matrix. In the ^{19}F MAS NMR spectrum the signal for the teflate groups at –47 ppm and its shoulder at –42 ppm can still be detected, which suggests that immobilization of Et_3SiH at ACF-teflate has no significant influence on its bulk structure. Spin-echo experiments did not show the presence of terminal fluorine atoms anymore. The ^1H-^{19}Si CP MAS NMR spectrum exhibits three signals at 74, 38 and 10 ppm, presumably corresponding to a silylium-like species, Et_3SiF and Et_2SiF_2, respectively (see SI).[22]

In conclusion, a unique mesoscopic, amorphous Lewis superacid was synthesized by doping an aluminium chlorofluoride with sterically demanding teflate anions. Such an anion doping with large groups is exceptional for the synthesis of aluminium fluoride materials. It is intriguing that the two distinct types of teflate groups appear to be present in the mesoscopic material. In addition, the [$^-$OTeF$_5$] moieties seem to remain their identity in the bulk structure, which leads presumably to highly distorted structure. As a consequence, ACF-teflate is highly Lewis acidic and catalyzes dehydrofluorination reactions of fluoroalkanes at room temperature.

Acknowledgements

We acknowledge financial support from the CRC 1349 “Fluorine Specific Interactions” funded by the German Research Foundation (project number 387284271). The authors would like to thank Diamond Light Source for beamtime (proposal CY28776), and the staff of beamline I15-1, in particular Dr. Maria Diaz-Lopez for assistance with the HEXD data collection. We thank Dr. Mike Ahrens for helpful discussions.

Keywords: Lewis superacids • C–F activation • silanes • aluminium teflates • aluminium fluorides

[1] a) J. L. Delattre, P. J. Chupas, C. P. Grey, A. M. Stacy, *J. Am. Chem. Soc.* **2001**, *123*, 5364–5365; b) H. Bozorgzadeh, E. Kemnitz, M. Nickkho-Amiry, T. Skapin, J. M. Winfield, *J. Fluorine Chem.* **2001**, *107*, 45–52; c) T. Krahl, E. Kemnitz, *Cat. Sci. Technol.* **2017**, *7*, 773–796.

[2] a) Carl G. Krespan, V. A. Petrov, B. E. Smart (DuPont de Nemours), U.S.A. 5416246, **1992**; b) T. Krahl, E. Kemnitz, *J. Fluorine Chem.* **2006**, *127*, 663–678.

[3] a) G. Meißner, K. Kretschmar, T. Braun, E. Kemnitz, *Angew. Chem. Int. Ed.* **2017**, *56*, 16338–16341; b) G. Meißner, D. Dirican, C. Jäger, T. Braun, E. Kemnitz, *Cat. Sci. Technol.* **2017**, *7*, 3348–3354; c) M. Ahrens, G. Scholz, T. Braun, E. Kemnitz, *Angew. Chem. Int. Ed.* **2013**, *52*, 5328–5332; d) M.-C. Kervarec, C. P. Marshall, T. Braun, E. Kemnitz, *J. Fluorine Chem.* **2019**, *221*, 61–65.

[4] M.-C. Kervarec, E. Kemnitz, G. Scholz, S. Rudić, T. Braun, C. Jäger, A. A. L. Michalchuk, F. Emmerling, *Chem. Eur. J.* **2020**, *26*, 7314–7322.

[5] E. Kemnitz, U. Groß, S. Rüdiger, C. S. Shekar, *Angew. Chem. Int. Ed.* **2003**, *42*, 4251–4254.

[6] C. P. Marshall, G. Scholz, T. Braun, E. Kemnitz, *Cat. Sci. Technol.* **2020**, *10*, 391–402.

[7] C. P. Marshall, G. Scholz, T. Braun, E. Kemnitz, *Dalton Trans.* **2019**, *48*, 6834–6845.

[8] a) D. Lentz, K. Seppelt, *Angew. Chem. Int. Ed. Engl.* **1978**, *17*, 355–356; b) T. Birchall, R. D. Myers, H. De Waard, G. J. Schrobilgen, *Inorg. Chem.* **1982**, *21*, 1068–1073.

[9] A. Wiesner, T. W. Gries, S. Steinhauer, H. Beckers, S. Riedel, *Angew. Chem. Int. Ed* **2017**, *56*, 8263–8266.

[10] P. Tomar, T. Braun, E. Kemnitz, *Eur. J. Inorg. Chem.* **2019**, *2019*, 4735–4739.

[11] K. S. Sing, *Pure Appl. Chem.* **1985**, *57*, 603–619.

[12] B. Calvo, C. P. Marshall, T. Krahl, J. Kröhnert, A. Trunschke, G. Scholz, T. Braun, E. Kemnitz, *Dalton Trans.* **2018**, *47*, 16461–16473.

[13] T. Krahl, *Dissertation*, Humboldt University Berlin, **2005**

[14] a) T. Krahl, R. Stösser, E. Kemnitz, G. Scholz, M. Feist, G. Silly, J.-Y. Buzaré, *Inorg. Chem.* **2003**, *42*, 6474–6483; b) R. König, G. Scholz, R. Bertram, E. Kemnitz, *J. Fluorine Chem.* **2008**, *129*, 598–606; c) R. König, G. Scholz, A. Pawlik, C. Jäger, B. Van Rossum, H. Oschkinat, E. Kemnitz, *J. Phys. Chem. C* **2008**, *112*, 15708–15720.

[15] K. Chen, *Int J Mol Sci* **2020**, *21*, 5666.

[16] a) V. Lacassagne, C. Bessada, P. Florian, S. Bouvet, B. Ollivier, J.-P. Coutures, D. Massiot, *J. Phys. Chem. B* **2002**, *106*, 1862–1868; b) C. Bessada, V. Lacassagne, D. Massiot, P. Florian, J.-P. Coutures, E. Robert, B. Gilbert, *Zeitschrift für Naturforschung A* **1999**, *54*, 162–166.

[17] O. Lindqvist, *Acta Chem. Scand.* **1970**, *24*, 3178–3188.

[18] a) L. O. Müller, D. Himmel, J. Stauffer, G. Steinfeld, J. Slattery, G. Santiso-Quiñones, V. Brecht, I. Krossing, *Angew. Chem. Int. Ed.* **2008**, *47*, 7659–7663; b) L. Greb, *Chem. Eur. J.* **2018**, *24*, 17881–17896.

[19] a) V. A. Petrov, C. G. Krespan, B. E. Smart, *J. Fluorine Chem.* **1998**, *89*, 125–130; b) C. G. Krespan, V. A. Petrov, *Chem. Rev.* **1996**, *96*, 3269–3302.

[20] a) C. Bakewell, A. J. P. White, M. R. Crimmin, *Angew. Chem. Int. Ed.* **2018**, *57*, 6638–6642; b) T. Chu, I. Korobkov, G. I. Nikonov, *J. Am. Chem. Soc.* **2014**, *136*, 9195–9202; c) O. Kysliak, H. Görls, R. Kretschmer, *Chem. Commun.* **2020**, *56*, 7865–7868.

[21] N. Suzuki, T. Fujita, K. Y. Amsharov, J. Ichikawa, *Chem. Commun.* **2016**, *52*, 12948–12951.

[22] a) H. F. T. Klare, M. Oestreich, *Dalton Trans.* **2010**, *39*, 9176–9184; b) A. Martens, O. Petersen, H. Scherer, I. Riddlestone, I. Krossing, *Organometallics* **2018**, *37*, 706–711; c) W. Huynh, M. P. Conley, *Dalton Trans.* **2020**, *49*, 16453–16463; d) M. Wozniak, T. Braun, M. Ahrens, B. Braun-Cula, P. Wittwer, R. Herrmann, R. Laubenstein, *Organometallics* **2018**, *37*, 821–828; e) D. Cory, A. Wong, W. M. Ritchey, *J. Organomet. Chem.* **1982**, *235*, 277–285; f) X. Pan, M. Talavera, G. Scholz, T. Braun, *ChemCatChem* **2022**, e202200029.

...

4. Conclusion and Outlook

4.1. Conclusion

The first part of this thesis is focused on the investigation of the aluminum-based Lewis superacid $[Al(OTeF_5)_3]_2$ and its solvent adducts. An improved synthesis was developed which utilizes $AlMe_3$ and $HOTeF_5$ as reactants to obtain $[Al(OTeF_5)_3]_2$ in high purity. This development was essential, since the product obtained by the previously reported route[88] contained residual alkyl moieties as impurities, leading to undesired side reactions and a reduced thermal stability of the compound. The novel route gives access to solid $[Al(OTeF_5)_3]_2$ on a multigram scale, which is room temperature stable for several hours. During its synthesis, the partially-substituted compound $[Al(OTeF_5)_2Me]_2$ could be isolated and further analyzed. Also, the dimeric structure of $[Al(OTeF_5)_3]_2$ was proofed by solid-state MAS NMR spectroscopy.

The solvent-complexation of $[Al(OTeF_5)_3]_2$ was studied and, dependent on the used solvent, different coordination modes were observed for the isolated adducts. For nitrile solvents, such as acetonitrile and benzonitrile, a six-fold coordination at the Al center was achieved. The molecular structure was determined by single-crystal X-ray diffraction in case of the benzonitrile complex $[Al(OTeF_5)_3(PhCN)_3]$. Furthermore, it was shown that in weakly coordinating solvents such as CH_2Cl_2 and *o*-DFB these nitrile adducts undergo autoionization. Addition of 2,2'-bipyridine resulted in the crystallization of a corresponding autoionization product $[Al(OTeF_5)_2(bipy)_2][Al(OTeF_5)_4(bipy)]$. With weakly coordinating solvents like fluorobenzene or SO_2ClF monomeric adducts were formed. The complexes $[Al(OTeF_5)_3(PhF)_2]$ and $[Al(OTeF_5)_3(OSOClF)_2]$ display a trigonal-bipyramidal coordination sphere at the Al center. While the fluorobenzene adduct has to be stored at –25 °C, solutions of $[Al(OTeF_5)_3]_2$ in SO_2ClF are stable at room temperature. Additionally, it was possible to obtain the weak-bound toluene complex $[Al(OTeF_5)_3(\eta^1\text{-}C_7H_8)]$, which rapidly decomposes at temperatures above –20 °C.

Quantum-chemical calculations confirmed that the solvent-complexes of $Al(OTeF_5)_3$ exhibit high, but in comparison to the donor-free Lewis acid slightly diminished FIA values, which in the case of fluorobenzene, toluene and SO_2ClF still fulfill the requirement for Lewis superacidity. In Figure 16, selected solvent adducts and other aluminum-based Lewis superacids are ranked based on their FIA values, revealing the exceptionally high acidity of the pentafluoroorthotellurate derivatives. These computational results were further supported experimentally by the Gutmann-Beckett method and the abstraction of a fluoride ion from $[SbF_6]^-$. By reacting the weakly-bound solvent adducts with halide sources, the corresponding WCAs $[Al(OTeF_5)_3X]^-$ (X = F, Cl, Br) were formed. In solution those anions undergo ligand scrambling. Stochiometric addition of a $[OTeF_5]^-$ source yielded the known WCA $[Al(OTeF_5)_4]^-$, while an excess of $[OTeF_5]^-$ led to the dianionic species $[Al(OTeF_5)_5]^{2-}$. Reactions with silyl halides such as Me_3SiF or Me_3SiCl resulted in the formation of $Me_3SiOTeF_5$ and the corresponding aluminum halides.

Finally, this study of Lewis superacidic aluminum pentafluoroorthotellurates paved the way to apply these derivatives, for example, in the field of reactive cation synthesis and the development of new heterogeneous catalysts.

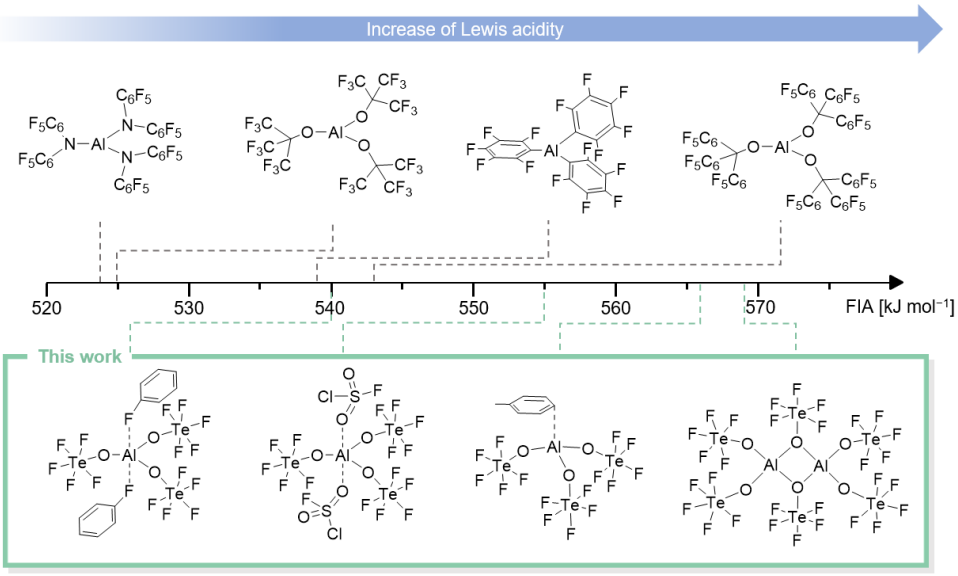

Figure 16. Fluoride ion affinity ranking of literature-known aluminum-based Lewis superacids and a selection of Lewis acidic pentafluoroorthotellurate derivatives calculated on BP86/def-SV(P) level of theory.

The second part of this thesis is concerned with the application of strong Lewis (and Brønsted) acids for the synthesis of highly reactive cations. Firstly, the perfluorinated tritylium cation $[C(C_6F_5)_3]^+$ was studied. So far, this cation was only obtainable in superacidic media such as "magic acid" (HSO_3F/SbF_5) or oleum. Reactions of the chloride precursor $C(C_6F_5)_3Cl$ either with the Lewis superacid $[Al(OTeF_5)_3]_2$ in SO_2ClF or with the Brønsted superacid $[H–C_6F_2H_4][Al(OTeF_5)_4]$ led in both cases to the successful formation of $[C(C_6F_5)_3]^+$. The molecular structure in the solid state of this cation was characterized for the first time by single-crystal X-ray diffraction of the compound $[C(C_6F_5)_3][Al(OTeF_5)_4]$ (cf. Figure 17). These novel reaction routes allow the handling of uncoordinated $[C(C_6F_5)_3]^+$ in organic solvents and its usage for further reactions.

In previous quantum-chemical studies the high Lewis acidity of $[C(C_6F_5)_3]^+$ was already reported. A special aspect is its remarkably high hydride ion affinity (HIA) of 955 kJ mol^{-1} when compared to its non-fluorinated analogue $[C(C_6H_5)_3]^+$ (HIA = 801 kJ mol^{-1}). These results were also proven in experiment by reacting $[C(C_6F_5)_3][Al(OTeF_5)_3Cl]$ with isobutane. Hereby, a hydride abstraction occured, forming the compound $HC(C_6F_5)_3$ and presumably the cation $[C(CH_3)_3]^+$ that subsequently polymerized. Another distinctive feature of $[C(C_6F_5)_3]^+$ is its high oxidation potential. Cyclovoltametric measurements of $[C(C_6F_5)_3][Al(OTeF_5)_4]$ in *o*-DFB displayed a formal oxidation potential of 1.11 V vs. Fc/Fc^+. Compared to the oxidation potential of non-fluorinated $[C(C_6H_5)_3]^+$ ($E^\circ = -0.11$ V) it is a drastic increase. The high oxidation potential of $[C(C_6F_5)_3]^+$ is explained by the strong electron-withdrawing properties of the perfluorinated phenyl groups, which was further supported by quantum-chemical calculations. In addition, the oxidative strength of $[C(C_6F_5)_3]^+$ was experimentally demonstrated by the oxidation of tris-(4-bromophenyl)amin with $[C(C_6F_5)_3][Al(OTeF_5)_4]$ to its radical cation. The latter species is also known as "Magic blue" and commonly employed in organic chemistry as a strong oxidizer.

Secondly, the isolation and characterization of an organic fluoronium ion was investigated. While a handful of inorganic fluoronium cations and their structure were already reported, a structural proof for an organic representative of the type $[R_2F]^+$ (R = organic residue) was still missing. So far, only NMR

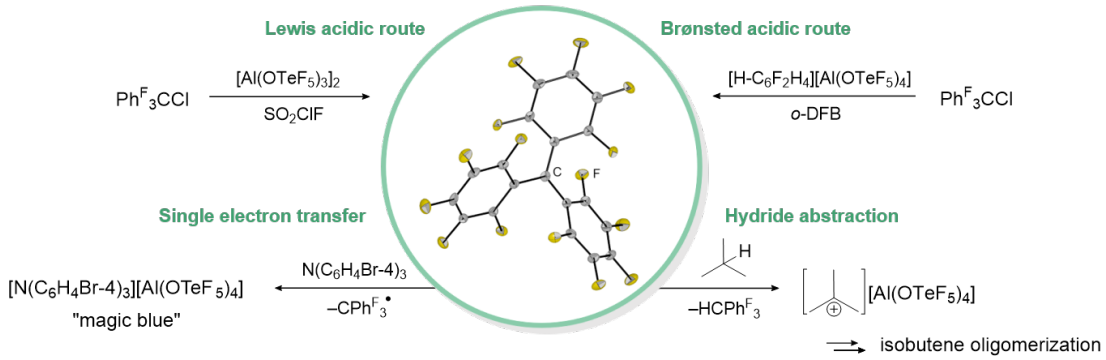

Figure 17. Synthesis and reactivity of the perfluorinated trityl cation $[C(C_6F_5)_3]^+$.

spectroscopic studies of a cage-like, organic fluoronium ion have been reported. While it was not possible to isolate and crystallize this compound with the Lewis acid $Al(OTeF_5)_3$, the reaction of the double norbornyl-type precursor with $SbF_5{\cdot}SO_2$ in SO_2ClF yielded success (see Figure 18). This route enabled the first crystallographic characterization of an organic fluoronium ion as an $[Sb_2F_{11}]^-$ salt and confirmed the expected symmetrical C–F–C bonding situation. Additionally, this compound was analyzed by vibrational spectroscopy and quantum-chemical calculations. An AIM analysis and the subsequent comparison with the heavier halonium homologues revealed in the case of the fluoronium ion a high charge-shift character of the C–F bonds instead of a covalent or ionic bonding situation.

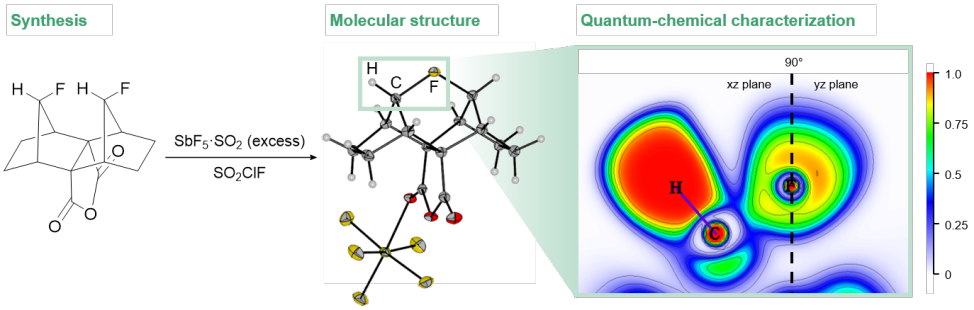

Figure 18. Synthesis and characterization of the organic fluoronium cation.

Lastly, the synthesis of a teflate-doped material was envisioned. A suitable candidate for this study was aluminum chlorofluoride $AlCl_xF_{3-x}$ (x = 0.3 - 0.05; ACF), a Lewis acidic material which has been already applied as heterogeneous catalyst, e.g. for C–F bond cleavage reactions. The reaction of a mixture of aluminum chloride $AlCl_3$ with 5 mol% $[Al(OTeF_5)_3]_2$ and CCl_3F yielded a yellow solid on multi-gram scale. Powder X-ray diffraction and BET measurements revealed a mesoporous, amorphous material. STEM measurements and EDX analysis showed sphere-shaped particles which tend to agglomerate. This particles possess a homogeneous dispersion of the elements Al, Cl, F, O and Te with the elemental composition of $AlCl_{0.1}F_{2.8}(OTeF_5)_{0.1}$. Solid-state MAS NMR spectroscopy, PDF and EXAFS measurements confirmed intact $OTeF_5$ groups. By IR spectroscopy of adsorbed CD_3CN the Lewis superacidic nature of the material was shown. The new ACF-teflate catalyzed the isomerization of 1,2-dibromohexafluoropropane to 2,2-dibromohexafluoropropane at room temperature. Performing this reaction at ambient conditions is only promoted by very strong Lewis acids such as ACF. Furthermore, the catalytic dehydrofluorination of fluoropentane and fluoroheptane through addition of Et_3SiH in deuterated benzene yielded the E/Z

isomers of 2-pentene, 2-heptene and 3-heptene together with H_2. In contrast, the analogous reaction with non-doped ACF resulted in the formation of Friedel-Craft products. These results indicate an exclusive reaction pathway for ACF-teflate.

This thesis laid ground for future applications of Lewis superacidic aluminum pentafluoroorthotellurates. It was shown, that strong Lewis acids are key reagents to answer fundamental questions in chemistry, such as the bonding situation in organic fluoronium ions, and they give synthetic access to new reactive species, such as the perfluorinated tritylium ion. Finally, this thesis touched on the development of new amorphous materials, which combine the high acidity of molecular Lewis superacids with the advantages of heterogeneous catalysts.

On a broader perspective, this work contributed to a fundamental understanding of the chemistry of aluminum pentafluoroorthotellurates. While there have already been spectacular synthetic results in conjunction with ionic aluminum pentafluoroorthotellurates reported, deeper insights on the structure and reactivity of the neutral counterpart were missing. This work resolved many of those questions such as the fluxional behavior in different solvents, more information on its structure in the solid state and the previously instability of the neat compound. Moreover, these neutral aluminum pentafluoroorthotellurates were shown to act as bridging link between molecular and solid Lewis acids such as ACF. In this regard, the similarities and differences of the pentafluoroorthotellurate group compared with the fluoride ligand were elaborated. From a theoretical point of view, the fluoride ion affinity of $Al(OTeF_5)_3$ clearly surpasses the values of hypothetically monomeric AlF_3, which might be explained by a reduced π-backbonding in case of the $[OTeF_5]^-$ compared to the F^- ligand. At the same time, the sterical demand of the teflate group results in a dimeric $[Al(OTeF_5)_3]_2$ in contrast to solid AlF_3. With this dimeric form and its solvent adducts, model reactions can be performed to further understand the interactions of solid Lewis acids with substrate molecules. Additionally, the oxidation resistance of the pentafluoroorthotellurate group was proven with the successful stabilization of the perfluorinated tritylium ion. On the downside, small nucleophiles such as F^- still can access the aluminum center, resulting in the substitution of $[OTeF_5]^-$ groups. Future endeavors could tackle these limitations by using five and sixfold coordinated pentafluoroorthotellurates based on As and Sb, resulting in a more effectively shielded central atom. Furthermore, the teflate group itself could be modified by substitution of F atoms with bulkier, electron-withdrawing groups such as CF_3 or C_6F_5.

4.2. Outlook

An interesting application for Lewis acidic aluminum pentafluoroorthotellurates might be found in the area of frustrated Lewis pair chemistry. In terms of small molecule activation (see Section 1.4.3), Lewis superacids can lead to different reaction pathways. With the right combination of $Al(OTeF_5)_3$ and sterically encumbered phosphines or N-heterocyclic carbenes, highly active cooperative or frustrated Lewis pairs might become accessible. They could be used for the activation and heterolytic cleavage of inert substrates. Furthermore, the formation of a frustrated radical pair based on $Al(OTeF_5)_3$ might be of interest. This phenomenon is closely related to FLP chemistry and allows radical reaction pathways when the redox potential of the Lewis pair is correctly aligned.[312] This was exemplary shown with the Lewis pair $P(t\text{-}Bu)_3/Al(C_6F_5)_3$ compared to $P(Mes)_3/Al(C_6F_5)_3$. While the former showed typical FLP reactivity, the latter resulted in different reaction products, which was explained by the formation of a frustrated radical pair $[P(Mes)_3]^{\cdot+}[Al(C_6F_5)_3]^{\cdot-}$.[313]

As shown in Section 3.2, the perfluorinated tritylium cation possesses a largely increased hydride ion affinity when compared to the non-fluorinated analogue. This opens up the possibility to employ this perfluorinated cation in the field of silylium-catalyzed hydrodefluorination reactions. As Ozerov and co-workers pointed out in a computational study, the hydride ion affinity of $[C(C_6H_5)_3]^+$ barely matches with that of the silylium cation $[Et_3Si]^+$.[314] Nevertheless, this is the standard reagent for the hydride abstraction to initiate silylium-driven hydrodefluorination reactions. The hydrodefluorination of perfluoroalkanes is still a synthetic challenge and simple trialkylsilylium ions are not electrophilic enough to promote those reactions. With the perfluorinated $[C(C_6F_5)_3]^+$ in hand, it could be possible to perform hydride abstraction reaction at hydrosilanes with electron-withdrawing substituents. If such a reaction succeed, a silylium cation with an increased electrophilicity is formed, which subsequently might be able to abstract a fluoride even from a perfluorinated alkane as substrate (see Figure 19).

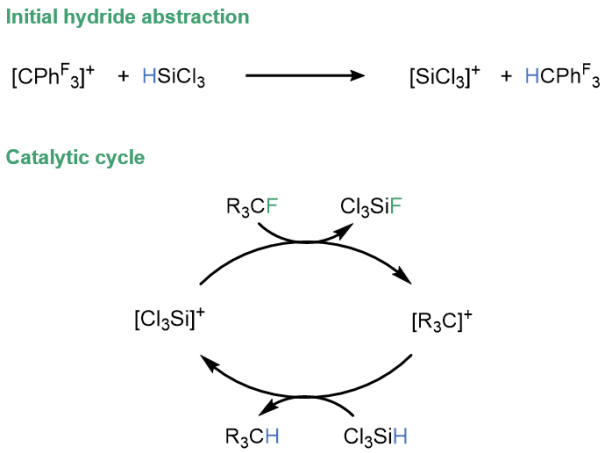

Figure 19. Initial generation of trichlorosilylium $[Cl_3Si]^+$ and catalytic hydrodefluorination cycle.

Similar to the known catalytic hydrodefluorination, a catalytic cycle could also be achieved with this reaction system. A feasible silane for this task could be Cl_3SiH, since this compound is also abundantly available.

5. References

[1] S. Arrhenius, *Z. Phys. Chem.* **1887**, *1*, 631–648.

[2] J. N. Brønsted, *Recl. Trav. Chim. Pays-Bas* **1923**, *42*, 718–728.

[3] T. M. Lowry, *J. Chem. Technol. Biotechnol.* **1923**, *42*, 43–47.

[4] G. N. Lewis, *J. Frankl. Inst.* **1938**, *226*, 293–313.

[5] H. Lux, *Z. Elektrochem. Angew. Phys. Chem.* **1939**, *45*, 303–309.

[6] H. Flood, T. Förland, L. G. Sillén, A. Linnasalmi, P. Laukkanen, *Acta Chem. Scand.* **1947**, *1*, 592–604.

[7] J. E. Huheey, E. A. Keiter, R. L. Keiter, *Anorganische Chemie: Prinzipien von Struktur und Reaktivität*, 2., neubearb. Aufl., de Gruyter, Berlin and New York, **1995**.

[8] S. P. L. Sørensen, *Biochem. Z.* **1909**, 131–304.

[9] L. P. Hammett, A. J. Deyrup, *J. Am. Chem. Soc.* **1932**, *54*, 2721–2739.

[10] G. A. Olah, G. K. Surya Prakash, Á. Molnr, J. Sommer, *Superacid Chemistry*, John Wiley & Sons, Inc, Hoboken, NJ, USA, **2009**.

[11] D. Fărcaşiu, A. Ghenciu, *J. Am. Chem. Soc.* **1993**, *115*, 10901–10908.

[12] D. Himmel, S. K. Goll, I. Leito, I. Krossing, *Angew. Chem. Int. Ed.* **2010**, *49*, 6885–6888.

[13] D. Himmel, V. Radtke, B. Butschke, I. Krossing, *Angew. Chem. Int. Ed.* **2018**, *57*, 4386–4411.

[14] R. G. Pearson, *J. Am. Chem. Soc.* **1963**, *85*, 3533–3539.

[15] R. S. Drago, B. B. Wayland, *J. Am. Chem. Soc.* **1965**, *87*, 3571–3577.

[16] H. Mayr, M. Breugst, A. R. Ofial, *Angew. Chem. Int. Ed.* **2011**, *50*, 6470–6505.

[17] T. E. Mallouk, G. L. Rosenthal, G. Mueller, R. Brusasco, N. Bartlett, *Inorg. Chem.* **1984**, *23*, 3167–3173.

[18] J. W. Larson, T. B. McMahon, *Inorg. Chem.* **1987**, *26*, 4018–4023.

[19] A. P. Altshuller, *J. Am. Chem. Soc.* **1955**, *77*, 6187–6188.

[20] K. O. Christe, D. A. Dixon, D. McLemore, W. W. Wilson, J. A. Sheehy, J. A. Boatz, *J. Fluor. Chem.* **2000**, *101*, 151–153.

[21] C. G. Krespan, V. A. Petrov, *Chem. Rev.* **1996**, *96*, 3269–3302.

[22] H. Böhrer, N. Trapp, D. Himmel, M. Schleep, I. Krossing, *Dalton Trans.* **2015**, *44*, 7489–7499.

[23] Z. M. Heiden, A. P. Lathem, *Organometallics* **2015**, *34*, 1818–1827.

[24] S. Ilic, A. Alherz, C. B. Musgrave, K. D. Glusac, *Chem. Soc. Rev.* **2018**, *47*, 2809–2836.

[25] H. Großekappenberg, M. Reißmann, M. Schmidtmann, T. Müller, *Organometallics* **2015**, *34*, 4952–4958.

[26] S. A. Couchman, D. J. D. Wilson, J. L. Dutton, *Eur. J. Org. Chem.* **2014**, *2014*, 3902–3908.

[27] D. F. Shriver, B. Swanson, *Inorg. Chem.* **1971**, *10*, 1354–1365.

[28] B. von Ahsen, B. Bley, S. Proemmel, R. Wartchow, H. Willner, F. Aubke, *Z. Anorg. Allg. Chem.* **1998**, *624*, 1225–1234.

[29] M. A. Beckett, G. C. Strickland, J. R. Holland, K. Sukumar Varma, *Polymer* **1996**, *37*, 4629–4631.

[30] E. Mayer, F. Sladky, *Inorg. Chem.* **1975**, *14*, 589–592.

[31] R. F. Childs, D. L. Mulholland, A. Nixon, *Can. J. Chem.* **1982**, *60*, 809–812.

[32] P. Erdmann, L. Greb, *Angew. Chem. Int. Ed.* **2022**, *61*, e202114550.

[33] R. G. Parr, L. v. Szentpály, S. Liu, *J. Am. Chem. Soc.* **1999**, *121*, 1922–1924.

[34] A. R. Jupp, T. C. Johnstone, D. W. Stephan, *Dalton Trans.* **2018**, *47*, 7029–7035.

[35] L. Greb, *Chem. Eur. J.* **2018**, *24*, 17881–17896.

[36] *The IUPAC Compendium of Chemical Terminology*, (Ed.: V. Gold), International Union of Pure and Applied Chemistry (IUPAC), Research Triangle Park, NC, **2019**.

[37] K. Seppelt, *Angew. Chem. Int. Ed.* **1982**, *21*, 877–888.

[38] A. Engelbrecht, F. Sladky, *Angew. Chem.* **1964**, *76*, 379–380.

[39] K. Seppelt, D. Nothe, *Inorg. Chem.* **1973**, *12*, 2727–2730.

[40] D. Lentz, K. Seppelt, *Z. Anorg. Allg. Chem.* **1983**, *502*, 83–88.

[41] F. Sladky, H. Kropshofer, *J. Chem. Soc., Chem. Commun.* **1973**, 600.

[42] D. Lentz, K. Seppelt, *Z. Anorg. Allg. Chem.* **1980**, *460*, 5–16.

[43] T. Drews, K. Seppelt, *Z. Anorg. Allg. Chem.* **1991**, *606*, 201–207.

[44] M. A. Ellwanger, C. von Randow, S. Steinhauer, Y. Zhou, A. Wiesner, H. Beckers, T. Braun, S. Riedel, *ChemComm* **2018**, *54*, 9301–9304.

[45] D. Lentz, K. Seppelt, *Angew. Chem. Int. Ed.* **1978**, *17*, 355–356.

[46] F. Sladky, H. Kropshofer, H. Kropshofer, *Inorg. Nucl. Chem. Lett.* **1972**, *8*, 195–197.

[47] T. Birchall, R. D. Myers, H. d. Waard, G. J. Schrobilgen, *Inorg. Chem.* **1982**, *21*, 1068–1073.

[48] D. Lentz, H. Pritzkow, K. Seppelt, *Angew. Chem. Int. Ed.* **1977**, *16*, 729–730.

[49] D. Lentz, H. Pritzkow, K. Seppelt, *Inorg. Chem.* **1978**, *17*, 1926–1931.

[50] D. Lentz, K. Seppelt, *Angew. Chem. Int. Ed.* **1979**, *18*, 66–67.

[51] P. Huppmann, H. Hartl, K. Seppelt, *Z. Anorg. Allg. Chem.* **1985**, *524*, 26–32.

[52] F. W. B. Einstein, P. R. Rao, J. Trotter, N. Bartlett, *J. Chem. Soc., A* **1967**, 478.

[53] K. Seppelt, *Chem. Ber.* **1976**, *109*, 1046–1052.

[54] K. Seppelt, *Chem. Ber.* **1975**, *108*, 1823–1829.

[55] G. A. Olah, G. K. Prakash, J. Sommer, *Science* **1979**, *206*, 13–20.

[56] L. O. Müller, D. Himmel, J. Stauffer, G. Steinfeld, J. Slattery, G. Santiso-Quiñones, V. Brecht, I. Krossing, *Angew. Chem. Int. Ed.* **2008**, *47*, 7659–7663.

[57] A. Y. Timoshkin, G. Frenking, *Organometallics* **2008**, *27*, 371–380.

[58] L. A. Mück, A. Y. Timoshkin, G. Frenking, *Inorg. Chem.* **2012**, *51*, 640–646.

[59] P. Erdmann, J. Leitner, J. Schwarz, L. Greb, *ChemPhysChem* **2020**, *21*, 987–994.

[60] A. J. Edwards, P. Taylor, *J. Chem. Soc., D* **1971**, 1376–1377.

[61] H. D. B. Jenkins, I. Krossing, J. Passmore, I. Raabe, *J. Fluor. Chem.* **2004**, *125*, 1585–1592.

[62] R. Steudel, *Chemie der Nichtmetalle: Synthesen - Strukturen - Bindung - Verwendung*, de Gruyter, Berlin, Boston, **2013**.

[63] M. Finze, E. Bernhardt, M. Zähres, H. Willner, *Inorg. Chem.* **2004**, *43*, 490–505.

[64] A. Terheiden, E. Bernhardt, H. Willner, F. Aubke, *Angew. Chem. Int. Ed.* **2002**, *41*, 799–801.

[65] M. Finze, E. Bernhardt, A. Terheiden, M. Berkei, H. Willner, D. Christen, H. Oberhammer, F. Aubke, *J. Am. Chem. Soc.* **2002**, *124*, 15385–15398.

[66] M. Gerken, G. Pawelke, E. Bernhardt, H. Willner, *Chem. Eur. J.* **2010**, *16*, 7527–7536.

[67] A. G. Massey, A. J. Park, *J. Organomet. Chem.* **1964**, *2*, 245–250.

[68] F. Focante, P. Mercandelli, A. Sironi, L. Resconi, *Coord. Chem. Rev.* **2006**, *250*, 170–188.

[69] K. Ishihara, N. Hanaki, M. Funahashi, M. Miyata, H. Yamamoto, *Bull. Chem. Soc. Jpn.* **1995**, *68*, 1721–1730.

[70] J. Zhou, S. J. Lancaster, D. A. Walker, S. Beck, M. Thornton-Pett, M. Bochmann, *J. Am. Chem. Soc.* **2001**, *123*, 223–237.

[71] G. Erker, *Dalton Trans.* **2005**, 1883–1890.

[72] D. W. Stephan, *J. Am. Chem. Soc.* **2015**, *137*, 10018–10032.

[73] L. A. Körte, J. Schwabedissen, M. Soffner, S. Blomeyer, C. G. Reuter, Y. V. Vishnevskiy, B. Neumann, H.-G. Stammler, N. W. Mitzel, *Angew. Chem. Int. Ed.* **2017**, *56*, 8578–8582.

[74] A. Engelbrecht, E. Tschager, *Z. Anorg. Allg. Chem.* **1977**, *433*, 19–25.

[75] G. A. Olah, K. Laali, O. Farooq, *J. Org. Chem.* **1984**, *49*, 4591–4594.

[76] G. A. Olah, O. Farooq, S. M. F. Farnia, J. A. Olah, *J. Am. Chem. Soc.* **1988**, *110*, 2560–2565.

[77] B. Cremer-Lober, H. Butler, D. Naumann, W. Tyrra, *Z. Anorg. Allg. Chem.* **1992**, *607*, 34–40.

[78] A. P. Davis, M. Jaspars, *Angew. Chem. Int. Ed.* **1992**, *31*, 470–471.

[79] Y. Li, C. Topf, X. Cui, K. Junge, M. Beller, *Angew. Chem. Int. Ed.* **2015**, *54*, 5196–5200.

[80] K. Thenert, K. Beydoun, J. Wiesenthal, W. Leitner, J. Klankermayer, *Angew. Chem. Int. Ed.* **2016**, *55*, 12266–12269.

[81] D. B. G. Williams, M. L. Shaw, M. J. Green, C. W. Holzapfel, *Angew. Chem. Int. Ed.* **2008**, *47*, 560–563.

[82] D. B. G. Williams, M. Lawton, *Tetrahedron Lett.* **2006**, *47*, 6557–6560.

[83] A. Hermannsdorfer, M. Driess, *Angew. Chem. Int. Ed.* **2021**, *60*, 13656–13660.

[84] K. Seppelt, *Chem. Ber.* **1977**, *110*, 1470–1476.

[85] D. Lentz, K. Seppelt, *Angew. Chem. Int. Ed.* **1978**, *17*, 356–361.

[86] M. J. Collins, G. J. Schrobilgen, *Inorg. Chem.* **1985**, *24*, 2608–2614.

[87] M. Gerken, P. Kolb, A. Wegner, H. P. Mercier, H. Borrmann, D. A. Dixon, G. J. Schrobilgen, *Inorg. Chem.* **2000**, *39*, 2813–2824.

[88] A. Wiesner, T. W. Gries, S. Steinhauer, H. Beckers, S. Riedel, *Angew. Chem. Int. Ed.* **2017**, *56*, 8263–8266.

[89] G. S. Hair, A. H. Cowley, R. A. Jones, B. G. McBurnett, A. Voigt, *J. Am. Chem. Soc.* **1999**, *121*, 4922–4923.

[90] D. Chakraborty, E. Y.-X. Chen, *Organometallics* **2003**, *22*, 207–210.

[91] D. Chakraborty, E. Y.-X. Chen, *Macromolecules* **2002**, *35*, 13–15.

[92] S. Feng, G. R. Roof, E. Y.-X. Chen, *Organometallics* **2002**, *21*, 832–839.

[93] T. Belgardt, J. Storre, H. W. Roesky, M. Noltemeyer, H.-G. Schmidt, *Inorg. Chem.* **1995**, *34*, 3821–3822.

[94] J. Chen, E. Y.-X. Chen, *Dalton Trans.* **2016**, *45*, 6105–6110.

[95] J. Chen, E. Y.-X. Chen, *Angew. Chem. Int. Ed.* **2015**, *54*, 6842–6846.

[96] A. K. Jaiswal, K. K. K. Goh, S. Sung, R. D. Young, *Org. Lett.* **2017**, *19*, 1934–1937.

[97] G. Ménard, D. W. Stephan, *Angew. Chem.* **2012**, *124*, 4485–4488.

[98] G. Ménard, D. W. Stephan, *Angew. Chem. Int. Ed.* **2012**, *51*, 4409–4412.

[99] G. Ménard, T. M. Gilbert, J. A. Hatnean, A. Kraft, I. Krossing, D. W. Stephan, *Organometallics* **2013**, *32*, 4416–4422.

[100] D. M. C. Ould, J. L. Carden, R. Page, R. L. Melen, *Inorg. Chem.* **2020**, *59*, 14891–14898.

[101] D. Chakraborty, E. Y.-X. Chen, *Inorg. Chem. Commun.* **2002**, *5*, 698–701.

[102] A. Kraft, J. Beck, G. Steinfeld, H. Scherer, D. Himmel, I. Krossing, *Organometallics* **2012**, *31*, 7485–7491.

[103] M. Rohde, L. O. Müller, D. Himmel, H. Scherer, I. Krossing, *Chem. Eur. J.* **2014**, *20*, 1218–1222.

[104] A. Martens, O. Petersen, H. Scherer, I. Riddlestone, I. Krossing, *Organometallics* **2018**, *37*, 706–711.

[105] A. Martens, P. Weis, M. C. Krummer, M. Kreuzer, A. Meierhöfer, S. C. Meier, J. Bohnenberger, H. Scherer, I. Riddlestone, I. Krossing, *Chem. Sci.* **2018**, *9*, 7058–7068.

[106] A. Kraft, N. Trapp, D. Himmel, H. Böhrer, P. Schlüter, H. Scherer, I. Krossing, *Chem. Eur. J.* **2012**, *18*, 9371–9380.

[107] A. Kraft, J. Possart, H. Scherer, J. Beck, D. Himmel, I. Krossing, *Eur. J. Inorg. Chem.* **2013**, *2013*, 3054–3062.

[108] J. Possart, A. Martens, M. Schleep, A. Ripp, H. Scherer, D. Kratzert, I. Krossing, *Chem. Eur. J.* **2017**, *23*, 12305–12313.

[109] J. F. Kögel, D. A. Sorokin, A. Khvorost, M. Scott, K. Harms, D. Himmel, I. Krossing, J. Sundermeyer, *Chem. Sci.* **2018**, *9*, 245–253.

[110] J. F. Kögel, A. Y. Timoshkin, A. Schröder, E. Lork, J. Beckmann, *Chem. Sci.* **2018**, *9*, 8178–8183.

[111] J. F. Kögel, D. A. Sorokin, M. Scott, K. Harms, D. Himmel, I. Krossing, J. Sundermeyer, *Dalton Trans.* **2022**, 4829–4835.

[112] I. M. Riddlestone, S. Keller, F. Kirschenmann, M. Schorpp, I. Krossing, *Eur. J. Inorg. Chem.* **2019**, *2019*, 59–67.

[113] A. L. Liberman-Martin, R. G. Bergman, T. D. Tilley, *J. Am. Chem. Soc.* **2015**, *137*, 5328–5331.

[114] D. Hartmann, M. Schädler, L. Greb, *Chem. Sci.* **2019**, *10*, 7379–7388.

[115] R. Maskey, M. Schädler, C. Legler, L. Greb, *Angew. Chem. Int. Ed.* **2018**, *57*, 1717–1720.

[116] D. Hartmann, L. Greb, *Angew. Chem. Int. Ed.* **2020**, *59*, 22510–22513.

[117] N. Ansmann, D. Hartmann, S. Sailer, P. Erdmann, R. Maskey, M. Schorpp, L. Greb, *Angew. Chem. Int. Ed.* **2022**, e202203947.

[118] T. Thorwart, D. Roth, L. Greb, *Chem. Eur. J.* **2021**, *27*, 10422–10427.

[119] D. Roth, H. Wadepohl, L. Greb, *Angew. Chem. Int. Ed.* **2020**, *59*, 20930–20934.

[120] F. S. Tschernuth, T. Thorwart, L. Greb, F. Hanusch, S. Inoue, *Angew. Chem. Int. Ed.* **2021**, *60*, 25799–25803.

[121] T. Keith Hollis, W. Odenkirk, N. P. Robinson, J. Whelan, B. Bosnich, *Tetrahedron* **1993**, *49*, 5415–5430.

[122] A. Corma, H. García, *Chem. Rev.* **2003**, *103*, 4307–4365.

[123] R. Craciun, D. Picone, R. T. Long, S. Li, D. A. Dixon, K. A. Peterson, K. O. Christe, *Inorg. Chem.* **2010**, *49*, 1056–1070.

[124] R. Craciun, R. T. Long, D. A. Dixon, K. O. Christe, *J. Phys. Chem. A* **2010**, *114*, 7571–7582.

[125] J. B. Lambert, S. Zhang, C. L. Stern, J. C. Huffman, *Science* **1993**, *260*, 1917–1918.

[126] K.-C. Kim, C. A. Reed, D. W. Elliott, L. J. Mueller, F. Tham, L. Lin, J. B. Lambert, *Science* **2002**, *297*, 825–827.

[127] C. B. Caputo, L. J. Hounjet, R. Dobrovetsky, D. W. Stephan, *Science* **2013**, *341*, 1374–1377.

[128] B. Pan, F. P. Gabbaï, *J. Am. Chem. Soc.* **2014**, *136*, 9564–9567.

[129] J. Belzner, *Angew. Chem. Int. Ed.* **1997**, *36*, 1277–1280.

[130] J. Y. Corey, *J. Am. Chem. Soc.* **1975**, *97*, 3237–3238.

[131] C. A. Reed, Z. Xie, R. Bau, A. Benesi, *Science* **1993**, *262*, 402–404.

[132] K. Müther, P. Hrobárik, V. Hrobáriková, M. Kaupp, M. Oestreich, *Chem. Eur. J.* **2013**, *19*, 16579–16594.

[133] R. Panisch, M. Bolte, T. Müller, *J. Am. Chem. Soc.* **2006**, *128*, 9676–9682.

[134] S. Duttwyler, Q.-Q. Do, A. Linden, K. K. Baldridge, J. S. Siegel, *Angew. Chem. Int. Ed.* **2008**, *47*, 1719–1722.

[135] P. Romanato, S. Duttwyler, A. Linden, K. K. Baldridge, J. S. Siegel, *J. Am. Chem. Soc.* **2011**, *133*, 11844–11846.

[136] H. F. T. Klare, L. Albers, L. Süsse, S. Keess, T. Müller, M. Oestreich, *Chem. Rev.* **2021**, *121*, 5889–5985.

[137] H. F. T. Klare, *ACS Catal.* **2017**, *7*, 6999–7002.

[138] C. Douvris, O. V. Ozerov, *Science* **2008**, *321*, 1188–1190.

[139] V. Fasano, J. H. W. LaFortune, J. M. Bayne, M. J. Ingleson, D. W. Stephan, *Chem. Commun.* **2018**, *54*, 662–665.

[140] T. Krahl, E. Kemnitz, *Catal. Sci. Technol.* **2017**, *7*, 773–796.

[141] T. Krahl, E. Kemnitz, *J. Fluor. Chem.* **2006**, *127*, 663–678.

[142] E. Kemnitz, U. Gross, S. Rüdiger, C. S. Shekar, *Angew. Chem. Int. Ed.* **2003**, *42*, 4251–4254.

[143] K. K. Samudrala, W. Huynh, R. W. Dorn, A. J. Rossini, M. P. Conley, *Angew. Chem. Int. Ed.* **2022**, e202205745.

[144] H. F. T. Klare, M. Oestreich, *Dalton Trans.* **2010**, *39*, 9176–9184.

[145] V. J. Scott, R. Celenligil-Cetin, O. V. Ozerov, *J. Am. Chem. Soc.* **2005**, *127*, 2852–2853.

[146] H. Amii, K. Uneyama, *Chem. Rev.* **2009**, *109*, 2119–2183.

[147] M. F. Ibad, P. Langer, A. Schulz, A. Villinger, *J. Am. Chem. Soc.* **2011**, *133*, 21016–21027.

[148] R. T. Mathers, S. P. Lewis, *J. Polym. Sci. A Polym. Chem.* **2012**, *50*, 1325–1332.

[149] G. A. Olah, O. Farooq, C. X. Li, M. A. M. F. Farnia, J. J. Aklonis, *J. Appl. Polym. Sci.* **1992**, *45*, 1355–1360.

[150] G. A. Olah, O. Farooq, S. M. F. Farnia, A. H. Wu, *J. Org. Chem.* **1990**, *55*, 1516–1522.

[151] K. Hara, R. Akiyama, M. Sawamura, *Org. Lett.* **2005**, *7*, 5621–5623.

[152] H. F. T. Klare, K. Bergander, M. Oestreich, *Angew. Chem. Int. Ed.* **2009**, *48*, 9077–9079.

[153] M. Yanagisawa, T. Shimamura, D. Iida, J. I. Matsuo, T. Mukaiyama, *Chem. Pharm. Bull.* **2000**, *48*, 1838–1840.

[154] Parks, Blackwell, Piers, *J. Org. Chem.* **2000**, *65*, 3090–3098.

[155] M. Ahrens, G. Scholz, T. Braun, E. Kemnitz, *Angew. Chem. Int. Ed.* **2013**, *52*, 5328–5332.

[156] G. Meißner, K. Kretschmar, T. Braun, E. Kemnitz, *Angew. Chem. Int. Ed.* **2017**, *56*, 16338–16341.

[157] X. Pan, M. Talavera, G. Scholz, T. Braun, *ChemCatChem* **2022**, *14*, e202200029.

[158] K. Teinz, S. Wuttke, F. Börno, J. Eicher, E. Kemnitz, *J. Catal.* **2011**, *282*, 175–182.

[159] M.-C. Kervarec, C. P. Marshall, T. Braun, E. Kemnitz, *J. Fluor. Chem.* **2019**, *221*, 61–65.

[160] A. K. Siwek, M. Ahrens, M. Feist, T. Braun, E. Kemnitz, *ChemCatChem* **2017**, *9*, 839–845.

[161] B. Calvo, J. Wuttke, T. Braun, E. Kemnitz, *ChemCatChem* **2016**, *8*, 1945–1950.

[162] G. A. Olah, *J. Org. Chem.* **2001**, *66*, 5943–5957.

[163] F. Kehrmann, F. Wentzel, *Ber. Dtsch. Chem. Ges.* **1901**, *34*, 3815–3819.

[164] P. Mehlmann, T. Witteler, L. F. B. Wilm, F. Dielmann, *Nat. Chem.* **2019**, *11*, 1139–1143.

[165] G. A. Olah, *Angew. Chem. Int. Ed.* **1995**, *34*, 1393–1405.

[166] P. v. R. Schleyer, W. E. Watts, R. C. Fort, M. B. Comisarow, G. A. Olah, *J. Am. Chem. Soc.* **1964**, *86*, 5679–5680.

[167] M. Saunders, P. v. R. Schleyer, G. A. Olah, *J. Am. Chem. Soc.* **1964**, *86*, 5680–5681.

[168] S. Winstein, E. Clippinger, R. Howe, E. Vogelfanger, *J. Am. Chem. Soc.* **1965**, *87*, 376–377.

[169] H. C. Brown, *Acc. Chem. Res.* **1983**, *16*, 432–440.

[170] G. A. Olah, G. K. S. Prakash, M. Saunders, *Acc. Chem. Res.* **1983**, *16*, 440–448.

[171] F. Scholz, D. Himmel, H. Scherer, I. Krossing, *Chem. Eur. J.* **2013**, *19*, 109–116.

[172] F. Scholz, D. Himmel, F. W. Heinemann, P. v. R. Schleyer, K. Meyer, I. Krossing, *Science* **2013**, *341*, 62–64.

[173] A. J. Edwards, R. J. C. Sills, *J. Chem. Soc., A* **1970**, 2697–2699.

[174] A. J. Edwards, G. R. Jones, *J. Chem. Soc., A* **1969**, 1467–1470.

[175] K. O. Christe, X. Zhang, J. A. Sheehy, R. Bau, *J. Am. Chem. Soc.* **2001**, *123*, 6338–6348.

[176] A. Vij, F. S. Tham, V. Vij, W. W. Wilson, K. O. Christe, *Inorg. Chem.* **2002**, *41*, 6397–6403.

[177] M. D. Lind, K. O. Christe, *Inorg. Chem.* **1972**, *11*, 608–612.

[178] J. F. Lehmann, G. J. Schrobilgen, K. O. Christe, A. Kornath, R. J. Suontamo, *Inorg. Chem.* **2004**, *43*, 6905–6921.

[179] G. A. Olah, J. R. DeMember, Y. K. Mo, J. J. Svoboda, P. Schilling, J. A. Olah, *J. Am. Chem. Soc.* **1974**, *96*, 884–892.

[180] R. Minkwitz, V. Gerhard, *Z. Naturforsch. B* **1991**, *46*, 561–565.

[181] V. Nguyen, X. Cheng, T. H. Morton, *J. Am. Chem. Soc.* **1992**, *114*, 7127–7132.

[182] N. Solcà, O. Dopfer, *J. Am. Chem. Soc.* **2003**, *125*, 1421–1430.

[183] H. Wang, C. E. Webster, L. M. Pérez, M. B. Hall, F. P. Gabbaï, *J. Am. Chem. Soc.* **2004**, *126*, 8189–8196.

[184] M. D. Struble, M. T. Scerba, M. Siegler, T. Lectka, *Science* **2013**, *340*, 57–60.

[185] M. G. Holl, C. R. Pitts, T. Lectka, *Acc. Chem. Res.* **2020**, *53*, 265–275.

[186] C. R. Pitts, M. G. Holl, T. Lectka, *Angew. Chem. Int. Ed.* **2018**, *57*, 1924–1927.

[187] K. O. Christe, R. Haiges, M. Rahm, D. A. Dixon, M. Vasiliu, *J. Fluor. Chem.* **2017**, *204*, 6–10.

[188] N. Bartlett, F. Einstein, D. F. Stewart, J. Trotter, *J. Chem. Soc., A* **1967**, 1190–1193.

[189] N. Bartlett, F. Einstein, D. F. Stewart, J. Trotter, *Chem. Commun.* **1966**, 550–552.

[190] H. S. A. Elliott, J. F. Lehmann, H. P. A. Mercier, H. D. B. Jenkins, G. J. Schrobilgen, *Inorg. Chem.* **2010**, *49*, 8504–8523.

[191] V. M. McRae, R. D. Peacock, D. R. Russell, *J. Chem. Soc., D* **1969**, 62–63.

[192] D. E. McKee, A. Zalkin, N. Bartlett, *Inorg. Chem.* **1973**, *12*, 1713–1717.

[193] J. F. Lehmann, D. A. Dixon, G. J. Schrobilgen, *Inorg. Chem.* **2001**, *40*, 3002–3017.

[194] K. Leary, A. Zalkin, N. Bartlett, *Inorg. Chem.* **1974**, *13*, 775–779.

[195] H. P. A. Mercier, M. D. Moran, J. C. P. Sanders, G. J. Schrobilgen, R. J. Suontamo, *Inorg. Chem.* **2005**, *44*, 49–60.

[196] D. W. Stephan, *Org. Biomol. Chem.* **2012**, *10*, 5740–5746.

[197] J. Paradies, *Angew. Chem. Int. Ed.* **2014**, *53*, 3552–3557.

[198] C. M. Mömming, E. Otten, G. Kehr, R. Fröhlich, S. Grimme, D. W. Stephan, G. Erker, *Angew. Chem. Int. Ed.* **2009**, *48*, 6643–6646.

[199] X. Zhao, A. J. Lough, D. W. Stephan, *Chem. Eur. J.* **2011**, *17*, 6731–6743.

[200] M. A. Dureen, D. W. Stephan, *J. Am. Chem. Soc.* **2009**, *131*, 8396–8397.

[201] J. S. J. McCahill, G. C. Welch, D. W. Stephan, *Angew. Chem. Int. Ed.* **2007**, *46*, 4968–4971.

[202] G. C. Welch, D. W. Stephan, *J. Am. Chem. Soc.* **2007**, *129*, 1880–1881.

[203] G. C. Welch, R. R. San Juan, J. D. Masuda, D. W. Stephan, *Science* **2006**, *314*, 1124–1126.

[204] P. Spies, G. Erker, G. Kehr, K. Bergander, R. Fröhlich, S. Grimme, D. W. Stephan, *Chem. Commun.* **2007**, 5072–5074.

[205] M. Ghara, S. Giri, P. Das, P. K. Chattaraj, *J. Chem. Sci.* **2022**, *134*, 1535.

[206] G. Ménard, D. W. Stephan, *Dalton Trans.* **2013**, *42*, 5447–5453.

[207] Y. Zhang, G. M. Miyake, E. Y.-X. Chen, *Angew. Chem. Int. Ed.* **2010**, *49*, 10158–10162.

[208] Y. Zhang, G. M. Miyake, M. G. John, L. Falivene, L. Caporaso, L. Cavallo, E. Y.-X. Chen, *Dalton Trans.* **2012**, *41*, 9119–9134.

[209] M. Reißmann, A. Schäfer, S. Jung, T. Müller, *Organometallics* **2013**, *32*, 6736–6744.

[210] R. J. Gillespie, *Acc. Chem. Res.* **1968**, *1*, 202–209.

[211] R. J. Gillespie, T. E. Peel, E. A. Robinson, *J. Am. Chem. Soc.* **1971**, *93*, 5083–5087.

[212] E. Paenurk, K. Kaupmees, D. Himmel, A. Kütt, I. Kaljurand, I. A. Koppel, I. Krossing, I. Leito, *Chem. Sci.* **2017**, *8*, 6964–6973.

[213] D. Himmel, S. K. Goll, I. Leito, I. Krossing, *Chem. Eur. J.* **2011**, *17*, 5808–5826.

[214] I. A. Koppel, R. W. Taft, F. Anvia, S.-Z. Zhu, L.-Q. Hu, K.-S. Sung, D. D. DesMarteau, L. M. Yagupolskii, Y. L. Yagupolskii, *J. Am. Chem. Soc.* **1994**, *116*, 3047–3057.

[215] E. Raamat, K. Kaupmees, G. Ovsjannikov, A. Trummal, A. Kütt, J. Saame, I. Koppel, I. Kaljurand, L. Lipping, T. Rodima, V. Pihl, I. A. Koppel, I. Leito, *J. Phys. Org. Chem.* **2013**, *26*, 162–170.

[216] R. J. Gillespie, T. E. Peel, *J. Am. Chem. Soc.* **1973**, *95*, 5173–5178.

[217] R. J. Gillespie, J. Liang, *J. Am. Chem. Soc.* **1988**, *110*, 6053–6057.

[218] G. A. Olah, *Science* **1970**, *168*, 1298–1311.

[219] G. A. Olah, *Angew. Chem. Int. Ed.* **1973**, *12*, 173–212.

[220] P. M. Esteves, A. Ramírez-Solís, C. J. A. Mota, *J. Am. Chem. Soc.* **2002**, *124*, 2672–2677.

[221] R. Taube, S. Wache, *J. Organomet. Chem.* **1992**, *428*, 431–442.

[222] M. Brookhart, B. Grant, A. F. Volpe, *Organometallics* **1992**, *11*, 3920–3922.

[223] I. Krossing, A. Reisinger, *Eur. J. Inorg. Chem.* **2005**, *2005*, 1979–1989.

[224] P. Jutzi, C. Müller, A. Stammler, H.-G. Stammler, *Organometallics* **2000**, *19*, 1442–1444.

[225] C. A. Reed, *Acc. Chem. Res.* **1998**, *31*, 133–139.

[226] M. Juhasz, S. Hoffmann, E. Stoyanov, K.-C. Kim, C. A. Reed, *Angew. Chem. Int. Ed.* **2004**, *43*, 5352–5355.

[227] C. A. Reed, K.-C. Kim, L. J. Mueller, R. D. Bolskar, *Science* **2000**, *289*, 101–104.

[228] C. A. Reed, K.-C. Kim, E. S. Stoyanov, D. Stasko, F. S. Tham, L. J. Mueller, P. D. W. Boyd, *J. Am. Chem. Soc.* **2003**, *125*, 1796–1804.

[229] S. Cummings, H. P. Hratchian, C. A. Reed, *Angew. Chem. Int. Ed.* **2016**, *55*, 1382–1386.

[230] M. Nava, I. V. Stoyanova, S. Cummings, E. S. Stoyanov, C. A. Reed, *Angew. Chem. Int. Ed.* **2014**, *53*, 1131–1134.

[231] E. S. Stoyanov, S. P. Hoffmann, M. Juhasz, C. A. Reed, *J. Am. Chem. Soc.* **2006**, *128*, 3160–3161.

[232] A. Wiesner, S. Steinhauer, H. Beckers, C. Müller, S. Riedel, *Chem. Sci.* **2018**, *9*, 7169–7173.

[233] S. Hämmerling, G. Thiele, S. Steinhauer, H. Beckers, C. Müller, S. Riedel, *Angew. Chem. Int. Ed.* **2019**, *58*, 9807–9810.

[234] I. M. Riddlestone, A. Kraft, J. Schaefer, I. Krossing, *Angew. Chem. Int. Ed.* **2018**, *57*, 13982–14024.

[235] I. Krossing, A. Reisinger, *Coord. Chem. Rev.* **2006**, *250*, 2721–2744.

[236] P. J. Malinowski, D. Himmel, I. Krossing, *Angew. Chem. Int. Ed.* **2016**, *55*, 9259–9261.

[237] Y. Li, M. Cokoja, F. E. Kühn, *Coord. Chem. Rev.* **2011**, *255*, 1541–1557.

[238] D. S. McGuinness, A. J. Rucklidge, R. P. Tooze, A. M. Z. Slawin, *Organometallics* **2007**, *26*, 2561–2569.

[239] A. B. A. Rupp, I. Krossing, *Acc. Chem. Res.* **2015**, *48*, 2537–2546.

[240] V. Aravindan, J. Gnanaraj, S. Madhavi, H.-K. Liu, *Chem. Eur. J.* **2011**, *17*, 14326–14346.

[241] K. Xu, *Chem. Rev.* **2014**, *114*, 11503–11618.

[242] R. V. Honeychuck, W. H. Hersh, *Inorg. Chem.* **1989**, *28*, 2869–2886.

[243] W. H. Hersh, *J. Am. Chem. Soc.* **1985**, *107*, 4599–4601.

[244] H. Willner, M. Bodenbinder, R. Bröchler, G. Hwang, S. J. Rettig, J. Trotter, B. von Ahsen, U. Westphal, V. Jonas, W. Thiel, F. Aubke, *J. Am. Chem. Soc.* **2001**, *123*, 588–602.

[245] T. Drews, K. Seppelt, *Angew. Chem. Int. Ed.* **1997**, *36*, 273–274.

[246] I. Bernhardi, T. Drews, K. Seppelt, *Angew. Chem. Int. Ed.* **1999**, *38*, 2232–2233.

[247] Z. Mazej, E. A. Goreshnik, *J. Fluor. Chem.* **2015**, *175*, 47–50.

[248] A. J. Edwards, G. R. Jones, *J. Chem. Soc., A* **1971**, 2318–2320.

[249] H. Hartl, J. Nowicki, R. Minkwitz, *Angew. Chem. Int. Ed.* **1991**, *30*, 328–329.

[250] S. Seidel, K. Seppelt, *Science* **2000**, *290*, 117–118.

[251] K. Fujiki, S.-y. Ikeda, H. Kobayashi, A. Mori, A. Nagira, J. Nie, T. Sonoda, Y. Yagupolskii, *Chem. Lett.* **2000**, *29*, 62–63.

[252] J. H. Golden, P. F. Mutolo, E. B. Lobkovsky, F. J. DiSalvo, *Inorg. Chem.* **1994**, *33*, 5374–5375.

[253] E. Y. Chen, T. J. Marks, *Chem. Rev.* **2000**, *100*, 1391–1434.

[254] J. Powell, A. Lough, T. Saeed, *J. Chem. Soc., Dalton Trans.* **1997**, 4137–4138.

[255] E. Bernhardt, G. Henkel, H. Willner, G. Pawelke, H. Bürger, *Chem. Eur. J.* **2001**, *7*, 4696–4705.

[256] P. Pröhm, J. R. Schmid, K. Sonnenberg, P. Voßnacker, S. Steinhauer, C. J. Schattenberg, R. Müller, M. Kaupp, S. Riedel, *Angew. Chem. Int. Ed.* **2020**, *59*, 16002–16006.

[257] M. Finze, E. Bernhardt, H. Willner, *Angew. Chem. Int. Ed.* **2007**, *46*, 9180–9196.

[258] T.-T.-T. Nguyen, D. Türp, M. Wagner, K. Müllen, *Angew. Chem. Int. Ed.* **2013**, *52*, 669–673.

[259] M. Niemann, B. Neumann, H.-G. Stammler, B. Hoge, *Eur. J. Inorg. Chem.* **2019**, *2019*, 3462–3475.

[260] H. Biller, S. Lerch, K. Tölke, H.-G. Stammler, B. Hoge, T. Strassner, *Chem. Eur. J.* **2021**, *27*, 13325–13329.

[261] L. A. Bischoff, J. Riefer, R. Wirthensohn, T. Bischof, R. Bertermann, N. V. Ignat'ev, M. Finze, *Chem. Eur. J.* **2020**, *26*, 13615–13620.

[262] N. Tiessen, B. Neumann, H.-G. Stammler, B. Hoge, *Chem. Eur. J.* **2020**, *26*, 13611–13614.

[263] M.-C. Chen, J. A. S. Roberts, A. M. Seyam, L. Li, C. Zuccaccia, N. G. Stahl, T. J. Marks, *Organometallics* **2006**, *25*, 2833–2850.

[264] J. A. S. Roberts, M.-C. Chen, A. M. Seyam, L. Li, C. Zuccaccia, N. G. Stahl, T. J. Marks, *J. Am. Chem. Soc.* **2007**, *129*, 12713–12733.

[265] Y. Sun, M. V. Metz, C. L. Stern, T. J. Marks, *Organometallics* **2000**, *19*, 1625–1627.

[266] S. M. Ivanova, B. G. Nolan, Y. Kobayashi, S. M. Miller, O. P. Anderson, S. H. Strauss, *Chem. Eur. J.* **2001**, *7*, 503–510.

[267] I. Krossing, *Chem. Eur. J.* **2001**, *7*, 490–502.

[268] I. Krossing, *J. Am. Chem. Soc.* **2001**, *123*, 4603–4604.

[269] I. Krossing, L. van Wüllen, *Chem. Eur. J.* **2002**, *8*, 700–711.

[270] W. Unkrig, M. Schmitt, D. Kratzert, D. Himmel, I. Krossing, *Nat. Chem.* **2020**, *12*, 647–653.

[271] I. Krossing, A. Bihlmeier, I. Raabe, N. Trapp, *Angew. Chem. Int. Ed.* **2003**, *42*, 1531–1534.

[272] Matti Reißmann, Dissertation, Carl von Ossietzky Universität Oldenburg, **2014**.

[273] S. P. Smidt, N. Zimmermann, M. Studer, A. Pfaltz, *Chem. Eur. J.* **2004**, *10*, 4685–4693.

[274] A. J. Rucklidge, D. S. McGuinness, R. P. Tooze, A. M. Z. Slawin, J. D. A. Pelletier, M. J. Hanton, P. B. Webb, *Organometallics* **2007**, *26*, 2782–2787.

[275] M. J. Hanton, K. Tenza, *Organometallics* **2008**, *27*, 5712–5716.

[276] M. Gonsior, I. Krossing, L. Müller, I. Raabe, M. Jansen, L. van Wüllen, *Chem. Eur. J.* **2002**, *8*, 4475–4492.

[277] J. Bohnenberger, W. Feuerstein, D. Himmel, M. Daub, F. Breher, I. Krossing, *Nat. Commun.* **2019**, *10*, 624.

[278] M. Schmitt, M. Mayländer, J. Goost, S. Richert, I. Krossing, *Angew. Chem. Int. Ed.* **2021**, *60*, 14800–14805.

[279] W. Unkrig, F. Zhe, R. Tamim, F. Oesten, D. Kratzert, I. Krossing, *Chem. Eur. J.* **2021**, *27*, 758–765.

[280] K. Shelly, C. A. Reed, Y. J. Lee, W. R. Scheidt, *J. Am. Chem. Soc.* **1986**, *108*, 3117–3118.

[281] D. Stasko, C. A. Reed, *J. Am. Chem. Soc.* **2002**, *124*, 1148–1149.

[282] Z. Xie, T. Jelinek, R. Bau, C. A. Reed, *J. Am. Chem. Soc.* **1994**, *116*, 1907–1913.

[283] Z. Xie, J. Manning, R. W. Reed, R. Mathur, P. D. W. Boyd, A. Benesi, C. A. Reed, *J. Am. Chem. Soc.* **1996**, *118*, 2922–2928.

[284] S. Körbe, P. J. Schreiber, J. Michl, *Chem. Rev.* **2006**, *106*, 5208–5249.

[285] C. A. Reed, *Acc. Chem. Res.* **2010**, *43*, 121–128.

[286] L. Toom, A. Kütt, I. Leito, *Dalton Trans.* **2019**, *48*, 7499–7502.

[287] W. H. Knoth, H. C. Miller, J. C. Sauer, J. H. Balthis, Y. T. Chia, E. L. Muetterties, *Inorg. Chem.* **1964**, *3*, 159–167.

[288] A. R. Pitochelli, F. M. Hawthorne, *J. Am. Chem. Soc.* **1960**, *82*, 3228–3229.

[289] V. Geis, K. Guttsche, C. Knapp, H. Scherer, R. Uzun, *Dalton Trans.* **2009**, 2687–2694.

[290] A. Avelar, F. S. Tham, C. A. Reed, *Angew. Chem. Int. Ed.* **2009**, *48*, 3491–3493.

[291] M. Kessler, C. Knapp, V. Sagawe, H. Scherer, R. Uzun, *Inorg. Chem.* **2010**, *49*, 5223–5230.

[292] W. Gu, O. V. Ozerov, *Inorg. Chem.* **2011**, *50*, 2726–2728.

[293] C. Bolli, J. Derendorf, C. Jenne, H. Scherer, C. P. Sindlinger, B. Wegener, *Chem. Eur. J.* **2014**, *20*, 13783–13792.

[294] S. V. Ivanov, S. M. Miller, O. P. Anderson, K. A. Solntsev, S. H. Strauss, *J. Am. Chem. Soc.* **2003**, *125*, 4694–4695.

[295] H. P. A. Mercier, J. C. P. Sanders, G. J. Schrobilgen, *J. Am. Chem. Soc.* **1994**, *116*, 2921–2937.

[296] P. K. Hurlburt, O. P. Anderson, S. H. Strauss, *J. Am. Chem. Soc.* **1991**, *113*, 6277–6278.

[297] P. K. Hurlburt, O. P. Anderson, S. H. Strauss, *Can. J. Chem.* **1992**, *70*, 726–731.

[298] P. K. Hurlburt, J. J. Rack, S. F. Dec, O. P. Anderson, S. H. Strauss, *Inorg. Chem.* **1993**, *32*, 373–374.

[299] P. K. Hurlburt, J. J. Rack, J. S. Luck, S. F. Dec, J. D. Webb, O. P. Anderson, S. H. Strauss, *J. Am. Chem. Soc.* **1994**, *116*, 10003–10014.

[300] D. M. van Seggen, P. K. Hurlburt, M. D. Noirot, O. P. Anderson, S. H. Strauss, *Inorg. Chem.* **1992**, *31*, 1423–1430.

[301] P. Ulferts, K. Seppelt, *Z. Anorg. Allg. Chem.* **2004**, *630*, 1589–1593.

[302] H. P. A. Mercier, M. D. Moran, G. J. Schrobilgen, C. Steinberg, R. J. Suontamo, *J. Am. Chem. Soc.* **2004**, *126*, 5533–5548.

[303] A. Wiesner, L. Fischer, S. Steinhauer, H. Beckers, S. Riedel, *Chem. Eur. J.* **2019**, *25*, 10441–10449.

[304] S. Hämmerling, P. Voßnacker, S. Steinhauer, H. Beckers, S. Riedel, *Chem. Eur. J.* **2020**, *26*, 14377–14384.

[305] J. Foropoulos, D. D. DesMarteau, *Inorg. Chem.* **1984**, *23*, 3720–3723.

[306] P. Murmann, R. Schmitz, S. Nowak, N. V. Ignat'ev, P. Sartori, I. Cekic-Laskovic, M. Winter, *J. Electrochem. Soc.* **2015**, *162*, A1738–A1744.

[307] F. J. Waller, A. G. M. Barrett, D. C. Braddock, D. Ramprasad, R. M. McKinnell, A. J. P. White, D. J. Williams, R. Ducray, *J. Org. Chem.* **1999**, *64*, 2910–2913.

[308] A. G. M. Barrett, D. C. Braddock, D. Catterick, D. Chadwick, J. P. Henschke, *Synlett* **2000**, *6*, 847–849.

[309] J. Nishikido, F. Yamamoto, H. Nakajima, Y. Mikami, Y. Matsumoto, K. Mikami, *Synlett* **1999**, *12*, 1990–1992.

[310] R. Filler, C.-S. Wang, M. A. McKinney, F. N. Miller, *J. Am. Chem. Soc.* **1967**, *89*, 1026–1027.

[311] G. A. Olah, M. B. Comisarow, *J. Am. Chem. Soc.* **1967**, *89*, 1027–1028.

[312] A. Dasgupta, E. Richards, R. L. Melen, *Angew. Chem. Int. Ed.* **2021**, *60*, 53–65.

[313] L. Liu, L. L. Cao, Y. Shao, G. Ménard, D. W. Stephan, *Chem* **2017**, *3*, 259–267.

[314] D. G. Gusev, O. V. Ozerov, *Chem. Eur. J.* **2011**, *17*, 634–640.

6. List of Publications

Publications

An Amorphous Teflate Doped Aluminium Chlorofluoride: A Solid Lewis Superacid for the Dehydrofluorination of Fluoroalkanes
Minh Bui, Kurt F. Hoffmann, Christian Heinekamp, Kerstin Scheurell, Gudrun Scholz, Tomasz Stawski, Franziska Emmerling, Thomas Braun, Sebastian Riedel **2022**, DOI: 10.26434/chemrxiv-2022-vr6fm
https://doi.org/10.26434/chemrxiv-2022-vr6fm

Air-stable aryl derivatives of pentafluoroorthotellurate
Daniel Wegener, Kurt F. Hoffmann, Alberto Pérez-Bitrián, Ilayda Bayindir, Amiera N. Hadi, Anja Wiesner, Sebastian Riedel *Chem. Commun.* **2022**, *69*, 9694.
https://doi.org/10.1039/D2CC03936B

Unravelling the Role of the Pentafluoroorthotellurate Group as a Ligand in Nickel Chemistry
Alberto Pérez-Bitrián, Kurt F. Hoffmann, Konstantin B. Krause, Günther Thiele, Christian Limberg, Sebastian Riedel *Chem. Eur. J.* **2022**, e202202016.
https://doi.org/10.1002/chem.202202016

Insights on the Lewis Superacid $Al(OTeF_5)_3$: Solvent Adducts, Characterization and Properties
Kurt F. Hoffmann, Anja Wiesner, Simon Steinhauer, Sebastian Riedel *Chem. Eur. J.* **2022**, e202201958.
https://doi.org/10.1002/chem.202201958

The Tris(pentafluorophenyl)methylium Cation: Isolation and Reactivity
Kurt F. Hoffmann, David Battke, Paul Golz, Susanne M. Rupf, Moritz Malischewski, Sebastian Riedel *Angew. Chem. Int. Ed.* **2022**, *61* e202203777.
https://doi.org/10.1002/anie.202203777

Structural proof of a $[C\text{-}F\text{-}C]^+$ fluoronium cation
Kurt F. Hoffmann, Anja Wiesner, Carsten Müller, Simon Steinhauer, Helmut Beckers, Muhammad Kazim, Cody Ross Pitts, Thomas Lectka, Sebastian Riedel *Nat. Commun.* **2021**, *12*, 5275.
https://doi.org/10.1038/s41467-021-25592-6

Dual-stimuli pseudorotaxane switches under kinetic control
Marius Gaedke, Henrik Hupatz, Hendrik V. Schröder, Simon Suhr, Kurt F. Hoffmann, Arto Valkonen, Biprajit Sarkar, Sebastian Riedel, Kari Rissanen, Christoph Schalley
Org. Chem. Front. **2021**, *8*, 3659.
https://doi.org/10.1039/D1QO00503K

Salts of the weakly coordinating anion $[Al(OTeF_5)_4]$ containing reactive counterions
Kurt F. Hoffmann, Anja Wiesner, Noah Subat, Simon Steinhauer, Sebastian Riedel *Z. Anorg. Allg. Chem.* **2018**, *644*, 1344.
https://doi.org/10.1002/zaac.201800174

Conference Contributions

Poster:
The Tris(pentafluorophenyl)methylium Cation: Structural Proof and Reactivity
20th European Symposium on Fluorine Chemistry
2022, Berlin, Germany.

Structural Proof of a $[C–F–C]^+$ Fluoronium Cation
GDCh-Wissenschaftsforum Chemie
2021, Online Format.

Solvent-stabilized, Lewis Superacidic Aluminum Pentafluoroorthotellurato Derivatives
GDCh-Wissenschaftsforum Chemie
2019, Aachen, Germany.

Solvent-stabilized, Lewis Superacidic Aluminum Pentafluoroorthotellurato Derivatives
19th European Symposium on Fluorine Chemistry
2019, Warsaw, Poland.

The Lewis Superacid $Al(OTeF_5)_3$
22nd International Symposium on Fluorine Chemistry
2018, Oxford, United Kingdom.

Talk:
Die Lewis-Supersäure $Al(OTeF_5)_3$
18. Deutscher Fluortag
2018, Schmitten, Germany.

January 5, 2023

A. Supporting Information of Publications

A.1. Insights on the Lewis Superacid $Al(OTeF_5)_3$: Solvent Adducts, Characterization and Properties

Chemistry–A European Journal

Supporting Information

Insights on the Lewis Superacid $Al(OTeF_5)_3$: Solvent Adducts, Characterization and Properties

Kurt F. Hoffmann, Anja Wiesner, Simon Steinhauer, and Sebastian Riedel*

Table of Content

NMR Spectra **2**
Vibrational Spectra **5**
Crystal data **6**
Quantum-chemical calculations **7**

NMR Spectra

NMR spectra of $[C(C_6H_5)_3][Al(OTeF_5)_{4-n}Cl_n]$ (n = 0,1,2,3)

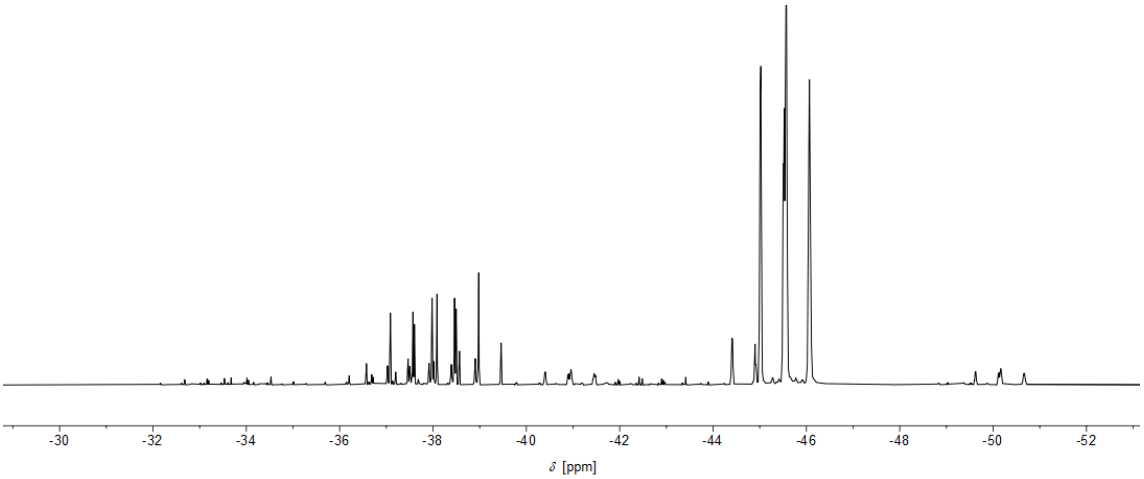

Figure S1. ^{19}F NMR spectrum (377 MHz, CD_2Cl_2, 22 °C) of $[C(C_6H_5)_3][Al(OTeF_5)_{4-n}Cl_n]$ (n = 0,1,2,3).

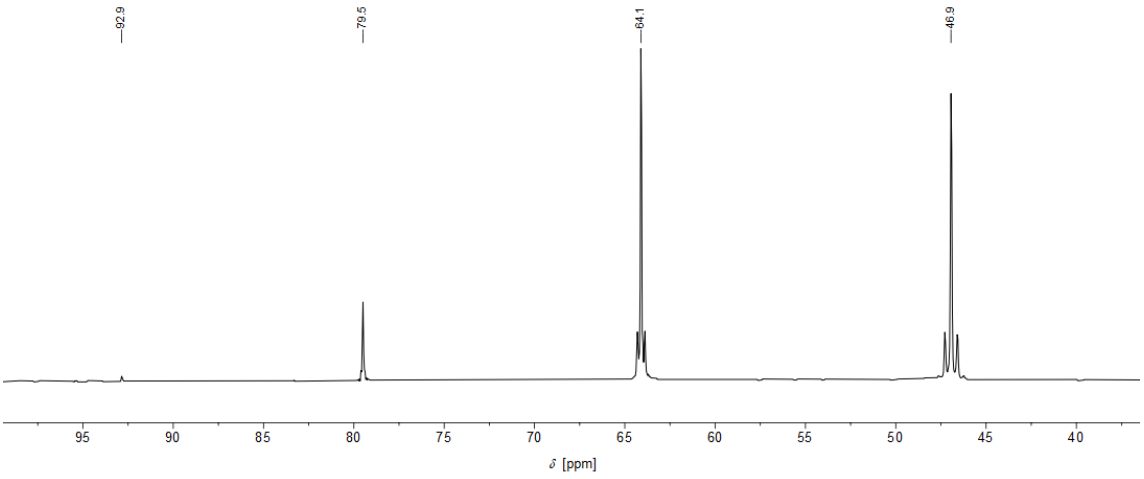

Figure S2. ^{27}Al NMR spectrum (104 MHz, CD_2Cl_2, 22 °C) of $[C(C_6H_5)_3][Al(OTeF_5)_{4-n}Cl_n]$ (n = 0,1,2,3).

NMR spectra of autoionized $[Al(OTeF_5)_3(PhCN)_3]$ in CD_2Cl_2

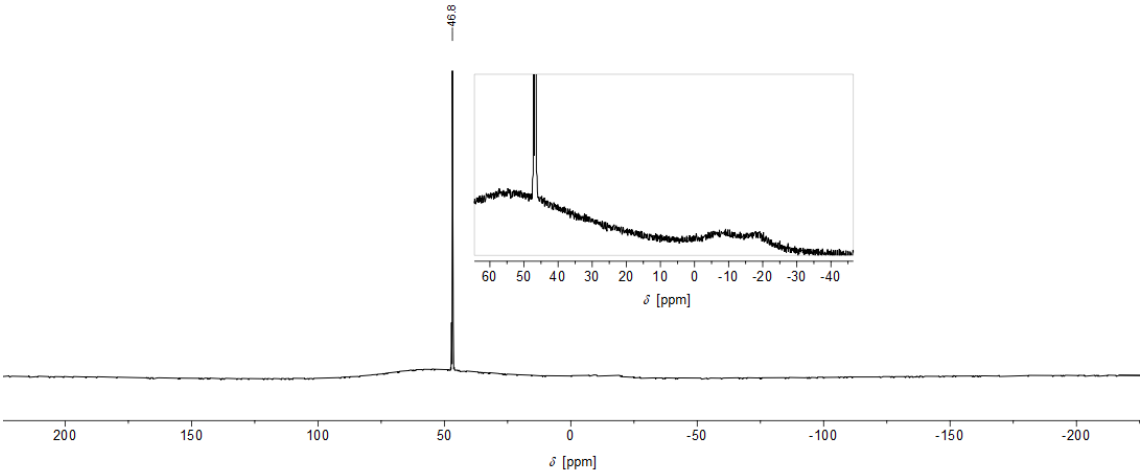

Figure S3. ^{27}Al NMR spectrum (104 MHz, CD_2Cl_2, 22 °C) of $[Al(OTeF_5)_3(PhCN)_3]$ and its autoionization products..

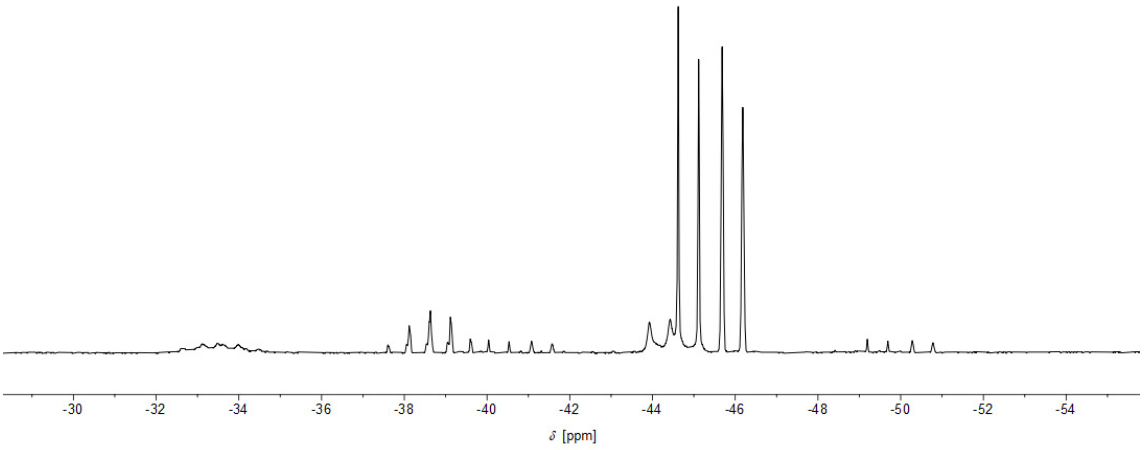

Figure S4. ^{19}F NMR spectrum (377 MHz, CD_2Cl_2, 22 °C) of $[Al(OTeF_5)_3(PhCN)_3]$ and its autoionization products.

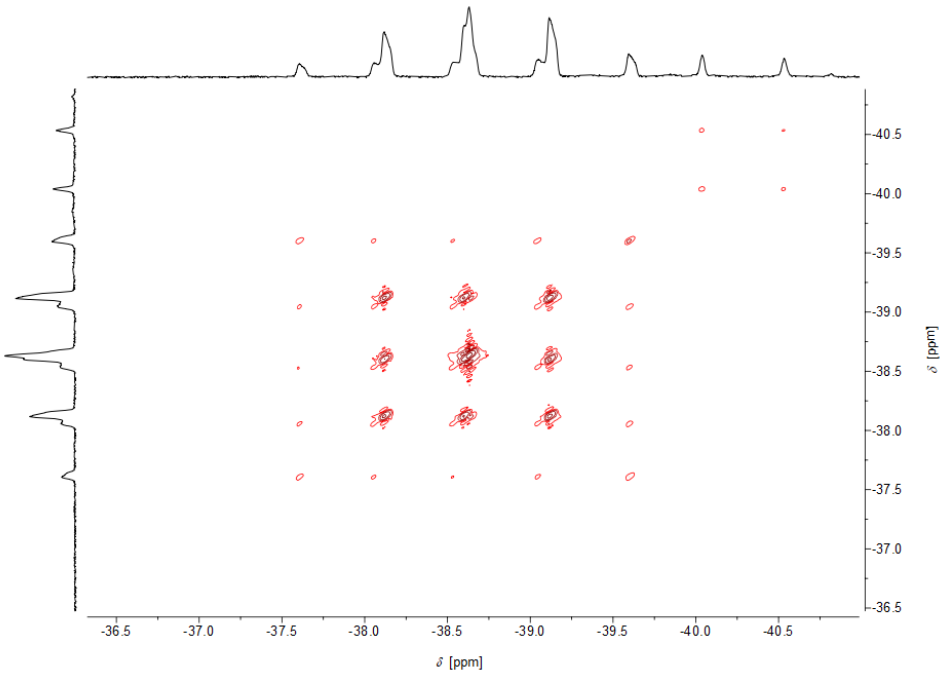

Figure S5. $^{19}F,^{19}F$ EXSY NMR (377 MHz, CD_2Cl_2, 22 °C, mixing time 1.0 s) of $[Al(OTeF_5)_3(PhCN)_3]$.

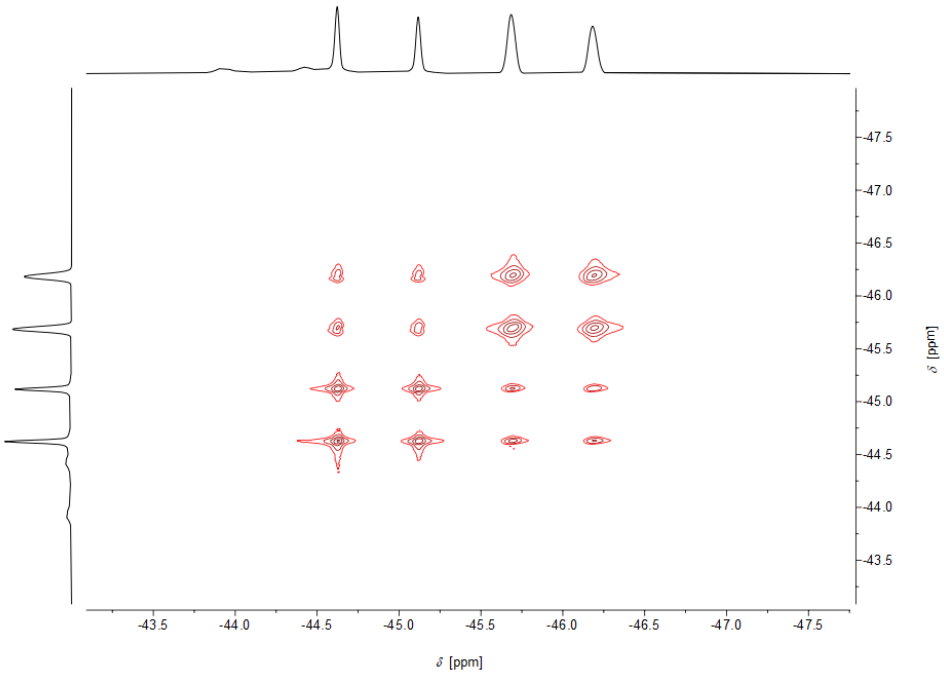

Figure S6. $^{19}F,^{19}F$ EXSY NMR (377 MHz, CD_2Cl_2, 22 °C, mixing time 1.0 s) of $[Al(OTeF_5)_3(PhCN)_3]$.

Vibrational Spectra

Infrared spectrum of $[Al(OTeF_5)_2Me]_2$ and $[Al(OTeF_5)_3]_2$

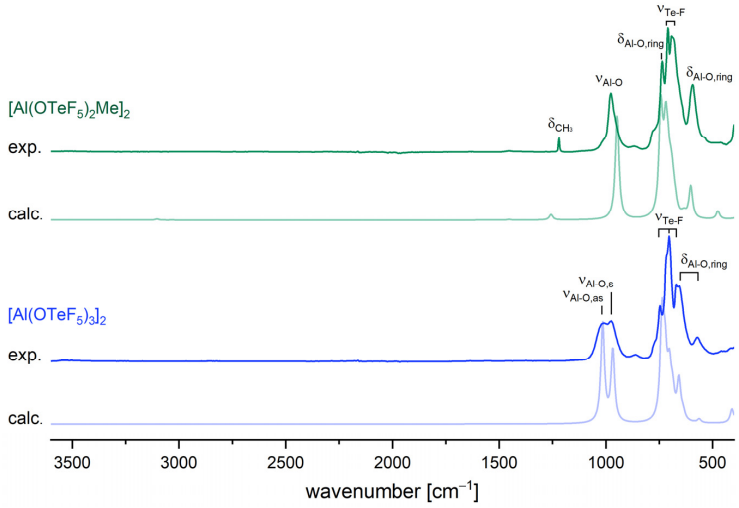

Figure S7. Experimental and calculated IR spectra of $[Al(OTeF_5)_2Me]_2$ (top, green) and $[Al(OTeF_5)_3]_2$ (bottom, blue). Calculations were performed on the B3LYP/def2-TZVPP level of theory.

Raman spectrum of $[Al(OTeF_5)_2Me]_2$ and $[Al(OTeF_5)_3]_2$

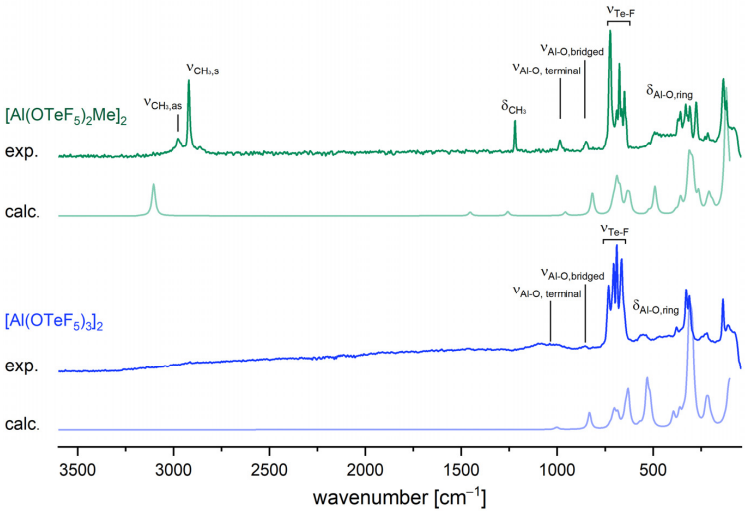

Figure S8. Experimental and calculated Raman spectra of $[Al(OTeF_5)_2Me]_2$ (top, green) and $[Al(OTeF_5)_3]_2$ (bottom, blue). Calculations were performed on B3LYP/def2-TZVPP level of theory.

Crystal data

	$[Al(OTeF_5)_2Me]_2$	$[Al(OTeF_5)_3(PhCN)_3]$	$[Al(OTeF_5)_2(bipy)_2]$ $[Al(OTeF_5)_4(bipy)]$	$[Al(OTeF_5)_3(PhF)_2]$	$[Al(OTeF_5)_3(SO_2ClF)_2]$
CCDC number	2165632	2165805	2165786	2161784	2161790
empirical formula	$C_4H_{12}Al_4F_{40}O_8Te_8$	$C_{21}H_{15}AlF_{15}N_3O_3Te_3$	$C_{30}H_{24}Al_2F_{30}N_6O_6Te_6$	$C_{12}H_{10}AlF_{17}O_3Te_3$	$AlCl_2F_{17}O_7S_2Te_3$
formula weight	2076.86	1052.14	1954.11	934.98	979.80
temperature [K]	100.0	100.0	100.0	100.0	100.0
crystal system	monoclinic	monoclinic	triclinic	monoclinic	triclinic
space group	$P2_1/n$	$P2_1/c$	$P\bar{1}$	$P2_1/n$	$P\bar{1}$
a [pm]	797.34(4)	1423.20(10)	929.15(6)	1422.04(8)	950.95(9)
b [pm]	956.42(5)	427.30(3)	1763.64(12)	867.36(5)	1034.61(9)
c [pm]	1394.58(8)	1610.83(11)	1787.83(10)	1957.19(13)	1282.11(11)
α [°]	90	90	62.239(2)	90	68.344(3)
β [°]	90.669(2)	98.909(2)	81.870(2)	103.301(2)	70.816(3)
γ [°]	90	90	89.249(2)	90	63.920(3)
volume [Å^3]	1063.42(10)	9677.8(11)	2561.8(3)	2349.3(2)	1031.89(16)
Z	1	12	2	4	2
ρ_{calcd} [g · cm^{-3}]	3.243	2.166	2.533	2.643	3.153
μ [mm^{-1}]	5.696	2.838	3.563	3.887	4.890
F(000)	928.0	5880.0	1804.0	1712.0	888.0
dimension [mm]	0.236 × 0.169 × 0.152	0.25 × 0.2 × 0.15	0.24 × 0.1 × 0.04	0.18 × 0.17 × 0.12	0.365 × 0.361 × 0.256
radiation	MoKα (λ = 0.71073)	MoKα (λ = 0.71073)	MoKα (λ = 0.71073)	MoKα (λ = 0.71073)	MoKα (λ = 0.71073)
2Θ range for data collection/°	4.258 to 59.95	4.564 to 55.664	4.436 to 56.798	5.16 to 52.822	4.546 to 55.026
index ranges	-11 ≤ h ≤ 9, -13 ≤ k ≤ 13, -19 ≤ l ≤ 19	-18 ≤ h ≤ 18, -56 ≤ k ≤ 56, -21 ≤ l ≤ 21	-12 ≤ h ≤ 12, -23 ≤ k ≤ 23, -21 ≤ l ≤ 23	-17 ≤ h ≤ 17, -10 ≤ k ≤ 10, -24 ≤ l ≤ 24	-12 ≤ h ≤ 12, -13 ≤ k ≤ 13, -16 ≤ l ≤ 16
reflections collected	24018	253100	247447	33084	12875
independent reflections	3080 [R_{int} = 0.0381, R_{sigma} = 0.0234]	22876 [R_{int} = 0.0433, R_{sigma} = 0.0200]	12835 [R_{int} = 0.0430, R_{sigma} = 0.0140]	4814 [R_{int} = 0.0528, R_{sigma} = 0.0314]	4656 [R_{int} = 0.0432, R_{sigma} = 0.0494]
data/restraints/parameters	3080/0/147	22876/0/1302	12835/282/831	4814/0/325	4656/638/496
goodness-of-fit on F^2	1.099	1.112	1.095	1.051	1.061
final *R* indexes [$I > 2\sigma(I)$]	R_1 = 0.0393, wR_2 = 0.0940	R_1 = 0.0350, wR_2 = 0.0676	R_1 = 0.0266, wR_2 = 0.0623	R_1 = 0.0242, wR_2 = 0.0510	R_1 = 0.0287, wR_2 = 0.0634
final *R* indexes [all data]	R_1 = 0.0457, wR_2 = 0.1012	R_1 = 0.0432, wR_2 = 0.0702	R_1 = 0.0312, wR_2 = 0.0652	R_1 = 0.0352, wR_2 = 0.0549	R_1 = 0.0326, wR_2 = 0.0652
largest diff. peak/hole [e Å^{-3}]	2.64/-1.83	1.41/-1.39	1.59/-2.19	0.52/-1.27	0.72/-1.44

	$[Al(OTeF_5)_3(\eta^1\text{-}C_7H_8)]$	$[Al(OTeF_5)_3(OEt_2)_2]$	$[NEt_4]_2[Al(OTeF_5)_5]$	$[Al(OTeF_5)_3(OPEt_3)]$
CCDC number	2165797	2165785	2167629	2170700
empirical formula	$C_{14}H_{16}AlF_{15}O_3Te_3$	$C_8H_{20}AlF_{15}O_5Te_3$	$C_{16}H_{40}AlF_{25}N_2O_5Te_5$	$C_6H_{15}AlF_{15}O_4PTe_3$
formula weight	927.05	891.02	1480.48	876.93
temperature [K]	100.0	100.0	100.0	150.0
crystal system	monoclinic	triclinic	monoclinic	orthorhombic
space group	$P2_1/c$	$P\bar{1}$	$P2_1/c$	*Pbca*
a [pm]	879.92(8)	948.83(5)	1863.99(18)	1590.90(7)
b [pm]	1912.07(18)	953.82(5)	1252.02(12)	1630.61(7)
c [pm]	1548.37(12)	1351.99(6)	1772.81(16)	1714.91(7)
α [°]	90	79.239(2)	90	90
β [°]	99.002(3)	72.354(2)	94.300(4)	90
γ [°]	90	87.553(2)	90	90
volume [Å^3]	2573.0(4)	1145.37(10)	4125.7(7)	4448.7(3)
Z	4	2	4	8
ρ_{calcd} [g · cm^{-3}]	2.393	2.584	2.384	2.619
μ [mm^{-1}]	3.537	3.972	3.658	4.154
F(000)	1712.0	824.0	2752.0	3216.0
dimension [mm]	0.14 × 0.13 × 0.04	0.16 × 0.094 × 0.046	0.19 × 0.14 × 0.04	0.18 × 0.15 × 0.104
radiation	MoKα (λ = 0.71073)	MoKα (λ = 0.71073)	MoKα (λ = 0.71073)	MoKα (λ = 0.71073)
2Θ range for data collection/°	4.686 to 52.126	4.348 to 61.098	4.466 to 56.74	4.294 to 52.838
index ranges	-10 ≤ h ≤ 10, -23 ≤ k ≤ 23, -19 ≤ l ≤ 18	-13 ≤ h ≤ 13, -13 ≤ k ≤ 13, -16 ≤ l ≤ 19	-24 ≤ h ≤ 24, -16 ≤ k ≤ 16, -23 ≤ l ≤ 23	-19 ≤ h ≤ 19, -20 ≤ k ≤ 20, -21 ≤ l ≤ 21
reflections collected	22774	56863	156748	70037
independent reflections	5077 [R_{int} = 0.0754, R_{sigma} = 0.0541]	7003 [R_{int} = 0.0558, R_{sigma} = 0.0311]	10271 [R_{int} = 0.0600, R_{sigma} = 0.0235]	4569 [R_{int} = 0.0559, R_{sigma} = 0.0187]
data/restraints/parameters	5077/13/271	7003/0/293	10271/991/763	4569/413/311
goodness-of-fit on F^2	1.323	1.180	1.129	1.072
final *R* indexes [$I > 2\sigma(I)$]	R_1 = 0.0678, wR_2 = 0.1188	R_1 = 0.0341, wR_2 = 0.0527	R_1 = 0.0442, wR_2 = 0.0909	R_1 = 0.0242, wR_2 = 0.0431
final *R* indexes [all data]	R_1 = 0.0825, wR_2 = 0.1223	R_1 = 0.0440, wR_2 = 0.0548	R_1 = 0.0547, wR_2 = 0.0982	R_1 = 0.0330, wR_2 = 0.0459
largest diff. peak/hole [e Å^{-3}]	1.19/-1.35	0.89/-1.60	1.37/-1.77	1.07/-1.01

Quantum-chemical calculations

$Al(OTeF_5)_3$

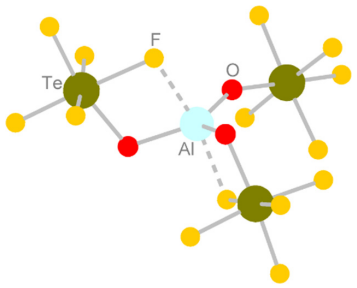

Figure S9. Representation of the B3LYP/def2-TZVPP structure of $Al(OTeF_5)_3$.

Al	-0.0154814	-0.2726284	0.2380079
O	-1.2150192	-1.6099189	0.2188792
Te	-1.858025	-1.7990648	1.9410794
F	-2.228418	-1.676358	3.7448521
F	-3.2075098	-0.5482842	1.707018
F	-0.5271402	-2.9989231	2.4273624
F	-0.5568303	-0.3105929	2.1825416
F	-3.0407199	-3.1811759	1.6577531
O	-0.5413155	1.325125	-0.0481248
Te	-0.6539851	2.8788385	-1.0391523
F	-0.7800246	4.4498125	-2.0174793
F	-2.0818445	2.2194246	-2.0275142
F	0.7737349	3.6341692	-0.1229922
F	0.5225159	2.2408741	-2.3338798
F	-1.8344846	3.6138593	0.1851539
O	1.6931933	-0.6379979	0.6599469
Te	2.5425389	-1.1453158	-0.9005797
F	2.9955182	-1.582618	-2.634162
F	3.0295077	0.5879675	-1.3401595
F	2.0716012	-2.930996	-0.7098563
F	0.6905554	-0.7726229	-1.5611246
F	4.2216328	-1.4835738	-0.2275697

$[Al(OTeF_5)_3]_2$

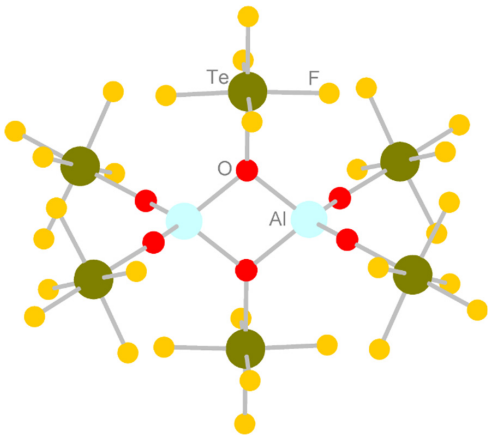

Figure S10. Representation of the B3LYP/def2-TZVPP structure of $[Al(OTeF_5)_3]_2$.

O	-1.4930305	2.1896381	-0.2767368
Te	-2.6470583	3.6140652	0.0228695
F	-3.8113447	5.0216138	0.3245977
F	-3.9988501	2.7359959	-0.8867214
F	-1.3432751	4.5522506	0.9597441
F	-2.1248447	4.4420252	-1.5503481
F	-3.2294561	2.8578109	1.6172466
O	1.47706	2.2066219	0.2369161
Te	2.6274369	3.6314827	-0.074022
F	3.7892503	5.0386468	-0.3863367
F	2.1086607	4.4664612	1.4965332
F	3.2056546	2.8673107	-1.6661743
F	1.3197935	4.5631386	-1.0116021
F	3.9833327	2.7597541	0.8358979
O	-1.4789384	-2.202007	-0.2427287
Te	-2.6340976	-3.6213529	0.0767392
F	-3.8004543	-5.0229981	0.3985197
F	-3.2089307	-2.845011	1.664112
F	-2.1183256	-4.4677639	-1.4885854
F	-1.3285911	-4.5514535	1.0188458
F	-3.9870594	-2.7508552	-0.8384706
O	1.4921224	-2.1935953	0.269627
Te	2.6436121	-3.6225345	-0.021176
F	3.8063834	-5.03311	-0.3159772
F	1.3400142	-4.5600328	-0.9584854
F	3.9937989	-2.7442902	0.8905543
F	2.1142487	-4.4446341	1.5527079
F	3.2321289	-2.8714023	-1.615457
Al	-0.0043695	1.4170581	-0.0135024
O	-0.1535843	0.0086776	1.1968077
Te	-0.3382248	0.0208286	3.116416
F	-0.5120992	0.0316488	4.9465403
F	1.4960966	0.0279101	3.3072707
F	-2.1732851	0.0141106	2.9537881
F	-0.3249469	-1.8299382	3.0611031
F	-0.3367753	1.8705495	3.0372695
Al	0.0052831	-1.4170809	0.0087401
O	0.1560708	-0.0086024	-1.2013979
Te	0.3480949	-0.0230182	-3.1202101
F	0.5300923	-0.0367044	-4.9495997
F	2.182635	-0.0131357	-2.9500178
F	-1.4852181	-0.0329699	-3.3189239
F	0.3318195	1.8276573	-3.0680115
F	0.3491701	-1.872766	-3.0383616

$[Al(OTeF_5)_3F]^-$

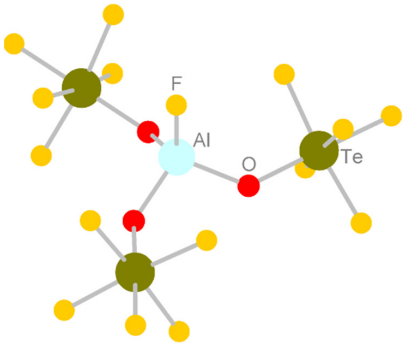

Figure S11. Representation of the B3LYP/def2-TZVPP structure of $[Al(OTeF_5)_3F]^-$.

O	-1.5463191	-0.2801372	0.5217827
Te	-2.5250278	-1.1545196	1.8577326
F	-2.7914381	-2.7104752	0.7929917
Al	0.1925518	0.0807057	0.2943045
F	2.3753416	-1.7044053	-2.6296602
Te	2.6820221	-1.9093634	-0.7611651
F	3.2215533	-2.1999151	1.0425133
F	-2.4040392	0.2908222	3.0922809
O	0.2616829	1.1881487	-1.1116047
Te	-0.3187476	2.9476271	-1.3864487
F	-1.1874354	3.0619573	0.3117506
O	0.9270971	-1.4442571	-0.2971982
F	-3.5510063	-2.0478683	3.1947791
F	-4.1702226	-0.4518669	1.2124829
F	-0.9844525	-1.9635291	2.6482528
F	-0.9019009	4.7377081	-1.6916792
F	-1.959732	2.4122816	-2.1908225
F	1.2512886	3.7254705	-0.6381403
F	0.4827542	3.0154881	-3.1098445
F	4.4599697	-2.409526	-1.2377858
F	3.3277562	-0.1133291	-0.6688633
F	2.2296214	-3.750751	-0.9126338
F	0.9286825	0.679734	1.6669752

$[Al(OTeF_5)_3(\eta^1\text{-}C_7H_8)]$

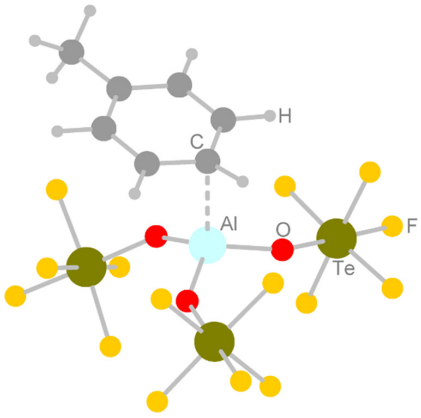

Figure S12. Representation of the B3LYP/def2-TZVPP structure of $[Al(OTeF_5)_3(\eta^1\text{-}C_7H_8)]$.

O	-1.3645142	0.0472616	0.8383873
Te	-2.0247602	-0.9220591	2.2642332
F	-0.8693236	-2.3472871	1.9657889
Al	0.0842052	0.5030815	0.0144527
F	3.2735168	-1.4518198	-0.6971698
Te	3.355718	-0.1378949	0.6109738
F	3.5812761	1.2018469	1.8908453
F	-3.2266079	0.4432291	2.6764494
O	0.1000744	0.2054927	-1.6897126
Te	-0.9183405	-0.2130364	-3.1710909
F	-2.4976445	0.3596441	-2.3556755
O	1.5215121	-0.0616924	0.8037575
F	-2.7207759	-1.8649171	3.7033038
F	-3.3136934	-1.7214252	1.1988772
F	-0.8004867	-0.1684789	3.4535181
F	-1.9271266	-0.6017863	-4.6792363
F	-1.237547	-1.9454691	-2.5830916
F	-0.6929694	1.5083491	-3.8559252
F	0.579457	-0.7800341	-4.1011201
F	5.2024022	-0.1733742	0.4403084
F	3.3354972	1.1880333	-0.713347
F	3.5018473	-1.4273841	1.9309405
C	-1.951805	3.5472675	1.5957221
C	-0.7335497	3.2601129	2.2252987
C	0.3741602	2.8735289	1.4933308
C	0.2809421	2.7344364	0.0912297
C	-0.9338018	3.0628015	-0.5485858
C	-2.0306255	3.4466468	0.201083
H	-0.6577867	3.3459344	3.3011814
H	1.3128721	2.6709089	1.9907999
H	1.1882941	2.6349594	-0.5012941
H	-1.0008055	3.0134289	-1.6268035
C	-3.1560707	3.9263926	2.4038704
H	-3.8464	4.5420932	1.8288546
H	-3.6912716	3.0230675	2.7082804
H	-2.8758123	4.4618862	3.3103096
H	-2.962405	3.6782877	-0.297653

$[Al(OTeF_5)_3(SO_2ClF)]$

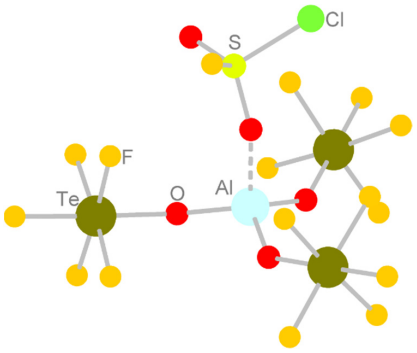

Figure S13. Representation of the B3LYP/def2-TZVPP structure of $[Al(OTeF_5)_3(SO_2ClF)]$.

O	-1.6592433	0.7148916	-0.6009423
Te	-3.364701	0.4311416	0.0548061
F	-3.7917254	-0.7446366	-1.3157064
Al	-0.0721226	0.0673813	-0.4207161
F	0.3395392	-3.9310304	-2.0915278
Te	1.1141499	-3.0967332	-0.634333
F	1.9519698	-2.3477315	0.8736738
F	-3.0555693	1.5639602	1.5024347
O	1.1915196	1.0607705	-1.0391452
Te	1.8705479	2.7787433	-0.958564
F	3.5627879	2.1374761	-0.5521731
O	0.0656577	-1.594959	-0.855081
F	-5.0677968	0.153948	0.7351987
F	-4.0348	1.8488294	-0.9269576
F	-2.7879589	-1.0057863	1.1098063
F	2.5684274	4.4926598	-0.8417563
F	1.4878106	2.8888833	0.876345
F	2.2857932	2.7723444	-2.7621977
F	0.2202367	3.5519195	-1.3246753
F	2.1646332	-4.6026743	-0.3734969
F	2.4720564	-2.4253162	-1.7067669
F	-0.1377897	-3.8735557	0.4995897
O	0.1651496	0.1042847	1.4736431
F	0.3061131	1.2980448	3.4921178
Cl	0.3525177	-1.3905595	3.7991572
S	0.9397938	0.1414216	2.6950853
O	2.3366892	0.2854494	2.6709802

$[Al(OTeF_5)_3(SO_2ClF)_2]$

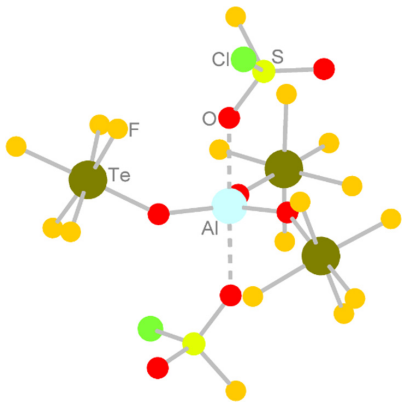

Figure S14. Representation of the B3LYP/def2-TZVPP structure of $[Al(OTeF_5)_3(SO_2ClF)_2]$.

Te	10.0161653	6.2782047	10.9361748
Te	10.9493527	11.9846492	9.3144023
Te	8.0640841	8.3097546	5.7191609
S	6.9010151	9.5609002	10.1436922
Cl	6.0578466	11.1129064	9.2276187
Al	9.7932361	8.8235004	8.6290342
Cl	13.8320818	8.1058191	8.4863993
S	12.6225164	8.2284827	6.9077405
F	9.1625566	12.5135547	9.1991334
F	11.2861285	12.7614866	7.6655026
F	8.543996	7.0932321	11.74685
F	11.119615	6.9515188	12.2676554
F	6.919034	9.7658341	5.9196719
F	12.7567993	11.582785	9.4978082
O	6.1327563	8.3928884	9.9769105
F	11.3063798	13.6344905	10.0871165
O	10.6181329	10.3528492	8.5279562
F	6.7859619	10.0431297	11.6095795
F	11.4600028	5.3533879	10.2135727
F	9.7094279	4.8117313	12.0314282
F	8.880489	5.4909523	9.6887203
O	12.9908846	9.2970521	6.0675927
O	8.3148047	9.5908647	9.8775039
F	9.1748303	6.8556662	5.3765248
F	12.9848867	6.8938579	6.2097644
F	10.6325748	11.3380496	11.0342899
F	9.4334968	9.4641547	5.1960047
F	7.5456027	8.2405452	3.9381935
O	11.2676577	8.0349153	7.3454599
F	6.6621127	7.1608498	6.1057485
O	8.5453573	8.391163	7.4972084
O	10.3434378	7.7355094	9.8644008

[Al(OTeF$_5$)$_3$(FSO$_2$Cl)]

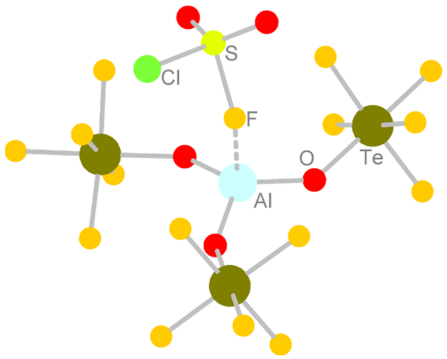

Figure S15. Representation of the B3LYP/def2-TZVPP structure of [Al(OTeF$_5$)$_3$(FSO$_2$Cl)].

O	-1.5193188	0.5808734	-0.5931293
Te	-3.2575665	-0.0605561	-0.6248653
F	-2.8018669	-1.4973683	-1.7124723
Al	0.1068868	0.0816244	-0.3790791
F	2.5651854	-2.630755	-1.9881324
Te	1.6423081	-2.9298912	-0.4088936
F	0.8056013	-3.3095575	1.2164442
F	-3.8302447	1.3162311	0.476215
O	1.3090529	1.2311502	-0.7914391
Te	1.783191	2.9959281	-0.4834915
F	3.2505296	2.4775531	0.5271401
O	0.4504497	-1.5557189	-0.7511884
F	-4.9974184	-0.7004349	-0.6211969
F	-3.669395	0.951174	-2.1189389
F	-2.9372605	-1.1196182	0.8862975
F	2.2580262	4.7556261	-0.1482299
F	0.7490187	3.0423277	1.0789561
F	2.83228	3.0347478	-2.0067491
F	0.3337883	3.6410526	-1.4487293
F	2.8195107	-4.3143306	-0.0435576
F	2.8046623	-1.7857477	0.4985474
F	0.5441017	-4.1509568	-1.2607171
F	0.2828311	0.0142367	1.5595825
O	-1.4516186	1.2542576	2.8427759
Cl	-0.8645408	-1.3812751	3.6533607
S	-0.3299012	0.4538685	3.1345301
O	0.8404477	0.8527882	3.8088774

[Al(OTeF$_5$)$_3$(PhF)]

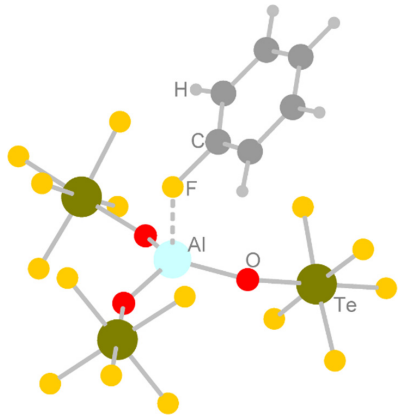

Figure S16. Representation of the B3LYP/def2-TZVPP structure of [Al(OTeF$_5$)$_3$(PhF)].

O	-1.3574532	-0.2727724	0.588358
Te	-2.3136574	-1.5139294	1.5758084
F	-2.3109655	-2.7493432	0.1859088
Al	-0.0032917	-0.1012996	-0.4551293
F	1.6989851	-2.2610785	-3.2578369
Te	2.3829898	-2.2493572	-1.5343431
F	3.188199	-2.267195	0.151038
F	-2.3684339	-0.3625722	3.0322396
O	-0.1615304	1.0160851	-1.7506316
Te	-0.7765345	2.7239013	-2.1093536
F	-0.9373877	3.1128148	-0.2816502
O	0.8217235	-1.5614625	-0.8232104
F	-3.2717263	-2.7396205	2.5851355
F	-3.9257775	-0.8293364	0.9729439
F	-0.7549108	-2.2780055	2.257861
F	-1.3812043	4.4424876	-2.4558129
F	-2.5482459	2.1692529	-2.1412262
F	0.9473537	3.4160796	-2.0747304
F	-0.638824	2.4454042	-3.9330973
F	3.9619877	-2.945266	-2.2124298
F	3.0894456	-0.5453897	-1.8174806
F	1.7915884	-3.9824485	-1.2692607
F	1.2278039	0.8184905	0.6512098
H	3.0240774	-0.4770933	4.6057875
C	2.3989003	0.2197726	4.0651469
C	1.7807609	1.2737181	4.7298545
H	1.9275188	1.3951719	5.7941514
C	0.9743394	2.1722884	4.0387151
H	0.495849	2.9902414	4.5588473
C	0.7733856	2.0287296	2.6677074
H	0.1564559	2.7055868	2.0951526
C	1.4077715	0.9658405	2.0793411
C	2.2178443	0.0469896	2.6941111
H	2.6814633	-0.7589149	2.1439448

$[Al(OTeF_5)_3(PhF)_2]$

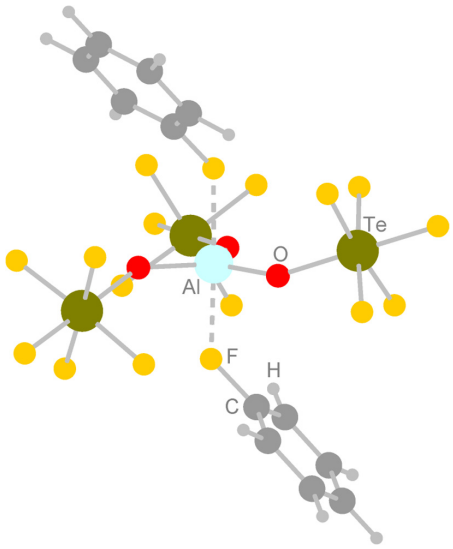

Figure S17. Representation of the B3LYP/def2-TZVPP structure of $[Al(OTeF_5)_3(PhF)_2]$.

Te	-0.9734327	0.9462411	-3.1501031
Te	1.1588097	2.0805517	2.365333
Te	-0.1716671	-3.3255445	0.9736657
Al	-0.0505676	-0.0654089	-0.0117749
F	-1.8074049	1.1457159	-4.7968066
F	0.1381309	2.356877	-3.617127
F	0.1943361	-0.2487888	-3.9639077
F	-2.1577894	-0.4480817	-2.7994032
F	-2.215334	2.1609599	-2.4689639
F	2.1096551	3.3872579	3.2796951
F	-0.1779762	3.3474522	2.10866
F	1.9978518	2.6722144	0.8024259
F	2.5847001	0.9318164	2.6822111
F	0.3909529	1.592675	3.9811246
F	-0.1055044	-4.890403	1.969733
F	-1.3808765	-4.1711971	-0.1477227
F	-1.5734907	-2.7736472	2.0765791
F	1.0482762	-2.5968459	2.1787109
F	1.2390547	-3.9990641	-0.0402009
F	-2.096405	0.1182679	0.2862501
F	1.9942933	-0.2453798	-0.2465606
O	-0.1349723	0.7832676	-1.517932
O	0.195919	0.78849	1.4716042
O	-0.235291	-1.7883062	-0.0358824
C	-2.9250787	0.8317135	1.1797317
C	-3.406513	2.0484468	0.7583954
H	-3.1453827	2.4429387	-0.2122456
C	-4.2408862	2.7323455	1.638961
H	-4.6404916	3.6941831	1.3487624
C	-4.5560334	2.1856429	2.8783852
H	-5.2031727	2.7257043	3.5557318
C	-4.0422329	0.9479449	3.2516025
H	-4.2868432	0.5231659	4.2153401
C	-3.2059738	0.243024	2.389966
H	-2.7919319	-0.720134	2.648328
C	2.8611158	-0.3508289	-1.3570954
C	3.3926236	0.8158742	-1.8533997
H	3.137729	1.7700117	-1.4166834
C	4.2624742	0.6984748	-2.9341551
H	4.7015231	1.5905602	-3.3589274
C	4.5624282	-0.5526039	-3.4637006
H	5.2378994	-0.6328039	-4.3042979
C	3.9977452	-1.7006753	-2.9184216
H	4.2316227	-2.6728485	-3.3298391
C	3.1243426	-1.6118172	-1.8371641
H	2.6716644	-2.4847363	-1.3906959

$[Al(OTeF_5)_3(MeCN)]$

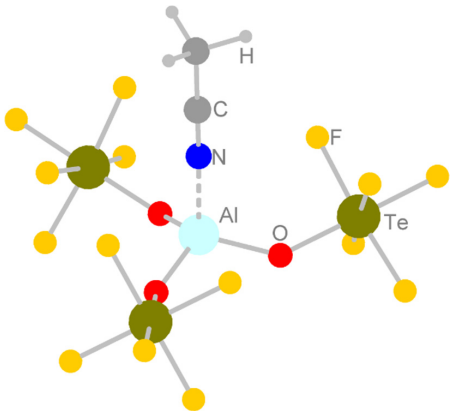

Figure S18. Representation of the B3LYP/def2-TZVPP structure of $[Al(OTeF_5)_3(MeCN)]$.

O	-1.9648925	-0.819232	-0.1963196
Te	-2.8152015	-1.605493	1.2391308
F	-3.1169665	-3.1846733	0.3148771
Al	-0.3643834	-0.3756579	-0.6925619
F	2.3501423	-2.0246658	-3.1150025
Te	2.4081239	-2.1796014	-1.2673118
F	2.6279762	-2.3389649	0.580413
F	-2.5520314	-0.0922556	2.3078174
O	-0.3451833	0.8473366	-1.919866
Te	-0.6752961	2.6509055	-2.1189549
F	-1.7163815	2.7098639	-0.5654777
O	0.6253848	-1.7421657	-1.0823492
F	-3.6652843	-2.3764799	2.6983678
F	-4.4589891	-0.9483387	0.6971033
F	-1.209306	-2.2923	1.9124664
F	-0.9866048	4.4715375	-2.3057262
F	-2.1922714	2.3520652	-3.1420898
F	0.8105801	3.106401	-1.0765928
F	0.3661446	2.7287768	-3.6476274
F	4.2051797	-2.6172791	-1.429428
F	2.9379729	-0.3876776	-1.1259186
F	2.0120457	-3.9844471	-1.3844527
N	0.4442654	0.4397231	0.8664418
C	0.9049847	0.9357394	1.7870865
C	1.4841156	1.5637457	2.9486961
H	0.7520226	1.5706505	3.7568249
H	2.3674173	1.0050429	3.2594529
H	1.7664362	2.5874441	2.7010009

$[Al(OTeF_5)_3(MeCN)_3]$

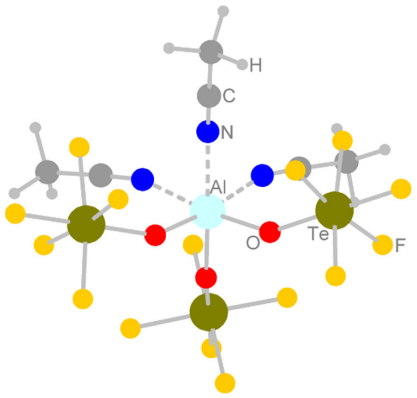

Figure S19. Representation of the B3LYP/def2-TZVPP structure of $[Al(OTeF_5)_3(MeCN)_3]$.

O	-1.0640556	-0.2607397	1.1095797
Te	-0.849383	-0.1452905	2.9076246
F	-1.9861514	-1.5888467	3.2493621
Al	-0.3461082	-0.701894	-0.5143833
F	0.3835034	1.2723515	2.8166471
O	-0.4951934	0.9824172	-1.2128612
Te	0.20802	2.2837552	-2.2635914
F	0.7353726	3.3332967	-0.809124
N	0.624424	-1.3276593	-2.2301677
F	-0.640189	-0.0264408	4.759129
F	-2.2527713	1.0547745	3.1000648
F	0.6145163	-1.3378526	2.9703635
F	0.9215319	3.6310745	-3.3411803
F	-1.40436	3.1951348	-2.3867273
F	1.9450309	1.5420415	-2.3012686
F	-0.151296	1.3769897	-3.8717283
N	1.5389765	-0.2170647	0.1820627
O	-1.9242142	-1.2970743	-1.2225892
N	0.052026	-2.5971743	0.208893
F	-2.9671409	-3.6282797	-0.3059966
Te	-2.8801777	-2.6710945	-1.9229131
F	-3.8706929	-4.0782252	-2.6473168
F	-1.3638834	-3.6988146	-2.3851893
F	-2.866931	-1.9500405	-3.6467899
F	-4.509115	-1.8590809	-1.5573648
C	1.2121331	-1.7050119	-4.7225466
C	0.900926	-1.5074549	-3.3247687
C	3.4771132	1.0706365	1.3152282
C	2.4099636	0.3350213	0.6755461
C	-0.0540543	-3.6140932	0.7203294
C	-0.238567	-4.8888457	1.3763112
H	-1.2419218	-5.2516332	1.1511955
H	-0.1331099	-4.7596786	2.4533704
H	0.4980114	-5.6078694	1.0195791
H	4.2894222	0.3979699	1.588086
H	3.0795809	1.5456865	2.2126409
H	3.8477358	1.8360935	0.6336539
H	2.2688068	-1.9403868	-4.8446011
H	0.9782259	-0.7870354	-5.2625726
H	0.6070459	-2.5215021	-5.1162964

$[Al(OTeF_5)_3(PhCN)]$

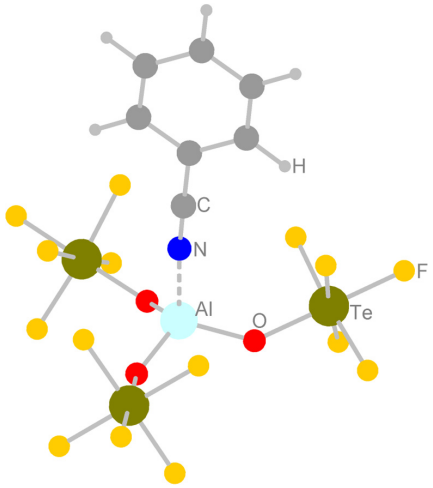

Figure S20. Representation of the B3LYP/def2-TZVPP structure of $[Al(OTeF_5)_3(PhCN)]$.

O	-1.2234647	-0.9538218	-1.0841076
Te	-1.8353611	-2.6696911	-0.8125232
F	-1.4174828	-3.1922031	-2.5416187
Al	0.0446908	0.1114682	-0.556472
F	3.4749067	1.3685022	-2.1804378
Te	3.3782311	-0.0006204	-0.93119
F	3.4347956	-1.3305693	0.3777995
F	-2.2893468	-2.3059391	0.9713101
O	-0.3552764	1.785369	-0.7686536
Te	-1.5265673	3.0445697	-0.1024163
F	-2.4942532	1.7553361	0.8514071
O	1.5850397	-0.2896077	-1.2472996
F	-2.4637605	-4.3925654	-0.5157049
F	-3.5489259	-2.2060794	-1.3417929
F	-0.1676651	-3.2642145	-0.2104056
F	-2.6946368	4.3149725	0.5842378
F	-2.6875839	2.8605159	-1.5390326
F	-0.4751142	3.3202482	1.4154219
F	-0.6378315	4.4156832	-0.975066
F	5.1840082	0.2785932	-0.5966958
F	3.0185059	1.2489983	0.4190214
F	3.86525	-1.2374121	-2.221012
N	0.1897492	-0.1987734	1.3315104
C	0.2157753	-0.4431453	2.453263
H	1.9929206	-0.1185017	6.6478648
C	1.231364	-0.5303752	6.0006919
C	0.2551476	-1.378908	6.5181204
H	0.2637664	-1.6230314	7.5719726
C	-0.7314406	-1.9171296	5.6952411
H	-1.4840053	-2.5750667	6.1066038
C	-0.7525761	-1.6119125	4.3449751
H	-1.5088375	-2.0203712	3.6893288
C	0.2335514	-0.756057	3.8306703
C	1.2302048	-0.2111243	4.6537364
H	1.9803294	0.4447802	4.23519

$[Al(OTeF_5)_3(PhCN)_3]$

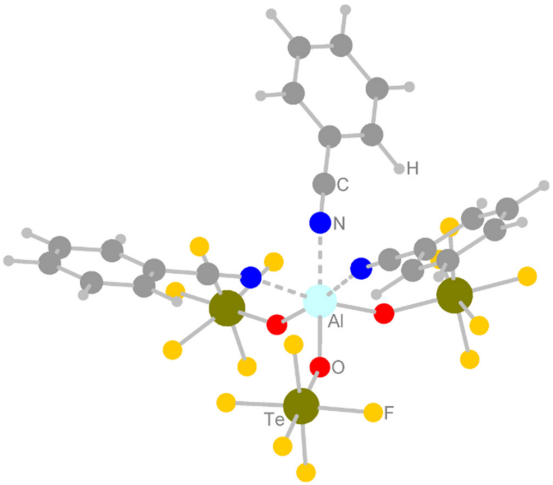

Figure S21. Representation of the B3LYP/def2-TZVPP structure of $[Al(OTeF_5)_3(PhCN)_3]$.

O	-0.9967725	-0.8011577	1.342996
Te	-1.036157	-1.5046955	3.0139367
F	-1.2124912	-3.2601032	2.3969566
Al	-0.0130089	-0.0009824	0.0184608
F	-0.7861424	0.1407463	3.8780051
O	-0.973995	1.5572027	0.0513056
Te	-1.0117088	3.3504808	-0.218925
F	-1.2712596	3.7299673	1.5921067
N	1.2908903	0.7745955	-1.3834211
F	-1.0806748	-2.2417407	4.7316621
F	-2.8801219	-1.3367122	3.1581491
F	0.8358166	-1.7827765	3.121157
F	-1.052236	5.2003803	-0.4813803
F	-2.8458905	3.3777909	-0.5135634
F	0.8477638	3.5874017	0.0466072
F	-0.6922628	3.2345127	-2.0634972
N	1.2747522	0.8096097	1.4047419
O	-0.9823785	-0.7312416	-1.3567627
N	1.2550107	-1.621147	0.0407064
F	-1.0253643	-3.410422	-1.7763035
Te	-1.0380023	-1.8376799	-2.7912942
F	-1.1065865	-2.9558265	-4.2874016
F	0.8396311	-1.9857566	-2.9654539
F	-0.9809657	-0.4224626	-4.0233357
F	-2.8942807	-1.8406685	-2.8471885
H	3.9701945	2.7898058	-2.3572492
C	3.5320876	2.6222479	-3.3309684
C	2.3818816	1.8330095	-3.4538151
C	1.7905778	1.2514792	-2.2994806
C	1.7887671	1.6124921	-4.7037961
H	0.8958353	1.0078282	-4.7760954
C	2.3601678	2.1860606	-5.8289729
H	1.9081398	2.0242446	-6.7977284
C	3.5050234	2.9688963	-5.71218
H	3.9430592	3.4147787	-6.5952831
C	4.0889529	3.1868918	-4.4669612
H	4.9753989	3.8001947	-4.3818658
H	2.4687891	0.3563607	4.6264663
C	2.6540219	1.4180139	4.5454262
C	2.3220139	2.0952546	3.3653378
C	1.7480525	1.3782454	2.2813032
C	2.5260274	3.4757698	3.2421858
C	3.0734918	4.1721661	4.3080328
C	3.4111636	3.5029082	5.4812132
H	3.8342998	4.0541888	6.3104507
C	3.2006202	2.1316705	5.5999418
H	3.4553973	1.6198586	6.5176578
H	2.2417353	-4.0632451	2.2689306
C	2.5270041	-4.5741802	1.3601233
H	3.2443351	-6.330947	2.3459136
C	3.0839311	-5.8426998	1.3946147
C	2.3184455	-3.9569329	0.1200735
C	1.7353821	-2.6620576	0.0749753
C	3.4264448	-6.4883322	0.2095764
C	2.6558653	-4.6038399	-1.0755507
C	3.2117107	-5.8720452	-1.0203282
H	3.8571559	-7.4802348	0.2444008
H	2.4680125	-4.11613	-2.0216262
H	3.4710441	-6.3830187	-1.9372402
H	2.2433488	3.9806138	2.3291431
H	3.2297153	5.2389302	4.2262016

[Al(OTeF$_5$)$_3$(Et$_2$O)]

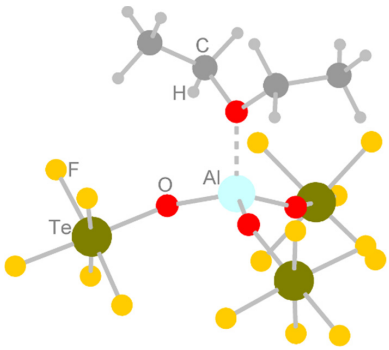

Figure S22. Representation of the B3LYP/def2-TZVPP structure of [Al(OTeF$_5$)$_3$(Et$_2$O)].

Te	0.3475401	0.8101471	-3.1991144
Te	0.7034086	-3.1163599	0.8561381
Te	-0.0651754	2.335533	2.0068034
Al	-0.7125426	-0.2118943	-0.1375418
F	0.0278413	-0.9790218	-3.6218115
F	1.9550408	0.3375451	-2.3922277
F	1.3246995	1.7169103	3.0631108
F	0.2262317	4.0266792	2.711144
F	1.2606477	0.9497186	-4.8076486
F	0.7083898	2.6043281	-2.9087114
F	-1.2070878	1.2740549	-4.1112211
F	1.1320757	2.7605944	0.6495497
F	-0.5192788	-4.2942646	0.087871
F	-1.4618309	3.0745506	1.0085492
F	-0.5650718	-2.7168719	2.1794954
F	1.9776428	-3.6250991	-0.3868861
F	-1.259538	2.0341672	3.4032966
F	1.9477214	-2.0500643	1.7303759
O	-0.3868217	0.6480265	1.3298651
O	-2.5384816	-0.5663934	-0.0499073
O	-0.599507	0.6770221	-1.6178971
F	1.2612295	-4.5238266	1.9294087
O	0.114757	-1.736438	-0.2167504
C	-3.3430785	-0.8403366	-1.259362
H	-2.9863988	-0.1336884	-2.003147
H	-4.3684553	-0.5831692	-1.0047289
C	-3.2246111	-0.812627	1.2363402
H	-2.4305502	-0.9559355	1.9636096
H	-3.7608501	-1.7536769	1.1260334
C	-4.1290954	0.3367015	1.6152982
H	-4.583776	0.1128592	2.5817013
H	-4.9356506	0.4842936	0.8974624
H	-3.5696983	1.2652188	1.712919
C	-3.2035595	-2.2743352	-1.716807
H	-2.1762002	-2.5098727	-1.9905712
H	-3.8282042	-2.4175101	-2.6001547
H	-3.5328911	-2.9814941	-0.955754

[Al(OTeF$_5$)$_3$(Et$_2$O)$_2$]

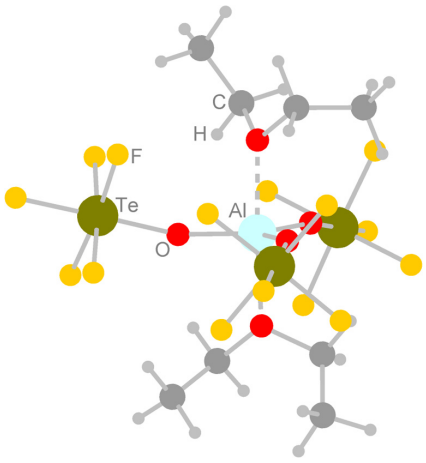

Figure S23. Representation of the B3LYP/def2-TZVPP structure of [Al(OTeF$_5$)$_3$(Et$_2$O)$_2$].

Te	5.5979325	3.7347362	5.253538
Te	10.8903802	0.5946733	2.8222348
Te	7.9634559	5.5953248	1.002465
Al	8.3605305	2.9989786	3.3068593
F	5.095431	2.0146883	5.7681768
F	4.7569865	3.4807015	3.6085595
F	7.7857804	4.7131725	-0.6262003
F	7.6725375	7.1819627	0.0796749
F	3.9578698	4.31717	5.9031002
F	5.9626382	5.5045963	4.8038082
F	6.2827848	4.0338304	6.9597225
F	6.1220484	5.498438	1.2564502
F	12.1253763	1.1047429	4.1203782
F	8.1203077	6.6231005	2.549833
O	7.1468328	1.6203354	2.4383088
F	11.6350504	1.8255199	1.633286
F	10.2600024	-0.7539274	3.9413868
F	9.7813107	5.8393394	0.6665305
F	9.7836728	-0.0362669	1.451969
O	8.2671846	4.0054308	1.8658314
O	9.6162527	4.3151078	4.2370598
O	7.2332993	3.1474271	4.6610647
F	12.1621469	-0.6203452	2.221443
O	9.6537171	1.7864687	3.445241
C	9.5922581	4.5733732	5.6756169
H	8.5578982	4.781246	5.9176035
H	10.1600766	5.4847344	5.8444767
C	6.9915991	1.4768668	0.9861611
H	7.1042586	0.4181291	0.7564679
H	7.8268065	2.0050532	0.537619
C	10.9239052	4.540222	3.6172378
H	10.8096268	4.2095079	2.5900727
H	11.6473835	3.8857463	4.1028207
C	6.8929788	0.3924879	3.1926144
H	7.1482783	0.6335321	4.2202732
H	7.5907549	-0.3635133	2.8325938
C	5.6731123	2.0307899	0.4876799
H	5.6609595	1.9712719	-0.6023825
H	5.550023	3.0741571	0.7685513
H	4.8209702	1.47206	0.8687751
C	11.3701376	5.9896736	3.6488777
H	12.2484587	6.0843747	3.0084717

H	11.6587335	6.3251859	4.6439407
H	10.5983459	6.6518318	3.2619801
C	5.4624757	-0.0996573	3.1084983
H	5.2012954	-0.446345	2.1096241
H	4.7543665	0.6667273	3.416794
H	5.3584941	-0.9483146	3.7869387
C	10.1311182	3.4231487	6.5027592
H	9.5353417	2.5221017	6.3665108
H	10.0833056	3.701333	7.557028
H	11.1692391	3.1915309	6.266232

$[Al(OTeF_5)_2Me]_2$

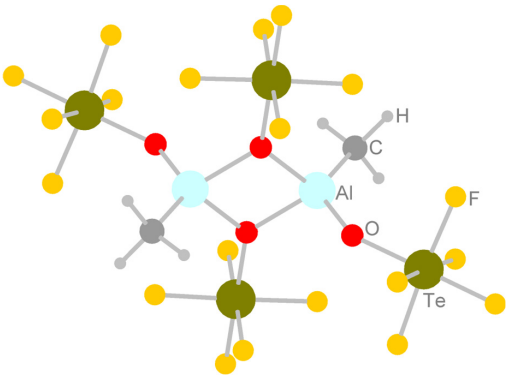

Figure S24. Representation of the BP86/def-SV(P) structure of $[Al(OTeF_5)_2Me]_2$.

C	-1.6594461	2.4951904	-0.2564480
O	1.5633360	2.0826647	0.0429539
Te	2.5913295	3.6162917	-0.0496177
F	3.6359734	5.1463628	-0.1412347
F	1.9175632	4.2554877	1.5631690
F	3.3315847	3.0922308	-1.6712519
F	1.2608646	4.5503122	-0.9646559
F	3.9810759	2.7867924	0.8555633
O	-1.5529453	-2.0755860	-0.0426786
Te	-2.6046279	-3.5938947	0.0244642
F	-3.6748097	-5.1074942	0.0898235
F	-3.3692604	-3.0637335	1.6325739
F	-1.9084284	-4.2391262	-1.5764395
F	-1.3061709	-4.5498237	0.9621607
F	-3.9625129	-2.7399486	-0.9060260
C	1.6658525	-2.5095077	0.2697993
Al	-0.0500286	1.4551178	-0.0700496
O	-0.0956252	0.0566541	1.2154535
Te	-0.2803230	0.1401124	3.1103740
F	-0.4576010	0.2154419	4.9434755
F	1.5557252	0.1266984	3.3271239
F	-2.1232239	0.1582281	2.9687961
F	-0.2949972	-1.7146013	3.1573173
F	-0.2592965	1.9913648	3.0049451
Al	0.0631227	-1.4601494	0.0796996
O	0.1155026	-0.0613456	-1.2042942
Te	0.2921264	-0.1476201	-3.0998833
F	0.4615995	-0.2267897	-4.9335454
F	2.1354030	-0.1777490	-2.9652886
F	-1.5446825	-0.1228424	-3.3091514
F	0.3180921	1.7067210	-3.1493442
F	0.2599767	-1.9986187	-2.9918586
H	-1.6234794	3.1141322	-1.1546550
H	-1.7944831	3.1673777	0.5930315
H	-2.5446756	1.8599131	-0.3221271
H	1.8090677	-3.1684762	-0.5886766
H	1.6163971	-3.1426779	1.1574149
H	2.5528449	-1.8792791	0.3567467

$Al(C_6F_5)_3$

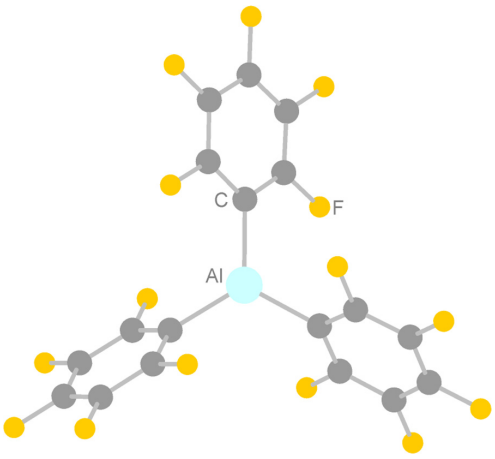

Figure S25. Representation of the BP86/def-SV(P) structure of $Al(C_6F_5)_3$.

C	2,5581884	0,7360921	1,4532835
C	1,3052162	0,5627493	2,0555348
F	1,0934578	1,0149188	3,3138883
C	0,2201274	-0,0736178	1,4285962
F	-0,9705738	-0,2179110	2,0424568
C	0,3907904	-0,5688283	0,1252515
F	-0,6283173	-1,1845399	-0,5007484
C	1,6294353	-0,4276945	-0,5196103
F	1,7877871	-0,9137707	-1,7666358
C	2,6788352	0,2225073	0,1568763
F	3,8482348	0,3179185	-0,5203053
F	4,2866830	3,6618397	0,0221924
F	6,3734296	4,3573390	-1,5699947
C	5,4788522	3,0616003	0,2470019
C	6,5370803	3,4388986	-0,5980450
C	5,6042468	2,1190731	1,2753006
C	7,7921122	2,8335691	-0,4196565
F	8,8252831	3,1728330	-1,2119837
C	6,8698635	1,5365210	1,4048705
C	7,9657864	1,8718262	0,5881643
F	7,1004219	0,5882780	2,3445806
F	9,1701530	1,2891833	0,7497087
F	3,3525059	-1,2836461	3,7446942
F	4,2580965	-2,4410787	6,0185718
C	4,2089303	-0,5666565	4,5113171
C	4,6665648	-1,2011827	5,6823507
C	4,6093570	0,7177855	4,1266768
C	5,5700260	-0,5217177	6,5154829
F	6,0212902	-1,1052578	7,6408805
C	5,5172872	1,3490824	4,9867755
C	6,0078058	0,7673987	6,1680698
F	5,9798135	2,5865771	4,6867840
F	6,8820464	1,4109489	6,9664626
Al	4,0001884	1,7482251	2,4769679
F	3,3409944	3,2415666	2,9911094

$[Al(C_6F_5)_3F]^-$

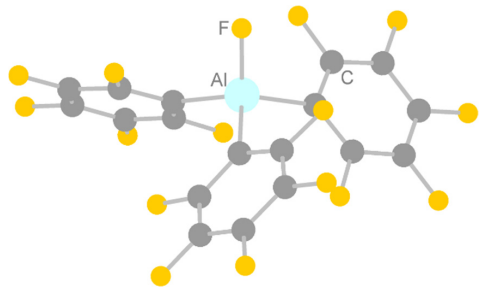

Figure S26. Representation of the BP86/def-SV(P) structure of $[Al(C_6F_5)_3F]^-$.

C	2,5581884	0,7360921	1,4532835
C	1,3052162	0,5627493	2,0555348
F	1,0934578	1,0149188	3,3138883
C	0,2201274	-0,0736178	1,4285962
F	-0,9705738	-0,2179110	2,0424568
C	0,3907904	-0,5688283	0,1252515
F	-0,6283173	-1,1845399	-0,5007484
C	1,6294353	-0,4276945	-0,5196103
F	1,7877871	-0,9137707	-1,7666358
C	2,6788352	0,2225073	0,1568763
F	3,8482348	0,3179185	-0,5203053
F	4,2866830	3,6618397	0,0221924
F	6,3734296	4,3573390	-1,5699947
C	5,4788522	3,0616003	0,2470019
C	6,5370803	3,4388986	-0,5980450
C	5,6042468	2,1190731	1,2753006
C	7,7921122	2,8335691	-0,4196565
F	8,8252831	3,1728330	-1,2119837
C	6,8698635	1,5365210	1,4048705
C	7,9657864	1,8718262	0,5881643
F	7,1004219	0,5882780	2,3445806
F	9,1701530	1,2891833	0,7497087
F	3,3525059	-1,2836461	3,7446942
F	4,2580965	-2,4410787	6,0185718
C	4,2089303	-0,5666565	4,5113171
C	4,6665648	-1,2011827	5,6823507
C	4,6093570	0,7177855	4,1266768
C	5,5700260	-0,5217177	6,5154829
F	6,0212902	-1,1052578	7,6408805
C	5,5172872	1,3490824	4,9867755
C	6,0078058	0,7673987	6,1680698
F	5,9798135	2,5865771	4,6867840
F	6,8820464	1,4109489	6,9664626
Al	4,0001884	1,7482251	2,4769679
F	3,3409944	3,2415666	2,9911094

$Al[N(C_6F_5)_2]_3$

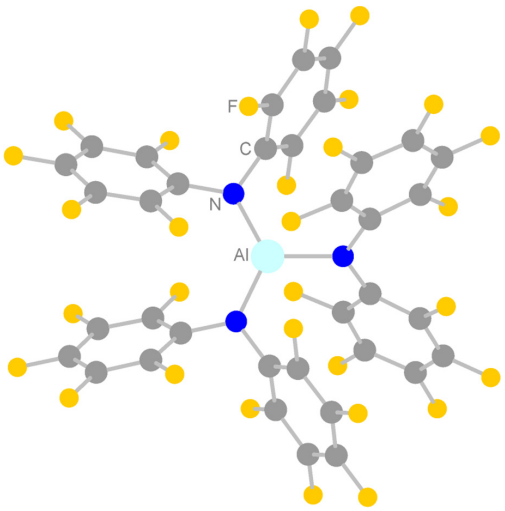

Figure S27. Representation of the BP86/def-SV(P) structure of $Al[N(C_6F_5)_2]_3$.

F	0.5581502	2.1025306	-0.8730444
F	1.6608077	3.8824144	-2.6987592
C	1.8122236	1.8965897	-1.3984916
C	2.3367464	2.7959470	-2.3287447
C	2.4703684	0.7322748	-0.9512876
C	3.6012637	2.5113993	-2.8807607
F	4.1467514	3.3421252	-3.7714817
C	3.7134731	0.4502163	-1.5643278
C	4.2889761	1.3502554	-2.4800403
F	4.3712424	-0.6821499	-1.2775831
F	5.4784684	1.0727835	-3.0178087
F	0.4657042	-2.2245495	0.8147397
F	1.5059771	-4.0242284	2.6328932
C	1.7141603	-2.0481382	1.3285438
C	2.2176386	-2.9600652	2.2614027
C	2.4212781	-0.9103603	0.8837976
C	3.4884113	-2.7194765	2.8184152
F	4.0033956	-3.5698372	3.7089690
C	3.6696604	-0.6681244	1.5028912
C	4.2169956	-1.5838284	2.4193063
F	4.3621925	0.4452764	1.2184205
F	5.4133909	-1.3429422	2.9608146
N	1.7764029	-0.0677919	-0.0347734
F	-2.6168003	-2.2557531	-2.9384335
F	1.7957075	-3.5891447	-3.9803670
F	0.2666286	-2.9247468	-1.8368633
C	1.2242575	-2.3830700	-3.9203115
C	0.4344880	-2.0274316	-2.8129267
F	-5.2410518	-1.7645748	-3.4188533
F	2.1293800	-1.8139013	-6.0403609
C	1.3916348	-1.4759932	-4.9817518
C	-3.1471674	-1.0995819	-2.5167412
C	-0.1794804	-0.7588162	-2.7217245
N	-0.9625877	-0.3744558	-1.5933469
C	0.7820641	-0.2091564	-4.9232176
C	-4.5084026	-0.8570439	-2.7676014
C	0.0181863	0.1385653	-3.7975521
F	0.9541248	0.6614575	-5.9225964
C	-2.3388535	-0.1577089	-1.8361421
F	-0.5288903	1.3617835	-3.7423841
C	-5.1123375	0.3260525	-2.3038715
F	-6.4103688	0.5479774	-2.5224857
C	-2.9753818	1.0230773	-1.3945417
C	-4.3403682	1.2704385	-1.6040493
F	-2.2435050	1.9459058	-0.7350158
F	-4.8990601	2.4015255	-1.1635524
F	-0.5739100	-1.3348498	3.7376146
F	-5.0126525	-2.0492314	1.3696762
F	-2.3533113	-1.8087490	0.8325309
C	-4.3540729	-0.9530901	1.7576356
C	-2.9820255	-0.8180741	1.4922703
F	1.0105390	-0.7892410	5.8890574
F	-6.3286073	-0.0567983	2.7299583
C	-5.0271535	0.0628811	2.4588649
C	0.0983421	-0.1758837	3.7786910
C	-2.2475122	0.3239023	1.8806413
N	-0.8652941	0.4421308	1.5928915
C	-4.3223172	1.2099760	2.8675430
C	0.9147821	0.0923433	4.8892645
C	-2.9571138	1.3406295	2.5631538
F	-4.9620352	2.1856893	3.5183666
C	-0.0236359	0.7366565	2.7042251
F	-2.3233355	2.4616905	2.9330040
C	1.6589186	1.2858471	4.9319001
F	2.4493372	1.5436835	5.9750249
C	0.7264382	1.9307878	2.7799029
C	1.5714942	2.2028631	3.8694214
F	0.6422589	2.8358414	1.7965699
F	2.2700136	3.3408720	3.9132065
Al	-0.0970676	0.0642809	-0.0308633

$[Al\{N(C_6F_5)_2\}_3F]^-$

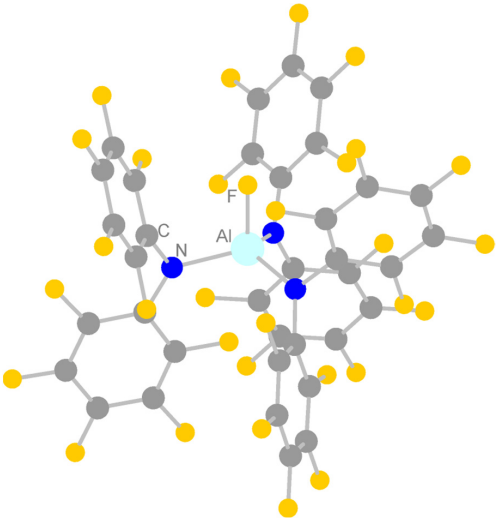

Figure S28. Representation of the BP86/def-SV(P) structure of $[Al\{N(C_6F_5)_2\}_3F]^-$.

F	-0.2077752	5.0627920	2.1555365
F	-0.1951305	7.3279805	0.6719352
C	0.5061456	5.0749856	1.0243455
C	0.5103756	6.2597356	0.2668382
C	1.2194087	3.9218863	0.6116143
C	1.2915579	6.3490118	-0.8969427
F	1.3094498	7.4832071	-1.6135845
C	2.0042070	4.0533911	-0.5625209
C	2.0430521	5.2380736	-1.3137115
F	2.7291920	3.0117917	-0.9902438
F	2.7873028	5.3144811	-2.4289001
F	2.9684365	0.6075918	0.4696129
F	5.1660542	-0.0644076	1.8991061
C	3.2491760	1.3142679	1.5656838
C	4.3994909	0.9652088	2.2943806
C	2.4160906	2.3844866	1.9725271
C	4.7838684	1.7198817	3.4137367
F	5.8922987	1.3974092	4.0987996
C	2.8368864	3.1289079	3.1005935
C	3.9985924	2.8110365	3.8180563
F	2.0950753	4.1640986	3.5213922
F	4.3576603	3.5324300	4.8932992
N	1.1967385	2.7017106	1.3213255
F	-2.5693465	0.3583429	-2.6923254
F	0.0428172	-3.6281856	-0.8843890
F	-1.3231975	-1.6769790	0.4342271
C	0.1479277	-2.3487871	-1.2779168
C	-0.5424097	-1.3352237	-0.5948658
F	-4.4304197	2.0406970	-3.6394696
F	1.5878459	-3.0015874	-3.0565712
C	0.9382996	-2.0313274	-2.3951952
C	-2.7715248	1.5136264	-2.0257104
C	-0.4400807	0.0163018	-0.9902548
N	-1.0563987	1.0496306	-0.2429840
C	1.0373415	-0.6971832	-2.8234955
C	-3.7565346	2.3816766	-2.5283788
C	0.3605480	0.3066126	-2.1157744
F	1.7857815	-0.3913013	-3.8954381
C	-2.0282803	1.8203576	-0.8515809
F	0.4700904	1.5778851	-2.5351188
C	-4.0618688	3.5913375	-1.8832268
F	-5.0104171	4.4097400	-2.3707203
C	-2.3765398	3.0504614	-0.2467582
C	-3.3615472	3.9222384	-0.7105890
F	-1.6889680	3.3731080	0.8822073
F	-3.6272616	5.0615863	-0.0574572
F	-3.4493203	-0.1073429	3.7449741
F	-5.0320696	4.3653191	3.4427317
F	-3.7693071	2.2920786	2.2341808
C	-3.8247203	3.9718361	3.8788498
C	-3.1591212	2.8993656	3.2607667
F	-3.3325763	-2.3409473	5.2921078
F	-3.8877136	5.6204374	5.5959035
C	-3.2468681	4.6103593	4.9883713
C	-2.2565443	-0.4992800	4.2198564
C	-1.8837286	2.4642203	3.6906869
N	-1.1849122	1.4000044	3.0771923
C	-1.9881931	4.1933778	5.4522266
C	-2.2095622	-1.6572819	5.0114151
C	-1.3289145	3.1352778	4.8085951
F	-1.4254451	4.8114925	6.5029582
C	-1.0964411	0.2453889	3.8954436
F	-0.1287188	2.7606988	5.2709915
C	-0.9763973	-2.1105186	5.5049915
F	-0.9190302	-3.2201816	6.2586639
C	0.1267751	-0.2225236	4.4348126
C	0.1951648	-1.3994862	5.1981606
F	1.2617040	0.4547853	4.2342023
F	1.3720785	-1.8259990	5.6839549
Al	-0.1813853	1.3938116	1.4585795
F	0.6505258	-0.0895985	1.6484193

$Al[OC(C_6F_5)_3]_3$

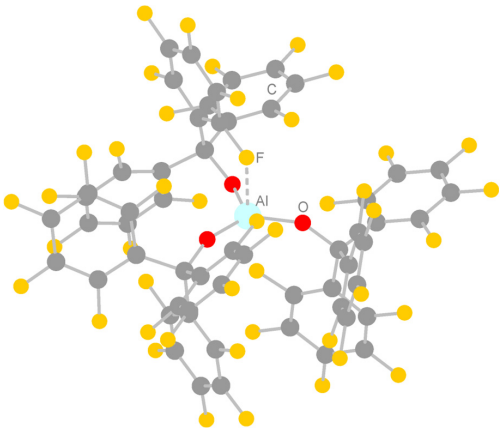

Figure S29. Representation of the BP86/def-SV(P) structure of $Al[OC(C_6F_5)_3]_3$.

C	-0.0116658	1.3478711	-3.1711144
C	-1.0458911	0.1741925	-3.0292969
C	-1.8504595	-0.1238281	-4.1524006
F	-1.7432161	0.5902719	-5.2873076
C	-2.8057230	-1.1525909	-4.1531628
F	-3.5261683	-1.3995789	-5.2514325
C	-3.0180891	-1.9047672	-2.9877140
F	-3.9220895	-2.8836968	-2.9714816
C	-2.2574491	-1.6200941	-1.8446660
F	-2.4472686	-2.3242265	-0.7253767
C	-1.3077048	-0.5817597	-1.8675512
F	-0.6499445	-0.3700478	-0.7167480
F	3.5117097	-0.9757417	-0.6457683
C	2.8523161	0.1651904	-0.8580115
C	1.8050076	0.2167875	-1.7859165
F	1.5204959	-0.9238667	-2.4405558
C	1.0528060	1.3854845	-2.0376274
C	1.4783472	2.5459225	-1.3618205
F	0.9005633	3.7429384	-1.5617054
C	2.5310128	2.5264766	-0.4251639
F	2.8867286	3.6509467	0.2017818
C	3.2318998	1.3370087	-0.1816614
F	4.2433574	1.3165202	0.6864375
F	-0.3458994	3.3303412	-5.4412181
C	-1.0598401	3.4757212	-4.3131067
C	-1.9675227	4.5545825	-4.3104969
F	-2.0668916	5.3394852	-5.3900279
C	-2.7587922	4.8172526	-3.1838325
F	-3.6127476	5.8400652	-3.1796908
C	-2.6352353	3.9882833	-2.0552882
F	-3.3681671	4.2259665	-0.9645362
C	-1.7277435	2.9206806	-2.0846224
F	-1.6262013	2.1721348	-0.9727957
C	-0.9157288	2.6230000	-3.2011433
O	0.6851588	1.1512212	-4.3511813
F	6.5292771	1.8369598	-9.0506197
F	4.9643635	1.6932155	-6.8865791
C	5.9418841	2.9480701	-8.5959814
C	5.1058151	2.8950573	-7.4697152
F	5.5148773	0.6692545	-2.3762845
F	7.4781000	2.4803409	-1.7425762
F	6.9920403	4.2532526	-10.2800631
C	5.5346229	1.8712117	-2.9577424
C	6.5393196	2.7942157	-2.6319824
C	6.1938613	4.1832408	-9.2147409
C	4.5492403	2.2259767	-3.8940748
C	6.5389169	4.0558816	-3.2531284
F	3.6026323	1.2458295	-4.1112247
O	2.6559198	2.7895794	-6.0035753
F	7.4792735	4.9496369	-2.9463401
C	4.5180263	3.4636481	-4.5515530
C	5.5424551	4.3651946	-4.1898508
C	4.4601520	4.0360525	-6.9412269
C	3.5264584	3.8229638	-5.6999376
F	5.5730656	5.5852605	-4.7445568
C	5.5964073	5.3425979	-8.6972171
F	1.8426091	5.0146536	-7.6260717
C	4.7647255	5.2633936	-7.5641207
C	2.6208697	5.0398381	-5.3692408
F	5.8358915	6.5268898	-9.2674909
C	1.7574410	5.5105764	-6.3839897
F	4.2697593	6.4274902	-7.1177516
F	3.1324162	5.1708336	-3.0178211
C	2.4214375	5.5823631	-4.0856969
C	0.8057531	6.5145909	-6.1634667
F	0.0319365	6.9432912	-7.1626944
C	1.4713097	6.5908766	-3.8349013
C	0.6474400	7.0474491	-4.8727712
F	1.3300391	7.0843753	-2.6010016
F	-0.2669130	7.9898235	-4.6412936
F	4.1587183	-3.8512380	-3.2404785
F	4.2815834	-2.2714877	-5.4084735
C	3.0332505	-3.5295145	-3.8833284
C	3.0750770	-2.7059202	-5.0169740
F	4.8330519	0.0981014	-10.7078604
F	5.8986158	-2.4141104	-11.0339003
F	1.7378225	-4.7687229	-2.3238254
C	4.4774906	-0.8947508	-9.8873149
C	5.0114418	-2.1813353	-10.0659919
C	1.7958766	-3.9996346	-3.4106535
C	3.5421420	-0.6674124	-8.8654655
C	4.5951668	-3.2197043	-9.2195679
F	3.0248100	0.5706637	-8.7951908

O	2.5441154	-0.1482990	-6.2454402
F	5.0855120	-4.4516781	-9.3848286
C	3.1202258	-1.6828957	-7.9768789
C	3.6497514	-2.9688199	-8.2074039
C	1.9183676	-2.3497929	-5.7481793
C	2.0768770	-1.2933100	-6.8772800
F	3.2869516	-4.0274502	-7.4676260
C	0.6262343	-3.6491732	-4.0970033
F	0.5959549	1.3325496	-7.1332312
C	0.6973528	-2.8244329	-5.2354899
C	0.7648409	-1.0410212	-7.6833146
F	-0.5650541	-4.0671143	-3.6494931
C	0.1435068	0.2096078	-7.8031335
F	-0.4861497	-2.5075281	-5.7985912
F	0.7031107	-3.3112712	-8.3846122
C	0.1834701	-2.0766965	-8.4463182
C	-0.9907592	0.4460329	-8.5958433
F	-1.5350938	1.6602149	-8.6551526
C	-0.9451429	-1.8870628	-9.2562664
C	-1.5342025	-0.6124360	-9.3394467
F	-1.4594682	-2.9043481	-9.9480163
F	-2.6050866	-0.4146978	-10.1052473
Al	1.9351103	1.3025761	-5.5217021

$[Al\{OC(C_6F_5)_3\}_3F]^-$

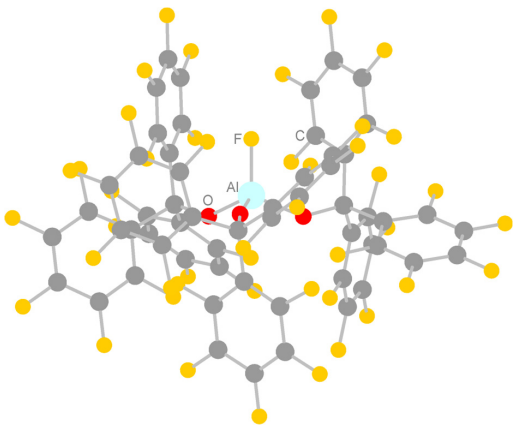

Figure S30. Representation of the BP86/def-SV(P) structure of $[Al\{OC(C_6F_5)_3\}_3F]^-$.

C	0.4168834	1.1364604	-2.4864938
C	-0.8386036	0.1842807	-2.3682325
C	-1.9313840	0.4542103	-3.2220034
F	-1.9224845	1.5191829	-4.0314276
C	-3.0878751	-0.3436070	-3.2458232
F	-4.1023136	-0.0456839	-4.0664245
C	-3.1909866	-1.4424359	-2.3790218
F	-4.2879244	-2.2095566	-2.3859356
C	-2.1387019	-1.7204650	-1.4960555
F	-2.2338209	-2.7563061	-0.6484525
C	-0.9937162	-0.9033026	-1.4873818
F	-0.0582223	-1.2253336	-0.5769918
F	3.8053235	-2.4002987	-2.0894467
C	3.3738790	-1.2075826	-1.6646393
C	2.1739739	-0.6676259	-2.1459076
F	1.4813939	-1.4127854	-3.0211542
C	1.6628309	0.5784863	-1.7191882
C	2.4331669	1.2631506	-0.7615388
F	2.0742807	2.4593473	-0.2652517
C	3.6387235	0.7399091	-0.2538242
F	4.3363915	1.4304050	0.6597199
C	4.1192662	-0.4919019	-0.7128748
F	5.2679236	-0.9894612	-0.2400754
F	0.4015900	3.8353292	-3.8399936
C	-0.1071393	3.7083019	-2.6089184
C	-0.6656020	4.8859235	-2.0704982
F	-0.6675546	6.0127659	-2.7923793
C	-1.2116746	4.8864948	-0.7805547
F	-1.7329211	6.0065687	-0.2651725
C	-1.2042857	3.6975989	-0.0333601
F	-1.7054277	3.6816387	1.2108701
C	-0.6493322	2.5403978	-0.5948854
F	-0.6303436	1.4386455	0.1783450
C	-0.0965816	2.4961877	-1.8915857
O	0.7674148	1.2220324	-3.7923394
F	7.6842861	1.2681096	-5.3240145
F	5.3037292	2.0637440	-4.4111784
C	6.9322279	2.0833668	-6.0754626
C	5.6711280	2.5016851	-5.6217253
F	3.9228598	4.8756257	-0.9025518
F	5.2448067	7.1992436	-1.5258683
F	8.6157248	2.1469121	-7.7545538
C	4.1206351	5.2078319	-2.1847733
C	4.7973323	6.3937882	-2.4975167
C	7.4154752	2.5383136	-7.3104633
C	3.6537311	4.3603898	-3.2120442
C	4.9984875	6.7309833	-3.8457131
F	3.0265034	3.2539250	-2.8013943
O	2.8446098	2.5557150	-5.3106271
F	5.6383543	7.8659019	-4.1652881
C	3.8385923	4.6696256	-4.5724758
C	4.5195083	5.8744201	-4.8456225
C	4.8329485	3.3532163	-6.3771867
C	3.4278548	3.7113343	-5.7485148
F	4.7160723	6.2585225	-6.1210815
C	6.6267456	3.4117023	-8.0701073
F	2.8110103	2.6221576	-8.2953084
C	5.3665310	3.8196344	-7.5943194
C	2.4543864	4.4046528	-6.7468808
F	7.0819573	3.8699850	-9.2459256
C	2.1567966	3.7475076	-7.9583762
F	4.7025914	4.6814334	-8.3841644
F	1.7813900	6.2171539	-5.3032234
C	1.6556812	5.5257133	-6.4510480
C	1.1950401	4.2080528	-8.8631852
F	0.9674478	3.5479689	-10.0072784
C	0.6797577	6.0106366	-7.3412522
C	0.4409978	5.3481748	-8.5507371
F	-0.0371424	7.0979308	-7.0216790
F	-0.4870343	5.8026723	-9.4009501
F	2.8858684	-4.4964551	-4.0460724
F	3.2284928	-2.1175126	-5.2286599
C	1.9856037	-4.0672622	-4.9392617
C	2.1361026	-2.8157585	-5.5604404
F	6.3600138	-0.4581329	-8.3517500
F	6.0941803	-2.2966462	-10.3685026
F	0.7436548	-6.0831163	-4.6973409
C	5.1616616	-1.0096503	-8.5990515
C	5.0338396	-1.9494465	-9.6287982
C	0.8991339	-4.8868470	-5.2785366
C	4.0463583	-0.6461539	-7.8147738
C	3.7756610	-2.5206168	-9.8785046
F	4.2893744	0.2478228	-6.8557032

O	1.8093351	-0.0304811	-6.1264876
F	3.6279689	-3.4186859	-10.8640113
C	2.7703657	-1.1978817	-8.0443466
C	2.6816191	-2.1380154	-9.0918100
C	1.2192679	-2.3236880	-6.5178021
C	1.5201392	-0.9005186	-7.1398413
F	1.4942095	-2.6987475	-9.3900661
C	-0.0156863	-4.4425541	-6.2414271
F	-1.0815077	-0.6796149	-6.0610193
C	0.1619613	-3.1909603	-6.8586299
C	0.3215796	-0.3311217	-7.9591859
F	-1.0527396	-5.2206238	-6.5868830
C	-0.9203047	-0.1915464	-7.3046489
F	-0.7482706	-2.8829596	-7.7982998
F	1.5375539	0.2372296	-9.9641414
C	0.4050220	0.2506647	-9.2380654
C	-2.0312211	0.4264257	-7.8875919
F	-3.1889885	0.5169482	-7.2217284
C	-0.6995673	0.8646587	-9.8575774
C	-1.9182384	0.9676936	-9.1771437
F	-0.5817895	1.3646271	-11.0951543
F	-2.9677987	1.5630328	-9.7572055
Al	1.3845074	1.5436317	-5.4046858
F	0.2088074	2.2984102	-6.3909330

$Al(OC_5NF_4)_3$

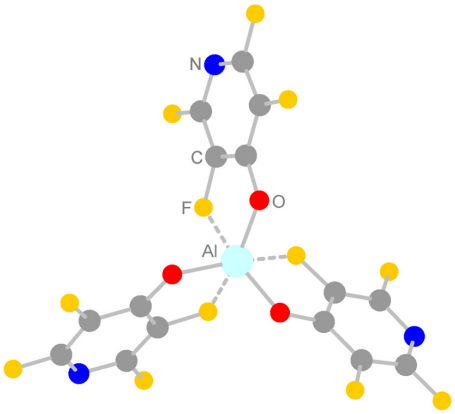

Figure S31. Representation of the BP86/def-SV(P) structure of $Al(OC_5NF_4)_3$.

Al	-0.0000000	-0.0000000	0.6712318
O	-1.5995034	-0.5245112	1.2664779
C	-2.2742252	-1.4658845	0.6214728
C	-3.5217939	-1.9892357	1.0342164
C	-4.1069367	-2.9825676	0.2260212
N	-3.5711724	-3.4518026	-0.8901935
C	-2.4062086	-2.9852894	-1.3008006
C	-1.7486380	-1.9992031	-0.5733516
F	-4.1101865	-1.5537225	2.1483305
F	-0.5187338	-1.4467841	-0.9360203
F	-1.8760628	-3.4762622	-2.4212236
F	-5.2812441	-3.4906175	0.6012680
O	1.2539917	-1.1229550	1.2664779
O	0.3455117	1.6474662	1.2664779
C	-0.1323806	2.7024791	0.6214728
C	2.4066058	-1.2365946	0.6214728
C	0.0381683	4.0445809	1.0342164
C	-0.5295109	5.0479953	0.2260212
N	-1.2037625	4.8186273	-0.8901935
C	-1.3822322	3.5764824	-1.3008006
C	-0.8570417	2.5139665	-0.5733516
C	2.6056797	-0.5147633	-0.5733516
C	3.7884407	-0.5911930	-1.3008006
N	4.7749349	-1.3668248	-0.8901935
C	4.6364476	-2.0654278	0.2260212
C	3.4836256	-2.0553451	1.0342164
F	-2.0725000	3.3628492	-2.4212236
F	-0.9935849	1.1726287	-0.9360203
F	-0.3823414	6.3190003	0.6012680
F	0.7095301	4.3363872	2.1483305
F	3.4006565	-2.7826647	2.1483305
F	5.6635854	-2.8283828	0.6012680
F	3.9485628	0.1134130	-2.4212236
F	1.5123186	0.2741554	-0.9360203

$[Al(OC_5NF_4)_3F]^-$

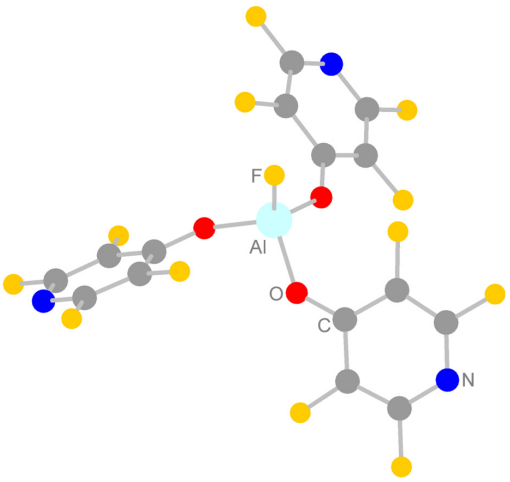

Figure S32. Representation of the BP86/def-SV(P) structure of $[Al(OC_5NF_4)_3F]^-$.

Al	0.0000000	-0.0000000	0.8316552
O	-1.6196791	-0.2338529	0.0970163
C	-2.5014946	-1.1957734	0.0010314
C	-2.4120967	-2.4297915	0.7053752
C	-3.4124653	-3.3939977	0.5434103
N	-4.4682492	-3.2346136	-0.2376634
C	-4.5780345	-2.0957202	-0.9028346
C	-3.6490047	-1.0515814	-0.8316294
F	-1.3599219	-2.6406318	1.5181423
F	-3.8201469	0.0809179	-1.5320303
F	-5.6595236	-1.9481314	-1.6925551
F	-3.3133019	-4.5549691	1.2164779
O	1.0123621	-1.2857568	0.0970163
O	0.6073170	1.5196097	0.0970163
C	0.2151771	2.7642445	0.0010314
C	2.2863175	-1.5684711	0.0010314
C	-0.8982129	3.3038328	0.7053752
C	-1.2330556	4.6522804	0.5434103
N	-0.5671330	5.4869241	-0.2376634
C	0.4740703	5.0125543	-0.9028346
C	0.9138062	3.6859215	-0.8316294
C	2.7351986	-2.6343401	-0.8316294
C	4.1039642	-2.9168341	-0.9028346
N	5.0353822	-2.2523105	-0.2376634
C	4.6455208	-1.2582828	0.5434103
C	3.3103095	-0.8740412	0.7053752
F	1.1426305	5.8753569	-1.6925551
F	1.9801504	3.2678853	-1.5320303
F	-2.2880680	5.1468881	1.2164779
F	-1.6068933	2.4980428	1.5181423
F	2.9668152	0.1425890	1.5181423
F	5.6013699	-0.5919190	1.2164779
F	4.5168931	-3.9272254	-1.6925551
F	1.8399965	-3.3488032	-1.5320303
F	-0.0000000	0.0000000	2.5140458

$[Al(OTeF_5)_5]^{2-}$

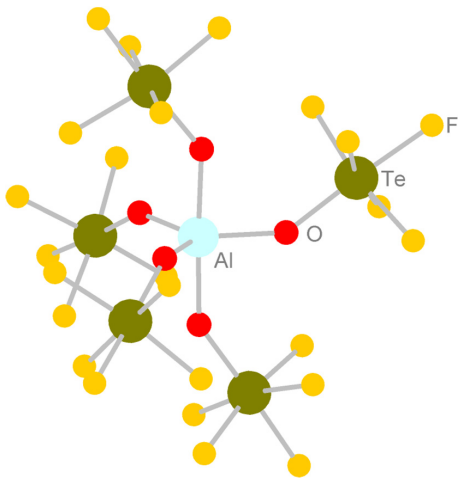

Figure S33. Representation of the B3LYP/def2-TZVPP structure of $[Al(OTeF_5)_5]^{2-}$.

Te	0,5105596	0,2097674	-3,3693125
F	1,2722123	0,1639034	-5,092757
F	-0,9931172	-0,5560967	-4,1795802
F	-0,1260249	1,8980965	-3,8723827
F	2,1191782	1,0047198	-2,8414941
F	1,241698	-1,4977223	-3,1710539
O	-0,2878594	0,2900614	-1,7383464
Al	-0,1104581	0,0674588	0,0589846
O	0,6394392	1,3773747	1,086325
O	-1,7835826	0,9160055	0,2942385
O	-0,8438189	-1,4430569	0,7686635
O	1,585526	-0,7342847	-0,1087974
Te	0,3479381	2,9878033	1,8867397
Te	-3,5377085	0,6952875	-0,1157388
Te	-0,6499978	-3,2007241	1,1888592
Te	3,325461	-0,6933008	0,4095081
F	0,1395619	4,6534154	2,7459717
F	-1,1593332	2,4743515	2,8673436
F	1,8455417	3,773261	1,0847302
F	-0,7199806	3,7260255	0,5406722
F	1,4135136	2,5418539	3,3602724
F	-5,3795054	0,5361168	-0,5017682
F	-4,0508218	2,1959202	0,8853267
F	-3,9346403	-0,3878849	1,3634016
F	-3,3468687	-0,8295662	-1,1890583
F	-3,4890515	1,77453	-1,6492817
F	-1,7064729	-3,0431515	2,7270734
F	-2,1751485	-3,7118501	0,2335631
F	0,3989313	-3,6664886	-0,2856186
F	0,8725196	-2,9797592	2,2529284
F	-0,5253239	-5,0223449	1,6580791
F	5,1438807	-0,706699	0,9173058
F	3,4245367	-2,5482325	0,6511041
F	3,9812262	-0,9370106	-1,3285091
F	2,989578	-0,4806564	2,2409634
F	3,5684119	1,1528771	0,2216447

Me_3SiF

Si	-0.0430541	0.0000935	-0.0022416
C	-0.0396398	-1.6781919	-0.7318168
C	-0.0379295	1.4709838	-1.0909968
C	-0.0530159	0.2074585	1.8159551
H	0.8456071	-1.7981384	-1.3664674
H	-0.9040342	-1.7913157	-1.3954153
H	-0.054228	-2.4690992	0.0161714
H	-0.0180927	1.2184628	-2.1497985
H	0.8254775	2.1017039	-0.852471
H	-0.9240382	2.0811934	-0.8825614
H	0.8170949	-0.3000938	2.2470126
H	-0.9327501	-0.2928952	2.2359021
H	-0.0508851	1.2508097	2.1268189

$[Me_3Si]^+$

Si	2.1627348	1.5902503	-0.000005
F	3.7834859	1.5901311	0.0000253
C	1.6118297	0.8009966	-1.6014181
C	1.6118028	3.3716991	0.1171485
C	1.6117956	0.5981561	1.4842719
H	1.9804593	1.3594345	-2.4640235
H	0.5218225	0.7683298	-1.6675619
H	1.9806113	-0.223221	-1.6840603
H	1.980439	3.9553023	-0.7286194
H	1.980509	3.8395207	1.0320262
H	0.5218018	3.4453311	0.1220027
H	1.9805096	-0.4280842	1.432049
H	0.5217891	0.5571943	1.5455958
H	1.9804996	1.0388194	2.4125588

A.2. The Tris(pentafluorophenyl)methylium Cation: Isolation and Reactivity

Angewandte Chemie
Eine Zeitschrift der Gesellschaft Deutscher Chemiker

Supporting Information

The Tris(pentafluorophenyl)methylium Cation: Isolation and Reactivity

*K. F. Hoffmann, D. Battke, P. Golz, S. M. Rupf, M. Malischewski, S. Riedel**

WILEY-VCH

SUPPORTING INFORMATION

Table of Contents

Experimental Procedures 2
NMR Spectra 4
Variable-Temperature NMR Spectra 10
EPR Spectra 13
Crystal data 14
Summary of crystal data and refinement results 14
$C(C_6F_5)_3H$ 15
$[C(C_6F_5)_3][Al(OTeF_5)_4]$ 17
Quantum-chemical calculations 20
CPh_3 radical 20
$[CPh_3]^+$ cation 21
CPh^F_3 radical 22
$[CPh^F_3]^+$ cation 23
$HCPh^F_3$ 25
References 26
Author Contributions ..... **Fehler! Textmarke nicht definiert.**

Experimental Procedures

All preparative work was carried out using standard Schlenk techniques. Glassware was greased with Triboflon III. The pentafluoroorthotelluric acid $HOTeF_5$[1] and $[Al(OTeF_5)_3]_2$[2] were prepared as described elsewhere. All solid materials were handled inside a glove box with an atmosphere of dry argon (O_2 < 0.5 ppm, H_2O < 0.5 ppm). All solvents were freshly dried with CaH_2 before use and stored on molecular sieve. NMR spectra were recorded on a JEOL 400 MHz ECS or ECZ spectrometer. Chemical shifts and couplings constants of strongly coupled spin systems are given as simulated by *gNMR*.[3] Crystal data was collected with Mo*K*α radiation on a Bruker D8 Venture diffractometer with a CMOS area detector. Single crystals were picked at −40 °C under nitrogen atmosphere and mounted on a 0.15 mm Micromount using perfluoroether oil. The structure was solved with the ShelXT[4] structure solution program using intrinsic phasing and refined with the ShelXL[5] refinement package using least squares on weighted F2 values for all reflections using OLEX2.[6] CCDC 2154970 and CCDC 2153771 contain the supplementary crystallographic data for this paper. These data are provided free of charge by The Cambridge Crystallographic Data Centre. Cyclic voltammetry was performed on an Interface 1010 B Potentiostat/Galvanostat/ZRA from Gamry Instruments. The investigations were carried out starting from 0 V going to the reduction first and then to the oxidation. The measurements were performed at a scan rate of 100 mV/s in anhydrous solvents under argon atmosphere without extra supporting and platinum wires as working-, counter-, and quasi-reference electrodes. The voltammograms were internally referenced against $Fc^{0/+}$. The compound was freshly prepared in the cyclic voltammetry cell with a concentration of 0.078 M in *ortho*-difluorobenzene. The Turbomole program[7] was used to perform calculations at the unrestricted Kohn-Sham DFT level, using the B3LYP hybrid functional[8] (with RI[9]) in conjunction with the valence triple-ζ basis set with two sets of polarization functions (def2-TZVPP)[10]. Minima on potential energy surfaces were characterized by normal mode analysis. Thermochemical data is provided without counterpoise correction but including zero-point energy correction as obtained from harmonic vibrational frequencies.

$C(C_6F_5)_3OH$

In a Schlenk flask fine magnesium powder (2.43 g, 100 mmol, 3 eq.) was suspended in diethylether (150 ml) and cooled to 0 °C. Bromopentafluorobenzene (24.7, 100 mmol, 3 eq.) was added dropwise and the mixture was allowed to warm to room temperature. After 4 hours, methyl chloroformate (3.15 g, 33 mmol, 1 eq.) was added in small portions and the reaction mixture was consecutively stirred for 36 hours at room temperature, finally followed by 4 hours stirring under reflux conditions. Afterwards, the mixture was treated with diluted HCl solution (10 %, 20 ml) and then extracted with diethyl ether (3x 30 ml). The collected organic phases were washed with dist. water (3x 30 ml) and Brine solution (3x 30 ml). After drying with $MgSO_4$, all volatiles were removed under reduced pressure. The resulting crude oil was then refined via fractionated sublimation. The first fraction (50 °C, $1*10^{-3}$ mbar) belongs to the sideproduct decafluorobenzophenone. The desired product was collected at 100 °C and $1*10^{-3}$ mbar as yellow crystals (6.73 g, 35 %). ^{1}H NMR (400 MHz, $CDCl_3$, 22 °C): δ = 4.29 (s, 1H, -O*H*) ppm; ^{19}F NMR (377 MHz, $CDCl_3$, 22 °C): δ = –140.0 (m, 6 *ortho*-F), –151.0 (m, 3 *para*-F), –160.2 (m, 6 *meta*-F) ppm.

SUPPORTING INFORMATION

These data are in agreement with literature values of $C(C_6F_5)_3OH$.[11]

$C(C_6F_5)_3Cl$

This synthesis is a modified version of an already reported procedure.[11]

Tris(pentafluorophenyl)methanol $C(C_6F_5)_3OH$ (3.53 g, 7 mmol) was dissolved in thionyl chloride (25.00 g) resulting in a yellow solution. Pyridine (0.49 g, 7 mmol, 1 eq.) and dimethylformamide (0.52 g, 7 mmol, 1 eq.) were added and the mixture was brought to reflux at 80 °C for 48 hours under constant stirring. Afterwards, the mixture was cooled to room temperature and decanted on ice water. It was treated with small portions of saturated $NaHCO_3$ solution until the formation of gas stopped. The aqueous phase was extracted with dichloromethane (3x 30 ml). The collected organic phases were subsequently washed with saturated $NaHCO_3$ and Brine solution (each 3x 30 ml), dried with $MgSO_4$ and finally all volatiles were removed under reduced pressure. After recrystallization in *n*-pentane at –16 °C the product was obtained as yellow powder (0.95 g, 22 %).^{19}F NMR (377 MHz, $CDCl_3$, 22 °C): δ = –135.5 (m, 6 *ortho*-F), –150.0 (m, 3 *para*-F), –160.3 (m, 6 *meta*-F) ppm.

These data are in agreement with literature values of $C(C_6F_5)_3Cl$.[11]

$[C(C_6F_5)_3][Al(OTeF_5)_4]$

Triethylaluminum (41.7 mg, 0.37 mmol, 1 eq.) was dissolved in 4 ml of *ortho*-difluorobenzene and degassed. Afterwards, pentafluoroorthotelluric acid $HOTeF_5$ (350 mg, 1.46 mmol, 4 eq.) was condensed onto the frozen solution at –196 °C. Warming the mixture to –30 °C under constant stirring led to a clear yellow solution and gas evolution. After 10 minutes the gas evolution ceased and tris(pentafluorophenyl)methyl chloride (200 mg, 0.37 mmol, 1 eq.) was added via a funnel. The solution turned intense purple and a further gas evolution could be observed. Stock solutions can be prepared and directly used. NMR spectra were recorded at –40 °C.^{19}F NMR (282 MHz, $C_6H_4F_2$, ext. [D_6]acetone, –40 °C): δ = –40.1 (m, 1F_A, $^2J(^{19}F_A,^{19}F_B)$=186 Hz, $^1J(^{19}F_A,^{125}Te)$=3158 Hz), –47.2 (m, 4F_B, $^1J(^{19}F_B,^{125}Te)$=3471 Hz), –112.6 (m, 3 *para*-F), –127.7 (m, 6 *ortho*-F), –154.3 (m, 6 *meta*-F) ppm. ^{27}Al NMR (78 MHz, $C_6H_4F_2$, ext. [D_6]acetone, –40 °C): δ = 47 (s, $[Al(OTeF_5)_4]^-$) ppm.

$[C(C_6F_5)_3][Al(OTeF_5)_3Cl]$

In a J. Young NMR tube $[Al(OTeF_5)_3]_2$ (38 mg, 0.0025 mmol, 0.5 eq) was weighed in and SO_2ClF was condensed on top at −196 °C. Warming to −30 °C led to a clear, colorless solution. Afterwards, tris(pentafluoro-phenyl)methyl chloride (28 mg, 0.05 mmol) was added. Shaking of the mixture led to an intense purple-colored solution, which was analyzed by low-temperature NMR spectroscopy. ^{19}F NMR (377 MHz, SO_2ClF, ext. [D_6]acetone, –60 °C): δ = –38.9 (m, 1F_A, $^2J(^{19}F_A,^{19}F_B)$=176 Hz), –40.0 (m, 1$F_{A'}$, $^2J(^{19}F_{A'},^{19}F_{B'})$=182 Hz), –46.1 (m, 4$F_B$, $^1J(^{19}F_B,^{125}Te)$=3467 Hz), –46.5 (m, 4$F_{B'}$, $^1J(^{19}F_{B'},^{125}Te)$=3463 Hz) –112.6 (m, 3 *para*-F), –127.7 (m, 6 *ortho*-F), –154.3 (m, 6 *meta*-F) ppm; ^{27}Al NMR (78 MHz, SO_2ClF, ext. [D_6]acetone, –60 °C): δ = 80 (s, $[Al(OTeF_5)_2Cl_2]^-$), 63 (s, $[Al(OTeF_5)_3Cl]^-$), 48 (s, $[Al(OTeF_5)_4]^-$) ppm; ^{13}C NMR (101 MHz, SO_2ClF, ext. [D_6]acetone, –60 °C): 175.3 (central C), 155.6 (*para*-C), 149.0 *(ortho*-C), 140.2 (*meta*-C), 115.6 (*ipso*-C) ppm.

Reaction of $[C(C_6F_5)_3][Al(OTeF_5)_4]$ with isobutane

The reaction was performed in a J. Young NMR tube. To a cooled solution of $[Al(OTeF_5)_3]_2$ (44 mg, 0.03 mmol, 0.5 eq.) in SO_2ClF at −60 °C, tris(pentafluorophenyl)methyl chloride (33 mg, 0.06 mmol, 1 eq.) was added under an argon stream, forming a deep purple solution. Finally, isobutane (7 mg, 0.12 mmol, 4 eq.) was condensed on the mixture at −196 °C. The reaction mixture was then brought to –60 °C and further warming was monitored and analyzed with low-temperature NMR spectroscopy

Reaction of $[C(C_6F_5)_3][Al(OTeF_5)_4]$ with ferrocene

A stock-solution of $[C(C_6F_5)_3][Al(OTeF_5)_4]$ in *ortho*-difluorobenzene (0.05 mmol/ml) at –30 °C was treated with solid ferrocene (9 mg, 0.05 mmol). Upon contact the solution immediately changed its color to blue and further reacted to a green solution, indicating the successful formation of the ferrocenium cation. The mixture was analyzed by EPR spectroscopy

Reaction of $[C(C_6F_5)_3][Al(OTeF_5)_4]$ with tris-(4-bromophenyl)amine

A stock-solution of $[C(C_6F_5)_3][Al(OTeF_5)_4]$ in *ortho*-difluorobenzene (0.052 mmol/ml) at –30 °C was treated with solid tris-(4-bromophenyl)amine (13 mg, 0.052 mmoll). Upon contact the solution immediately changed its color to a dark blue, indicating the formation of the radical cationic ammoniumyl. The mixture was analyzed by EPR spectroscopy.

SUPPORTING INFORMATION

NMR Spectra

$C(C_6F_5)_3OH$

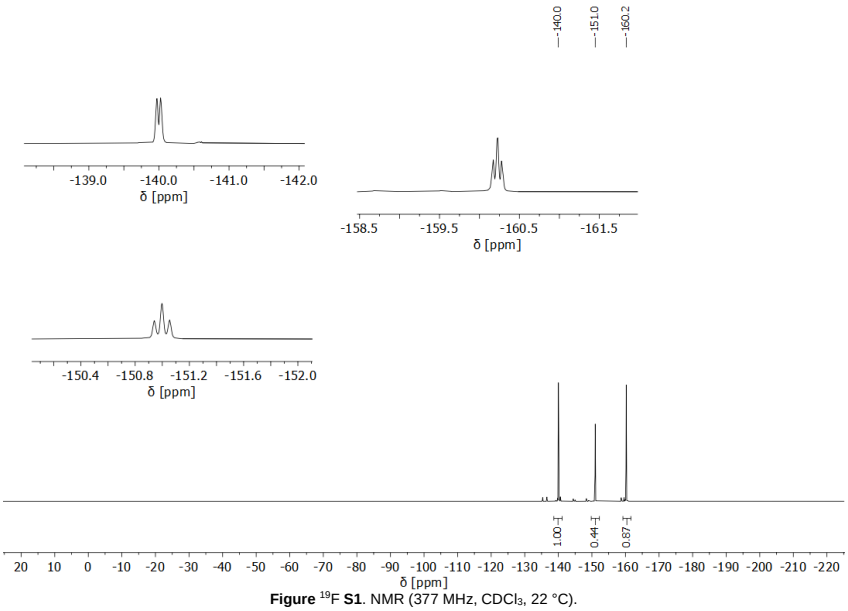

Figure ^{19}F **S1**. NMR (377 MHz, $CDCl_3$, 22 °C).

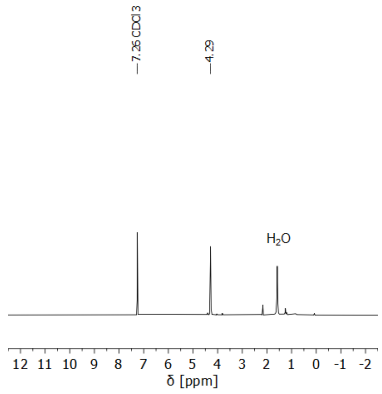

Figure S2. ^{1}H NMR (400 MHz, $CDCl_3$, 22 °C).

$C(C_6F_5)_3Cl$

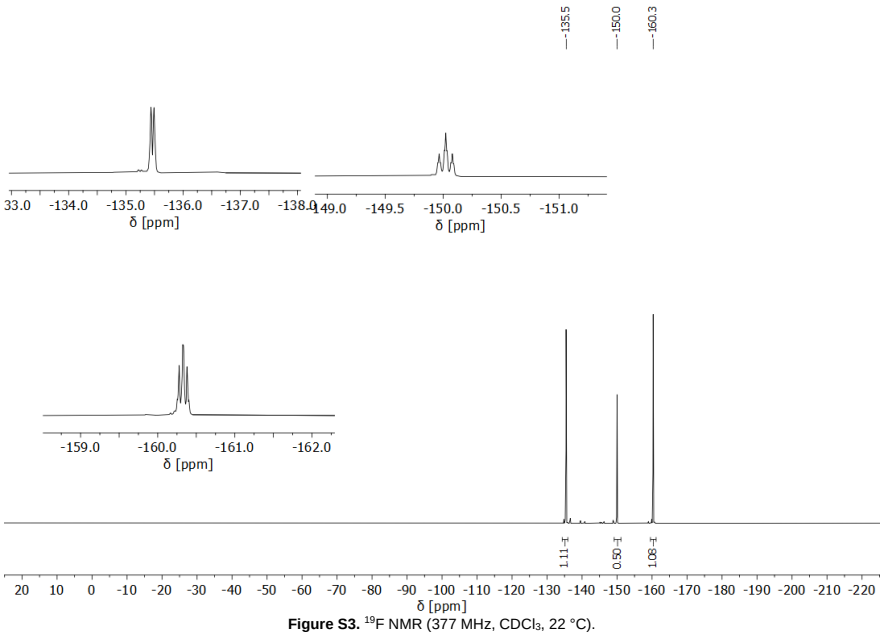

Figure S3. ^{19}F NMR (377 MHz, $CDCl_3$, 22 °C).

$[C(C_6F_5)_3][Al(OTeF_5)_4]$

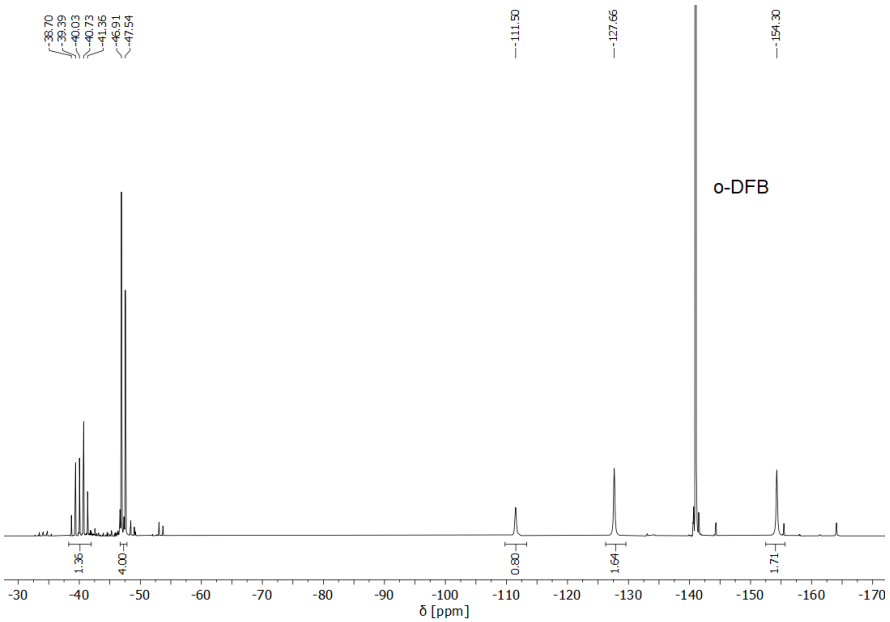

Figure S4. ^{19}F NMR (377 MHz, $C_6H_4F_2$, ext. $[D_6]$acetone, –40 °C).

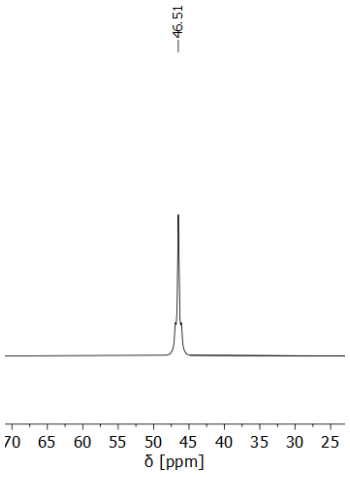

Figure S5. ^{27}Al NMR (78 MHz, $C_6H_4F_2$, ext. $[D_6]$acetone, –40 °C).

SUPPORTING INFORMATION

[C(C$_6$F$_5$)$_3$][Al(OTeF$_5$)$_3$Cl]

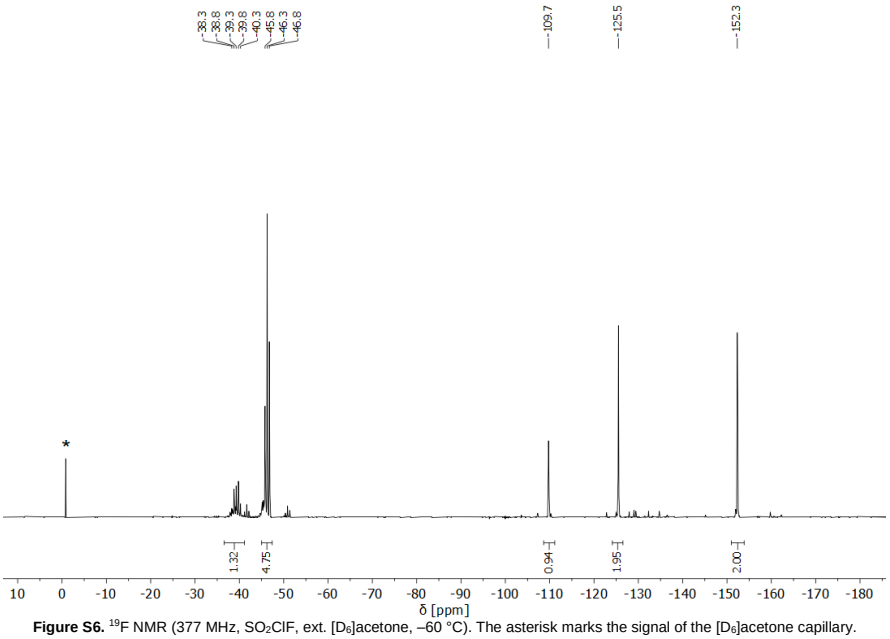

Figure S6. ^{19}F NMR (377 MHz, SO_2ClF, ext. [D$_6$]acetone, –60 °C). The asterisk marks the signal of the [D$_6$]acetone capillary.

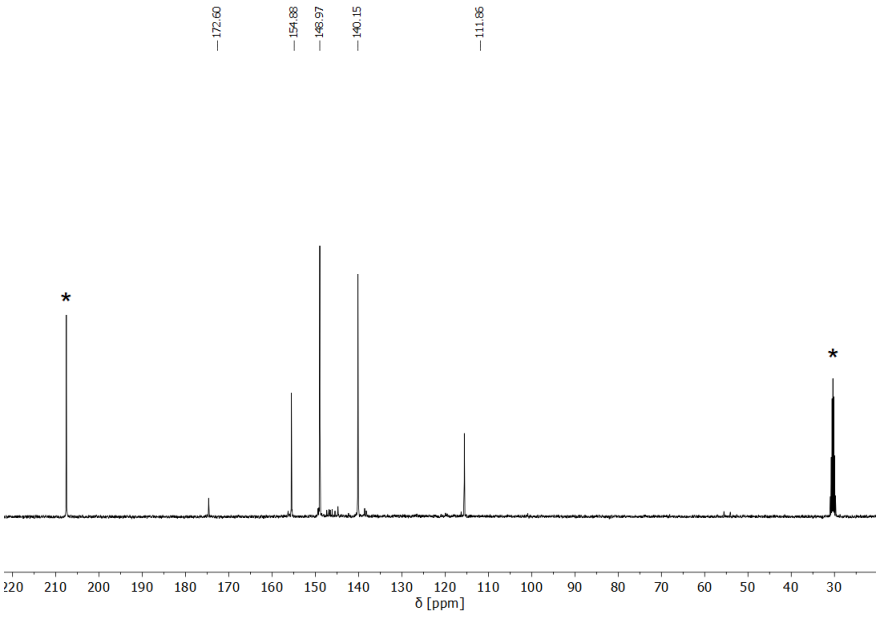

Figure S7. ^{13}C NMR (101 MHz, SO_2ClF, ext. [D$_6$]acetone, –60 °C). Asterisks mark the signals of the [D$_6$]acetone capillary.

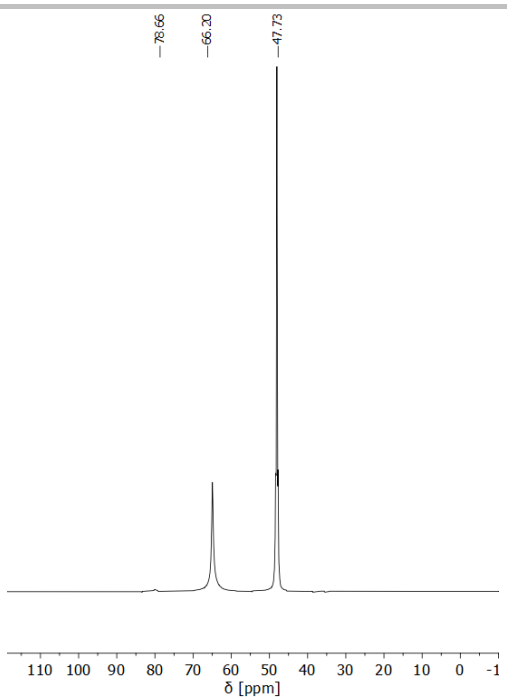

Figure S8. ^{27}Al NMR (78 MHz, SO_2ClF, ext. [D_6]acetone, –60 °C).

SUPPORTING INFORMATION

Decomposition of $[C(C_6F_5)_3][Al(OTeF_5)_4]$ in *o*-DFB at room temperature

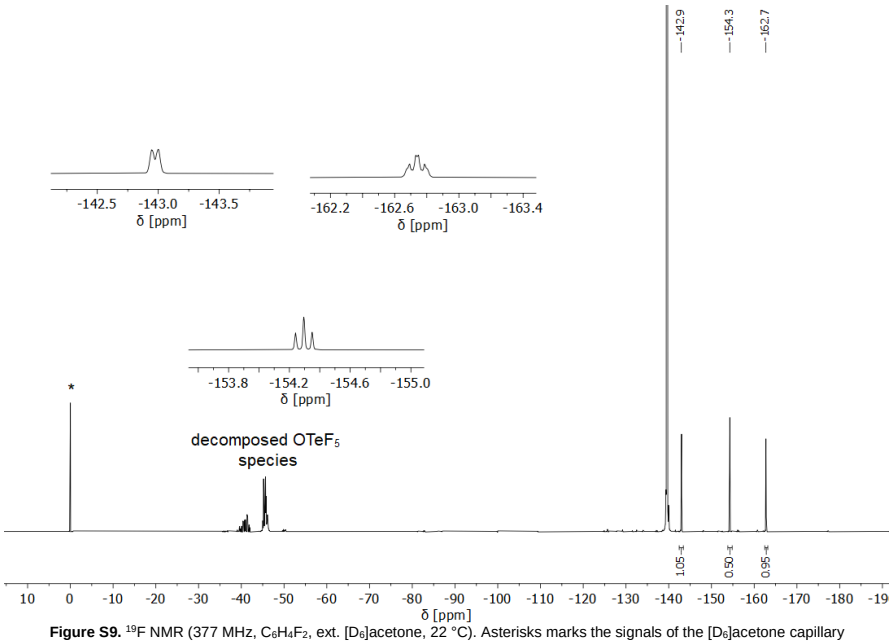

Figure S9. ^{19}F NMR (377 MHz, $C_6H_4F_2$, ext. $[D_6]$acetone, 22 °C). Asterisks marks the signals of the $[D_6]$acetone capillary

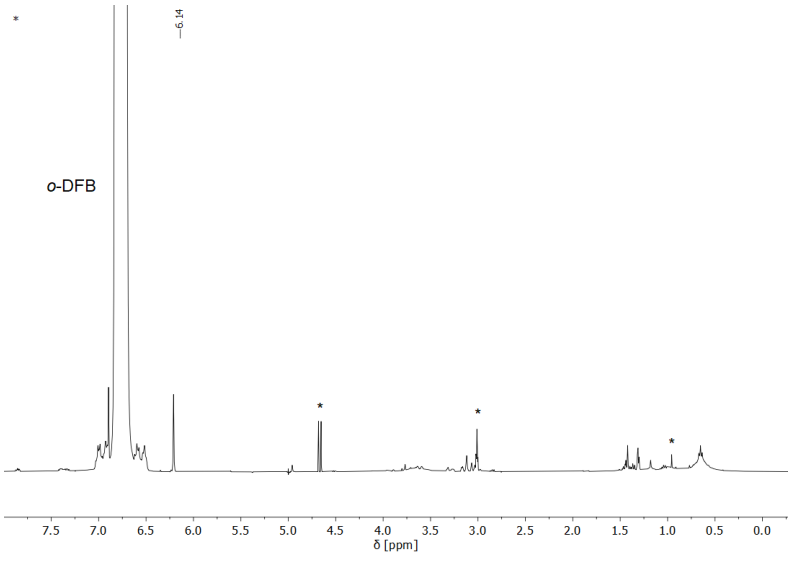

Figure S10. ^{19}F NMR (377 MHz, $C_6H_4F_2$, ext. $[D_6]$acetone, 22 °C). Asterisks mark the signals of the $[D_6]$acetone capillary.

Variable-Temperature NMR Spectra

After the sample has been warmed for several hours to 0 °C, the sample was measured again at –60 °C. The ^{19}F NMR spectrum reveals the complete conversion of cation $[C(C_6F_5)_3]^+$ to perfluorotrityl methane. Furthermore, the formation of $HOTeF_5$ was observed in the ^{19}F and ^1H NMR spectra, probably occurring due to partial decomposition of $[Al(OTeF_5)_{4-x}Cl_x]^-$ via the protonation of the Brønsted acidic *tert*-butyl cation. Similar decomposition reactions have been reported by Krossing et al. when they treated $AlBr_3$ with *tert*-butylbromide.[12] The broadened signals of the isobutane in the ^1H and ^{13}C NMR spectra are resolved again, suggesting that the dynamic exchange ceased. Additionally, several signals with low intensity in the range of 1 to 3 ppm in the ^1H NMR and 0 to 50 ppm in the ^{13}C NMR are observed, which correspond to isobutene oligomerization products. Still, no clearly assignable signals of the *tert*-butyl cation are found, which most likely reacted with the excess isobutane of the reaction mixture. Additional experiments were performed in which a slight excess of $HOTeF_5$ is added to the reaction of the Lewis acid $Al(OTeF_5)_3(SO_2ClF)$ and $C(C_6F_5)_3Cl$ in SO_2ClF in order to form HCl and therefore remove the chloride source before the isobutane is added. Furthermore, an equimolar amount of isobutane was used. These attempts also resulted in the rapid oligomerization of the formed *tert*-butyl cation at 0 °C and finally yielded the polymerization of the sample at room temperature.

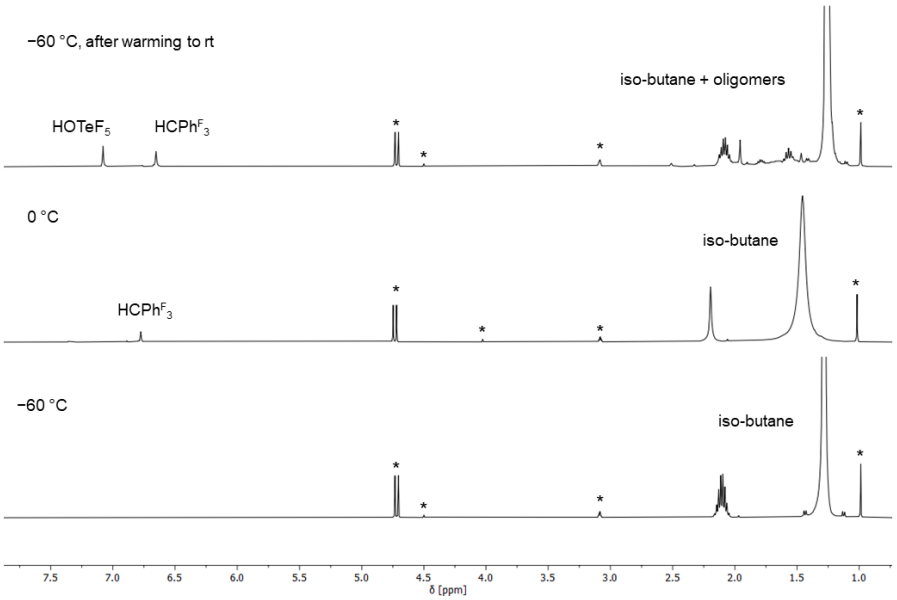

Figure S11. VT ^1H NMR (400 MHz, SO_2ClF, ext. $[D_6]$acetone) spectra of the reaction of $[CPh^F_3][Al(OTeF_5)_3Cl]$ with isobutane. Asterisk marks the signal of the external deuterated solvent capillary.

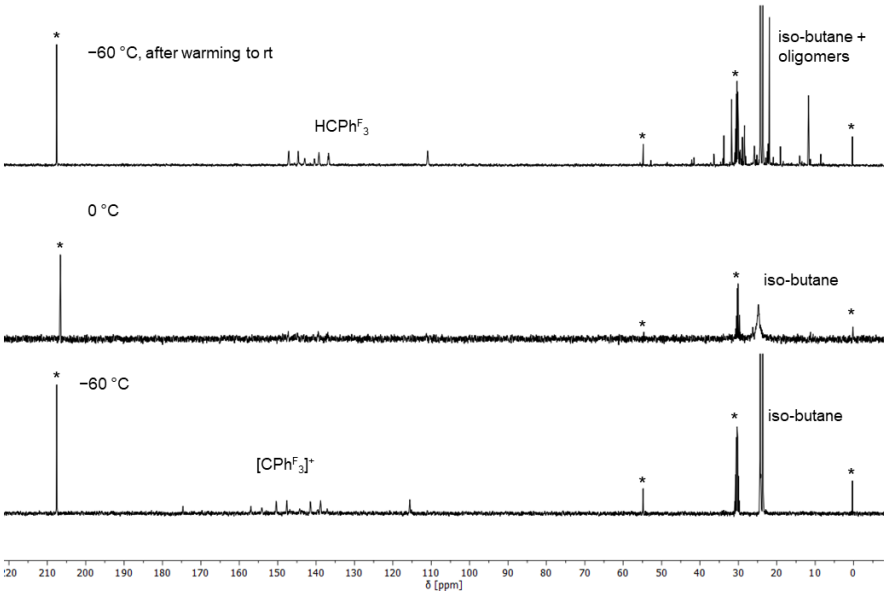

Figure S12. VT ^{13}C NMR (101 MHz, SO_2ClF, ext. [D$_6$]acetone) spectra of the reaction of [CPh$^{F}_{3}$][Al(OTeF$_5$)$_3$Cl] with isobutane. Asterisk marks the signal of the external deuterated solvent capillary.

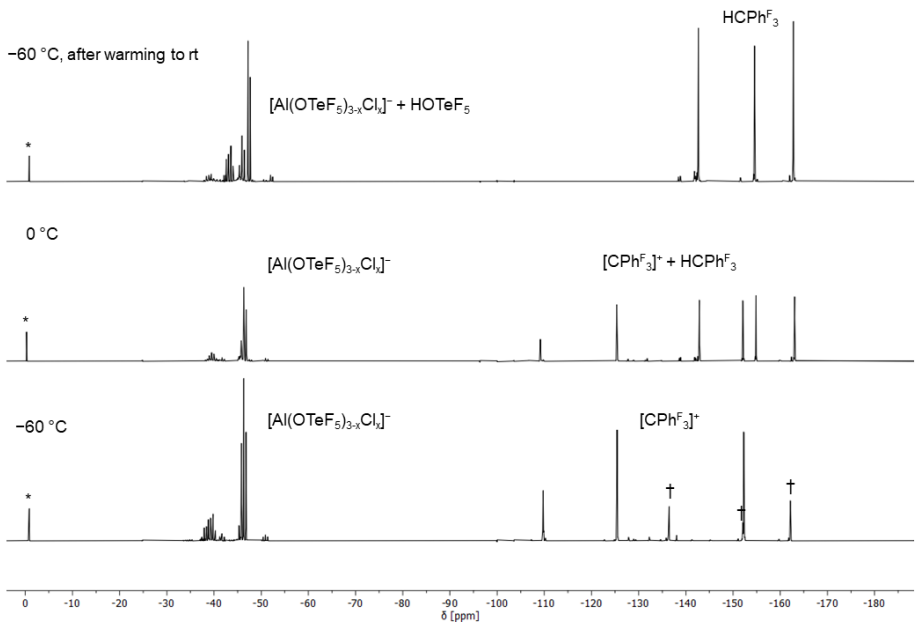

Figure S13. VT ^{19}F NMR (282 MHz, SO_2ClF, ext. [D$_6$]acetone) spectra of the reaction of [CPh$^{F}_{3}$][Al(OTeF$_5$)$_3$Cl] with isobutane. Asterisk denotes the signal of the external deuterated solvent capillary. Daggers denotes residual CPh$^{F}_{3}$Cl.

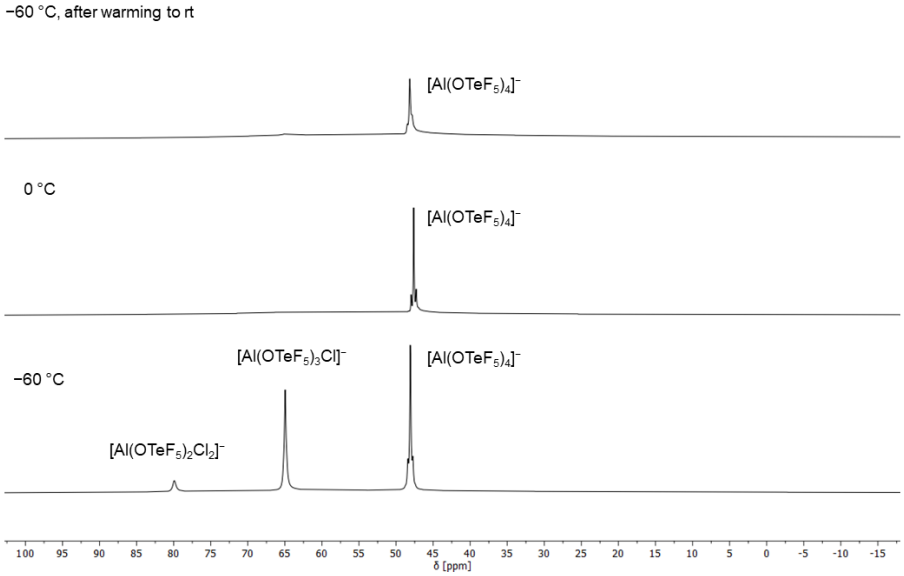

Figure S14. VT ^{27}Al NMR (78 MHz, SO_2ClF, ext. [D_6]acetone) spectra of the reaction of [CPh^F_3][$Al(OTeF_5)_3Cl$] with isobutane. Asterisk marks the signal of the external deuterated solvent capillary.

SUPPORTING INFORMATION

EPR Spectra

$$[Ph^F{}_3C][Al(OTeF_5)_4] + FeCp_2 \xrightarrow[-30\ °C \rightarrow r.t.]{\text{SET}\ o\text{-DFB}} Ph^F{}_3C^{\bullet} + [FeCp_2][Al(OTeF_5)_4]$$

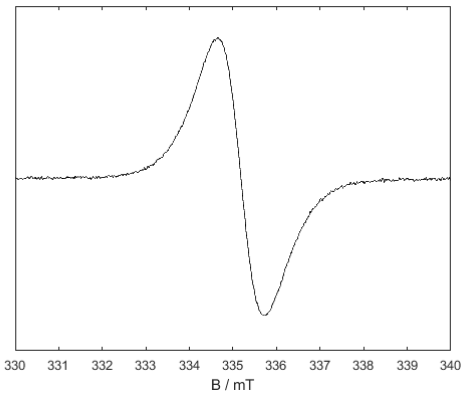

Figure S15. Experimental EPR spectrum showing the signal of the perfluorinated trityl radical $CPh^F{}_3$ at room temperature. The spectrum was recorded using the solution obtained after the reaction of $[CPh^F{}_3][Al(OTeF_5)_4]$ and ferrocene. The experimental *g* value is 2.0031.

$$[Ph^F{}_3C][Al(OTeF_5)_4] + N(C_6H_4Br\text{-}4)_3 \xrightarrow[-30\ °C \rightarrow r.t.]{\text{SET}\ o\text{-DFB}} Ph^F{}_3C^{\bullet} + [N(C_6H_4Br\text{-}4)_3][Al(OTeF_5)_4]$$

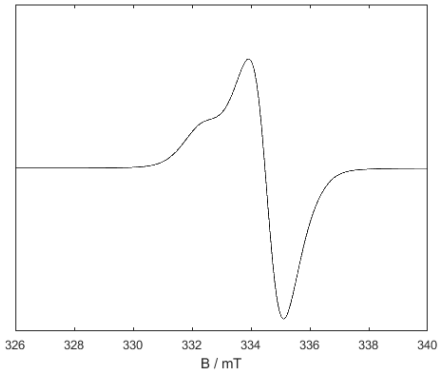

Figure S16. Experimental EPR spectrum showing two broad overlapped signals of the perfluorinated trityl radical $CPh^F{}_3$ and the ammoniumyl radical cation $[N(C_6H_4Br\text{-}4)_3][Al(OTeF_5)_4]$ at room temperature. The spectrum was recorded using the solution obtained after the reaction of $[CPh^F{}_3][Al(OTeF_5)_4]$ and the amine $N(C_6H_4Br\text{-}4)_3$.

WILEY-VCH

SUPPORTING INFORMATION

Crystal data

Summary of crystal data and refinement results

	$C(C_6F_5)_3H$	$[C(C_6F_5)_3][Al(OTeF_5)_4]$
CCDC number	2154970	2153771
empirical formula	$C_{19}HF_{15}$	$AlC_{19}F_{35}O_4Te_4$
formula weight	514.20	1494.57
temperature [K]	100	100
crystal system	trigonal	monoclinic
space group	$R\bar{3}$	$C2/c$
a [pm]	3785.7(4)	1383.99(18)
b [pm]	3785.7(4)	2029.23(18)
c [pm]	610.10(7)	1400.13(15)
α [°]	90	90
β [°]	90	115.648(5)
γ [°]	120	90
volume [Å^3]	7572.2(17)	3544.7(7)
Z	18	4
ρ_{calcd} [g · cm^{-3}]	2.030	2.801
μ [mm^{-1}]	0.236	3.500
dimension [mm]	0.949 × 0.058 × 0.052	0.459 × 0.164 × 0.03
color	colorless	colorless
reflection collected	20405	105750
independent reflections	3096 [R_{int} = 0.0692]	3642 [R_{int} = 0.0467]
data/retrains/parameters	3096/0/307	3642/612/363
goodness-of-fit on F^2	0.993	1.147
final R indexes [$I > 2\sigma(I)$]	R_1 = 0.0463 wR_2 = 0.1069	R_1 = 0.0349 wR_2 = 0.0763
final R indexes [all data]	R_1 = 0.0734 wR_2 = 0.1216	R_1 = 0.0388 wR_2 = 0.0786

SUPPORTING INFORMATION

$C(C_6F_5)_3H$

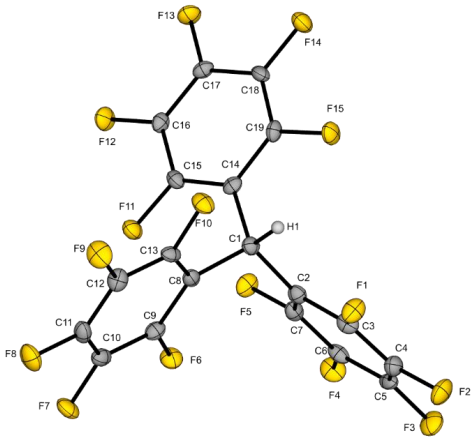

Figure S17. Molecular structure of $C(C_6F_5)_3H$.

Table S1. Bond Lengths for $C(C_6F_5)_3H$.

Atom	Atom	Length/Å	Atom	Atom	Length/Å
F1	C3	1.346(3)	C2	C3	1.382(4)
F2	C4	1.335(3)	C2	C7	1.387(4)
F3	C5	1.336(3)	C3	C4	1.381(4)
F4	C6	1.347(3)	C4	C5	1.377(4)
F5	C7	1.344(3)	C5	C6	1.380(4)
F6	C9	1.343(3)	C6	C7	1.375(4)
F7	C10	1.343(3)	C8	C9	1.388(4)
F8	C11	1.342(3)	C8	C13	1.385(4)
F9	C12	1.338(3)	C9	C10	1.386(4)
F10	C13	1.342(3)	C10	C11	1.370(4)
F11	C15	1.342(3)	C11	C12	1.379(4)
F12	C16	1.345(3)	C12	C13	1.382(4)
F13	C17	1.341(3)	C14	C15	1.383(4)
F14	C18	1.337(3)	C14	C19	1.384(4)
F15	C19	1.350(3)	C15	C16	1.381(4)
C1	C2	1.535(4)	C16	C17	1.374(4)
C1	C8	1.527(4)	C17	C18	1.377(4)
C1	C14	1.536(4)	C18	C19	1.372(4)

Table S2. Bond Angles for $C(C_6F_5)_3H$.

Atom	Atom	Atom	Angle/°	Atom	Atom	Atom	Angle/°
C2	C1	C14	113.5(2)	C11	C10	C9	119.9(3)
C8	C1	C2	114.6(2)	F8	C11	C10	120.3(3)
C8	C1	C14	113.4(2)	F8	C11	C12	120.1(3)
C3	C2	C1	118.7(3)	C10	C11	C12	119.6(3)
C3	C2	C7	116.0(3)	F9	C12	C11	120.0(3)
C7	C2	C1	125.4(3)	F9	C12	C13	120.6(3)
F1	C3	C2	119.8(3)	C11	C12	C13	119.4(3)
F1	C3	C4	117.0(3)	F10	C13	C8	119.9(3)
C4	C3	C2	123.2(3)	F10	C13	C12	117.0(3)

F2	C4	C3	120.7(3)	C12	C13	C8	123.1(3)
F2	C4	C5	120.1(3)	C15	C14	C1	125.3(3)
C5	C4	C3	119.2(3)	C15	C14	C19	115.7(3)
F3	C5	C4	120.6(3)	C19	C14	C1	119.0(3)
F3	C5	C6	120.2(3)	F11	C15	C14	120.7(3)
C4	C5	C6	119.3(3)	F11	C15	C16	117.0(3)
F4	C6	C5	119.8(3)	C16	C15	C14	122.3(3)
F4	C6	C7	120.0(3)	F12	C16	C15	120.4(3)
C7	C6	C5	120.2(3)	F12	C16	C17	119.8(3)
F5	C7	C2	120.4(3)	C17	C16	C15	119.8(3)
F5	C7	C6	117.4(3)	F13	C17	C16	119.7(3)
C6	C7	C2	122.2(3)	F13	C17	C18	120.5(3)
C9	C8	C1	125.5(3)	C16	C17	C18	119.8(3)
C13	C8	C1	118.9(3)	F14	C18	C17	119.9(3)
C13	C8	C9	115.6(3)	F14	C18	C19	121.1(3)
F6	C9	C8	120.4(3)	C19	C18	C17	119.0(3)
F6	C9	C10	117.1(3)	F15	C19	C14	119.4(3)
C10	C9	C8	122.5(3)	F15	C19	C18	117.1(3)
F7	C10	C9	120.0(3)	C18	C19	C14	123.4(3)
F7	C10	C11	120.1(3)				

Table S3. Hydrogen Atom Coordinates (Å×10^4) and Isotropic Displacement Parameters (Å^2×10^3) for $C(C_6F_5)_3H$.

Atom	x	y	z	U(eq)
H1	6442.03	5169.25	7875.25	18

$[C(C_6F_5)_3][Al(OTeF_5)_4]$

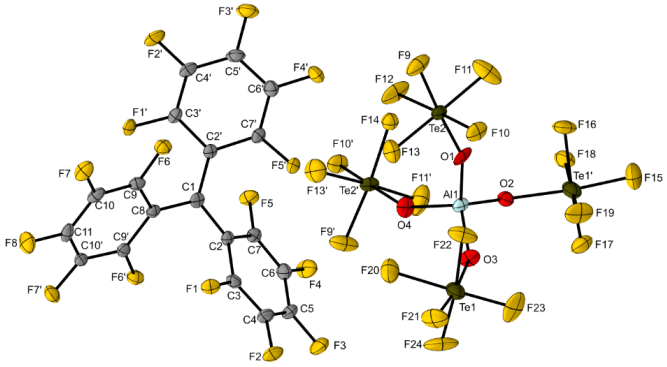

Figure S18. Molecular structure of $[C(C_6F_5)_3][Al(OTeF_5)_4]$.

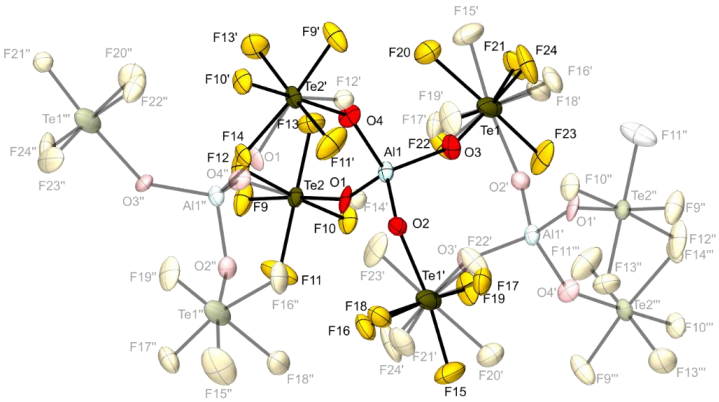

Figure S19. Molecular structure of the disordered anion in $[C(C_6F_5)_3][Al(OTeF_5)_4]$.

Table S4. Bond Lengths for $[C(C_6F_5)_3][Al(OTeF_5)_4]$.

Atom	Atom	Length/Å	Atom	Atom	Length/Å
Te2	F10	1.835(3)	F7	C10	1.333(6)
Te2	F9	1.839(3)	F5	C7	1.325(6)
Te2	F13	1.820(4)	F2	C4	1.334(6)
Te2	O1	1.78(3)	F4	C6	1.323(6)
Te2	F11	1.820(4)	F8	C11	1.319(9)
Te2	$O4^1$	1.88(2)	F3	C5	1.319(6)
Te2	F12	1.774(19)	Al1	O1	1.68(3)
Te2	F14	1.85(3)	Al1	O4	1.718(17)
Te1	F22	1.814(17)	Al1	O3	1.713(10)
Te1	$O3^2$	1.985(9)	Al1	O2	1.731(10)

Te1	F16	1.870(8)	C8	C9[3]	1.416(6)
Te1	O2	1.864(9)	C8	C9	1.416(6)
Te1	F18	2.008(9)	C8	C1	1.449(10)
Te1	F20	1.938(8)	C9	C10	1.371(7)
Te1	F15	1.789(9)	C2	C1	1.432(6)
Te1	F23	1.703(9)	C2	C3	1.430(7)
Te1	F19	1.604(9)	C2	C7	1.413(7)
Te1	F21	1.719(8)	C10	C11	1.390(7)
Te1	F24	1.825(9)	C4	C5	1.381(8)
Te1	F17	1.825(18)	C4	C3	1.371(7)
F6	C9	1.332(6)	C6	C5	1.386(8)
F1	C3	1.318(6)	C6	C7	1.378(7)

[1]1-X,+Y,3/2-Z; [2]1/2-X,3/2-Y,1-Z; [3]-X,+Y,1/2-Z

Table S5. Bond Angles for $[C(C_6F_5)_3][Al(OTeF_5)_4]$.

Atom	Atom	Atom	Angle/°	Atom	Atom	Atom	Angle/°
F10	Te2	F9	85.37(15)	F21	Te1	F22	90.7(7)
F10	Te2	O4[1]	175.6(7)	F21	Te1	O3[2]	172.1(5)
F10	Te2	F14	85.1(7)	F21	Te1	F20	87.0(5)
F9	Te2	O4[1]	93.8(9)	F21	Te1	F24	90.9(4)
F9	Te2	F14	170.5(7)	F24	Te1	O3[2]	87.3(5)
F13	Te2	F10	88.52(17)	F24	Te1	F20	86.7(5)
F13	Te2	F9	88.85(19)	F17	Te1	O3[2]	96.0(8)
F13	Te2	F11	174.99(19)	F17	Te1	F16	167.0(8)
F13	Te2	O4[1]	95.8(6)	F17	Te1	O2	90.4(5)
F13	Te2	F14	91.1(13)	F17	Te1	F18	83.7(8)
O1	Te2	F10	94.4(9)	O1	Al1	O4	107.9(18)
O1	Te2	F9	176.7(17)	O1	Al1	O3	114.9(11)
O1	Te2	F13	94.4(17)	O1	Al1	O2	107.2(18)
O1	Te2	F11	89.4(17)	O4	Al1	O2	110.8(8)
F11	Te2	F10	87.96(18)	O3	Al1	O4	108.0(11)
F11	Te2	F9	87.3(2)	O3	Al1	O2	108.0(5)
F11	Te2	O4[1]	87.7(6)	Al1	O1	Te2	156(3)
F11	Te2	F14	92.1(13)	C9	C8	C9[3]	115.9(6)
F12	Te2	F10	170.5(6)	C9	C8	C1	122.1(3)
F12	Te2	F9	87.3(8)	C9[3]	C8	C1	122.1(3)
F12	Te2	F13	85.2(6)	F6	C9	C8	120.1(5)
F12	Te2	F11	97.8(7)	F6	C9	C10	117.7(5)
F12	Te2	O4[1]	12.3(10)	C10	C9	C8	122.1(5)
F12	Te2	F14	102.2(11)	C3	C2	C1	121.7(5)
F14	Te2	O4[1]	95.7(11)	C7	C2	C1	122.3(5)
F22	Te1	O3[2]	90.2(7)	C7	C2	C3	116.0(4)
F22	Te1	F20	86.2(6)	F7	C10	C9	120.6(5)
F22	Te1	F24	172.6(7)	F7	C10	C11	119.4(5)
O3[2]	Te1	F18	162.8(4)	C9	C10	C11	120.0(5)
F16	Te1	O3[2]	97.0(4)	C2[3]	C1	C8	119.8(3)
F16	Te1	F18	83.8(4)	C2	C1	C8	119.8(3)
O2	Te1	O3[2]	77.8(4)	C2	C1	C2[3]	120.5(6)
O2	Te1	F16	92.0(4)	F8	C11	C10	120.1(3)
O2	Te1	F18	84.9(4)	F8	C11	C10[3]	120.1(3)
F20	Te1	O3[2]	85.3(4)	C10	C11	C10[3]	119.7(7)
F15	Te1	O3[2]	114.7(5)	F2	C4	C5	119.9(5)
F15	Te1	F16	87.6(4)	F2	C4	C3	119.7(5)
F15	Te1	O2	167.4(5)	C3	C4	C5	120.4(5)
F15	Te1	F18	82.6(5)	F4	C6	C5	119.5(5)
F15	Te1	F17	87.2(5)	F4	C6	C7	121.0(5)
F23	Te1	F22	93.7(6)	C7	C6	C5	119.6(5)

F23	Te1	O3[2]	92.3(4)	F3	C5	C4	119.8(5)
F23	Te1	F20	177.6(4)	F3	C5	C6	119.8(5)
F23	Te1	F21	95.5(5)	C4	C5	C6	120.4(5)
F23	Te1	F24	93.4(6)	F1	C3	C2	119.8(4)
F19	Te1	F22	96.3(8)	F1	C3	C4	118.8(5)
F19	Te1	O3[2]	19.0(5)	C4	C3	C2	121.3(5)
F19	Te1	F20	67.9(5)	F5	C7	C2	120.3(4)
F19	Te1	F23	109.8(5)	F5	C7	C6	117.5(5)
F19	Te1	F21	153.2(5)	C6	C7	C2	122.2(5)
F19	Te1	F24	79.1(5)	Al1	O2	Te1	133.9(6)

[1]1-X,+Y,3/2-Z; [2]1/2-X,3/2-Y,1-Z; [3]-X,+Y,1/2-Z

Table S6. Atomic Occupancy for $[C(C_6F_5)_3][Al(OTeF_5)_4]$.

Atom	Occupancy	Atom	Occupancy	Atom	Occupancy
Al1	0.5	O1	0.5	O4	0.5
F22	0.5	O3	0.5	F16	0.5
O2	0.5	F18	0.5	F20	0.5
F15	0.5	F23	0.5	F19	0.5
F21	0.5	F24	0.5	F17	0.5
F12	0.5	F14	0.5		

SUPPORTING INFORMATION

Quantum-chemical calculations

Structure optimizations were performed DFT level using the B3LYP functional together with def2-TZVPP basis set as implemented in the Turbomole V7.3 program.

CPh_3 radical

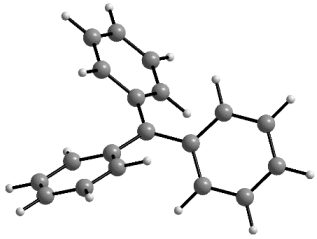

Figure S20. Representation of the B3LYP/def2-TZVPP structure of the CPh_3 radical.

```
$coord
   -3.13196863839529     -0.02141756615702      1.71721899799721  c
   -4.95758580017693     -2.02464255822518      2.23663245826561  c
   -7.58005563073335     -1.60577260294866      2.01265258089143  c
   -8.24785073380689      0.22825474950869      1.40953456077638  h
   -9.31053342158524     -3.51161881920265      2.49520960704563  c
  -11.30997974031826     -3.13724087759807      2.27732750314509  h
   -8.49234458559724     -5.89968458029861      3.23856910898188  c
   -9.84576075519705     -7.38364367144206      3.62202133278227  h
   -5.91234860498653     -6.35609994453278      3.48292257133340  c
   -5.25134162867099     -8.19774482484253      4.07987157020826  h
   -4.17528334390754     -4.46065945430963      2.98305653779683  c
   -2.18084585620237     -4.84008554594961      3.21039918270288  h
    1.97979776656735     -4.65570604630747     -3.69722113727487  h
    1.86123266209212     -3.16120310151079     -2.30523145472153  c
   -0.45151812048952     -2.59187384561587     -1.21567487947800  c
   -2.11269786619500     -3.63863338557835     -1.78008446243604  h
   -0.69532589410538     -0.63369240214670      0.57557353599355  c
    1.51525355351575      0.70993196989295      1.21604325954300  c
    1.40585375765980      2.20059738375591      2.60877193458144  h
    3.82849266366415      0.12148116789596      0.13782134391145  c
    5.49549985376024      1.16978344438648      0.69214102075028  h
    4.01991607613048     -1.81404894212709     -1.63457060291808  c
    5.82539359798795     -2.26645930664567     -2.48091030050482  h
   -1.82133105506026      4.21401008418346     -0.86641276628079  h
   -2.90719258346174      4.61838839824585      0.81622732221251  c
   -3.49616069281751      7.10201912483922      1.40406675552794  c
   -2.85049964962966      8.60864766516790      0.18000905229480  h
   -4.92218729753315      7.66398295894094      3.54304922565541  c
   -5.37341581683585      9.60411962662592      4.00466205182288  h
   -5.76149074098822      5.70066950506029      5.08121766269939  c
   -6.85340299153553      6.11285031919587      6.76133307797971  h
   -5.19442134343275      3.21340534922376      4.48752188300241  c
   -5.83770509116921      1.71463856703204      5.71776770897705  h
   -3.74371161607381      2.59771147620367      2.33876698657065  c
$end
```

E_{tot}= −732.8281357854 H

SUPPORTING INFORMATION

$[CPh_3]^+$ cation

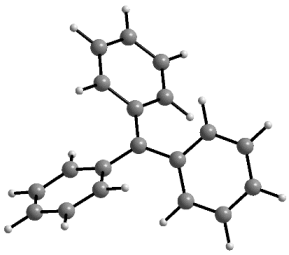

Figure S21. Representation of the B3LYP/def2-TZVPP structure of the $[CPh_3]^+$ cation.

```
$coord
   -3.13034876138922    -0.01950510799536     1.71921643722896  c
   -4.93667097029271    -2.00217547292532     2.23427640107620  c
   -7.56142615766595    -1.54944506711499     2.01312763734952  c
   -8.21826237519897     0.27715563159430     1.38132241869735  h
   -9.28100992260958    -3.46130662601394     2.46939856155231  c
  -11.27994157298732     -3.11054280103302     2.23328211175193  h
   -8.43716478978566    -5.84185041511979     3.22013344183803  c
   -9.79023975749378    -7.32656850586361     3.60031668544937  h
   -5.85949591666082    -6.32011104379028     3.48377102706351  c
   -5.21673419586087    -8.15844246734918     4.10135232144907  h
   -4.12208401869730    -4.43992550273455     2.96729501192002  c
   -2.12925208365253    -4.80054210010024     3.22399918212504  h
    1.92765959179923    -4.64949337237787    -3.68665614167781  h
    1.79735236620714    -3.16546307729286    -2.28847083796031  c
   -0.50477824529713    -2.61531297825473    -1.18520928618285  c
   -2.17471002389962    -3.64123059359770    -1.75623776751548  h
   -0.72080910939945    -0.62681974034324     0.58790023611610  c
    1.47681428310243     0.75473591184393     1.22512023176900  c
    1.36609777017015     2.22788590635518     2.63390908436641  h
    3.78225074223647     0.14795412497247     0.15904186664863  c
    5.45963162459463     1.17832116976508     0.70580979958482  h
    3.94521270004884    -1.79872447958049    -1.60918503955378  c
    5.74865460182843    -2.25161662109356    -2.45892035451986  h
   -1.79184670887454     4.16916313501642    -0.88389243869892  h
   -2.85914241392603     4.58147718142127     0.80673811408130  c
   -3.46926681287654     7.05360027306703     1.38715499401252  c
   -2.84015182199898     8.57005673736874     0.17107854881186  h
   -4.90474587143507     7.58845829454833     3.53110560978148  c
   -5.35577086895620     9.52792740028145     3.99442593152401  h
   -5.76277854666247     5.63805622716645     5.08130308691422  c
   -6.84537593373683     6.06526602754480     6.76044768365275  h
   -5.21913799275807     3.15551756953903     4.47997803218178  c
   -5.84186622162223     1.65245820931114     5.71289630674012  h
   -3.73618215377697     2.57130648750529     2.33445433225770  c
$end
```

E_{tot}= −732.6127398496 H

SUPPORTING INFORMATION

CPh^F_3 radical

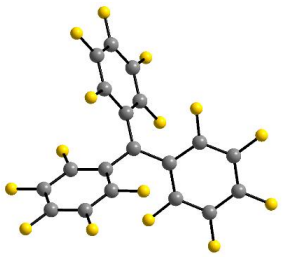

Figure 22. Representation of the B3LYP/def2-TZVPP structure of the CPh^F_3 radical.

$coord

0.00102095831423	-0.00589087565973	0.00801778726910	c
-1.82152910352303	-2.00315931051489	0.52915276113432	c
-4.43323105393526	-1.67697743004412	0.15706131329673	c
-5.31850549875523	0.50218192407784	-0.77007250157835	f
-6.17810287468856	-3.56283025959276	0.63717200121991	c
-8.62878580200458	-3.16711531176416	0.21575467539219	f
-5.36753163106176	-5.89476886542917	1.52911723906414	c
-7.02895482441862	-7.71831447986014	1.99088592776722	f
-2.80578995638073	-6.30272472566063	1.93179279976384	c
-2.01525359585412	-8.52118038427255	2.82184047457524	f
-1.09170826741715	-4.39216659209148	1.43746138651539	c
1.34096786557728	-4.86998780281962	1.93380340273554	f
5.11338473085629	-4.61814072727159	-6.08996900924995	f
4.98429096674587	-2.96340067833226	-4.19634556549664	c
2.68226141947498	-2.37693480373256	-3.10387667783727	c
0.62791561438334	-3.50556932012894	-4.05296779517895	f
2.43839720887598	-0.61749352355453	-1.12979196677633	c
4.69917423469118	0.51753472758734	-0.32120866889103	c
4.67250507230553	2.15924744734229	1.60218728524416	f
7.02142446834353	-0.04699214089245	-1.38208137458523	c
9.11831689998071	1.04879006848443	-0.52000482766640	f
7.17165126120826	-1.79471394485263	-3.33492310989912	c
9.39103715683998	-2.34469567169809	-4.37072032839057	f
1.12063294546648	4.16350061591777	-3.22901776693544	f
0.00368782745405	4.62472560410400	-1.00768626785207	c
-0.58009162635164	7.11325441834269	-0.45708087298921	c
-0.00190468529490	8.94866705430707	-2.08153229558881	f
-1.81008875951849	7.69728580483153	1.78691195431761	c
-2.37705057227108	10.08017695996412	2.33389844398078	f
-2.44325268381658	5.77127430161393	3.45474743394851	c
-3.59416579889494	6.32311275995127	5.62526990152057	f
-1.84697705325195	3.29541895740893	2.86476601460146	c
-2.43771390546845	1.52338037113236	4.56959801605902	f
-0.60603093761067	2.61450583310680	0.61784021050972	c

$end

E_{tot}= −2221.462296850 H

SUPPORTING INFORMATION

$[CPh^F_3]^+$ cation

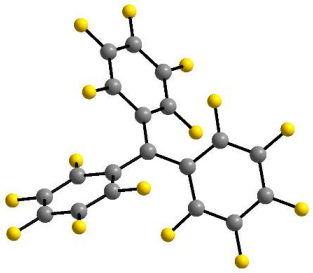

Figure S23. Representation of the B3LYP/def2-TZVPP structure of the $[CPh^F_3]^+$ cation.

```
$coord
   -3.12847519778563    -0.03427606137065     1.72822146445654  c
   -4.93970743187294    -2.00629125346953     2.24176378330425  c
   -7.57167506998977    -1.63373020801220     1.89791216029448  c
   -8.43311735217169     0.54493905178775     1.00250632940774  f
   -9.31262289323390    -3.52285039764603     2.33214446182964  c
  -11.74229083640152     -3.13778722756079     1.91425185350927  f
   -8.48889728953204    -5.86887697891823     3.21654009059876  c
  -10.13442534025011     -7.66061877466915     3.66030297845973  f
   -5.91947402989705    -6.31256399319108     3.62790083103769  c
   -5.16620700503527    -8.52319616055764     4.50571671300607  f
   -4.19512200180034    -4.42885981279714     3.11171431447322  c
   -1.77922089307287    -4.91241597336640     3.58083012896927  f
    1.98668030845786    -4.79764930398260    -4.19919776577930  f
    1.82389897630195    -3.07487925705258    -2.40167098406411  c
   -0.46237958531801    -2.53657382455660    -1.27258836654440  c
   -2.47986441698428    -3.77538471489228    -2.10188177407108  f
   -0.71930991579581    -0.64041815020000     0.60525100344119  c
    1.52978858760846     0.64239357502560     1.30113032051966  c
    1.48682920641729     2.36991152179240     3.11993133194211  f
    3.84080214759853     0.07745818737314     0.23885093761327  c
    5.90840592234744     1.26364083598089     0.97611253926368  f
    3.98916447665892    -1.77394782350118    -1.63631641566980  c
    6.16923684157296    -2.29337699265672    -2.68141490042123  f
   -1.82839198058644     4.14333222829216    -1.41859522728765  f
   -3.00786570801213     4.59123590385105     0.75020519429517  c
   -3.60165136180392     7.06665543564855     1.30627131551841  c
   -2.96416723176018     8.91305743657836    -0.24660955709049  f
   -4.89774339521536     7.61984890794082     3.53780073314571  c
   -5.43621440399136     9.96804261456755     4.09599795765257  f
   -5.62412508625126     5.68206545665473     5.17574327924069  c
   -6.81549428911881     6.23353655532936     7.29767368322188  f
   -5.08209391360525     3.20976241926809     4.55584553040179  c
   -5.75685065859233     1.43203069927408     6.19281422377032  f
   -3.73291984915130     2.55605039375651     2.33512506139000  c
$end
```

E_{tot}= −2221.192766570 H

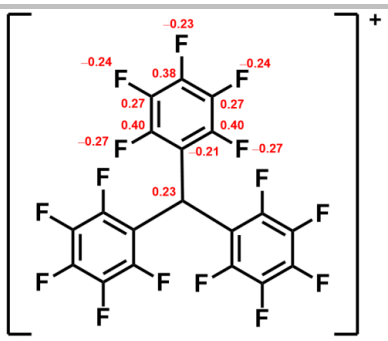

Figure S24. Visualization of the NPA charges

atomic populations from total density:

atom	charge	n(s)	n(p)	n(d)	n(f)	n(g)
1 c	0.22815	2.90596	2.85875	0.00548	0.00166	0
2 c	-0.207	2.92786	3.2709	0.00557	0.00267	0
3 c	0.39863	2.86748	2.72383	0.00829	0.00177	0
4 f	0.26632	3.82418	0.43424	0.00777	0.00013	0
5 c	0.26857	2.8775	2.84235	0.00967	0.00191	0
6 f	0.24373	3.82387	0.41166	0.00806	0.00014	0
7 c	0.37481	2.89338	2.72071	0.0094	0.00169	0
8 f	0.22447	3.82019	0.3953	0.00884	0.00015	0
9 c	0.26906	2.87763	2.84175	0.00966	0.00191	0
10 f	-0.24368	3.82381	5.41167	0.00807	0.00014	0
11 c	0.39892	2.86712	2.72388	0.0083	0.00177	0
12 f	-0.26632	3.82416	5.43426	0.00777	0.00013	0
13 f	-0.24371	3.82381	5.41169	0.00807	0.00014	0
14 c	0.26878	2.8777	2.84193	0.00968	0.00191	0
15 c	0.39917	2.86763	2.72315	0.00828	0.00177	0
16 f	-0.26642	3.82426	5.43427	0.00776	0.00013	0
17 c	-0.20669	2.92816	3.27029	0.00558	0.00267	0
18 c	0.3985	2.86756	2.72386	0.00831	0.00177	0
19 f	-0.26662	3.82429	5.43444	0.00776	0.00013	0
20 c	0.2691	2.87757	2.84176	0.00966	0.00191	0
21 f	-0.24366	3.82383	5.41163	0.00806	0.00014	0
22 c	0.37503	2.89337	2.72047	0.00943	0.00169	0
23 f	-0.2244	3.82016	5.39526	0.00884	0.00015	0
24 f	-0.26712	3.82431	5.43493	0.00775	0.00013	0
25 c	0.39747	2.86721	2.72524	0.0083	0.00177	0
26 c	0.26926	2.87758	2.84159	0.00966	0.00191	0
27 f	-0.24385	3.82388	5.41178	0.00806	0.00014	0
28 c	0.37376	2.89323	2.7219	0.00942	0.0017	0
29 f	-0.22485	3.82017	5.3957	0.00883	0.00015	0
30 c	0.26909	2.87756	2.84177	0.00967	0.00191	0
31 f	-0.24389	3.82383	5.41186	0.00806	0.00014	0
32 c	0.39793	2.86734	2.72467	0.00829	0.00177	0
33 f	-0.26677	3.82436	5.43453	0.00775	0.00013	0
34 c	-0.20672	2.9279	3.27056	0.00559	0.00267	0

$HCPh^F_3$

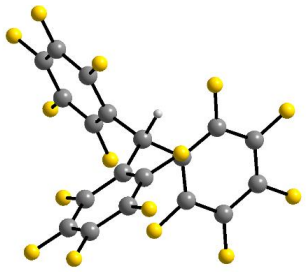

Figure S25. Representation of the B3LYP/def2-TZVPP structure of $HCPh^F_3$.

$coord

-0.43242750805016	0.11287100728542	-1.01694465034275	c
-2.03922444607518	-1.97147747845669	0.16868531523283	c
-4.56318751821306	-2.16573178580534	-0.56172538675342	c
-5.50559024607474	-0.51515944116360	-2.23850245870965	f
-6.17522204512185	-4.00559037141251	0.37377033186685	c
-8.57426308385832	-4.11283501738654	-0.38362839475288	f
-5.26455474365669	-5.74718980062378	2.10934125747594	c
-6.78299659498517	-7.52329601938330	3.03271351842612	f
-2.76161228374391	-5.61741055609950	2.87728256756725	c
-1.87524775217661	-7.27387751117889	4.55376308290948	f
-1.19361834355298	-3.74700264944628	1.91460353496209	c
1.18577059940600	-3.68975019177612	2.76416569249142	f
5.66679864136353	-3.79340607972783	-6.68647479870586	f
5.25788775266411	-2.58676493590162	-4.51436962413502	c
2.83042230996776	-1.90288992240869	-3.80530357976236	c
0.93091392594808	-2.50220258913728	-5.37314293914444	f
2.30422714258549	-0.62917780341081	-1.55964520559647	c
4.36772797027345	-0.07802330144498	-0.02385752962301	c
4.04938722075826	1.09262165442053	2.19291663899325	f
6.82036336628722	-0.72980133396256	-0.68916647605809	c
8.74261365993196	-0.16368854162681	0.83610426678460	f
7.27029121808692	-1.99039727979459	-2.94262556619541	c
9.61319589769076	-2.62677455878355	-3.58879923853098	f
-0.44128468939166	4.57468105473029	-3.81470785010133	f
-0.75698432718067	4.83741817862691	-1.31363995693545	c
-1.08992883108848	7.26050465379448	-0.37522951178299	c
-1.09160322572448	9.24686308057988	-1.92259140054532	f
-1.43196528911954	7.60345149216663	2.20177901000285	c
-1.75348334528894	9.91196736078589	3.13928524184582	f
-1.42966355507435	5.52178526101219	3.79431517485305	c
-1.74182486865912	5.83801019698880	6.27295761217810	f
-1.08222775561832	3.11850065993386	2.80180878998869	c
-1.05702930550392	1.19090881276050	4.43581567537661	f
-0.74367695006078	2.69981515017280	0.22705915311520	c
-1.25198299674452	0.36304860567308	-2.88601229639481	h

$end

E_{tot}= −-2222.093075202 H

References

[1] K. Seppelt, D. Nothe, *Inorg. Chem.* **1973**, *12*, 2727.
[2] A. Wiesner, T. W. Gries, S. Steinhauer, H. Beckers, S. Riedel, *Angew. Chem. Int. Ed. Engl.* **2017**, *56*, 8263; *Angew. Chem.* **2017**, *129*, 8375.
[3] Adept Scientific, *gNMR V 5.0*, **2005**.
[4] G. M. Sheldrick, *Acta Crystallogr. A* **2008**, *64*, 112.
[5] G. M. Sheldrick, *Acta Cryst. (Acta Crystallographica)* **2015**, *C71*, 3.
[6] O. V. Dolomanov, L. J. Bourhis, R. J. Gildea, J. A. K. Howard, H. Puschmann, *J. Appl. Cryst.* **2009**, *42*, 339.
[7] TURBOMOLE GmbH, *TURBOMOLE V7.3. a development of University of Karlsruhe and Forschungszentrum Karlsruhe*, **2018**.
[8] a) A. D. Becke, *Phys. Rev. A* **1988**, *38*, 3098; b) C. Lee, W. Yang, R. G. Parr, *Phys. Rev. B* **1988**, *37*, 785; c) S. H. Vosko, L. Wilk, M. Nusair, *Can. J. Phys.* **1980**, *58*, 1200.
[9] M. Sierka, A. Hogekamp, R. Ahlrichs, *J. Chem. Phys.* **2003**, *118*, 9136.
[10] F. Weigend, R. Ahlrichs, *Phys. Chem. Chem. Phys.* **2005**, *7*, 3297.
[11] E. G. Delany, S. Kaur, S. Cummings, K. Basse, D. J. D. Wilson, J. L. Dutton, *Chem. Eur. J.* **2019**, *25*, 5298.
[12] F. Scholz, D. Himmel, H. Scherer, I. Krossing, *Chem. Eur. J.* **2013**, *19*, 109.

A.3. Structural proof of a $[C–F–C]^+$ fluoronium cation

Structural Proof of a $[C–F–C]^+$ Fluoronium Cation

Kurt F. Hoffmann, Anja Wiesner, Carsten Müller, Simon Steinhauer, Muhammad Kazim, Cody Ross Pitts, Thomas Lectka[2*], Sebastian Riedel[1*]

Correspondence to: [1] s.riedel@fu-berlin.de; [2] lectka@jhu.edu

Supplementary Information:

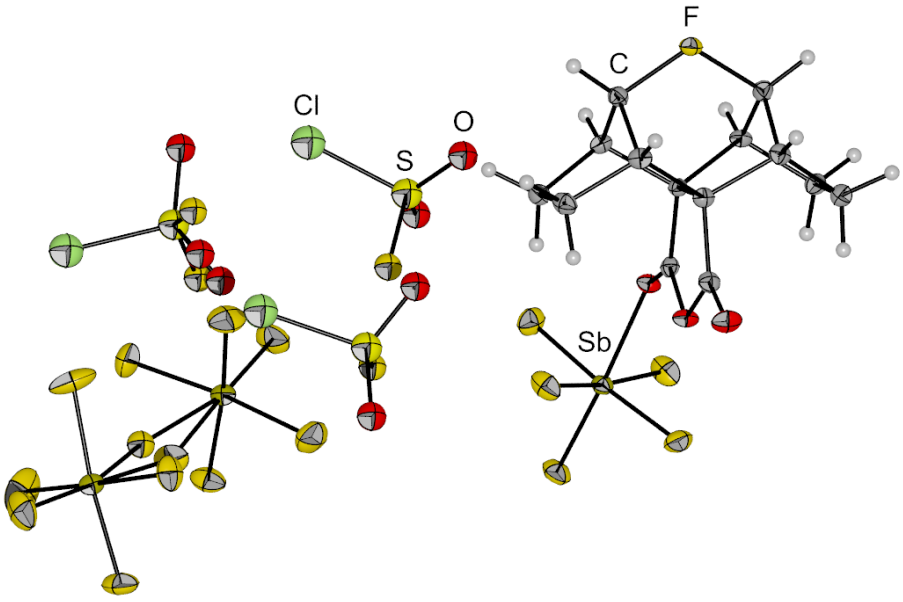

Supplementary Fig. 1. Molecular structure of $[1][Sb_2F_{11}]\cdot(SO_2ClF)_3$. Thermal ellipsoids set at 50 % probability.

Supplementary Table 1. Summary of crystal data and refinement results

	[1][Sb_2F_{11}]·(SO_2ClF)$_3$
CCDC number	CCDC-2049161
empirical formula	$C_{14}H_{14}Cl_3F_{20}O_9S_3Sb_3$
formula weight	1274.03
temperature [K]	100.0
crystal system	monoclinic
space group	$P2_1/c$
a [pm]	9.4660(4)
b [pm]	25.0063(11)
c [pm]	14.8266(7)
α [°]	90
β [°]	92.532(2)
γ [°]	90
volume [Å^3]	3506.2(3)
Z	4
ρ_{calcd} [g · cm^{-3}]	2.414
μ [mm^{-1}]	2.850
dimension [mm]	0.435 × 0.185 × 0.164
color	yellow
reflection collected	101280
independent reflections	8747 [R_{int} = 0.0981]
data/restraints/parameters	8747/29/498
goodness-of-fit on F^2	1.040
final *R* indexes [$I > 2\sigma(I)$]	R_1 = 0.0328 wR_2 = 0.0549
final *R* indexes [all data]	R_1 = 0.0562 wR_2 = 0.0579

Supplementary Table 2. Bond lengths of [1][Sb_2F_{11}]·(SO_2ClF)$_3$.

Atom	Atom	Length/Å	Atom	Atom	Length/Å	Atom	Atom	Length/Å
Sb1	F2	1.8611(16)	Sb2	F12A	2.11(3)	O2	C13	1.495(3)
Sb1	F6	1.8613(17)	S1S	Cl1S	1.9727(12)	O3	C13	1.164(4)
Sb1	F5	1.8564(18)	S1S	F1S	1.527(2)	C14	C7	1.497(4)
Sb1	F4	1.8625(17)	S1S	O2S	1.405(3)	C7	C6	1.556(4)
Sb1	O1	2.0971(18)	S1S	O1S	1.400(2)	C7	C12	1.561(4)
Sb1	F3	1.8628(18)	S2S	Cl2S	1.9713(11)	C7	C8	1.546(4)
Sb3	F17	1.8489(18)	S2S	F2S	1.538(2)	C11	C10	1.546(4)
Sb3	F12	2.027(10)	S2S	O4S	1.401(2)	C11	C1	1.516(4)
Sb3	F16	1.8548(18)	S2S	O3S	1.398(3)	C11	C12	1.549(4)
Sb3	F13	1.854(2)	S3S	Cl3S	1.9565(17)	C10	C9	1.560(4)
Sb3	F14	1.850(2)	S3S	O5S	1.387(3)	C6	C2	1.517(4)
Sb3	F15	1.8535(19)	S3S	F3S	1.709(9)	C6	C5	1.548(4)
Sb3	F12A	1.91(4)	S3S	O6S	1.323(7)	C1	C8	1.524(4)
Sb2	F10	1.8589(17)	S3S	F3AS	1.526(7)	C12	C13	1.506(4)
Sb2	F11	1.8558(19)	S3S	O6AS	1.360(7)	C12	C3	1.553(4)
Sb2	F12	2.033(6)	F1	C1	1.566(3)	C8	C9	1.546(4)
Sb2	F9	1.851(2)	F1	C2	1.587(3)	C4	C3	1.548(4)
Sb2	F7	1.8469(19)	O1	C14	1.243(3)	C4	C5	1.568(4)
Sb2	F8	1.8554(18)	O2	C14	1.306(3)	C2	C3	1.511(4)

Supplementary Table 3. Bond angles of $[1][Sb_2F_{11}]\cdot(SO_2ClF)_3$.

Atom	Atom	Atom	Angle/°	Atom	Atom	Atom	Angle/°	Atom	Atom	Atom	Angle/°
F2	Sb1	F6	94.66(8)	F7	Sb2	F12	178.0(4)	C1	F1	C2	115.64(17)
F2	Sb1	F4	93.88(8)	F7	Sb2	F9	94.03(10)	C14	O1	Sb1	129.82(18)
F2	Sb1	O1	176.97(8)	F7	Sb2	F8	95.15(9)	Sb3	F12	Sb2	155.9(7)
F2	Sb1	F3	91.80(8)	F7	Sb2	F12A	165(5)	C14	O2	C13	110.7(2)
F6	Sb1	F4	171.46(7)	F8	Sb2	F10	169.22(9)	O1	C14	O2	122.5(2)
F6	Sb1	O1	86.01(7)	F8	Sb2	F11	88.30(9)	O1	C14	C7	123.8(3)
F6	Sb1	F3	89.63(9)	F8	Sb2	F12	85.95(17)	O2	C14	C7	113.7(2)
F5	Sb1	F2	92.88(8)	F8	Sb2	F12A	84.6(19)	C14	C7	C6	113.7(2)
F5	Sb1	F6	89.48(9)	F1S	S1S	Cl1S	98.88(11)	C14	C7	C12	103.6(2)
F5	Sb1	F4	90.01(8)	O2S	S1S	Cl1S	109.41(12)	C14	C7	C8	116.8(2)
F5	Sb1	O1	84.16(8)	O2S	S1S	F1S	106.94(15)	C6	C7	C12	104.1(2)
F5	Sb1	F3	175.29(8)	O1S	S1S	Cl1S	108.97(13)	C8	C7	C6	112.4(2)
F4	Sb1	O1	85.46(7)	O1S	S1S	F1S	107.82(16)	C8	C7	C12	104.6(2)
F4	Sb1	F3	90.18(9)	O1S	S1S	O2S	122.26(17)	C10	C11	C12	110.7(2)
F3	Sb1	O1	91.16(8)	F2S	S2S	Cl2S	98.17(9)	C1	C11	C10	97.8(2)
F17	Sb3	F12	84.9(5)	O4S	S2S	Cl2S	108.52(11)	C1	C11	C12	99.5(2)
F17	Sb3	F16	90.58(9)	O4S	S2S	F2S	107.11(14)	C11	C10	C9	104.2(2)
F17	Sb3	F13	92.90(9)	O3S	S2S	Cl2S	110.33(12)	C2	C6	C7	99.0(2)
F17	Sb3	F14	172.59(11)	O3S	S2S	F2S	107.18(15)	C2	C6	C5	97.1(2)
F17	Sb3	F15	89.84(10)	O3S	S2S	O4S	122.68(16)	C5	C6	C7	111.2(2)
F17	Sb3	F12A	99(3)	O5S	S3S	Cl3S	109.55(14)	C11	C1	F1	109.5(2)
F16	Sb3	F12	84.13(18)	O5S	S3S	F3S	93.3(4)	C11	C1	C8	99.2(2)
F16	Sb3	F12A	95(4)	O5S	S3S	F3AS	114.6(4)	C8	C1	F1	108.1(2)
F13	Sb3	F12	177.0(5)	F3S	S3S	Cl3S	97.9(3)	C11	C12	C7	103.5(2)
F13	Sb3	F16	93.85(10)	O6S	S3S	Cl3S	116.6(4)	C11	C12	C3	112.6(2)
F13	Sb3	F12A	165(5)	O6S	S3S	O5S	128.6(4)	C13	C12	C7	105.3(2)
F14	Sb3	F12	87.7(5)	O6S	S3S	F3S	101.4(5)	C13	C12	C11	115.2(2)
F14	Sb3	F16	89.06(10)	F3AS	S3S	Cl3S	101.0(3)	C13	C12	C3	114.5(2)
F14	Sb3	F13	94.51(11)	O6AS	S3S	Cl3S	99.3(4)	C3	C12	C7	104.1(2)
F14	Sb3	F15	89.35(11)	O6AS	S3S	O5S	121.8(5)	C7	C8	C9	110.7(2)
F14	Sb3	F12A	74(3)	O6AS	S3S	F3AS	107.7(5)	C1	C8	C7	99.1(2)
F15	Sb3	F12	86.81(19)	O4S	S2S	Cl2S	108.52(11)	C1	C8	C9	97.5(2)
F15	Sb3	F16	170.85(10)	O4S	S2S	F2S	107.11(14)	C3	C4	C5	103.9(2)
F15	Sb3	F13	95.26(10)	O3S	S2S	Cl2S	110.33(12)	C8	C9	C10	104.0(2)
F15	Sb3	F12A	76(4)	O3S	S2S	F2S	107.18(15)	O2	C13	C12	106.7(2)
F10	Sb2	F12	83.45(18)	O3S	S2S	O4S	122.68(16)	O3	C13	O2	118.0(2)
F10	Sb2	F12A	85(2)	O5S	S3S	Cl3S	109.55(14)	O3	C13	C12	135.3(3)
F11	Sb2	F10	89.23(9)	O5S	S3S	F3S	93.3(4)	C6	C2	F1	108.4(2)
F11	Sb2	F12	87.3(5)	O5S	S3S	F3AS	114.6(4)	C3	C2	F1	108.4(2)
F11	Sb2	F12A	70(5)	F3S	S3S	Cl3S	97.9(3)	C3	C2	C6	99.9(2)
F9	Sb2	F10	90.18(9)	O6S	S3S	Cl3S	116.6(4)	C4	C3	C12	111.3(2)
F9	Sb2	F11	171.47(10)	O6S	S3S	O5S	128.6(4)	C2	C3	C12	99.5(2)
F9	Sb2	F12	84.2(5)	O6S	S3S	F3S	101.4(5)	C2	C3	C4	97.1(2)
F9	Sb2	F8	90.71(10)	F3AS	S3S	Cl3S	101.0(3)	C6	C5	C4	104.2(2)
F9	Sb2	F12A	101(5)	O6AS	S3S	Cl3S	99.3(4)	Sb3	F12A	Sb2	162(6)
F7	Sb2	F10	95.51(9)	O6AS	S3S	O5S	121.8(5)				
F7	Sb2	F11	94.49(10)	O6AS	S3S	F3AS	107.7(5)				

Supplementary Table 4. Calculated vibrational frequencies and C–X–C bond angles of different dimethyl halonium ions $[Me_2X]^+$ (X = F, Cl, Br, I), double-norbornyl type halonium ions $[DNTX]^+$ (C_{2v} symmetry) and HC-substituted $[R_2DNTX]^+$ halonium ions (R = F, Me, CF_3) at def2-TZVPP/B3LYP level of theory. Frequencies are given in cm^{-1}. Relative intensities are given in brackets.

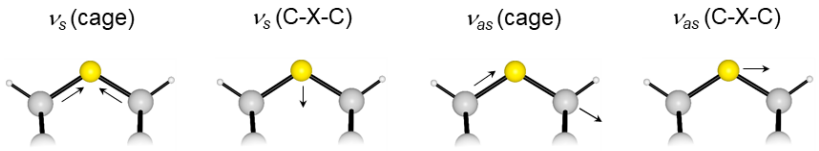

		νs (cage)	νs (C-X-C)	νas (cage)	νas (C-X-C)	<(C-X-C)
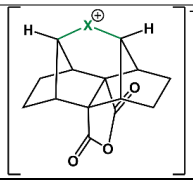	[DNTF]$^+$	724 (6)	488 (6)	588 (29)	304 (34)	115°
	[DNTCl]$^+$	711 (11)	386 (4)	657 (22)	313 (3)	98°
	[DNTBr]$^+$	710 (15)	368 (4)	651 (19)	253 (2)	92°
	[DNTI]$^+$	709 (18)	365 (3)	649 (14)	234 (1)	86°
		νs (C-X-C)	δ (C-X-C)	νas (C-X-C)		<(C-X-C)
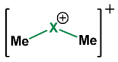	[Me_2F]$^+$	659 (12)	264 (1)	677 (100)		121°
	[Me_2Cl]$^+$	561 (41)	228 (1)	604 (100)		105°
	[Me_2Br]$^+$	500 (55)	187 (4)	517 (100)		101°
	[Me_2I]$^+$	470 (41)	160 (3)	484 (52)		98°
		νs (cage)	νs (C-X-C)	νas (cage)	νas (C-X-C)	<(C-X-C)
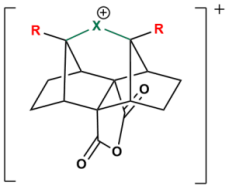	[F_2DNTF]$^+$ [a]	850/800	552/474	688	-168	115°
	[F_2DNTCl]$^+$	831/780	519/415	685	237	97°
	[$(CH_3)_2$DNTF]$^+$	708/679	546/467	638/552	176[b]	119°
	[$(CH_3)_2$DNTCl]$^+$	709/667	518/402	660/563	363[c]	102°
	[$(CF_3)_2$DNTF]$^+$	847/803	509	691/537	375	118°
	[$(CF_3)_2$DNTCl]$^+$	868/792	405	715/546[d]	376	101°

[a]: Transition state connecting two carbo-cationic structure
[b]: coupled with modes at 434, 341 and 161 cm^{-1}
[c]: coupled with mode at 278 cm^{-1}
[d]: coupled with modes at 764 and 742 cm^{-1}

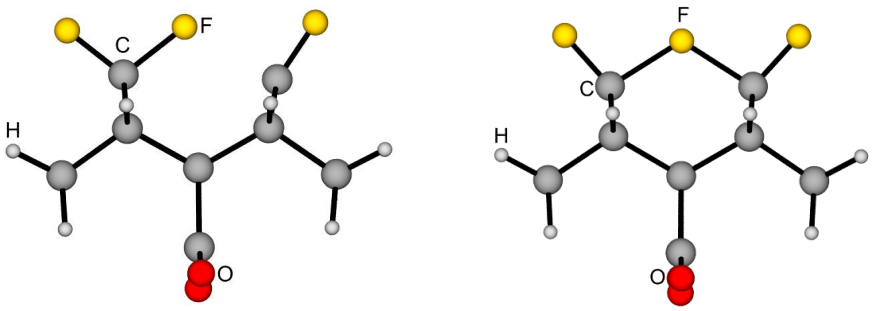

Supplementary Fig. 2. Calculated structures of $[F_2DNTF]^+$ (B3LYP/def2-TZVPP). Left: Ground state with carbo-cationic structure. Right: Transition state with C_{2v} symmetry.

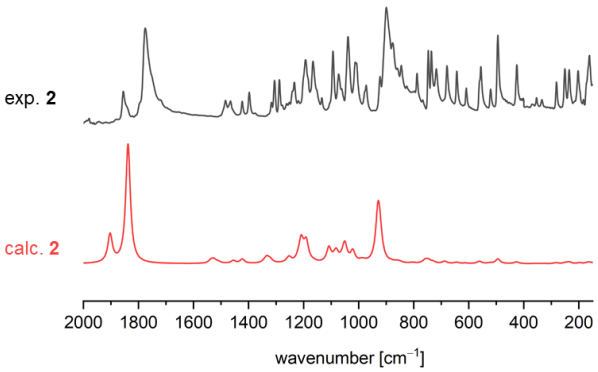

Supplementary Fig. 3. Experimental and calculated (B3LYP/def2-TZVPP) IR spectra of precursor **2**.

Supplementary Table 5. Selected experimental and calculated (B3LYP/def2-TZVPP) vibrations of precursor **2**.

Frequencies [cm^{-1}]		Assignments
experimental	calculated	
1855 (m)	1903 (m)	ν_s(C=O)
1775 (vs)	1838 (vs)	ν_{as}(C=O)
900 (vs)	930 (s)	ν_{as} (C-O-C)

vs=very strong, s=strong, m=medium

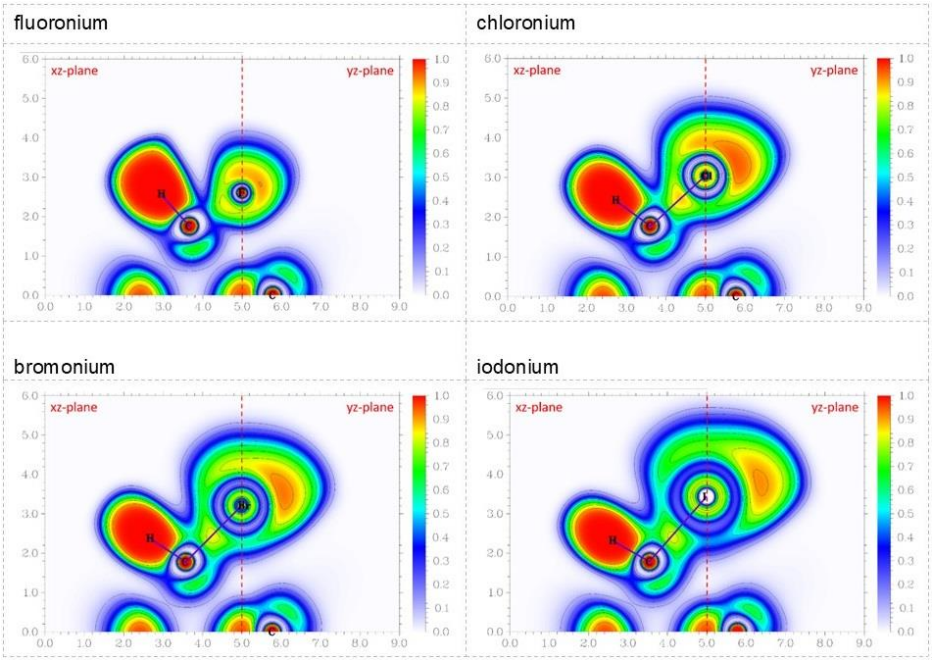

Supplementary Fig. 4. Electron localization function in the C–X–C plane ("xz-plane") and the plane containing the halogen's lone pairs, perpendicular to the former one (yz-plane). Both planes are merged at the molecule's main axis (dashed red line). ELF is defined from 0.0 (white) to 1.0 (red); contours are drawn in intervals of 0.1.

Supplementary Table 6. Atomic charges of fluoronium in C_{2v} symmetry.

Atom(s)	AIM	NBO	Mulliken	ChelpG	Merz-Kollmann	Voronoi	Löwdin
1 F	-0.521	-0.260	-0.136	-0.132	-0.094	0.058	0.382
2 O	-0.031	-0.490	-0.163	-0.441	-0.480	-0.100	0.399
3/13 C	-0.009	-0.119	-0.063	0.038	-0.120	-0.031	-0.067
4/9/14/25 C	0.041	-0.256	-0.046	-0.219	-0.237	-0.042	0.029
5/10/15/26 H	0.072	0.254	0.139	0.128	0.174	0.091	0.005
6/16/19/27 C	0.000	-0.388	-0.223	-0.036	-0.101	-0.042	0.100
7/18/21/28 H	0.056	0.238	0.140	0.067	0.106	0.082	0.001
8/17/20/29 H	0.050	0.233	0.147	0.075	0.108	0.066	0.002
11/23 C	0.245	0.285	0.150	0.284	0.258	0.116	0.083
12/24 H	0.141	0.236	0.177	0.135	0.160	0.117	0.012
22/30 C	1.556	0.788	0.286	0.734	0.839	0.225	-0.453
31/32 O	-1.101	-0.479	-0.216	-0.444	-0.448	-0.217	0.259

Supplementary Data Table 1. Cartesian coordinates.

Cartesian coordinates of optimized structures for AIM analysis on cc-pVTZ/B3LYP level of theory:

Fluoronium (C_{2v})

1	9	0.000000	0.000000	2.583669
2	8	0.000000	0.000000	-2.263264
3	6	0.000000	0.781841	-0.026580
4	6	1.291134	-1.151111	0.753468
5	1	1.295331	-2.153093	1.170604
6	6	2.560805	-0.783278	-0.056647
7	1	2.532376	-1.217377	-1.053202
8	1	3.447342	-1.179173	0.434062
9	6	-1.291134	1.151111	0.753468
10	1	-1.295331	2.153093	1.170604
11	6	1.340081	0.000000	1.733264
12	1	2.049299	0.000000	2.552572
13	6	0.000000	-0.781841	-0.026580
14	6	1.291134	1.151111	0.753468
15	1	1.295331	2.153093	1.170604
16	6	-2.560805	-0.783278	-0.056647
17	1	-3.447342	-1.179173	0.434062
18	1	-2.532376	-1.217377	-1.053202
19	6	2.560805	0.783278	-0.056647
20	1	3.447342	1.179173	0.434062
21	1	2.532376	1.217377	-1.053202
22	6	0.000000	-1.160633	-1.495304
23	6	-1.340081	0.000000	1.733264
24	1	-2.049299	0.000000	2.552572
25	6	-1.291134	-1.151111	0.753468
26	1	-1.295331	-2.153093	1.170604
27	6	-2.560805	0.783278	-0.056647
28	1	-2.532376	1.217377	-1.053202
29	1	-3.447342	1.179173	0.434062
30	6	0.000000	1.160633	-1.495304
31	8	0.000000	-2.240491	-1.982386
32	8	0.000000	2.240491	-1.982386

Chloronium (C_{2v})

1	17	0.000000	-2.731549	0.000000
2	8	0.000000	2.549200	0.000000
3	6	0.000000	0.312500	-0.781800
4	6	-1.291100	-0.467500	1.151100
5	1	-1.295300	-0.884600	2.153100
6	6	-2.560800	0.342600	0.783300
7	1	-2.532400	1.339200	1.217400
8	1	-3.447300	-0.148100	1.179200
9	6	1.291100	-0.467500	-1.151100
10	1	1.295300	-0.884600	-2.153100
11	6	-1.397787	-1.466505	0.000000
12	1	-2.263869	-2.120155	0.000000
13	6	0.000000	0.312500	0.781800
14	6	-1.291100	-0.467500	-1.151100
15	1	-1.295300	-0.884600	-2.153100
16	6	2.560800	0.342600	0.783300
17	1	3.447300	-0.148100	1.179200
18	1	2.532400	1.339200	1.217400
19	6	-2.560800	0.342600	-0.783300
20	1	-3.447300	-0.148100	-1.179200
21	1	-2.532400	1.339200	-1.217400
22	6	0.000000	1.781300	1.160600
23	6	1.397787	-1.466505	0.000000
24	1	2.263869	-2.120155	0.000000
25	6	1.291100	-0.467500	1.151100
26	1	1.295300	-0.884600	2.153100
27	6	2.560800	0.342600	-0.783300
28	1	2.532400	1.339200	-1.217400
29	1	3.447300	-0.148100	-1.179200
30	6	0.000000	1.781300	-1.160600
31	8	0.000000	2.268300	2.240500
32	8	0.000000	2.268300	-2.240500

Bromonium (C_{2v})

1	35	0.000000	-2.902612	0.000000
2	8	0.000000	2.549200	0.000000
3	6	0.000000	0.312500	-0.781800
4	6	-1.291100	-0.467500	1.151100
5	1	-1.295300	-0.884600	2.153100
6	6	-2.560800	0.342600	0.783300
7	1	-2.532400	1.339200	1.217400
8	1	-3.447300	-0.148100	1.179200
9	6	1.291100	-0.467500	-1.151100
10	1	1.295300	-0.884600	-2.153100
11	6	-1.424617	-1.465524	0.000000
12	1	-2.324301	-2.071049	0.000000
13	6	0.000000	0.312500	0.781800
14	6	-1.291100	-0.467500	-1.151100
15	1	-1.295300	-0.884600	-2.153100
16	6	2.560800	0.342600	0.783300
17	1	3.447300	-0.148100	1.179200
18	1	2.532400	1.339200	1.217400
19	6	-2.560800	0.342600	-0.783300
20	1	-3.447300	-0.148100	-1.179200
21	1	-2.532400	1.339200	-1.217400
22	6	0.000000	1.781300	1.160600
23	6	1.424617	-1.465524	0.000000
24	1	2.324301	-2.071049	0.000000
25	6	1.291100	-0.467500	1.151100
26	1	1.295300	-0.884600	2.153100
27	6	2.560800	0.342600	-0.783300
28	1	2.532400	1.339200	-1.217400
29	1	3.447300	-0.148100	-1.179200
30	6	0.000000	1.781300	-1.160600
31	8	0.000000	2.268300	2.240500
32	8	0.000000	2.268300	-2.240500

Iodonium (C_{2v})

1	53	0.000000	0.000000	2.513071
2	8	0.000000	0.000000	-3.162435
3	6	0.000000	0.781800	-0.925735
4	6	1.291100	-1.151100	-0.145735
5	1	1.295300	-2.153100	0.271365
6	6	2.560800	-0.783300	-0.955835
7	1	2.532400	-1.217400	-1.952435
8	1	3.447300	-1.179200	-0.465135
9	6	-1.291100	1.151100	-0.145735
10	1	-1.295300	2.153100	0.271365
11	6	1.448222	0.000000	0.856152
12	1	2.385120	0.000000	1.401621
13	6	0.000000	-0.781800	-0.925735
14	6	1.291100	1.151100	-0.145735
15	1	1.295300	2.153100	0.271365
16	6	-2.560800	-0.783300	-0.955835
17	1	-3.447300	-1.179200	-0.465135
18	1	-2.532400	-1.217400	-1.952435
19	6	2.560800	0.783300	-0.955835
20	1	3.447300	1.179200	-0.465135
21	1	2.532400	1.217400	-1.952435
22	6	0.000000	-1.160600	-2.394535
23	6	-1.448222	0.000000	0.856152
24	1	-2.385120	0.000000	1.401621
25	6	-1.291100	-1.151100	-0.145735
26	1	-1.295300	-2.153100	0.271365
27	6	-2.560800	0.783300	-0.955835
28	1	-2.532400	1.217400	-1.952435
29	1	-3.447300	1.179200	-0.465135
30	6	0.000000	1.160600	-2.394535
31	8	0.000000	-2.240500	-2.881535
32	8	0.000000	2.240500	-2.881535

Cartesian coordinates of optimized structures on def2-TZVPP/B3LYP level of theory:

Fluoronium $[1]^+$

$coord

11.09534536303368	28.13188835984827	14.98931574951190	sb
0.57216723090669	27.18635296840741	23.97693675753127	f
13.45970764792514	29.37169543806405	12.66314411910007	f
12.89869675354930	25.34190635722174	16.30878115398685	f
12.09698277036908	30.08465590272153	17.82438207564522	f
8.48036251955925	30.57788399531997	14.44804876626062	f
8.08177167933374	26.82694386471859	18.02505495499407	o
9.34066589251418	25.91085935379019	12.79127053555617	f
4.52061988878575	26.56302996220730	15.65722640554323	o
0.41113278846160	26.36550555200010	14.29478224964746	o
5.78132212388425	26.74627742697040	17.86817302069135	c
3.99550155498554	26.88659795507331	20.09253621459212	c
0.06286343958818	24.41190855002334	20.10573586467333	c
-2.00256669452309	24.38557524609745	20.03144500624721	h
1.35875178479745	21.93440946445377	19.20817075374301	c
1.39819224350847	21.81648614264561	17.13967932670655	h
0.29382714193859	20.28758632118030	19.87534246517582	h
4.01058707044167	29.46752030419488	21.51105958559663	c
5.41507262608422	29.60911305426804	23.02124085695728	h
1.27290479063495	24.54918693602359	22.70119959849152	c
0.63307960097336	23.30212823780058	24.21928585693571	h
1.30113896917773	26.76909683044017	18.85237041330019	c
4.03216740479310	24.58832335931228	21.92544025283144	c
5.43459036956572	24.72225006565212	23.43854940285828	h
1.30791392793588	31.60185939963047	18.38883428935081	c
0.22051961140715	33.32312531942887	18.77016712795976	h
1.35226794681177	31.37049788611540	16.32994868629854	h
4.05453080686021	22.05554586373663	20.44262096387240	c
4.36737729390755	20.47044804863183	21.73787402062116	h
5.60253257414828	22.00519103120543	19.06465760867153	h
1.80424062170627	26.54155988477370	16.03994744661705	c
1.25576295438694	29.61736689579349	22.26185907906203	c
0.59451265755745	31.07472635593292	23.56804894504331	h
0.03867448585722	29.29349207141757	19.69160857607504	c
-2.02704809660869	29.28298040929766	19.62039067964281	h
4.00534297198925	31.72041463847492	19.62270396968651	c
5.55225457735762	31.56520806418354	18.24995482487319	h
4.29496277014760	33.50037467875320	20.64117661561667	h

$[Sb_2F_{11}]^-$

$coord

3.87268788333358	-0.09894696956553	0.00716070108642	sb
-3.87106180713710	0.09657821958757	-0.01277906084533	sb
3.18342454007231	1.65349371533709	3.03110677998590	f
-0.00223942088031	-0.18049990697928	-0.57843781185082	f
7.40868981086617	-0.03892792783807	0.49198105490099	f
4.08985798566229	-1.85886318631115	-3.08816893251563	f
-3.26604319661623	3.44691384990498	1.04002256439009	f
-7.40188892547857	0.33336050787399	0.45537915223984	f
-4.01199458317984	-3.28272924388573	-1.14461879401264	f
-3.26498416123545	-1.05426170745525	3.30421156245971	f
-4.00850489931800	1.20626944810937	-3.40002027407987	f
3.45338159547559	-3.20035256431438	1.71377775106013	f
3.82957426312473	2.98597174246114	-1.78070366486947	f

Precursor 2

$coord

0.41781573334380	25.43754234821739	24.88988623714344	f
7.95218255080806	26.79989990358887	18.04600445513265	o
4.29652909826633	26.61665200324481	15.88724251763853	o
0.22793878235309	26.46242005688439	14.66989844692075	o
5.70540658466113	26.79911951309763	18.10347670431808	c
3.93555706332755	26.96593916967636	20.35859227165888	c
0.11496912567343	24.34086981279938	20.27443076468609	c
-1.93464089090401	24.22468356832750	20.20784982173707	h
1.49957705643056	22.07436347852333	19.01254786481486	c
1.51386692173675	22.16979551375601	16.96122429239659	h

0.54981001828699	20.31818268432746	19.51177075899795	h
4.03494983113528	29.65198712300927	21.57712703252322	c
5.47825930121785	29.86118459734848	23.02435444424643	h
1.34813731823086	24.00653384820365	22.89199225647063	c
1.14580610375334	22.06373866617729	23.54387364535686	h
1.23819806641386	26.84999337283288	19.17937788516309	c
4.07479950162451	24.50919127616777	22.00217331826874	c
5.52081925778058	24.54022364202098	23.46111159202404	h
1.43166876934926	31.55421366392643	18.26243712386893	c
0.45271502187929	33.34308240129546	18.51312380074426	h
1.44390082316876	31.15563012338758	16.24590423475416	h
4.22275013303083	22.19231188548677	20.19850918598694	c
4.63010229477829	20.49301330935876	21.28590960723543	h
5.70601588656829	22.35448083949612	18.78774287662409	h
1.70554631404996	26.62493122475932	16.35537999422840	c
1.28298450773030	30.03788632974857	22.43788277287040	c
0.84725849783879	32.53773163636995	23.18231120145295	f
0.08466116536951	29.48246322768367	19.84685652068797	c
-1.96730049951306	29.54029968936661	19.76266484237666	h
4.13891351260622	31.67131540713741	19.44896659589750	c
5.64023093674998	31.33785529377679	18.08558868845336	h
4.48509881318468	33.51683563466127	20.28286951886025	h
0.65539711360971	28.88208428007490	23.98613949589301	h

[DNTF]$^+$

$coord

0.62903568283625	27.17298445796316	23.92159109701894	f
8.07856945357527	26.85696481285739	17.84738964852043	o
4.45291128427226	26.61110531628079	15.61363070759538	o
0.38689764877892	26.42686067099202	14.33683571558249	o
5.84114881258226	26.81038949855044	17.83832040575475	c
4.03191218555459	26.94436673880458	20.06055962338056	c
0.14500924431308	24.41814258306388	20.06943202153789	c
-1.90513381121230	24.36362003198772	20.00038036324571	h
1.46346277527762	21.96613744302900	19.15426538343608	c
1.50115237499959	21.86046788654414	17.10163047313296	h
0.42971043231209	20.31541661339373	19.81530905013500	h
4.00082771774082	29.50325147452042	21.49965437443050	c
5.39213118763003	29.65591777224739	23.00073572766194	h
1.35103174846976	24.54966384364540	22.65879625422651	c
0.73208806491786	23.30736521101023	24.16579139583224	h
1.34504850554597	26.79566097638355	18.83368875036909	c
4.09924238190754	24.63652531330480	21.87326990345215	c
5.49134762142820	24.77228568383275	23.37520464073304	h
1.26966352713846	31.61909371204081	18.41123948692532	c
0.16888106131252	33.30854207217045	18.81617234948391	h
1.31002121765530	31.41183276272340	16.36650773461949	h
4.15408095867805	22.11573019261776	20.38039528269804	c
4.48278527604875	20.53964052669656	21.65940492915440	h
5.68442968815264	22.09530542666814	19.00733637624777	h
1.85444509625285	26.58826290881372	16.01853196108277	c
1.24893877316845	29.60011408074350	22.26880479938782	c
0.57519577846263	31.03145576062675	23.57042219627753	h
0.04704012358508	29.28455019730367	19.69374678160445	c
-2.00341485645549	29.24551578882527	19.62251615502302	h
3.96066521329003	31.76592173727553	19.63813571363634	c
5.49297076580742	31.63528648522188	18.27400065472762	h
4.22226124040187	33.53112970508958	20.66018358264897	h

[DNTCl]$^+$

$coord

0.00000000000000	0.00000000000000	5.27106239521996	cl
0.00000000000000	0.00000000000000	-4.61318355979169	o
0.00000000000000	1.47487823363886	-0.37866368450989	c
2.47788421815234	-2.17540670325418	1.03860713823379	c
2.51036727783312	-4.07778110941794	1.80828946247499	h
4.81858109059850	-1.48023311220189	-0.58259715627306	c
4.70855408391570	-2.29664686845931	-2.46581124257644	h
6.52408028693769	-2.22903617860494	0.28956444298374	h
-2.47788421815234	2.17540670325418	1.03860713823379	c
-2.51036727783312	4.07778110941794	1.80828946247499	h
2.68559021570232	0.00000000000000	2.92676002870376	c
4.30480696789164	0.00000000000000	4.18850348554270	h

0.00000000000000	-1.47487823363886	-0.37866368450989	c
2.47788421815234	2.17540670325418	1.03860713823379	c
2.51036727783312	4.07778110941794	1.80828946247499	h
-4.81858109059850	-1.48023311220189	-0.58259715627306	c
-6.52408028693769	-2.22903617860494	0.28956444298374	h
-4.70855408391570	-2.29664686845931	-2.46581124257644	h
4.81858109059850	1.48023311220189	-0.58259715627306	c
6.52408028693769	2.22903617860494	0.28956444298374	h
4.70855408391570	2.29664686845931	-2.46581124257644	h
0.00000000000000	-2.19014356126564	-3.15967221246382	c
-2.68559021570232	0.00000000000000	2.92676002870376	c
-4.30480696789164	0.00000000000000	4.18850348554270	h
-2.47788421815234	-2.17540670325418	1.03860713823379	c
-2.51036727783312	-4.07778110941794	1.80828946247499	h
-4.81858109059850	1.48023311220189	-0.58259715627306	c
-4.70855408391570	2.29664686845931	-2.46581124257644	h
-6.52408028693769	2.22903617860494	0.28956444298374	h
0.00000000000000	2.19014356126564	-3.15967221246382	c
0.00000000000000	-4.23010334968507	-4.08197232467304	o
0.00000000000000	4.23010334968507	-4.08197232467304	o

[DNTBr]$^+$

$coord

0.00000000000000	0.00000000000000	5.59854979991570	br
0.00000000000000	0.00000000000000	-4.57788273771324	o
0.00000000000000	1.47343681101759	-0.34009472067078	c
2.49537860177614	-2.17523898796772	1.05048688723752	c
2.54196487967722	-4.07984510626205	1.81324551866535	h
4.81038407749094	-1.48089318818146	-0.61581710583899	c
4.67016212073147	-2.29681294620007	-2.49730646214463	h
6.52941416286428	-2.22991847155006	0.22853500790013	h
-2.49537860177614	2.17523898796772	1.05048688723752	c
-2.54196487967722	4.07984510626205	1.81324551866535	h
2.76911866699108	0.00000000000000	2.93040297316913	c
4.44797190215980	0.00000000000000	4.10931739741494	h
0.00000000000000	-1.47343681101759	-0.34009472067078	c
2.49537860177614	2.17523898796772	1.05048688723752	c
2.54196487967722	4.07984510626205	1.81324551866535	h
-4.81038407749094	-1.48089318818146	-0.61581710583899	c
-6.52941416286428	-2.22991847155006	0.22853500790013	h
-4.67016212073147	-2.29681294620007	-2.49730646214463	h
4.81038407749094	1.48089318818146	-0.61581710583899	c
6.52941416286428	2.22991847155006	0.22853500790013	h
4.67016212073147	2.29681294620007	-2.49730646214463	h
0.00000000000000	-2.18884024376465	-3.12288654687132	c
-2.76911866699108	0.00000000000000	2.93040297316913	c
-4.44797190215980	0.00000000000000	4.10931739741494	h
-2.49537860177614	-2.17523898796772	1.05048688723752	c
-2.54196487967722	-4.07984510626205	1.81324551866535	h
-4.81038407749094	1.48089318818146	-0.61581710583899	c
-4.67016212073147	2.29681294620007	-2.49730646214463	h
-6.52941416286428	2.22991847155006	0.22853500790013	h
0.00000000000000	2.18884024376465	-3.12288654687132	c
0.00000000000000	-4.22904725811963	-4.04536032578199	o
0.00000000000000	4.22904725811963	-4.04536032578199	o

[DNTI]$^+$

$coord

0.00000000000000	0.00000000000000	5.99195696048093	i
0.00000000000000	0.00000000000000	-4.54296354236039	o
0.00000000000000	1.47188732219168	-0.30174977272553	c
2.51378220166008	-2.17412027569925	1.06118469716450	c
2.57313569316580	-4.08336297360798	1.81163892587750	h
4.79975509494393	-1.48082039794966	-0.65027828219451	c
4.63117252393844	-2.29577974927352	-2.52999399204245	h
6.53191118855401	-2.22998481143278	0.16639983880631	h
-2.51378220166008	2.17412027569925	1.06118469716450	c
-2.57313569316580	4.08336297360798	1.81163892587750	h
2.84383287089420	0.00000000000000	2.94534654769552	c
4.59757453490064	0.00000000000000	4.00949489861719	h
0.00000000000000	-1.47188732219168	-0.30174977272553	c
2.51378220166008	2.17412027569925	1.06118469716450	c
2.57313569316580	4.08336297360798	1.81163892587750	h

-4.79975509494393	-1.48082039794966	-0.65027828219451	c
-6.53191118855401	-2.22998481143278	0.16639983880631	h
-4.63117252393844	-2.29577974927352	-2.52999399204245	h
4.79975509494393	1.48082039794966	-0.65027828219451	c
6.53191118855401	2.22998481143278	0.16639983880631	h
4.63117252393844	2.29577974927352	-2.52999399204245	h
0.00000000000000	-2.18733277015050	-3.08614467352053	c
-2.84383287089420	0.00000000000000	2.94534654769552	c
-4.59757453490064	0.00000000000000	4.00949489861719	h
-2.51378220166008	-2.17412027569925	1.06118469716450	c
-2.57313569316580	-4.08336297360798	1.81163892587750	h
-4.79975509494393	1.48082039794966	-0.65027828219451	c
-4.63117252393844	2.29577974927352	-2.52999399204245	h
-6.53191118855401	2.22998481143278	0.16639983880631	h
0.00000000000000	2.18733277015050	-3.08614467352053	c
0.00000000000000	-4.22779642215375	-4.00934608434971	o
0.00000000000000	4.22779642215375	-4.00934608434971	o

$[(CH_3)_2F]^+$

$coord

-7.21178698055431	-2.15036805233638	-0.08574713464112	c
-2.17569534244732	-2.33435253793977	0.06026251353845	c
-4.75985064336209	-3.29322082103004	0.95266954255819	f
-8.61079932230119	-3.26677823977091	0.90641391428433	h
-7.12078402132827	-2.49336484006848	-2.10205815235469	h
-7.13457023274653	-0.18340440452723	0.47623680718163	h
-2.15201241343958	-0.35879148015890	0.59651683566919	h
-2.16476119340744	-2.69932510314026	-1.95420588816326	h
-0.92137056735281	-3.52905450507286	1.14991156192670	h

$[(CH_3)_2Cl]^+$

$coord

-2.74940855722662	0.12273921311639	-0.10373808284162	c
2.75257938294357	-0.07443095932565	0.06003815624264	c
-0.09698215038874	-1.53980428082857	1.40500068872604	cl
-4.39688948724873	-0.78324511501959	0.71978524410537	h
-2.58830312515236	-0.22025789915257	-2.11725951762158	h
-2.58708686276909	2.09393352910595	0.43060088596045	h
2.70062179364348	1.90412530812094	0.58916555387076	h
2.68619355139871	-0.40789985519255	-1.96038746537809	h
4.27927545479973	-1.09515994082437	0.97679453693595	h

$[(CH_3)_2Br]^+$

$coord

-2.90592724284390	0.14581896324264	-0.12057657933605	c
2.91107894720162	-0.06631976017248	0.04837628090630	c
-0.10793487316150	-1.71288054257974	1.57056867818872	br
-4.58972636689088	-0.73085316537955	0.65692445602397	h
-2.69223038553339	-0.19477492064566	-2.12831171902648	h
-2.70913445250679	2.10811529291477	0.42972110142138	h
2.81350790147972	1.91078585170088	0.57145022650600	h
2.80157898293334	-0.41439056550041	-1.96635359489260	h
4.47878748932174	-1.04550115358045	0.93820115020878	h

$[(CH_3)_2I]^+$

$coord

-3.08835274618120	0.16478022935070	-0.13716450911544	c
3.09499971831997	-0.06058910016267	0.04234325802871	c
-0.12120578424990	-1.92124517575004	1.76102927761576	i
-4.82088947470275	-0.65759238975392	0.59172156281031	h
-2.84883790426908	-0.17365133635600	-2.14244227541951	h
-2.86601404309598	2.12557695416154	0.40912449802697	h
2.97193184372001	1.91641738323474	0.56072465245956	h
2.96040057635575	-0.40406286408596	-1.97172641195501	h
4.71796781410314	-0.98963370063837	0.88638994754865	h

$[F_2DNTF]^+$ (ground state)

$coord

-0.41516332840997	0.00009459289085	4.63446378593041	f
-0.04389974677222	-0.00004864482538	-4.55658864718025	o
0.00785633339142	1.48825144576630	-0.32348581595427	c
2.49995132559086	-2.21374919650710	1.05546344467431	c
2.57283156272630	-4.07559034764483	1.90882288040558	h
4.85724766528326	-1.49100182021306	-0.60668880664510	c
4.68349613948191	-2.31190222442410	-2.48227496782468	h
6.57125747769032	-2.24093421029241	0.24251544913609	h
-2.46852349354219	2.18258514853313	1.09414360244774	c
-2.49694521617597	4.07130264526178	1.89832073879030	h
2.82022567800066	0.00025346516500	2.74757898661822	c
4.18465811439661	0.00033287445737	4.72660340958414	f
0.00798570391048	-1.48821773592402	-0.32339858479923	c
2.49979545385202	2.21406487096864	1.05531049982805	c
2.57273862273914	4.07601795761231	1.90841537986082	h
-4.79678918966581	-1.48230596886229	-0.53469645069279	c
-6.49959572704755	-2.21914219428434	0.34753636488055	h
-4.69954192207717	-2.29756972351397	-2.41843322263787	h
4.85711701242808	1.49123704646576	-0.60689556728375	c
6.57104824765233	2.24151308260617	0.24214113916846	h
4.68306708116726	2.31193475540554	-2.48253986038338	h
0.00413306326151	-2.19247902836923	-3.11286404915908	c
-2.58658931756518	-0.00001678972883	2.98144714469459	c
-4.54401569730814	-0.00012011893918	4.55486748295819	f
-2.46830145497073	-2.18270745091273	1.09427736219934	c
-2.49650779459687	-4.07137977219747	1.89858400692394	h
-4.79691452376916	1.48181222294718	-0.53482093804660	c
-4.69977085342855	2.29692943304786	-2.41862051855686	h
-6.49977519594662	2.21854342699537	0.34738631798686	h
0.00383972623145	2.19236643091508	-3.11300270770748	c
0.05790044160921	-4.23060284056691	-4.03180605859742	o
0.05718381186341	4.23052866816750	-4.03192348929910	o

$[F_2DNTF]^+$ (C_{2v} transition state)

$coord

-0.41516332840997	0.00009459289085	4.63446378593041	f
-0.04389974677222	-0.00004864482538	-4.55658864718025	o
0.00785633339142	1.48825144576630	-0.32348581595427	c
2.49995132559086	-2.21374919650710	1.05546344467431	c
2.57283156272630	-4.07559034764483	1.90882288040558	h
4.85724766528326	-1.49100182021306	-0.60668880664510	c
4.68349613948191	-2.31190222442410	-2.48227496782468	h
6.57125747769032	-2.24093421029241	0.24251544913609	h
-2.46852349354219	2.18258514853313	1.09414360244774	c
-2.49694521617597	4.07130264526178	1.89832073879030	h
2.82022567800066	0.00025346516500	2.74757898661822	c
4.18465811439661	0.00033287445737	4.72660340958414	f
0.00798570391048	-1.48821773592402	-0.32339858479923	c
2.49979545385202	2.21406487096864	1.05531049982805	c
2.57273862273914	4.07601795761231	1.90841537986082	h
-4.79678918966581	-1.48230596886229	-0.53469645069279	c
-6.49959572704755	-2.21914219428434	0.34753636488055	h
-4.69954192207717	-2.29756972351397	-2.41843322263787	h
4.85711701242808	1.49123704646576	-0.60689556728375	c
6.57104824765233	2.24151308260617	0.24214113916846	h
4.68306708116726	2.31193475540554	-2.48253986038338	h
0.00413306326151	-2.19247902836923	-3.11286404915908	c
-2.58658931756518	-0.00001678972883	2.98144714469459	c
-4.54401569730814	-0.00012011893918	4.55486748295819	f
-2.46830145497073	-2.18270745091273	1.09427736219934	c
-2.49650779459687	-4.07137977219747	1.89858400692394	h
-4.79691452376916	1.48181222294718	-0.53482093804660	c
-4.69977085342855	2.29692943304786	-2.41862051855686	h
-6.49977519594662	2.21854342699537	0.34738631798686	h
0.00383972623145	2.19236643091508	-3.11300270770748	c
0.05790044160921	-4.23060284056691	-4.03180605859742	o
0.05718381186341	4.23052866816750	-4.03192348929910	o

[F_2DNTCl]$^+$

$coord

-0.00000153248771	0.00004325990948	5.36600627068124	cl
-0.00006851382897	-0.00008330606743	-4.52690009254079	o
0.00005016754658	1.48403884065569	-0.28996164994520	c
2.50225538553096	-2.19159532054451	1.07502951992788	c
2.56119662036951	-4.07784785073641	1.88013618502498	h
4.80918266948879	-1.48302697357035	-0.60819843655940	c
4.64886062204107	-2.30044612948728	-2.48619964073287	h
6.53223741606460	-2.22418439531771	0.22875147798314	h
-2.50220897989265	2.19162130907341	1.07495353381032	c
-2.56110413057419	4.07788781739481	1.88003082093730	h
2.75697196261833	-0.00004612657229	2.91957341093281	c
4.75916538342324	-0.00005737633339	4.43000007491787	f
-0.00000882248908	-1.48407294926883	-0.28992275785639	c
2.50220949386499	2.19160324241986	1.07514971279853	c
2.56099849354202	4.07780757326892	1.88037716457405	h
-4.80917414505784	-1.48323226564273	-0.60806648778394	c
-6.53220834357323	-2.22426120228229	0.22903960724125	h
-4.64892068945766	-2.30088678377598	-2.48596920932777	h
4.80931357144223	1.48323873179109	-0.60789239931549	c
6.53229089735191	2.22405473330642	0.22951498591410	h
4.64936116225446	2.30109262510979	-2.48573168727389	h
-0.00025495892529	-2.19074308756585	-3.08114087255633	c
-2.75695281597163	0.00011330308799	2.91955135943663	c
-4.75915904212916	0.00019076017209	4.42996164357900	f
-2.50219062973040	-2.19157833156982	1.07518367834284	c
-2.56103863011140	-4.07777021867435	1.88044059432150	h
-4.80922880568584	1.48303377371978	-0.60810618867941	c
-4.64917344737189	2.30065429856342	-2.48603760882811	h
-6.53224086378050	2.22397798160650	0.22911753181675	h
0.00010896242364	2.19063086566685	-3.08120904868312	c
-0.00061016575633	-4.23051841352609	-3.99874662032976	o
0.00034170886144	4.23036161518913	-3.99889656050784	o

[$(CH_3)_2$DNTF]$^+$

$coord

0.68365192263414	27.16484972999767	23.80135195900626	f
8.10065523364110	26.85170432160530	17.79706560326634	o
4.47765954977840	26.60728829417867	15.56355457595093	o
0.41440747129021	26.42541733227945	14.28583740442742	o
5.86197705682938	26.80624108184850	17.79056058453135	c
4.05186391271919	26.94121803559202	20.01456546037870	c
0.19387773309444	24.38150800347974	19.98183245402316	c
-1.85629041654535	24.30336365457790	19.90686618643729	h
1.54919208980377	21.98673035287990	18.96498227602479	c
1.59277803156957	21.95816859868685	16.91057021206323	h
0.54372521431110	20.29214838234947	19.55158010929348	h
4.03644784822219	29.52778713749547	21.40283767311221	c
5.43350800276566	29.70364623837760	22.89726343543559	h
1.38278773850686	24.42961788446645	22.60157887008405	c
0.52402815160613	22.73978982896075	24.68607479520960	c
1.36767024470444	26.79270476976773	18.78815358815310	c
4.13582489961450	24.59968741274765	21.78179655932160	c
5.53329930283529	24.71253193167409	23.28206466350438	h
1.35413897171810	31.57324042760937	18.22816281136518	c
0.28042317449159	33.29546996970520	18.55522680516337	h
1.40136306635666	31.29074168872592	16.19326022342634	h
4.24005166583480	22.13703335670699	20.19242687460197	c
4.61019740966962	20.51768327203979	21.40302600302863	h
5.76167775693238	22.19422564564742	18.81187077118154	h
1.87936194026331	26.58596806238441	15.97137415702999	c
1.27599505848047	29.71037412043175	22.19495095470248	c
0.34305292291182	31.66337392208982	23.99884921086595	c
0.09410750743105	29.30870996506697	19.60258607659825	c
-1.95731739024943	29.29112684038397	19.52302831366717	h
4.04680480528931	31.71939051871743	19.45334167054286	c
5.57157966116480	31.50968190720486	18.09205222755626	h
4.35004061008450	33.51882961506868	20.39972726383341	h
-1.68035253595379	31.47633788812311	24.32002726113435	h
0.68875054289663	33.53095862007491	23.19904587180696	h
1.34621707241228	31.55433335342601	25.79173128862086	h
0.87895764522927	20.78221748826856	24.14845679241266	h
-1.49492410943327	22.94476495168022	25.02492347589885	h
1.56319973730631	23.11374139671840	26.42196143717204	h

$[(CH_3)_2DNTCl]^+$

$coord

0.32765877466908	27.21648243621750	24.57181774547504	cl
8.03607593899264	26.86070930126256	17.93409710008409	o
4.41722750243517	26.61613058746680	15.69738880998571	o
0.35452496584610	26.43594141247262	14.42387860249930	o
5.79687701490289	26.81506855861500	17.92623274059025	c
3.98442499371559	26.94999690873953	20.15464595073909	c
0.15800393584120	24.34347262048667	20.06578190787264	c
-1.89046648071298	24.23325467975762	19.97211610152452	h
1.55740905504661	22.01796708273415	18.94137063221910	c
1.60059390980327	22.07257155477519	16.88808200134761	h
0.58247553403362	20.28173116134062	19.45047313674422	h
3.99834840553459	29.57667423458721	21.48146378260879	c
5.40872788666749	29.78134468089348	22.96020439432885	h
1.33790400259561	24.25756769862513	22.71761781156890	c
0.62267693182084	22.16873147394847	24.53308150688361	c
1.30631701192267	26.80313303030088	18.93062285724609	c
4.09797925976548	24.55955173551868	21.86559301588209	c
5.51100032840305	24.63959214887258	23.35424393126299	h
1.36910216708152	31.53963359232003	18.20951304011140	c
0.32532385791905	33.29333554904631	18.44938650602370	h
1.42284859878985	31.17247744547499	16.18905917506535	h
4.24690252264318	22.16682186451120	20.16922671197340	c
4.65625897355803	20.50592139691325	21.30764271494088	h
5.76108358193766	22.30627139143271	18.78767984349401	h
1.82053887870553	26.59586232002231	16.10928084324446	c
1.22576507410825	29.89633842412049	22.28407647100824	c
0.42235724276746	32.20750008572733	23.76064209959990	c
0.05876147440388	29.36023324504349	19.67968167585731	c
-1.99210262755618	29.37314348506450	19.57573795315510	h
4.05866267069592	31.68719248077693	19.43922587067539	c
5.58142631144259	31.39915380957814	18.09134838152626	h
4.39716649272867	33.51670941710379	20.31150010630015	h
-1.59984131657717	32.18017534445175	24.14576882355516	h
0.82710243015045	33.90325815576945	22.67222119316548	h
1.44648284429510	32.34779727968161	25.54092529778948	h
1.10244786233593	20.34365108065575	23.71864334781442	h
-1.40087374208879	22.17146968684307	24.91227848417083	h
1.64321723159357	22.34573863988724	26.31201533249874	h

$[(CF_3)_2DNTF]^+$

$coord

0.71189366084464	27.16171990212476	23.73403903611093	f
8.12275386879251	26.84804728737697	17.76298061889423	o
4.49979239065252	26.60505980899153	15.52355321635580	o
0.43436012184596	26.42385720618432	14.24319322690462	o
5.88709040147200	26.80273367135268	17.74601361693943	c
4.07322857206579	26.93706461850785	19.97357225626757	c
0.20195903639282	24.37158919867194	19.92959290256885	c
-1.84752565191840	24.29672949076661	19.86709139681686	h
1.56915341297802	21.98187489129511	18.90797864212712	c
1.60352940659340	21.97861316979468	16.85318294153035	h
0.57293743072336	20.28275491741264	19.48709452711594	h
4.06785851181198	29.53008861498667	21.36579253717182	c
5.45181507724391	29.70244126548199	22.87109521753973	h
1.40738606159015	24.48414428493168	22.53246533887503	c
0.48198456860137	22.84438613975238	24.76450457472696	c
1.38598586693309	26.79078556149854	18.74351969435676	c
4.16440586081678	24.58591191546692	21.73935854433256	c
5.55145943880599	24.69527467980811	23.24783607547091	h
1.39064506560140	31.57144783198368	18.17332783284054	c
0.32784961743962	33.29980863082525	18.48359858993387	h
1.43879787210177	31.26005917304955	16.14268693133743	h
4.25832782381858	22.12889869630974	20.13439899981184	c
4.62574639181201	20.50231534653281	21.33117851573829	h
5.78363486685761	22.21096373604539	18.75927213806345	h
1.90244580179595	26.58352906360931	15.92216411130697	c
1.30511520192217	29.64482832730938	22.13865103107229	c
0.30364129578872	31.57162627553434	24.09199357342020	c
0.10817121455391	29.31593634398065	19.54913615127204	c
-1.94241297383031	29.30361582876573	19.47753206981951	h
4.07635008192590	31.71814452351190	19.40839022041949	c

5.61174628267911	31.49003175899401	18.06216395642257	h
4.37138407755084	33.51970661303118	20.34733108428006	h
-2.13137702159546	31.14338941726648	24.56137887365218	f
0.56174793767108	33.90613063812999	23.17591217026897	f
1.60513511644769	31.38858280802706	26.23816442786979	f
0.86372129851284	20.40987030924179	24.23210170036151	f
-1.97512881449047	23.21933038783872	25.15771636845705	f
1.75478032740854	23.43135146116953	26.85454609859537	f

$[(CF_3)_2DNTCl]^+$

$coord

0.34713212916643	27.21432075834682	24.53343295605000	cl
8.05240714414426	26.86215497868246	17.90441546201235	o
4.43267946119367	26.61354827564698	15.66496950886053	o
0.36698700249675	26.43100247164752	14.39317169943429	o
5.81591304427592	26.81348697476916	17.88871338505291	c
4.00089133500882	26.94781261293062	20.12254365269172	c
0.17030569964225	24.32972573528593	20.01904831729296	c
-1.87700226604731	24.21654408801807	19.93321708679742	h
1.58936543540413	22.02295560097943	18.87418052950684	c
1.62061872849704	22.11510011087088	16.82226921559351	h
0.63431259201943	20.27415202898324	19.36233540065168	h
4.02787193104874	29.58484594961891	21.43985230795377	c
5.43214891805292	29.79415522542812	22.92189186487138	h
1.35823063974686	24.30792218966903	22.66920397553189	c
0.56860200214570	22.23705638079702	24.61335862576290	c
1.32100333376585	26.80050732193795	18.89784755456798	c
4.12847483865614	24.54548296785633	21.82654858832038	c
5.53662756223107	24.62167105779996	23.31836025319821	h
1.40260889646555	31.52293771673243	18.13955211961715	c
0.37698639670529	33.28669691346125	18.34722489483716	h
1.45170137939176	31.11099036928314	16.12798435777012	h
4.27869045195915	22.17387896668466	20.09600074645364	c
4.70250551759558	20.49819705835043	21.19976417678901	h
5.78944658125887	22.36047214930985	18.71697375709221	h
1.83741564743259	26.59198065825254	16.07114851871254	c
1.24832660060853	29.84011841774341	22.24275191421562	c
0.39299406663663	32.15153909166984	23.85956966028365	c
0.06995658376706	29.36778288247601	19.63038120393830	c
-1.97995002667839	29.38471937261606	19.53335013303532	h
4.08906581319271	31.67236217042409	19.36994441262091	c
5.61487257247283	31.34588532458050	18.03486730457220	h
4.43343139104906	33.51128049165541	20.21054977866990	h
-2.07460978215830	31.96385324105824	24.38478938342417	f
0.78023377631493	34.33309346718511	22.67993025875608	f
1.67938138385398	32.18891376203738	26.03681452582835	f
1.12578912894214	19.92304643306782	23.81683216495214	f
-1.92510781948934	22.35837402790880	25.01924648991212	f
1.76008140944803	22.62407655179639	26.81147302341749	f

A.4. An Amorphous Teflate Doped Aluminium Chlorofluoride: A Solid Lewis Superacid for the Dehydrofluorination of Fluoroalkanes

Supporting information

An Amorphous Teflate Doped Aluminium Chlorofluoride: A Solid Lewis Superacid for the Dehydrofluorination of Fluoroalkanes

Minh Bui,[a] Kurt Hoffmann,[b] Thomas Braun,*[a] Sebastian Riedel,*[b] Christian Heinekamp,[a],[c] Kerstin Scheurell,[a] Gudrun Scholz,[a] Tomasz M. Stawski,[c] Franziska Emmerling[a],[c]

[a] M. Bui, Prof. Dr. T. Braun, C. Heinekamp, Dr. K. Scheurell, Dr. G. Scholz, Priv.-Doz. Dr. F. Emmerling
Department of Chemistry, Humboldt-Universität zu Berlin
Brook-Taylor-Straße 2, D-12489 Berlin, Germany
E-mail: thomas.braun@chemie.hu-berlin.de
[b] K. Hoffmann, Prof. Dr. S. Riedel
Institut für Chemie und Biochemie, Freie Universität Berlin
Fabeckstraße 34/36, D-14195 Berlin, Germany
E-Mail: s.riedel@fu-berlin.de
[c] C. Heinekamp, Dr. Tomasz M. Stawski, Priv.-Doz. Dr. F. Emmerling
BAM Federal Institute for Materials Research and Testing
Richard-Willstätter-Straße 11, D-12489 Berlin, Germany

Content:

General techniques and materials 2
NMR spectroscopy 2
X-ray powder diffraction 7
Infrared spectroscopy 7
Surface area determination and pore size analysis 8
Pair distribution function (PDF) 9
Extended X-ray absorption fine structure (EXAFS) 10
Transmission electron microscopy 11
Thermogravimetric analysis (TGA) / Differential scanning calorimetry (DSC) 11
Temperature programmed desorption 12
Synthesis of pentafluoroorthotellurate doped aluminium chlorofluoride (ACF-teflate) 12
Isomerization of 1,2-dibromohexafluoropropane to 2,2-dibromohexafluoropropane 12
Formation of ACF-teflate·Et_3SiH 13
Formation of ACF-teflate·1-fluoropentane 13
Formation of ACF-teflate·CD_3CN 13
Formation of ACF-teflate·^{15}N-Pyridine 13
Reactivity studies towards liquid fluoroalkanes (n-fluoropentane, n-fluoroheptan) 13
Reactivity studies towards gaseous fluoroalkanes (difluoromethane, 1,1-difluoroethane) . 13
Literature 16

General techniques and materials

The samples were prepared in a MBraun glovebox and all reactions were performed in JYoung NMR tubes using conventional Schlenk techniques. C_6D_6 was purchased from Eurisotrop and dried over K-Solvona and distilled before usage. ^{15}N-pyridine was purchased from Eurisotrop and used as received. Triethylsilane, 1-fluoropentane and 1-fluoroheptan were obtained from Sigma Aldrich and stored under an argon atmosphere in Schlenk flasks. $AlCl_3$ was purified by sublimation before usage. The gases difluoromethane and 1,1-difluoroethane were purchased from ABCR.

NMR spectroscopy

Liquid NMR spectra were measured at a Bruker DPX 300, Bruker AVANCE II 300 or a Bruker AVANCE II 500 spectrometer at room temperature with tetramethylsilane as external standard. ^{1}H NMR chemical shifts δ were referenced to residual C_6D_5H (δ = 7.16 ppm). ^{19}F NMR spectra were calibrated externally to $CFCl_3$ (δ = 0 ppm) and ^{13}C NMR spectra were referenced to C_6D_6 (δ = 128.06 ppm).

Solid-state MAS (magic angle spinning) nuclear magnetic resonance spectra were recorded at a Bruker AVANCE 400 (B_0 = 9.4 T) spectrometer at room temperature. Depending on the nucleus different rotor sizes were used: 2.5 mm rotors for ^{1}H, ^{19}F and ^{27}Al; 4 mm for ^{1}H-^{29}Si CP and ^{125}Te; 7 mm for ^{1}H-^{15}N CP. The chemical shifts were given with respect to a $CFCl_3$ standard for ^{19}F and an aqueous solution of $AlCl_3$ for ^{27}Al. For both nuclei AlF_3 was used as external standard. ^{125}Te NMR spectra were referenced to $Te(CH_3)_2$ and $Te(OH)_6$ as a external standard. The respective Larmor frequencies are ν_{1H} = 400.1 MHz, ν_{13C} = 100.6 MHz, ν_{19F} = 376.4MHz, ν_{15N} = 40.6 MHz, ν_{27Al} = 104.3 MHz, ν_{29Si} = 79.5 MHz and ν_{125Te} = 126.2 MHz. For ^{1}H-^{15}N CP MAS NMR measurements $^{15}ND_4Cl$ (^{15}N = -341 ppm) was used as external standard. The ^{1}H 90° pulse length was set as 2.6 µs. The contact time was 3 or 8 ms and the d1 time was 5 s. The ^{1}H-^{29}Si CP MAS NMR spectra were recorded by using a ^{1}H 90° pulse length of 2.65 µs at 6 dB while the contact time was 5 ms and d1 time was 5 s. As external standard Na_2SiF_6 (^{29}Si = 189.1 ppm) was used.

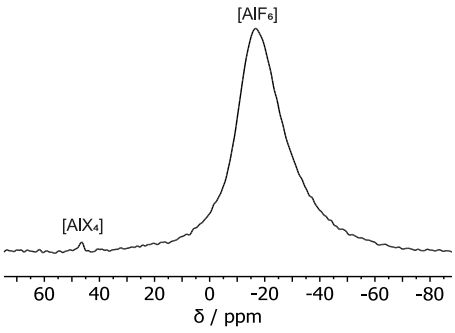

Figure 1. ^{27}Al MAS NMR spectrum ($\tilde{\nu}_{rot}$: 15 kHz) for ACF-teflate.

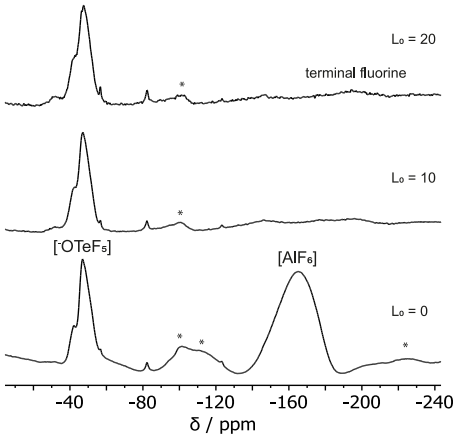

Figure 2. ^{19}F rotor synchronized spin-echo MAS NMR spectra ($\tilde{\nu}_{rot}$: 20 kHz) of ACF-teflate: Asterisks (*) represent spinning sidebands.

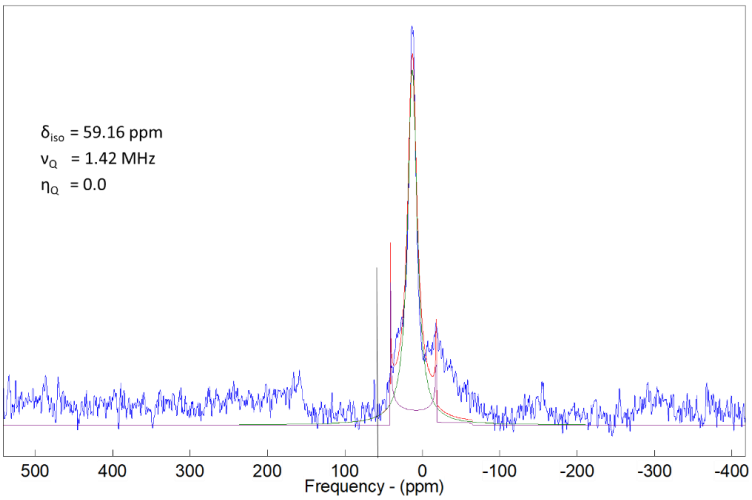

Figure 3. Calculated ^{27}Al MAS NMR spectrum ($\tilde{\nu}_{rot}$: 15 kHz) for $[Al(OTeF_5)_3]_2$ using DMFIT.

DMFIT [1] was used to calculate the measured ^{27}Al MAS NMR spectrum and to estimate the $\delta_{iso}(^{27}Al)$ value for $[Al(OTeF_5)_3]_2$. Due to the bad signal-to-noise ratio the calculated values should be considered very carefully. The quadrupolar frequency ν_Q and the quadrupolar asymmetry parameter η_Q are determined as 1.42 MHz and 0, respectively. Additionally, a distinct signal could be detected at around 13 ppm, which develops during the measurement. This might imply a decomposition of $[Al(OTeF_5)_3]_2$ into unknown aluminium entities during the measurement. The signal appears at a typical chemical shift region for $[AlF_xO_{6-x}]$ (x = 0-1) species.[2]

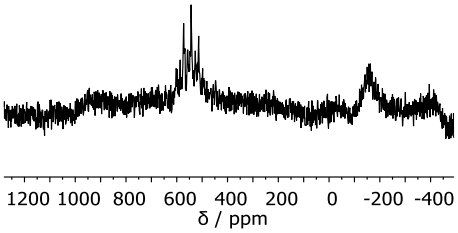

Figure 4. ^{125}Te MAS NMR spectrum ($\tilde{\nu}_{rot}$: 12 kHz) for ACF-teflate

The ^{125}Te MAS NMR spectrum for ACF-teflate shows a signal at 543 ppm which appears as a multiplet with a scalar ^{1}J(Te,F) coupling of about 3600 Hz.

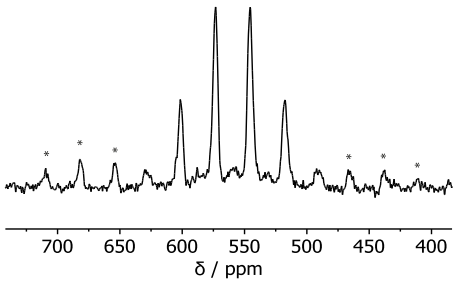

Figure 5. ^{125}Te MAS NMR spectrum ($\tilde{\nu}_{rot}$: 13:5 kHz) for $[PPh_4][Al(OTeF_5)_4]$. Asterisks (*) represent spinning sidebands.

In the ^{125}Te MAS NMR spectrum (Figure 5) one can detect a signal at 559 ppm which appears as a sextuplet (^{1}J(Te,F) = 3530 Hz) and can be assigned to the tellurium attached to five equivalent fluorine atoms. Therefore, the four fluorine atoms in the equatorial plain and the one fluorine atom in the axial position in the teflate group are indistinguishable.

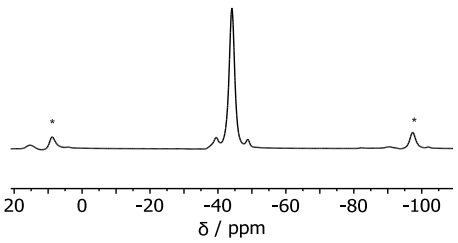

Figure 6. ^{19}F MAS NMR spectrum ($\tilde{\nu}_{rot}$: 20 kHz) for $[PPh_4][Al(OTeF_5)_4]$. Asterisks (*) represent spinning sidebands.

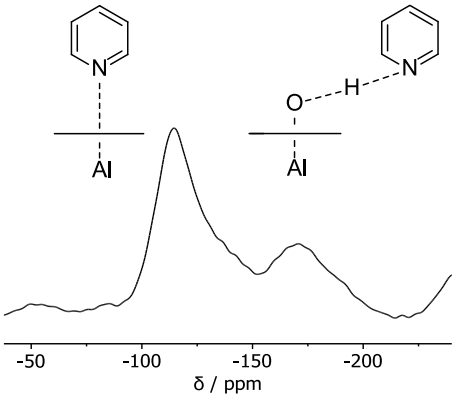

Figure 7. ^{1}H-^{15}N CP MAS NMR ($\tilde{\nu}_{rot}$: 3 kHz) spectrum for ACF-teflate treated with ^{15}N-pyridine.

^{15}N-labeled pyridine was adsorbed at ACF-teflate and a ^{1}H-^{15}N CP MAS NMR spectrum was measured (Figure 5). Signals at -114 and -170 with a shoulder at -137 ppm were detected. The high-field shifted signal can be assigned to ^{15}N-pyridine molecules that interact with Brønsted acid sites, whereas the other two signals indicate the presence of Lewis-acidic sites. Brønsted acid sites can be formed during the sample preparation.

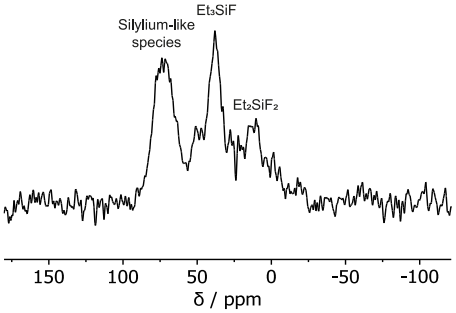

Figure 8. ^{1}H-^{29}Si CP MAS NMR spectrum ($\tilde{\nu}_{rot}$: 10 kHz) for ACF-teflate treated with Et_3SiH.

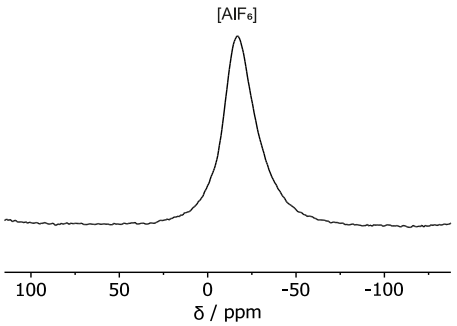

Figure 9. ^{27}Al MAS NMR spectrum ($\tilde{\nu}_{rot}$: 15 kHz) for ACF-teflate treated with Et_3SiH.

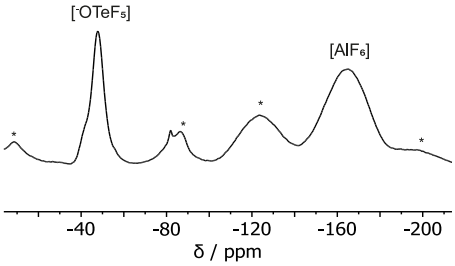

Figure 10. ^{19}F MAS NMR spectrum ($\tilde{\nu}_{rot}$: 15 kHz) for ACF-teflate treated with Et_3SiH. Asterisks (*) represent spinning sidebands.

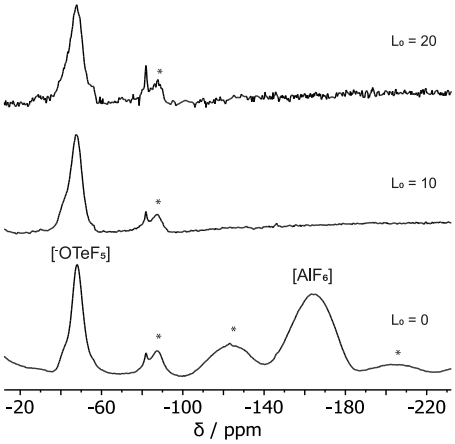

Figure 11. ^{19}F rotor synchronized spin-echo MAS NMR spectra ($\tilde{\nu}_{rot}$: 15 kHz) of ACF-teflate treated with Et_3SiH. Asterisks (*) represent spinning sidebands.

X-ray powder diffraction

X-ray powder diffraction measurements were performed on an STOE Stadi MP diffractometer equipped with a Dectris Mythen 1 K linear silicon strip detector and Ge(111)double-crystal monochromator (Mo-K radiation) in a transmission geometry.

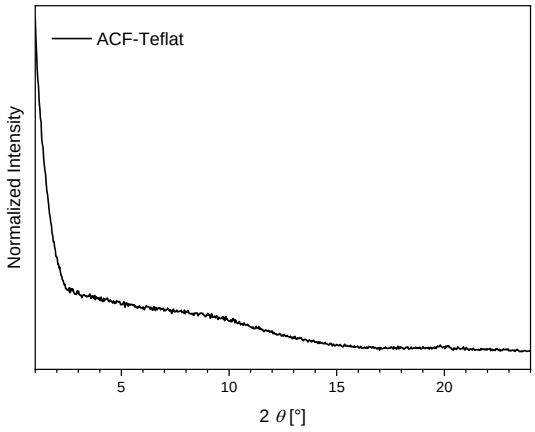

Figure 12. Powder XRD for ACF-teflate.

Similar to neat ACF, ACF-teflate exhibits no reflections in the powder X-ray diffractogram and can therefore also be characterized as an amorphous material.

Infrared spectroscopy

The IR-spectra were recorded in a glovebox at a Bruker Alpha II spectrometer with a diamond ATR (attenuated total reflectance) measuring unit (Pyroelectric DTGS detector).

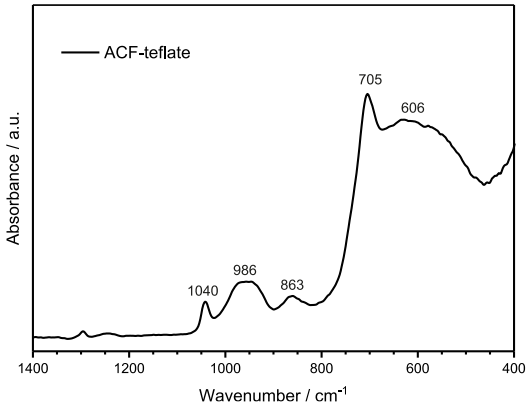

Figure 13. ATR-IR spectrum for ACF-teflate.

Surface area determination and pore size analysis

Low temperature adsorption isotherms of nitrogen at 77 k were determined with a Micro-meritics ASAP 2020. Approximately 150 mg of the samples were tempered at 200 °C for 10 h immediately before the measurement at the device. The evaluation was carried out according to the BET theory.[3] BJH method was used to determine the pore size.[4]

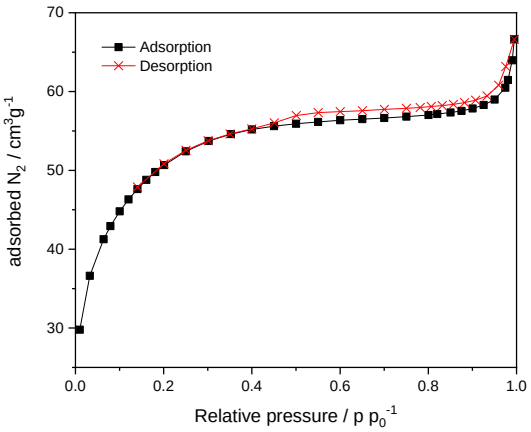

Figure 14. N2 adsorption and desorption isotherm for ACF-teflate at 77 K.

Pair distribution function (PDF)

High-energy X-ray diffraction (HEXD) measurements were performed at the beamline I15-1 of the Diamond Light Source (UK). The diffraction patterns were collected at 76 keV, which corresponded to a wavelength of 0.161669 Å. The 2D patterns were measured with a Perkin Elmer XRD 1611 CP3 detector (409.6 × 409.6 mm^2 active area, 100 µm pixel size) in Debye-Scherrer geometry. The powder samples were measured in spinning capillaries using the standard I15-1 setup. The q-range was calibrated using a CeO_2 standard. Dark current contributions were corrected automatically by the acquisition software. The as-obtained 2D patterns were reduced to raw 1D curves using DAWN. We obtained the atomic pair distribution functions (PDFs) from the diffraction patterns using the PDFgetX3 software,[5] which was also used for the background and Compton scattering subtractions. Further analysis was performed in Python using a DiffPy library.

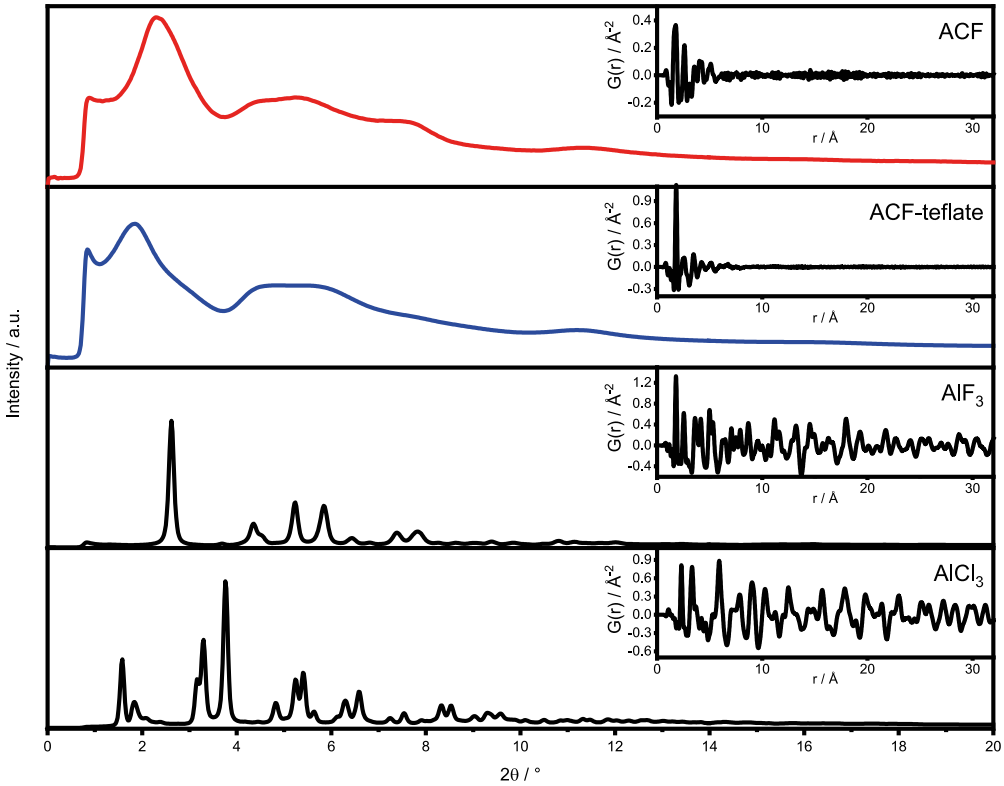

Figure 15. High-energy X-Ray Diffraction of ACF, ACF-Teflat, comm. AlF_3 and $AlCl_3$ (HEXD, wavelength 0.161669 Å) data obtained at I15-1 of the Diamond Light Source after background subtraction. Respective insets show the calculated PDFs up to a distance r = 30 Å.

Extended X-ray absorption fine structure (EXAFS)

EXAFS measurements were performed at the BAM*line* at BESSY-II [6], according to the experimental arrangement displayed in Figure 16. The beam was monochromatized using a double-crystal monochromator (DCM) installed at the beamline, with a resolution ($\Delta E/E$) of about $2x10^{-4}$. The slits were adjusted to provide a 4 mm (H) x 1 mm (V) spot size. The measurements were performed @ Te K-edge (31.814 keV) in transmission, as the sample preparation allowed choosing the adequate thickness for optimal absorption, establishing an edge jump factor of about 2. This was achieved by diluting the powder samples with Boron Nitride (BN). The excitation energy was varied from –200 to –20 eV below the edge in 10 eV steps, from –20 eV below the edge and 200 eV above the edge in 1 eV steps, and in the EXAFS region with a constant step in the *k*-space of 0.04 $Å^{-1}$ until *k* = 16 Å.

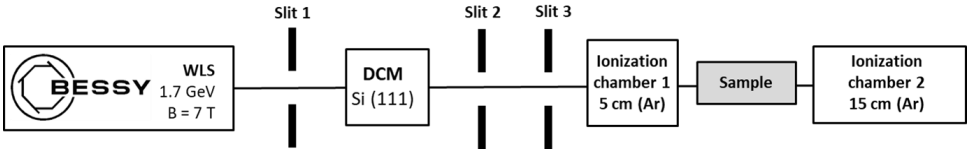

Figure 16. Layout of EXAFS experiments in transmission @ the BAMline, BESSY-II.

EXAFS data were processed by ATHENA and ARTEMIS.[7] This GUIs programs is part of the main package IFEFFIT (v. 1.2.12). The AutoBK background subtraction procedure was used with the Rbkg parameter set to 1.0 Å and kw=1. Afterwards all spectra were normalized to the far post-edge region, free from absorption features. Regarding the EXFAS region, with ATHENA one can plot $\chi(k)$against R(Å) and the oscillations represent different frequencies, which correspond to the different distances for each coordination shell. Hence, Fourier transforms (FT) are necessary for the analysis process. The FT from the k-space to R-space were performed with a Hanning-type window with a range of 1.5 to 14 Å. By analyzing the signal in the frequency domain in ATHENA the window range was selected to exclude the noisy part of the signal.

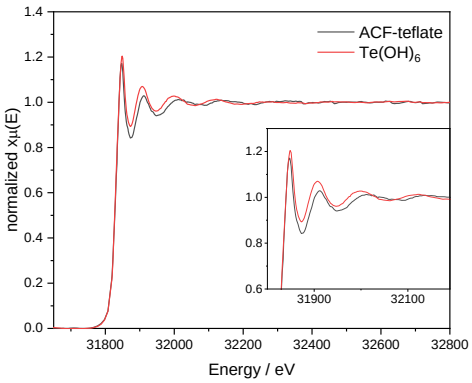

Figure 17. Normalized Te K-edge data of ACF-Teflat and $Te(OH)_6$.

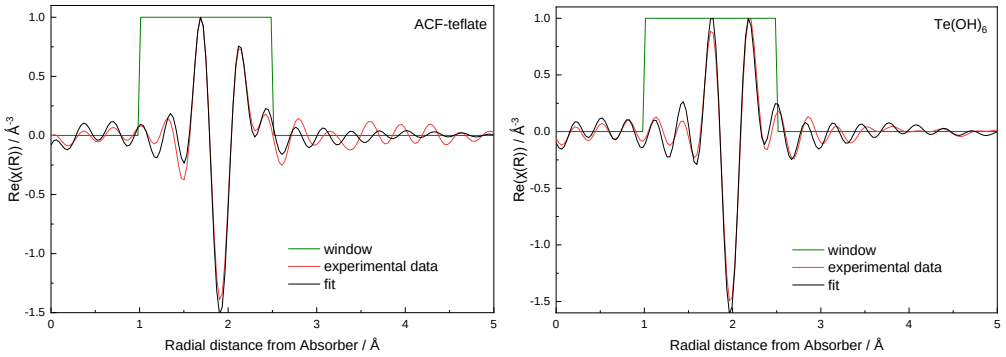

Figure 18. Te K-edge EXAFS data from ACF-Teflat (R=0.011) and $Te(OH)_6$ (R=0.009). Experimental data: red, fit results: black, fit window: green.

Transmission electron microscopy

High-resolution transmission electron microscopy (HRTEM), high-angle annular dark-field scanning transmission electron microscopy (HAADF-STEM) and energy dispersive X-ray analysis (EDX) elemental mapping were carried out on a FEI Talos F200S scanning/transmission electron microscope (S/TEM) at an acceleration voltage of 200 kV. A dry TEM grid preparation was carried out. Therefore, TEM grids were carefully swiped across the powder samples. The excess of powder on the grids were removed by tapping lightly.

Thermogravimetric analysis (TGA) / Differential scanning calorimetry (DSC)

The TGA and DSC measurements were performed on a TGA/DSC 3+ from Mettler Toledo, Switzerland. Samples were weight in in a glovebox and sealed with the A2 closing stamp. The closed crucible was pinned in a N_2 stream by the sample robot. The samples were heated from 25 to 600 °C at a rate of 10 K/min. Afterwards the samples were cooled down to 25 °C at the same rate.

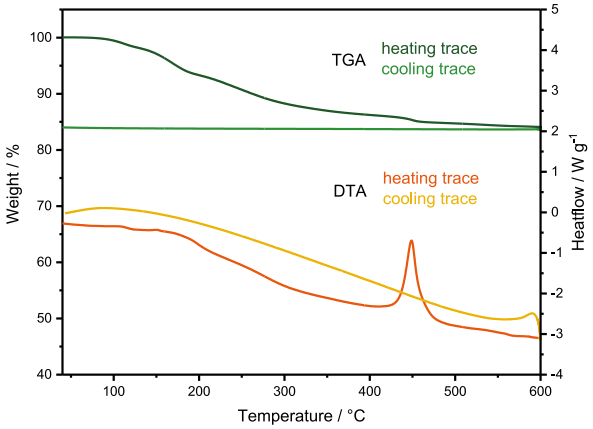

Figure 5. TPD profile for ACF-teflate and its TGA/DTA curve for heating and cooling process.

Temperature programmed desorption

NH_3-TPD were performed on the Autosorb iQ equipped with a TCD detector from Anton Paar. Approximately 200 mg of the sample were placed between two layers of quartz wool in a quartz cell. The cell was evacuated for 5 min and then tempered to 200 °C with a heating rate of 5 K/min while in a helium flow. Then, the cell was cooled down to 120 °C and NH_3 gas was added for 15 min. After that, the gas flow was changed again to helium and the detector was turned on. Helium was then flowed for 30 min to get rid of the non-adsorbed NH_3 on the sample surface. The TPD measurement was then performed starting at 80 °C until 510 °C with a heating rate of 10 K/min. The TPD profile for ACF-teflate revealed two maxima at around 208 and 349 °C for weak and medium/strong acidic sites, respectively.

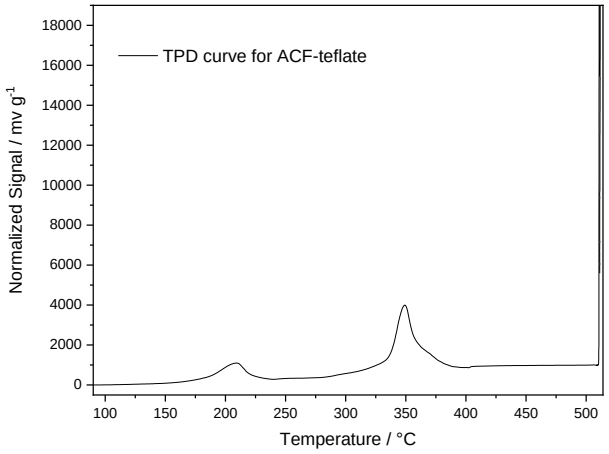

Figure 19. TPD curve for ACF-teflate showing two acidic sites for weak and medium/strong acidic sites.

Synthesis of pentafluoroorthotellurate doped aluminium chlorofluoride (ACF-teflate)

$AlCl_3$ (eq, 10.6 mmol, 1400 mg) and $Al_2(OTeF_5)_6$ (0.54 mmol, 400 mg) were placed in a round Schlenk flask and cooled down to –30 °C. Then, CCl_3F (53 mmol) was condensed five times onto the powder mixture. The resulting yellowish suspension was stirred for 1 h at –30 °C, then for 2h at 25 °C. A yellow powder in a quantitative amount was obtained after removal of the solvent under vacuum. EDX spectroscopy was performed to determine the chemical formula $AlCl_{0.1}F_{2.8}(OTeF_5)_{0.1}$.

Isomerization of 1,2-dibromohexafluoropropane to 2,2-dibromohexafluoropropane

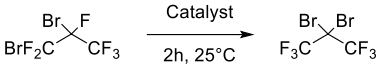

In a pear-shaped flask, 25 mg of the ACF-teflate were suspended in 250 µL of 1,2-dibromohexafluoropropane. The reaction mixture was stirred for two hours at 25 °C. After the reaction, CD_3Cl was added and the isomerization activity was investigated by ^{19}F NMR spectroscopy. The conversions were calculated by integration of the signals for the starting and isomerization compound. ACF-teflate can catalyze the isomerization with a conversion up to 70 %.

1,2-dibromohexafluoropropane

^{19}F-NMR (282 MHz, CD_3Cl): δ [ppm] = –58.1 (2F, m), –74.3 (3F, m), –133.2 (1F, m)

2,2-dibromohexafluoropropane

^{19}F-NMR (282 MHz, CD_3Cl): δ [ppm] = –72.1 (6F, s),

Formation of ACF-teflate·Et_3SiH

ACF-teflate (200 mg) was placed in a Schlenk flask and cooled down to 0 °C. Et_3SiH (1 mL) was carefully added to the powder to get a dark suspension (Attention: strong exothermic reaction!). The reaction mixture was stirred at 0 °C for 1 h and then at 25 °C for also 1 h. Afterwards, the excess of Et_3SiH was removed under vacuum to obtain a dark brown powder. The mass gain is 8 %.

Formation of ACF-teflate·1-fluoropentane

ACF-teflate (200 mg) was placed in a Schlenk flask and cooled down to 0 °C. 1-Fluoropentane (1 mL) was added to the powder to get a light brown suspension. The reaction mixture was stirred at 0 °C for 1 h and then at 25 °C for also 1 h. Afterwards, the excess of 1-fluoropentane was removed under vacuum to obtain a brown powder. The mass gain is 3 %.

Formation of ACF-teflate·CD_3CN

The powder ACF-teflate (200 mg) was suspended in an excess of CD_3CN in a Schlenk flask and stirred at 25 °C for two hours. The excess of CD_3CN was removed under vacuum to obtain a brown powder.

Formation of ACF-teflate·^{15}N-Pyridine

ACF-teflate (500 mg) was placed in a Schlenk flask and ^{15}N-pyridine (0.5 mL) was added to the powder. The reaction mixture was stirred at 25 °C for 2 h. Then the suspension was dried under reduced pressure.

Reactivity studies towards liquid fluoroalkanes (n-fluoropentane, n-fluoroheptan)

15 mg of ACF-teflate were placed in a JYoung NMR tube and Et_3SiH (0.02 mmol) was added resulting to a dark suspension. Then, the fluoroalkane (0.02 mmol) was added and gas evolution was observed. After that C_6D_6 was added to the reaction mixture. The products were analyzed by NMR spectroscopy.

Reactivity studies towards gaseous fluoroalkanes (difluoromethane, 1,1-difluoroethane)

In a JYoung NMR Tube 15 mg of ACF-teflate were suspended in Et_3SiH (0.02 mmol) resulting to a dark suspension. Then C_6D_6 was added and cooled down to –196 °C. Afterwards, the gases were condensed into the reaction mixture.

All conversions were determined by ^{1}H NMR spectroscopy. The yields for the dehydrofluorination reactions were calculated based on the conversion of fluoroalkanes into the olefines. The ratio of the isomers for the dehydrofluorination reactions were calculated by ^{13}C and ^{1}H NMR spectroscopy. For the Friedel Crafts type reactions the yields were determined based on the conversion of fluoroalkanes into the Friedel-Crafts products.

Table 1. Selected ^{1}H and ^{19}F NMR resonances of the reactants and products of the catalytic reactions in C_6D_6.

Reactant/product	δ(^{1}H NMR) in ppm	δ(^{13}C NMR) in ppm	δ(^{19}F NMR) in ppm
CH_2F_2	4.68 ppm (t, ^{2}J(H,F) = 50.2 Hz)	n.d.[a]	–142.2 ppm (t, ^{2}J(F,H) = 50.2 Hz)
CH_3CHF_2	5.30 ppm (tq, ^{2}J(H-F) = 57.1 Hz, ^{3}J(H,F) = 4.5 Hz, 1H, CHF_2), 0.93 ppm (td, ^{3}J(H,F) = 20.7 Hz, ^{3}J(H,F) = 4.5 Hz, 3H, CH_3)	n.d.[a]	–109.1 ppm (dq, ^{2}J(F,H) = 57.1 Hz, ^{3}J(F,H) = 20.7 Hz)
$F(CH_2)_4CH_3$	4.11 (dt, ^{2}J(H,F) = 47.6 Hz, ^{3}J(H,H) = 6.2 Hz, 2H, CH_2F)	n.d.[a]	–218.2 (hept, ^{2}J(F,H) = 24 Hz)
$F(CH_2)_6CH_3$	4.12 (dt, ^{2}J(H,F) = 47.4 Hz, ^{3}J(H,H) = 6.3 Hz, 2H, CH_2F)	n.d.[a]	–217.8 (hept, ^{2}J(F,H) = 24 Hz)
Et_3SiH	3.88 (hept, ^{3}J(H,H) = 3.1 Hz	n.d.[a]	-
H_2	4.47 (s)	n.d.[a]	-
HD	4.44 (t, ^{1}J(H,D) = 42 Hz)	n.d.[a]	-
Et_3SiF	n.d.[a]	n.d.[a]	–175.3 (m, ^{3}J(F,H) = 6.8 Hz)
Et_2SiF_2	n.d.[a]	n.d.[a]	–142.1 (m, ^{3}J(F,H) = 5.4 Hz)
(E)-pent-2-ene	5.41 (m, 2H, CH_3CH=$CH$$CH_2CH_3$), 1.95 (m, 2H, CH_3CH=$CHCH_2$$CH_3$), 1.59 (m, 3H, $CH_3$$CH$=$CHCH_2CH_3$)	n.d.[a]	-
(Z)-pent-2-ene	5.41 (m, 2H, CH_3CH=$CH$$CH_2CH_3$), 1.95 (m, 2H, CH_3CH=$CHCH_2$$CH_3$), 1.52 (m, 3H, $CH_3$$CH$=$CHCH_2CH_3$)	n.d.[a]	-
(E)-hept-2-ene	5.42 (m, 2H, CH_3CH=$CH$$(CH_2)_3CH_3$), 1.97 (m, 2H, CH_3CH=$CHCH_2$$(CH_2)_2CH_3$), 1.61 (m, 3H, $CH_3$$CH$=$CH(CH_2)_3CH_3$)	132.2 (CH_3C=C), 125.0 (CH_3C=C), 32.9 (C=C-CH_2), 32.5 (C-C-CH_3),23.4 (C-CH_3), 18.1 (CH_3-C=C), 14.7 (CH_2-CH_3)	-
(Z)-hept-2-ene	5.41 (m, 2H, CH_3CH=$CH$$(CH_2)_3CH_3$), 1.97 (m, 2H, CH_3CH=$CHCH_2$$(CH_2)_2CH_3$), 1.55 (m, 3H, $CH_3$$CH$=$CH(CH_2)_3CH_3$)	131.3 (CH_3C=C), 124.0 (CH_3C=C), 32.8 (C=C-CH_2), 27.1 (C-C-CH_3), 22.9 (C-CH_3), 14.4 (C-CH_3), 12.9 (CH_3-C=C)	-
(E)-hept-3ene	n.d.[a]	132.6 (CH_3-C-C=C), 129.7 (CH_3-C-C=C), 35.2 (CH_3-C), 26.2 (C=C-C), 23.4 (C-CH_3), 14.3 (CH_3-C), 13.9 (C-CH_3)	

(Z)-hept-3-ene	n.d.	132.2 (CH_3-C-C=*C*), 129.6 (CH_3-C-*C*=C), 29.3 (C=C-*C*), 23.5 (*C*-CH_3), 21.5 (CH_3-*C*), 14.2 (*C*H_3-C), 14.0 (C-*C*H_3)	
[d_n]-Ph_2CH_2	3.73 (s, CH_2)	n.d.[a]	-
[d_n]-Ph_2CHCH_3	2.44 (q, ^3J(H,H) = 7.6 Hz, 1H, C*H*), 1.46 (d, ^3J(H,H) = 7.6 Hz, 3H, C*H*$_3$)	n.d.[a]	-

[a] n.d. = not determined.

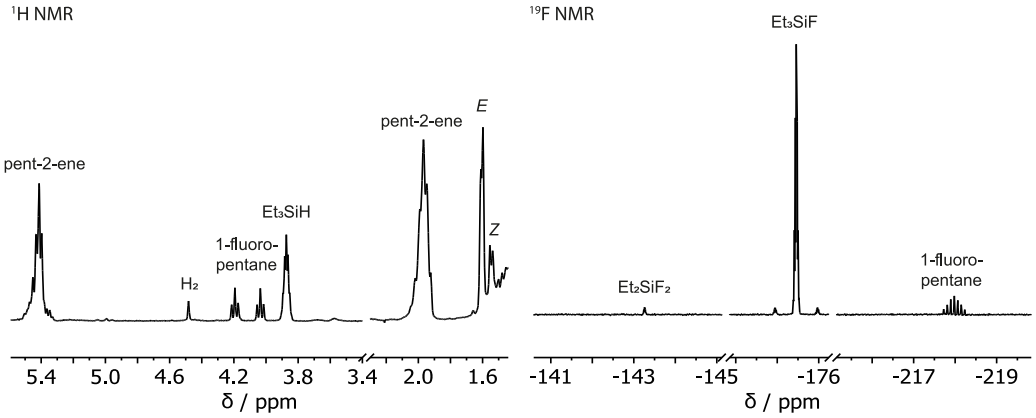

Figure 20. Parts of the ^{1}H NMR (300.1 Hz, C_6D_6) and ^{19}F NMR (105.1 Hz, C_6D_6) spectra for the ACF-teflate catalyzed dehydrofluorination reaction of 1-fluoropentane with Et_3SiH.

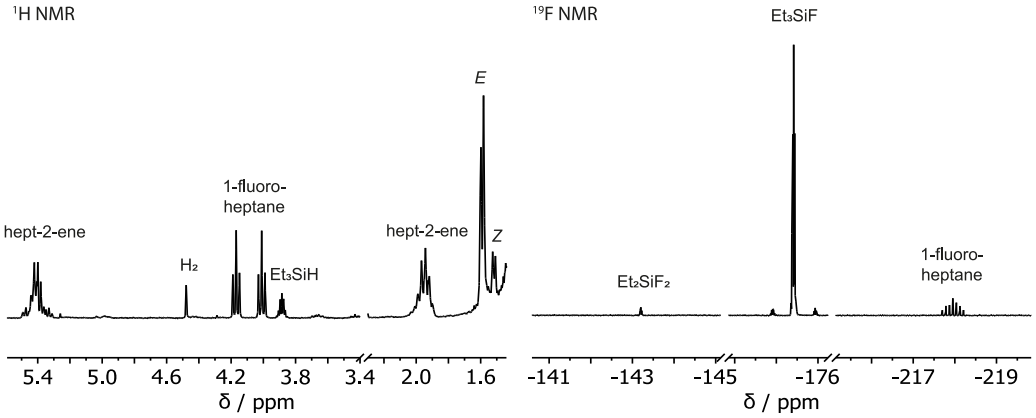

Figure 21. Parts of the ^{1}H NMR (300.1 Hz, C_6D_6) and ^{19}F NMR (105.1 Hz, C_6D_6) spectra for ACF-teflate catalyzed dehydrofluorination reaction of 1-fluoroheptane with Et_3SiH.

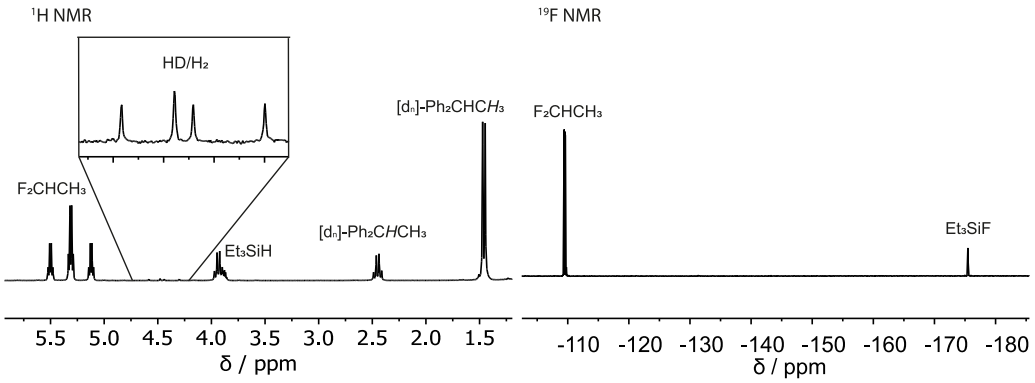

Figure 22. ^{1}H NMR (300.1 Hz, C_6D_6) and ^{19}F NMR (105.1 Hz, C_6D_6) spectra for ACF-teflate catalyzed Friedel-Crafts reaction of 1,1-difluoroethane with Et_3SiH.

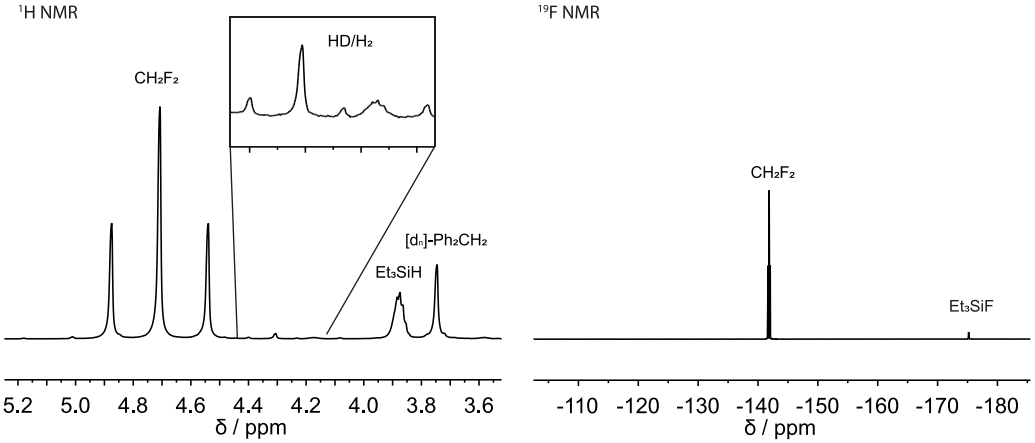

Figure 23. ^{1}H NMR (300.1 Hz, C_6D_6) and ^{19}F NMR (105.1 Hz, C_6D_6) spectra for the ACF-teflate catalyzed Friedel-Crafts reaction of difluoromethane with Et_3SiH.

Literature

[1] D. Massiot, F. Fayon, M. Capron, I. King, S. Le Calvé, B. Alonso, J.-O. Durand, B. Bujoli, Z. Gan, G. Hoatson, *Magn. Reson. Chem.* **2002**, *40*, 70–76.

[2] a) R. König, G. Scholz, A. Pawlik, C. Jäger, B. Van Rossum, H. Oschkinat, E. Kemnitz, *J. Phys. Chem. C* **2008**, *112*, 15708–15720; b) C. Bessada, V. Lacassagne, D. Massiot, P. Florian, J.-P. Coutures, E. Robert, B. Gilbert, *Zeitschrift für Naturforschung A* **1999**, *54*, 162–166.

[3] S. Brunauer, P. H. Emmett, E. Teller, *J. Am. Chem. Soc.* **1938**, *60*, 309–319.

[4] E. P. Barrett, L. G. Joyner, P. P. Halenda, *J. Am. Chem. Soc.* **1951**, *73*, 373–380.

[5] P. Juhás, T. Davis, C. L. Farrow, S. J. Billinge, *J. Appl. Crystallogr.* **2013**, *46*, 560–566.

[6] H. Riesemeier, K. Ecker, W. Görner, B. R. Müller, M. Radtke, M. Krumrey, *X-Ray Spectrom.* **2005**, *34*, 160–163.

[7] B. Ravel, M. Newville, *J. Synchrotron Rad.* **2005**, *12*, 537–541.